



Doktorego tesiak

Molecular recognition of the HIV-1 neutralizing MPER epitope reconstituted in membranes. Contribution of lipid composition and transmembrane domain inclusion.

Johana Torralba Iturbe

2022

Zuzendariak: José Luis Nieva Escandón eta
Beatriz Apellániz Unzalu

Biofisika Institutua (CSIC/EHU)
Biokimika eta Biología Molekularra saila

Acknowledgements

The present thesis was performed at Instituto Biofísica (CSIC, UPV/EHU) under the supervision of Drs. José Luis Nieva and Beatriz Apellániz. The work was supported by the Basque Government (IT1196-19), the Spanish MINECO (BIO2015-64421-R (MINECO/AEI/FEDER, UE)) and MCIU (RTI2018-095624-B-C21 (MCIU/AEI/FEDER, UE)). The author was a recipient of a predoctoral fellowship from the Basque Government.

Aitorpena

Tesi hau Biofísika Institutuan (CSIC, UPV/EHU) burutua izan da, José Luis Nieva eta Beatriz Apellániz Dk.-en zuzendaritzapean. Lanak Eusko Jaurlaritzaren (IT1196-19) Espainiako Gobernuaren MINECO (BIO2015-64421-R (MINECO/AEI/FEDER, UE)) eta MCIU (RTI2018-095624-B-C21 (MCIU/AEI/FEDER, UE)) diru-laguntzak jaso ditu. Autorea Eusko Jaurlaritzaren ikertzaile ez-doktoreen prestakuntzarako doktoratu aurreko laguntzaren onuraduna izan da.

AUTOREAREN ARGITALPENAK

- i) Christophe Caillat, Delphine Guilligay, Johana Torralba, Nikolas Friedrich, Jose L Nieva, Alexandra Trkola, Christophe J Chipot, François L Dehez, Winfried Weissenhorn (2021). Structure of HIV-1 gp41 with its membrane anchors targeted by neutralizing antibodies. *eLife*; 10:e65005. doi:10.7554/eLife.65005
- ii) Igor de la Arada *, Johana Torralba *, Igor Tascón, Adai Colom, Iban Ubarretxena-Belandia, José L R Arrondo, Beatriz Apellániz, José L Nieva. Conformational plasticity underlies membrane fusion induced by an HIV sequence juxtaposed to the lipid envelope (2021). *Sci Rep.*; 11(1):1278. doi:10.1038/s41598-020-80156-w
- iii) Johana Torralba, Igor de la Arada, Pablo Carra villa, Sara Insausti, Edurne Rujas, Eneko Largo, Christian Eggeling, José L R Arrondo, Beatriz Apellániz, José L Nieva (2020). Cholesterol Constrains the Antigenic Configuration of the Membrane-Proximal Neutralizing HIV-1 Epitope. *ACS Infect Dis.*; 6(8):2155-2168. doi:10.1021/acsinfecdis.0c00243
- iv) Victoria Oakes, Johana Torralba, Edurne Rujas, José L Nieva, Carmen Domene, Beatriz Apellaniz. Exposure of the HIV-1 broadly neutralizing antibody 10E8 MPER epitope on the membrane surface by gp41 transmembrane domain scaffolds (2018). *BBA-Biomembranes*; 1860(6):1259-1271. doi:10.1016/j.bbamem.2018.02.019
- v) Eneko Largo, Douglas P Gladue, Johana Torralba, Vicente M Aguilella, Antonio Alcaraz, Manuel V Borca, José L Nieva. Mutation-induced changes of transmembrane pore size revealed by combined ion-channel conductance and single vesicle permeabilization analyses (2018). *BBA – Biomembranes*; 1860(5):1015-1021. doi:10.1016/j.bbamem.2018.01.012
- vi) Pablo Carra villa, Antonio Cruz, Itziar Martin-Ugarte, Itziar R Oar-Arteta, Johana Torralba, Beatriz Apellaniz, Jesús Pérez-Gil, José Requejo-Isidro, Nerea Huarte, José L Nieva. Effects of HIV-1 gp41-Derived Virucidal Peptides on Virus-like Lipid Membranes (2017). *Biophys J.*;113(6):1301-1310. doi:10.1016/j.bpj.2017.06.061

AURKIBIDEA

| | |
|---|----|
| 1. SARRERA | 3 |
| 1.1 1 MOTAKO GIZA IMMUNOESKASIAREN BIRUSA | 4 |
| 1.1.1. GIB-1aren egitura eta infekzio zikloa | 4 |
| 1.1.2. Gainazaleko glikoproteina (Env), txertoen garapenerako itua | 9 |
| 1.2 ENV-EN OINARRITUTAKO IMMUNOGENOAK | 15 |
| 1.3 MPER EPITOPOA | 19 |
| 1.3.1. MPERen aldakortasun konformazionala | 20 |
| 1.3.2. M PER domeinura zuzendutako bnAb-ak | 22 |
| 1.3.3. M PER domeinuan oinarritutako txertoen saiakerak | 25 |
| 1.4 HELBURU NAGUSIAK | 27 |
| 1.4.1. Helburu zehatzak | 27 |
| 2.KAPITULUA..... | 29 |
| | 30 |
| 2. TEKNIKA ESPERIMENTALAK | 31 |
| 2.1 LIPIDOETAN OINARRITUTAKO SISTEMA EREDUAK | 31 |
| 2.1.1. Liposomen ekoizpena | 31 |
| 2.1.2. Lipido kontzentrazioaren determinazioa | 36 |
| 2.1.3. Peptidoen txertaketa besikuletan: sakarosa gradiente bidezko LPFen flotazioa | 38 |
| 2.1.4. Besikulen tamainaren zehaztapena DLS bitartez | 39 |
| 2.2 FAB-EN ADIERAZPENA, PURIFIKAZIOA ETA MARKAKETA | 41 |
| 2.2.1. Fab-en adierazpen eta purifikazioa bakterio zeluletan | 41 |
| 2.2.2. Proteinen zuzendutako markaketa | 44 |
| 2.3 TEKNIKA ESTRUKTURALAK | 46 |
| 2.3.1. Dikroismo zirkularreko espektroskopia (DC) | 46 |
| 2.3.2. Espektroskopia infragorria (IR) | 48 |
| 2.4 FLUORESZENTZIA OINARRITUTAKO MIKROSKOPIA AURRERATUA | 50 |
| 2.4.1. Mikroskopia konfokala | 50 |

| | |
|--|-----|
| 2.5 MIKROSKOPIA ELEKTRONIKOA | 58 |
| 2.6 INDAR ATOMIKOKO MIKROSKOPIOA | 59 |
| 2.6.1. Indar-espektroskopia | 62 |
| 2.6.2. Molekula bakarreko FS | 63 |
| 2.7 BIOLOGIA ZELULARRA: ZELULEN INFEKZIO ETA BIRUSEN NEUTRALIZAZIO SAIOAK..... | 67 |
| 2.7.1. Pseudobirusen ekoizpena..... | 68 |
| 2.7.2. Neutralizazio saioa | 70 |
| 2.8 TEKNIKA IMMUNOLOGIKOAK | 71 |
| 2.8.1. Untxien immunizazioa..... | 71 |
| 2.8.2. ELISA ez-zuzena..... | 73 |
| 3. RESULTS | 77 |
| 3.1 Conformational plasticity underlies membrane fusion induced by an HIV sequence juxtaposed to the lipid envelope | 77 |
| 3.1.1. Introduction..... | 78 |
| 3.1.2. Methods..... | 80 |
| 3.1.3. Results | 83 |
| 3.1.4. Discussion | 93 |
| | 98 |
| 3.2 Cholesterol constrains the antigenic configuration of the membrane-proximal neutralizing HIV-1 epitope | 99 |
| 3.2.1. Introduction..... | 100 |
| 3.2.2. Methods..... | 102 |
| 3.2.3. Results | 106 |
| 3.2.4. Discussion | 117 |
| | 122 |
| 3.3 Antibody accessibility to the nearly-pan-neutralizing HIV-1 MPER epitope modulated by the length of the Env glycoprotein membrane-spanning scaffold and the bilayer thickness..... | 123 |
| 3.3.1. Introduction..... | 124 |

| | |
|---|-----|
| 3.3.2. Methods..... | 125 |
| 3.3.3. Results | 127 |
| 3.3.4. Discussion..... | 135 |
| | 140 |
| 3.4 Anchoring of HIV-1 10E8 epitope through the transmembrane domain reverses MPER effects on the mechanical stability of the lipid bilayer and augments antibody binding affinity. Implications for liposome-based MPER vaccine design. | 141 |
| 3.4.1. Introduction..... | 142 |
| 3.4.2. Methods..... | 143 |
| 3.4.3. Results | 146 |
| 3.4.4. Discussion | 157 |
| 4. EZTABIDA OROKORRA | 163 |
| 4.1 ONDORIOA..... | 167 |

LABURDUREN ETA SINBOLOEN ZERRENDA

| | |
|--------|--|
| 2D-COS | Two-dimensional correlation spectroscopy |
| 6-HB | 6-helix bundle / 6-helize sorta |
| Adv | Adenovirus / Adenobirusa |
| AIDS | Acquired Immune Deficiency Syndrome |
| AFM | Atomic force microscopy / Indar atomikoko mikroskopia |
| APDMES | 3-aminopropyldimethylethoxysilane |
| ART | Antiretroviral therapy / Erretrobirusen kontrako tratamendua |
| ASA | Accessible surface area |
| ATR | Attenuated Total Reflectance |
| AZT | Azidothymidine / Azidotimidina |
| bnAb | Broadly neutralizing antibody / Espektro zabaleko antigorputz neutralizatzaila |
| BSA | Bovine serum albumin / Behi gazur albumina |
| BCR | B-cell receptor / B-zelulen hartzailea |
| CA | Capsid / Kapsidea |
| CCD | Charge-coupled device |
| CD | Circular dichroism / Dikroismo zirkularra |
| CD4bs | CD4-binding site / CD4-ren batuketa gunea |
| CD4mc | CD4-mimetic compound |
| CDC | Center for disease Control and Prevention / Amerikako gaixotasunen kontrolerako zentroa |
| CDRH3 | Third complementarity determining region of the heavy chain / Osagarritasuna determinatzen duen esualdea |
| Chol | Cholesterol / Kolesterola |
| C-MPER | C-terminal sequence of the MPER / C-muturreko MPER sekuentzia |

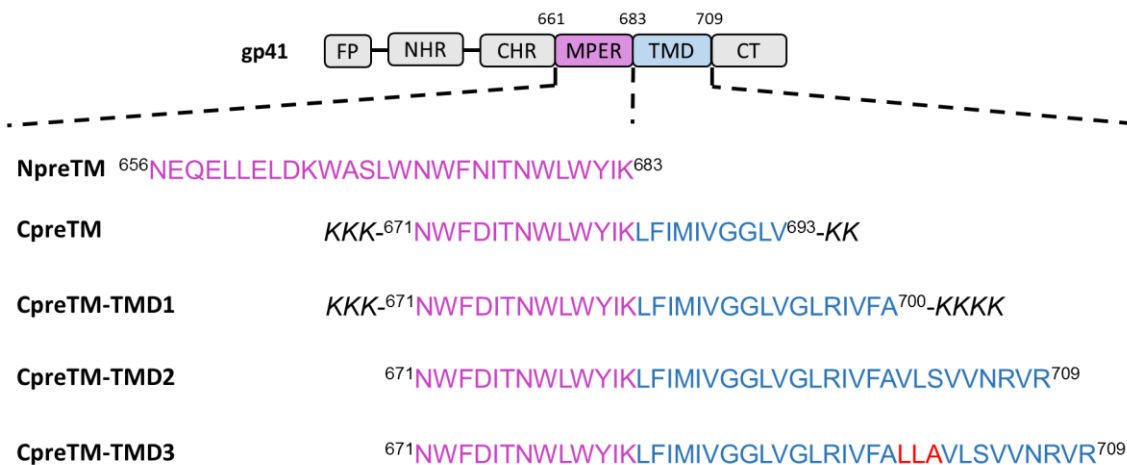
| | |
|-----------------|---|
| Cryo-EM | Cryogenic electron microscopy / Kriomikroskopia elektronikoa |
| CT | Cytoplasmic tail / Isats zitoplasmatikoa |
| CTL | Control / Kontrola |
| D _c | Hydrocarbon acyl chain thickness |
| D _{HH} | Headgroup to headrgroup distance |
| DHSM | Dihydrosphingomyelin |
| diPC | Diacyl PC |
| DLS | Dynamic light scattering / Argiaren sakabanatze teknika |
| DMEM | Dulbecco's modified Eagle's medium / Medioa |
| DMSO | Dimethylsulfoxide |
| DTT | Dithiothreitol |
| ELISA | Enzyme linked immunosorbent assay |
| EM | Electron microscopy / Mikroskopio elektronikoa |
| Env | Envelope glycoprotein / Bildukiko glikoproteina |
| eOD | Engineered outer domain |
| ER | Endoplasmic reticulum / Erretikulu endoplasmatikoa |
| etOH | Ethanol / Etanola |
| Fab | Fragment, antigen binding / Antigenoa batzen duen fragmentua |
| Fb | Breakthrough force |
| FDA | Food and drug administration / Elikagai eta botiken administrazioa |
| FP | Fusion peptide / Fusio peptidoa |
| FS | Force spectroscopy / Indar espektroskopia |
| GIB | Giza immunoeskasiaren birusa |
| GFP | Green fluorescent protein / Proteina fluoreszente berdea |
| Gp120 | HIV glycoprotein 120 kDa (surface subunit) / GIB 120 kDa glikoproteina (gainazaleko azpiunitatea) |

| | |
|--------------|--|
| Gp41 | HIV glycoprotein 41 kDa (transmembrane subunit) / GIB 41 kDa glikoproteina (transmintz azpiunitatea) |
| GT | Germline targeting / Lerro germinalera zuzendutako |
| GUV | Giant unilamellar vesicles / Lamela bakarreko besikula erraldoiak |
| HAART | Highly active antiretroviral therapy / Terapia anti-erretrobiral oso aktiboa |
| HC | Heavy chain / Kate astuna |
| HEK293 cells | Human embryonic kidney 293 cells / Giza enbrioiaaren giltzurrun 293 zelulak |
| HEPES | 4-(2-hydroxyethyl)piperazine-1-ethanesulfonic acid |
| HFIP | 1,1,1,3,3,3-hexafluoro-2-propanol |
| HIES | Hartutako immunoeskasiaren sindromea |
| HIV | Human immunodeficiency virus |
| HR | Heptad repeated region / Heptada errepikakorrak |
| IgG | Immunoglobulin G / G immunoglobulina |
| IN | Integrase / Integrasa |
| IPTG | Isopropyl-D-thiogalactopyranoside |
| IR | Infrared / Infragorria |
| Laurdan | 6-dodecanoyl-2-dimethylaminonaphthalene |
| LC | Light chain / Kate arina |
| LPF | Liposome-peptide formulation / Liposoma-peptido formulazioak |
| LUV | Large unilamellar vesicle / Lamela bakarreko besikula txikiak |
| MA | Matrix / Matrizea |
| MCS | Multiple cloning site / Klonazio gune anizkoitza |
| MHC | Major histocompatibility complex / Histokonpatibilitate konplexu nagusia |

| | |
|-----------------|---|
| MLV | Multilamellar vesicle / Lamela anitzeko besikulak |
| MPER | Membrane-proximal external régión / Mintzaren hurbileko kanpo-eskualdea |
| NA | Numerical apertura / Irekidura optikoa |
| NBD | 7-nitro-1,2,3-benzoxadiazole |
| NC | Nucleocapsid / Nukleokapsidea |
| NFL | Native flexibly linked |
| NHP | Non-human primates |
| NMR | Nuclear magnetic resonance / Erresonantzia magnetiko nuklearra |
| OD | Optical density / Dentsitate optikoa |
| ON | Over night / Gau osoz |
| PA | Phosphatidic acid |
| PBS | Phosphate-buffered saline / Fosfatodun indargetzailea |
| PDI | Polydispersity index / Polidispersio indizea |
| PE | Phosphatidylethanolamine |
| PI4P | Phosphatidylinositol-4-phosphate |
| POPC | 1-palmitoyl-2-oleoyl-sn-glycero-3-phosphocholine |
| PR | Protease /Proteasa |
| PS | Phosphatidylserine |
| PsV | Pseudovirus |
| PTM | Post-translational modifications / Itzulpen ondoko aldaketa |
| Rho | Lissamine rhodamine B sulfonyl chloride |
| RT ¹ | Reverse transcriptase / Alderantzizko transkriptasa |
| RT ² | Room temperature / Giro temperatura |
| SLB | Supported lipid bilayer / Finkatutako lipido geruzak |
| SDS | Sodium dodecyl sulfate |

| | |
|----------|--|
| SDS-PAGE | Sodium dodecyl sulfate polyacrylamide gel electrophoresis |
| SHM | Somatic hypermutation / Hipermutazio somatikoa |
| SM | Sphingomyelin / Esfingomielina |
| smFRET | Single molecule fluorescence resonance energy transfer / Molekula indibidualetan oinarritutako erresonantzia fluoreszentearen energia transferentzia |
| STED | Stimulated emission depletion microscopy / Igorpen-murriztuko kitzikapen mikroskopia |
| TEV | Tobacco etch virus |
| Tm | Melting temperature / Urtze tenperatura |
| UCA | Unmutated common ancestors / Mutatu gabeko aitzindari komuna |
| UFO | Uncleaved prefusion optimized |
| UNAIDS | The Joint United Nations programme on HIV and AIDS / GIB eta HIESaren Nazio Batuen programa |
| VLP | Virus like particle / Birus antzeko partikula |

**GIB-1AREN GP41-MPER-TMD DOMEINUTIK
ERATORRITAKO PEPTIDOEN SEKUENTZIAK**



LABURPENA

SARRERA

Giza Immunoeskasiaren birusa (GIB), Hartutako Immuno Eskasiaren Sindromearen (HIES) eragilea dena, 1983an Pasteur Institutuan isolatu zen lehen aldiz¹. UNAIDSek 2020an argitaratutako egunerezte txostenaren arabera, HIESaren pandemia hasi zenetik, kalkulatzen da GIBak munduan 76 milioi pertsona inguru kutsatu dituela eta horietatik 35 milioi, HIESak eragindako gaitzen ondorioz hil direla. Birus honen aurkikuntzatik urte ugari igaro badira ere, ez da orain arte honen aurkako behin betiko sendabiderik ezta txerto eraginkorrik aurkitu. Hala ere, erretrobirusaren kontrako tratamendua (ingelesetik *Antiretroviral Therapy*, ART) nabarmen murriztu du HIESak eragindako hilkortasuna, hasiera batean hilgarria zen gaixotasun hori kroniko bilakatzu eta gaixoen bizi-iraupena luzatzearekin batera, gaixotasunaren transmisioa murriztuz².

Ondorioz, GIB-1aren aurkako txerto eraginkor bat diseinatzea da pandemia kontrolatu eta gainditu ahal izateko ahalmen handia izan dezakeen estrategietako bat. Env proteina, GIB-1aren gainazalean kokatzen den eta sistema immuneak ezagutzeko eskuragarri dagoen proteina bakarra denez, birusen honen aurkako txerto potentzial baten garapenerako itu nagusia bilakatu da. Env, gp120 eta gp41 azpiunitateek osatzen duten heterodimeroen trimero bat da³. Gp120 azpiunitatea, gainazalean kokatzen da eta birusaren eta zelula ostalariaren arteko ezagumenduan parte hartzen du; gp41 azpiunitateak aldiz, mintza zeharkatzen du eta zelularen mintzaren eta birusaren mintzaren arteko fusioaz arduratzen da.

GIB-1aren infekzioa birusaren Env glikoproteinaren gp120 azpiunitatearen eta itu zelularen CD4 hartzailearen arteko loturarekin hasten da (1.2 irudia). Lotura honek, CCR5 edo CXCR4 kohartzaileen eta gp120 azpiunitateko V3 begiztaren arteko lotura ahalbidetuko duten zenbait konformazio aldaketa eragingo ditu. Ondoren, gp41 azpiunitateko N eta C muturreko heptada errepikakorrak (NHR eta CHR hurrenez hurren) agerian geratzen dira eta fusio peptidoa (FP) zelula ostalariaren mintzean txertatzen da⁴. Jarraian C eta N HR eskualdeak tolesten dira 6-HB egitura eratuz eta bi mintzen arteko hurbilketa eraginez. Gp41 azpiunitateko FPak eta mintz lipidikoan murgilduta aurkitzen den MPER eskualdeak (ingelesetik, *Membrane-Proximal External Region*) zelularen eta birusaren mintzak desegonkortzen dituzte^{5,6}, hauen arteko fusioa eraginez eta ondorioz, birusaren material genetikoa eta zenbait entzima zelula ostalariaren zitoplasman askatzea ahalbidetuz.

GIBaren aurkikuntzatik ia 40 urte igaro diren arren, ez da oraindik birus honen aurkako txerto eraginkorrik diseinatzea lortu; arrakasta falta hau bereziki, birusak garatu dituen immunitate sistemaren aurkako ihes mekanismoen ondorio izan daiteke. Birusaren gainazalean kokatzen den Env konplexua oso dinamiko eta ezegonkorra da eta oso kopuru txikian adierazten da GIBaren mintzaren gainazalean, horietako trimero batzuk gainera, ez-funtzionalak izan ohi dira⁷. Horrez gain, birusaren aniztasun genetikoa izugarri altua da, birusaren erretrontranskriptasa entzimak ez baitu akatsak zuzentzeko mekanismorik⁸. Ezaugarri honek izugarri zaitzen du sistema immunearen bidezko trimeroaren ezagumendua. Hala ere, zenbait gaixok GIBaren infekzioa blokeatzeko gai diren eta neutralizazio potentzia altua zein espektro zabala duten antigorputzak (bnAb, ingelesetik *broadly neutralizing antibodies*) garatzea lortzen dute; eta hauen isolamenduak, Env-en kontserbatutako gune zaugarrien identifikazioa ahalbidetu du (1.4 irudia). Espektro zabaleko antigorputzak garatu daitezen, denbora luzez eta etengabe egon behar dute antígeno biralekin kontaktuan; horregatik, urteak igaro ondoren, heltze prozesu luze baten ostean soili sortzen dira⁹ eta hipermutazio somatiko maila altuak izan ohi dituzte^{10,11}. Horrez gain, kate astuneko CDR3 begizta luzeak garatzen dituzte, Env trimeroan sakon eta ezkutuan dauden epitopoetara heltzeko gaitasuna ematen dietenak¹⁰.

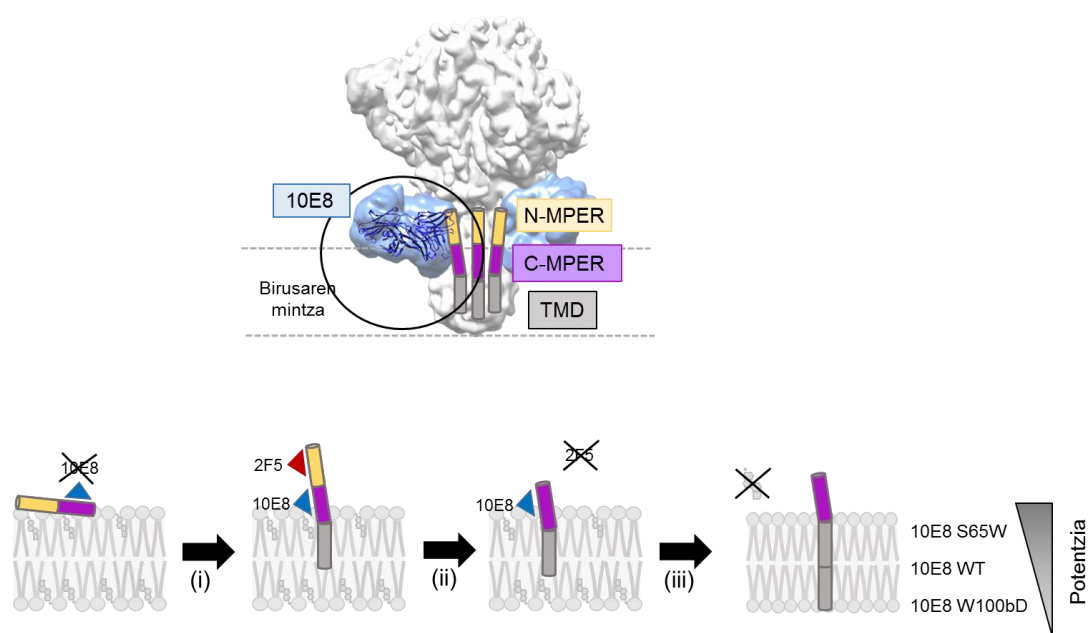
BnAb-ek dituzten ezaugarri bereziek eta heltze prozesu luzeen beharrak, txertaketa bidezko hauen indukzioa erronka handia suposatzen du. Hala ere, bnAb-en existentziak berak frogatzen du B zelulek infekzio naturalean sortzen duten erantzuna zenbaitetan, gai izan daitekela GIB-1aren aurkako antigorputz neutralizatzaileak sortzeko. Azkenaldian antigorputzen isolamendu tekniketan emandako hobekuntzek eta hauen lotura-guneen identifikazioak, GIBaren aurkako immunogenoen diseinu arrazionalerako oso baliagarria izan daitekeen informazioa eman du.

GIB-1aren aurkako identifikatutako bnAb-en artean, MPER sekuentziara zuzendutakoak, espektro zabalena erakusten dutenak dira. Izan ere, eskualde hau oso kontserbaturik dago, ezinbestekoa baita birusaren eta itu zelularen arteko fusioa eragiteko^{5,6}. Orain arte deskribaturiko anti-MPER antigorputzen artean, hobekien deskribaturik dagoena eta espektro zabal handiena erakusten duena, 10E8 bnAb-a da¹². MPER immunogeno bikaina dirudien arren, domeinu honetara zuzendutako txertoen saiakerek ez dute arrasta handirik lortu. MPER domeinura zuzendutako txertoen huts egitearen arrazoiatariko bat, eskualde honen malgutasunaren ondorioz, bnAb-en indukzioa eragiten duen MPERaren egitura, oraindik atomikoki ebatzia ez egotea izan daiteke. Bestalde, MPER mintzean txertaturik egoteak, honen konformaziorako eta beraz txertoen garapenerako, lipido ingurunea mantentzea

ezinbestekoa da. Baino, oraindik sakon aztertu beharra dago lipidoek MPER domeinuaren egituraren konfigurazioan zein immunogenizitatearen modulazioan duten zeregina, txertoek izan beharko luketen osaera lipidiko zehatza definitzeko.

Tesi honen helburu nagusia 10E8 moduko antigorputzen erantzuna eragiten duen MPER-TMDaren egitura zehatza imitatzeko behar diren baldintza egokiak definitzea litzateke, eskualde honetan oinarritutako immunogenoien diseinu arrazionalean laguntzeko hain zuen (1.irudia). Horretarako, MPER epitopoaren sekuentzia espezifika eta lipido-peptido txertoen lipido konposizio zehatza definitu nahi izan da.

EMAITZAK ETA EZTABAIKA



1. irudia. MPER domeinuan oinarritutako immunogenoak ekoizteko jarraitutako estrategia. A) cryo-EM berreraikuntzan oinarritutako 10E8 MPERari lotutako eredua (EMDB-3312). B) 10E8 antigenorputzak ezagutzen duen MPER epitopoaren egitura imitatzeko jarraitutako estrategia. i) Epitopoaren gainazaleko aurkezpen egonkorra, TMDa ainguraketa moduan erabiliz. ii) Erantzun immunea C-MPERera zuzentzeko, N-MPER domeinu immunogenikoaren ezabaketa. iii) LPF-en formulazioen optimizazioa 10E8 eta honen aldaerak erreferentzia gisa erabiliz. Peptidoaren aurkezpena hobetzen da transmintz domeinuaren sekuentziaren luzera handituz eta besikula lipidikoetatik kolesterola ezabatuz.

10E8k ezagutzen duen egitura imitatzen duen sekuentzia definitze aldera, tesi honetan jarraitutako estrategiaren lehenbiziko urratsa (1.irudia i), MPER-TMDan oinarritutako peptidoen egitura antigenikoa definitzea litzateke, mintzean perturbaziorik sortzen ez duena hain zuen. Lipido-peptido formulazio (LPF) egonkorra definitzeko, eta C-MPER

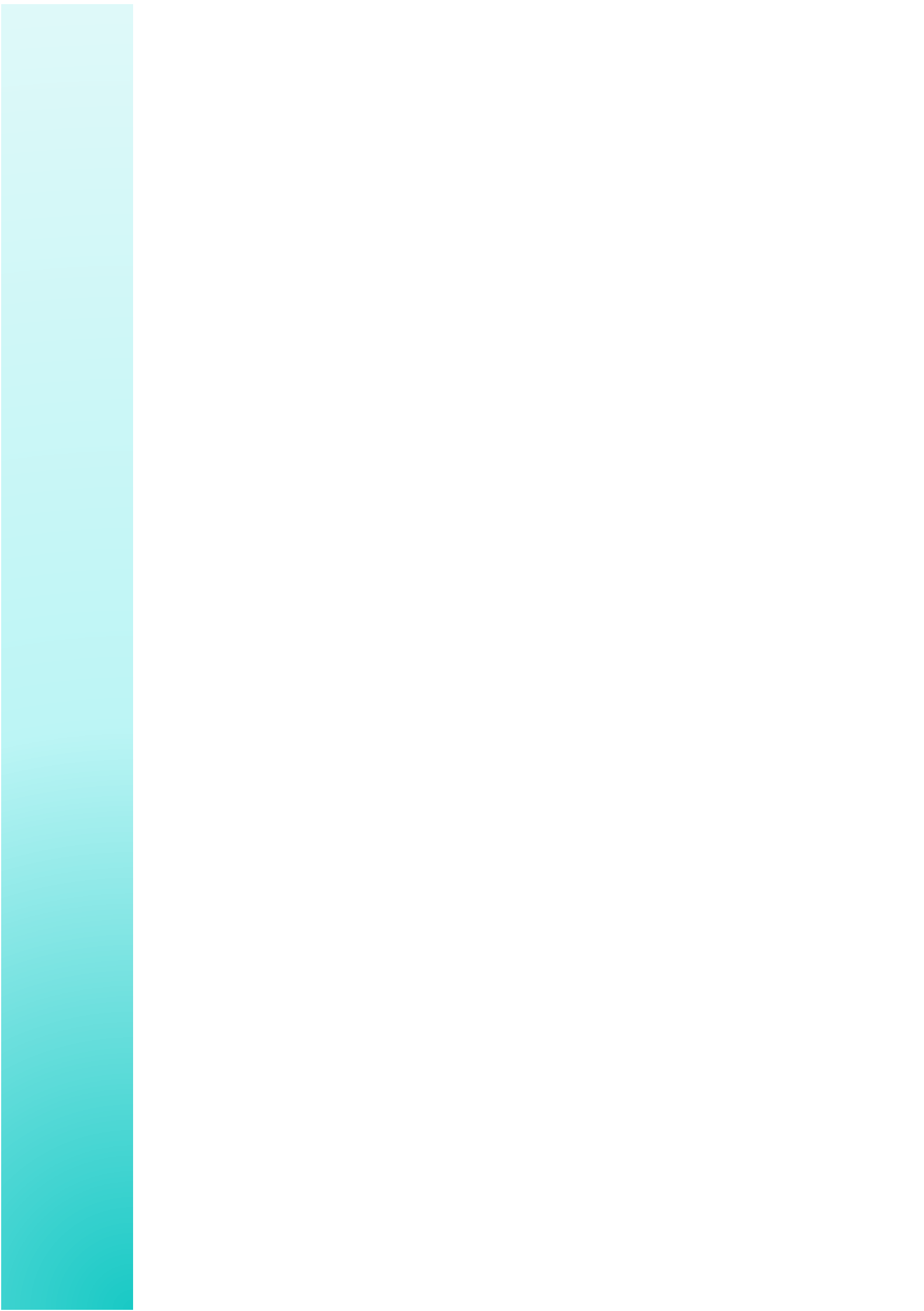
zonaldera zuzendutako erantzun immuneak lortzeko, N-MPER eremua ezabatzea egokiena dela ikusi izan da.

Halaber, txertoen diseinurako jarraitu den hurrengo estrategia, transmintz domeinuaren gehipena izan da. Izañ ere, uste da errekonstituzio prozesuaren ostean besikula lipidikoen gainazalean kokatuko den epitopoaren aurkezpena egokia eta egonkorra izan dadin, peptidoaren ainguraketan eta honen egituraren modulazioan parte hartuko duen sekuentzia hau gehitzea erabilgarria izan daitekeela. Beraz, mintza zeharkatzen duten sekuentziaren luzera desberdineko peptidoak diseinatu dira eta lipido konposizio desberdineko besikuletan hartzen duten egitura eta antigenizitatea aztertu da. Alde batetik, TMDaren gehipenak, bigeruzaren egonkortasun mekanikoa nabarmen hobetzen duela ikusi da, LPF egonkorraezko ezinbesteko ezaugarria alegia. Gainera, mintza zeharkatzen duen sekuentziaren luzerak, epitopoaren irisgarritasuna eta honekin batera antigorputzen afinitatea modula dezakela baiezttu da. Hain zuzen, LPFetan jarritako transmintz sekuentziaren luzera zenbat eta luzeagoa izan, 10E8 antigorputzaren ezagupena hobea dela frogatu da, epitopoaren esposizio maila emendatzen dela alegia.

Azkenik, tesi honetan ikertu den GIBaren aurkako txertoen diseinurako hirugarren estrategia, LPFek izan beharko luketen lipido konposizio zehatza definitzea izan da. Lipido konposizioa funsezko elementua da MPER-TMD domeinuan oinarritutako peptido-lipido txertoen diseinuan, lipidoek peptidoen egitura modulatzeko gaitasuna baitute eta ondorioz, epitopoa sistema immunera nola aurkeztuko den definituko dute. GIB-1aren mintza kolesterolean aberatsa denez, lipido honen kontzentrazio altua duten besikulen erabilpena aztertu da, peptidoak birusean duen ingurune natiboa imitatze aldera. Hala ere, kapituluetan zehar ikusi da besikulen kolesterol edukia handitzeak, negatiboki eragiten duela peptidoaren egitura, epitopoaren mintzean zeharreko ezkutaketa eraginez. Epitopoaren oklusioak, 10E8 bnAb-ak lotura gunera iristeko duen gaitasunaren murrizketa eta honekin batera, antigenizitatearen galera eragiten du. Tesi honetan beraz, C-MPER domeinuan oinarritutako txertoak ekoizteko, birusaren mintzak duen kolesterol kontzentrazioa imitatzea ez dela egokia ikusi izan da; hau da, anti-MPER antigorputzak sortzeko LPF-en formulazioak kolesterolik gabe diseinatu behar dira.

1.KAPITULUA

SARRERA ETA HELBURUAK



1. SARRERA

Hartutako Immuno Eskasiaren Sindromea (HIESa) Amerikako Gaixotasunen Kontrolerako eta Prebentziorako Zentroak (ingelesez *Center for Disease Control and Prevention, CDC*) diagnostikatu zuen lehen aldiz 1981eko ekainean. 1983an Luc Montagnierrek, Pasteur Institutuko bere taldearekin batera, erretrobirus berri bat aurkitu zuen HIESaz kutsatutako gaixoengandik hartutako laginak aztertzen ari zen bitartean¹. Urte bat beranduago, erretrobirus hau, HIESaren eragile bezala identifikatua izan zen¹³ eta 1986an Giza Immunoeskasiaren Birusaren (GIB) izena eman zitzzion¹⁴.

UNAIDsek 2020an argitaratutako txostenaren arabera, HIESaren pandemia hasi zenetik, GIBak munduan 76 milioi pertsona inguru kutsatu ditu, horietatik 35 milioi HIESak eragindako gaitzen ondorioz hil direlarik. Bestalde, gaur egun 38 milioi pertsona bizi dira HIESarekin eta 1.7 milioi infekzio berri gertatu ziren 2020an, batez ere Afrika ekialde eta hegoaldean. Orain arte behin betiko sendabiderik aurkitu ez bada ere, erretrobirusaren kontrako tratamenduak (ingelesetik *Antiretroviral Therapy, ART*) nabarmen murritz tu du HIESak eragindako hilkortasuna, terapia hau 2006tik 2019ra bitartean izandako heriotzen % 48ko beherakadaren erantzulea delarik.

Zidobudina (ZDV), azidotimidina (AZT) bezala ere ezaguna, FDAk (ingelesetik *Food and Drug Administration*) 1987an GIBari aurre egiteko onetsi zuen lehen botika izan zen. Ordutik, 220 tratamendu baino gehiago izan dira onartuak. Gaur egun infekzioa kontrolatzeko erabiltzen den erreferentziazko tratamenduak HAART (ingelesetik, *Highly Active Antiretroviral Therapy*) izena hartzen du eta botika ezberdinak konbinazioa da. Botika hauek nagusiki, birusaren alderantzizko transkriptasa (RT) eta proteasa (PR) entzimen aurka egiten dute, birusaren karga eta transmisio tasa murritzuz. Tratamendu honi esker, HIESa gaixotasun kroniko bilakatzea lortu den arren, gaixoen bizi-iraupena luzatuz eta gaixotasunaren transmisioa murritzuz², kutsatutako pertsonen % 60k bakarrik du terapia eskuragarri. Horrez gain, HAARTa ez da gai latentzia fasean dagoen birusa ezabatzeko, eta ondorioz, gaixoek bizitza guztian zehar jaso behar dute tratamendu hau, albo-ondorio ugari pairatuz¹⁵.

Hori dela eta, GIBaren aukako txerto eraginkor bat garatzea funtsezkoa da pandemia kontrolatu eta azkenean honekin amaitu ahal izateko. Txertoen garapenerako teknologia izugarri hobetu den arren, eta GIBa aurkitu zenetik 30 urte igaro diren arren, ez da oraindik birusen honen aurkako txertorik aurkitu.

1.1 1 MOTAKO GIZA IMMUNOESKASIAREN BIRUSA

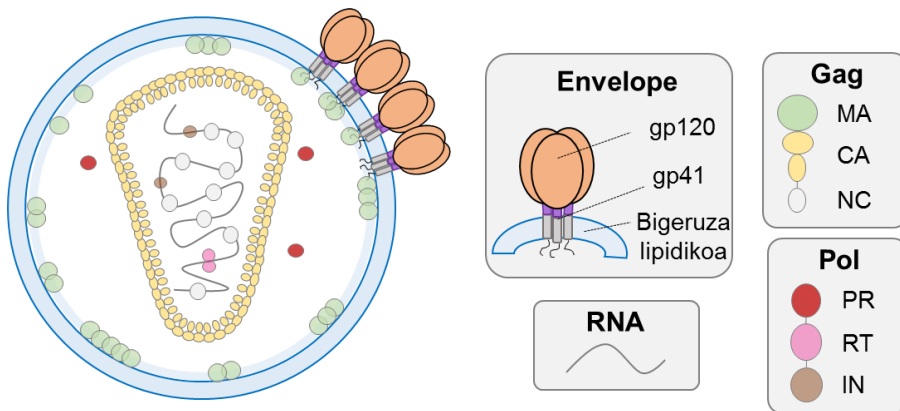
GIBa *Lentivirus* generoan, *Retroviridae* familiaren barruan sailkatzen da. Erretrobirusak ornodun espezie ezberdinetan aurkitu izan dira eta animalia zein gizakien gaixotasun askorekin erlazionaturik daude. Familia honek iraupen luzeko gaixotasunak eragiten ditu batez ere, inkubazio aldi luzekoak¹⁶.

Ezaugarri genetiko eta antigeno biralen desberdintasunetan oinarriturik, GIBa 1 eta 2 motetan sailkatu daiteke (GIB-1, GIB-2 hurrenez hurren). GIB-1ak birulentzia altuena du, errazago transmititzen da eta mundu mailan GIBak eragindako infekzio gehienen sortzailea da¹⁷. GIB-1aren andui desberdinak hiru talde nagusitan sailkatu daitezke: M (ingelesetik *Major*), N (ingelesetik *New*) eta O (ingelesetik *Outlier*)¹⁸. Era berean, M taldean kokatzen diren anduiak oso desberdinak direnez, A-tik K-rako kladoetan sailkatu ohi dira. Horietatik, B kladoa nagusiki Ipar Amerika eta Europan aurkitu daiteke eta ikerketa gehienen itua da. Zehazki, klado honen HXB2 hartu da erreferentzia gisa tesi lan honetan. GIB-2aren transmisio ahalmen baxuaren ondorioz, Mendebaldeko Afrikara mugatzen da¹⁹.

1.1.1. GIB-1aren egitura eta infekzio zikloa

GIB-1 birioi heldua mintz lipidiko batez inguratutako eta 100 nm-tako diametroa duen partikula esferikoa da (1.1 irudia). GIB-1aren genoma, nukleokapsidearen (NC) barruan kokatzen diren 9 kb-tako kate bakuneko bi RNA molekulek osatzen dute. RNArekin batera, birusaren NCaren barnean kokatzen diren elementu garrantzitsuenak alderantzizko transkriptasa (RT) eta integrasa (IN) entzimak dira. Nukleokapsidea NC proteinez eraturik eta kono itxura hartzen duen kapsideaz (CA) inguraturik dago. Birus honen genomak 9 gene ditu, baina funtsezkoak hiru dira: *gag*, *pol*, eta *env*. *Gag* matrizea (MA) osatuko duten egiturazko proteinen aitzindaria da, eta MA, CA, NC eta p6 kodetzen ditu. PR, RT eta IN entzimak *pol* geneak kodetzen ditu. *Env* genea, gp160 fusio glikoproteina (*Env*) kodetzen du eta aitzindari honen proteolisiaren bitartez, bi azpiunitate lortzen dira: gp120 (gainazaleko proteina) eta gp41 (transmintz proteina). Azpiunitate hauek, birusaren gainazalean kokatuko den Env trimerikoa osatuko dute²⁰, itu zelularen hartziale eta kohartzialearen batuketaren, eta jarraian ematen den zelula eta birusaren mintzen arteko fusioaren erantzulea alegia. Azkenik, GIB-1ak sei proteina gehigarri kodetzen ditu; horietatik hiru (*Vif*, *Vpr* eta *Nef*) birus partikulan daude, beste bi

(Tat eta Rev) gene erregulazioan funtsezkoak dira eta azken proteinak, Vpu-k, zeharka laguntzen du birioiak muntatzen.



1.1 irudia. GIB-1 birioi helduaren modelo eskematikoa. Birusaren proteina garrantzitsuenak irudikatu dira. GIB-1 esferikoa da eta honen gainazalean Env konplexua kokatzen da, gp120 eta gp41 azpiunitatez osaturik dagoena. Kono itxura hartzen duen kapsideak RNA, NC eta entzimak biralak babesten ditu. Irudia, ²¹-tik egokitua izan da.

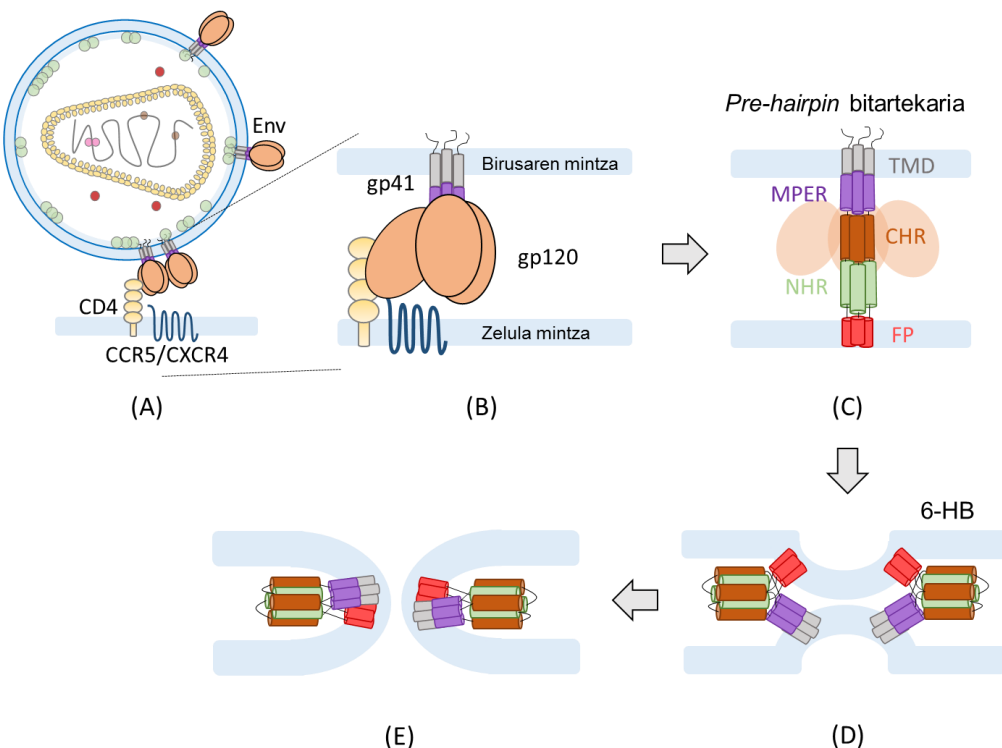
GIB-1ak CD4 hartzalea eta CCR5 edo CXCR4 kohartzaleak adierazten dituzten immunitate sistemako zelulak infektatzen ditu; horien artean, T linfozitoak, monozitoak, makrofagoak eta zelula dendritikoak. Infekzioa gertatzean, GIBaren aurkako CD8⁺ eta CD4⁺ T linfozito espezifikoak sortzen dira, erantzun zelular bat eragingo dute, karga birikoaren murriketa eragingo delarik. T linfozitoez gain, immunitate sistemako B zelulak ere aktibatu egiten dira; baina, antigorputzen bidezko hasierako erantzunak ez du birusaren erreplikazioa kontrolatzerik lortuko. Hain zuzen, hilabeteak behar dira birus autologoaren aurkako antigorputz neutralizatzailak garatzeko. Hala ere, GIBak immunitate sistematik ihes egiteko hainbat estrategia garatu ditu. Horien artean, birusaren mutazio-tasa alta, alderantzizko transkriptasak akatsak zuzentzeko mekanismorik ez duenaren ondorio ⁸. Honek, aldakortasun genetiko izugarria sortzen du birusean, funtzionalak diren eskualdeak ere oso aldakorrak bihurtuz, soilik euren funtzioa betetzeko ezinbestekoak diren hondakin kopurua mantentzen delarik ²². Honez gain, birusaren gainazalean kokatzen diren Env konplexu gutxi daude (8-14 espikula birioi bakoitzeko); horietako batzuk ez-funtzionalak dira eta are gehiago, gp120 azpiunitatearen berezko ezabaketa gertatu ohi da ⁷. Gainera, Env glikoproteinaren eskualde funtzionalak, oro har, glicosilazioz babesturik daude ²³, esterikoki izkutatuak fusio prozesua hasten den arte ²⁴, edo askotan, antigorputz ez-neutralizatzileen epitopo gainartzaile edo immunodominanteez inguraturik. Ihes mekanismo hauei esker,

infekzioa gertatu ostean, immunitate sistemaren erantzunari esker birus-karga gutxitzen den arren, ez da infekzioa guztiz ezabatzea lortzen.

Infekzio prozesua, birusaren Env-en gp120 azpiunitatearen eta zelularen CD4 hartzailaren arteko loturak abiarazten du. Lotura honek, konformazio aldaketa bat eragingo du, CXCR4 edo CCR5 kohartzailen ezagumendua ahalbidetuko duena eta mintzen arteko fusioa eragingo duena. Zelula eta birusaren arteko mintzen fusioa gertatzean, birusaren RNA eta zenbait entzima (RT, IN, erribonukleasa eta PR barne), zelula ostalariaren zitoplasman askatzen dira. Ondoren, birusaren RTak RNA kate bikoitzeko DNA erretrontranskribatuko du eta nukleoaren poroen bidez nukleo igaroko da MA, Vpr, IN eta faktore zelularrekin konplexu bat eratuz. Nukleoan, INak DNA birala zelula ostalariaren kromosoman integratuko du. Birusa orduan, latentzia-fasean sartuko da DNAren transkripzioa aktibatzeko seinale bat, hala nola, Tat proteinaren aktibitatea jaso arte. Transkripzioaren lehen urratsetan, RNA polimerasak mRNAk sortzen ditu Tat, Nef eta Ref-entzat. Berehala, beste proteina biral batzuen zein RNA genomikoaren ekoizpena emango da, Tat proteinaz kontrolatutako prozesua izanik. Berriki sintetizatutako egitura-proteinak mintz plasmatikora garaiatzen dira eta mihiatzatzen hasten dira konplexu bat eratzen den arte eta azkenean, birioi heldugabea gemazio bidez askatuko da. Une honetan, PRak Gag eta Gag-Pol poliproteina aitzindariak proteolizatuko ditu erreplikazio zikloa osatuz. Azkenik, birioi helduak infekzio ziklo berri bat abiarazi dezake ^{25,26}.

1.1.1.1 Env bidezko birus eta zelularen mintzen arteko fusioa

Mintzen arteko fusioa, termodinamikaren ikuspegitik, hesi kinetiko handiak gainditu behar dituen gertaera ez-onuragarria da, batez ere aldarapenezko hidratazio indarrak direla eta ²⁷. Birusaren mintzaren kasuan, aipaturiko hesi kinetikoa birusaren fusio proteinen birtolestean sortzen den energia askearekin gainditzen da ^{28,29}. GIB-1aren kasuan, Env glikoproteina da birusa itu zelulan sartzea ahalbidetzen duena (1.2 irudia). Zenbait ikerketek, fusioa eman dadin Env espikula gutxi nahikoak direla diote ³⁰⁻³², birioi helduan Env gutxi dagoenaren modeloarekin bat datorrena ⁷ alegia. Fusio prozesuaren lehen urratsa, birusaren gp120 eta zelularen CD4 hartzailaren arteko afinitate altuko elkarrekintza gertatzen denean ematen da (1.2 A irudia), fusio aurretik guztiz itxita dagoen trimeroaren irekiera eraginez ^{33,34}.



1.2. irudia. GIB-1aren fusio prozesuaren irudikapena. A) CD4 eta gp120 molekulen arteko loturak Env-en konformazio aldaketan eragiten du, B) g120 azpiunitateko V3 begizta CCR5 edo CXCR4 kohartzaleen arteko kontaktua ahalbidetzen duena. C) Kohartzalearekin elkarrekintza eman ondoren, gp41 azpiunitateko N eta C muturreko heptada errepikakorrak (NHR eta CHR) agerian geratzen dira eta fusio peptidoa (FP) zelula ostalararen mintzean txertatzen da, birusa zelula ostalarira ainguratzuz eta pre-hairpin bitartekaria eratuz. D) Jarraian, C eta N HR eskualdeak tolestu egiten dira eta 6-HBa eratzen dute. E) Birmoldaketa hauek birusaren mintzaren eta zelula ostalararen hurbilketa estua eragiten dute, hemifusio bitartekari bat eratuz eta azkenik fusio-poroa sortuz.

Elkarrekintza horrek eragindako konformazio aldaketek, gp120 azpiunitateko kohartzalearen lotura gunea agerian jarriko du, honen eta CCR5 edo CXCR5 zelulen kohartzalearen arteko lotura eraginez (1.2 B irudia)^{35,36}. Lotura honek, gp41 azpiunitatean mintzen arteko fusioa eragingo duten konformazio aldaketak sustatuko ditu. Lehenik eta behin, gp41eko N muturrean kokatzen den FPa itu zelularen mintzean txertatuko da zurtoin itxura duen pre-hairpin deituriko bitartekaria sortuz, non bi mintzak gp41en bitartez konektaturik dauden (1.2 C irudia)⁴. Jarraian, gp41eko monomero bakoitzaren NHR eta CHR domeinuak berrantolatzen dira sei-helize sorta (ingelesetik, *six-helix bundle*, 6-HB) deituriko egitura antiparaleloa sortuz, non FPa zelula mintzean txertaturik dagoen. Birusaren mintzean txertaketa, mintzetik gertu aurkitzen den MPER domeinuaren (ingelesetik, *Membrane Proximal External Region*) eta mintza zeharkatzen duen domeinuaren (TMD) bitartez ematen da (1.2 D irudia). Horrela, bi mintzak elkarrengana hurbiltzen dira, kanpoko bi lipido monogeruzen arteko fusioa gertatuz^{37,38}.

Ondoren, hemifusio bitartekaria hautsi eta fusio-poro bat eratzen da, 6-HB konformazioak erregulaturiko prozesua izanik (1.2 E irudia) ³⁹. Azken ezegonkortze urrats hauetan uste da MPER domeinuak funtsezko zeregina duela adabaki hidrofobiko txikiak eta mintzaren kurbaduraren estresa sorraraziz; jarduera hauek konposizio lipidikoak modulatu ditzakeelarik ⁴⁰⁻⁴³.

1.1.1.2 Birusaren mintza

Birus bilgarridunen lipidoek funtsezko eginkizuna dute birusaren infekzio zein morfogenesian. GIB-1ak zelula ostalariaren mintz plasmatikotik lortzen du bere lipido geruza, zeinetan erreplikazio zikloan Env proteinak txertatzen diren. Egitura proteina nagusia, Gag, mintz plasmatikora garraiatzen da eta nahikoa da birus ez-infekziosoak eratzeko. Birus infekziosoak sortzeko ostera, birusaren genoma, erreplikazio-entzimak eta gainazaleko glikoproteinak behar dira; guzti hauek Gag proteinak biltzen dituelarik ⁴⁴.

Pentsa zitekeen GIB-1ak infektatutako zelulen mintzetik eratorritako lipido geruza duenez, zelula ekoizlearen mintz plasmatikoaren antzeko osaera lipidikoa izatea. Hala ere, Aloia eta lankideek desberdintasunak antzeman zituzten GIB-1aren eta infektatutako zelularen mintzen konposizio lipidikoen artean. Ikerketa honen arabera, GIBaren mintza esfingolipidoetan eta kolesterolean (Chol) aberasturik egon ohi da eta ondorioz, honen jariakortasuna baxuagoa da infektatutako zelularekin alderatuta ^{45,46}.

Lipidoen masa espektrometrian egindako aurrerapenei esker, Aloia eta lankideek eginiko ikerketan ondorioztatutakoa berretsi ahal izan zen ⁴⁷. Hain zuzen, GIBaren partikulen lipidomaren analisi kuantitatiboak aditzera eman zuen mintzaren ordena sustatzen duten lipidoen, hala nola, esfingomielina (SM) eta Chol-a, GIBaren gainazalean metatzen direla, detergenteekiko erresistenteak diren mintz mikrodomeinuetan aurkitzen diren kontzentrazioetan hain zuzen. Chol-a da birusaren estalki lipidikoaren osagairik ugariena, lipido guztien ia % 50a izanik. Honekin bat etorri, GIBaren mintza oso ordenatua da ^{48,49}. Gainera, ikusi da GIBaren mintza zeramidetan, dihidroesfingomielinan (DHSM), aminofosfolipidoetan, fosfoetanolaminan eta fosfoinositidoetan aberasturik dagoela ^{47,50}. Fosfatidilserina (PS) eta fostadiletanolamina (PE) birioi helduen bigeruza lipidikoaren kanpo mintzean kokatzen dira batez ere ^{51,52}, ATP-menpekoak diren aminofosfolipido translokasek bultzatzen duten mintzean dagoen lipidoen banaketa asimetrikoaren galerarekin bat etorri.

Beraz, birusaren eta zelula mintzaren lipido konposizioan dagoen desberdintasun handiak eta honen konposizio bereziak, GIB-1aren gemazioa esfingolipido eta Chol-ean aberatsak diren nanodomeinuetatik ematen denaren hipotesia baieztatzen du⁵³⁻⁵⁵. Osaera lipidiko hau mantentzea garrantzi handikoa dela dirudi; izan ere, zelula ekoizleetan Chol-aren edo SM-aren sintesia inhibitzeak, edo Chol-a birus zein itzelulatik ezabatzeak, nabarmen murrizten du birusen ekoizpena eta hauen infektatzeko gaitasuna^{47,56,57}.

1.1.2. Gainazaleko glikoproteina (Env), txertoen garapenerako itua

GIB-1aren gainazalean eskuragarri dagoen proteina bakarra denez, Env espektro zabaleko antigorputz neutralizatzailen (ingelesetik, *bnAbs* edo *Broadly Neutralizing Antibodies*) itu bakarra da eta beraz, GIBaren aurkako txertoen garapenerako helburu nagusia⁵⁸. Hori dela eta, ahalegin handiak egin dira honen egitura eta funtzia aztertu eta ulertzeko. Aurretiaz aipatu moduan, Env mintza zeharkatzen duen proteina oligomerikoa da, 1 motako fusio-proteina biralen parte da eta hiru gp120 (gainazaleko azpiunitatea) eta hiru gp41 (transmintzeko azpiunitatea) azpiunitatez osatua dago, heterodimeroen trimero egonkor bat osatzen dutenak.

Env, erretikulu endoplasmaticoan (ER) sintetizatzen da gp160 aitzindari bezala. Bertan, itzulpen ondoko eraldaketa ugari pairatzen ditu; horien artean, disulfuro zubi kontserbakorren sorrera eta manosa ugari dituzten glikanoen gehikuntza²⁶. Aitzindaria jarraian, Golgi aparatura garaiatzen da, non itzulpen ondoko eraldaketa gehiago jasaten dituen, glikano konplexuen gehikuntza eta gp120 eta gp41 azpiunitateen proteolisia barne^{59,60}.

Gp120 azpiunitatea bi domeinu nagusitan tolesten da, kanpo eta barne domeinuetan alegia. Bost domeinu aldakorrak (V1-V5) beste bost domeinu konstanteekin (C1-C5) tartekatzen dira eta immunitate sistemari ikusgai gelditzen diren begizta aldakorrak eratzen dituzte. V1ek V2k eta V3k trimeroaren egonkortze domeinua osatzen dute mintzetik urrun gelditzen den espikularen goiko partean alboko gp120 protomeroekin elkarreraginez.

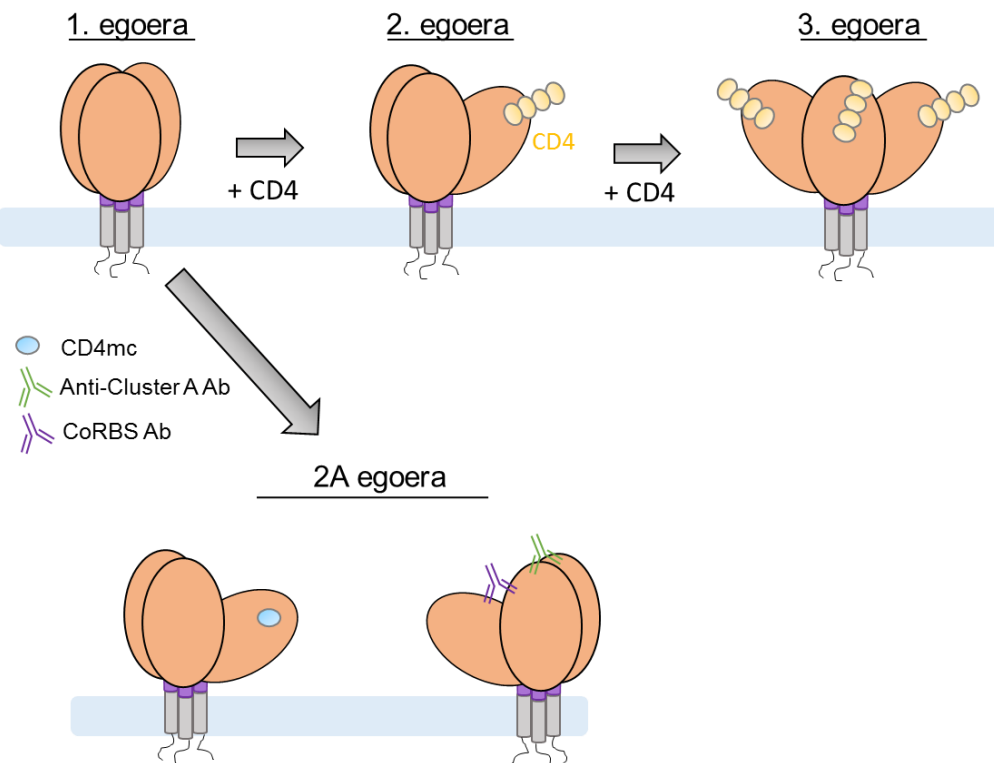
Env oso proteina ezegonkor eta dinamikoa denez, bere kristalizazioa eta estruktura atomikoaren zehaztapena errazteko, Env trimero mutatu edo ez-osoak erabili izan dira. Hasiera batean, gp120 nukleoa, V1-V2, V3 eta N muturreko eremua faltan zituela, bi

modutan kristalizatzea lortu zen: i) glikosilaziorik gabe eta CD4 amino muturreko bi domeinuekin eta 17b antigenoa batzen duen fragmentuarekin (Fab, ingelesetik *Fragment, antigen-binding*) konplexua eratuz^{61,62}, eta ii) guztiz glikosilatua eta inolako konplexurik eratu gabe⁶³. Ondoren, gp120 azpiunitatearen zenbait egitura atomiko ebatzi ziren, V3 begizta osorik zuena⁶⁴, N eta C muturreko luzapenekin⁶⁵ eta baita, elkarrekintzarik eratu gabe⁶⁶. Horrez gain, FP eta MPER domeinurik gabeko gp41 trimero disolbagarriaren egitura, fusio osteko konformazio egonkorrean, erresonantzia magnetiko nuklearraz (NMR) eta X-izpien kristalografiaz ebatzia izan zen⁶⁷⁻⁶⁹.

2013. urtean, lehen aldiz ebatzi zen Env trimero solugarriaren (SOSIP.664) egitura atomikoa kriomikroskopia elektronikoa (cryoEM) eta X-izpien kristalografia konbinatzu^{20,70}. Trimero hau, MPER, TMD eta isats zitoplasmatikoa (CT) faltan zituela eta anti-gp120 antigorputzekin lotuta ebatzi zen. SOSIP.664ren hasierako egituraren Env glikoproteinaren sekuentzia, A kladoaren BG505 anduitik eratorritakoa izan zen, egonkortzeko mutazio batzuk zituela: i) disulfuro zubi bat (SOS) sorrarazi zen gp120ren 501 eta gp41en 605 hondarren artean^{71,72}, ii) 559. posizioko isoleuzina proлина batez (IP) ordezkatu zen⁷³ eta iii) 664. hondarretik aurrerako sekuentzia ezabatu egin zen. Ostean, SOSIP egituraren ebazpena hobetza lortu da GIBaren aukako antigorputz desberdinei batuta^{74,75}. 2016. urtean ebatzi zen SOSIP mutaziorik gabeko bereizmen altuko lehen Env trimeroa⁷⁶. Kasu honetan, B kladoaren barnean sailkatzen den JR-LF andui basatia erabili zen, CTa faltan zuela eta PGT151 antigorputzari lotua⁷⁶.

1.1.2.1 Env-en malgutasuna, “arnasketa” prozesua

Aurretiaz aipatu bezala, GIB-1aren Env espikula oso proteina malgu eta dinamikoa da, eta berez igarotzen da konformazio itxi eta erlaxatuagoaren artean “arnasketa” deritzon prozesua jarraituz^{77,78} (1.3 irudia). Molekula-indibidualetan (ingelesetik, *single-molecule*) oinarritutako erresonantzia fluoreszentearen energia-transferentzia (smFRET) erabiliz eta analisi estrukturaletan oinarrituz, birioietan egindako esperimentuetatik ondorioztatutako emaitzek, irekiera maila desberdineko hurrengo lau konformazio desberdin definitu dituzte: 1, 2, 2A eta 3⁷⁹⁻⁸².



1.3 irudia. Env-en konformazio egoerak. Irudian, eskematikoki, GIB-1aren konformazio egoerak ageri dira. CD4 hartzaila lotu aurretik, orokorrean Env 1. egoeran, konformazio itxian ageri da. CD4rekin lotzean, Env partzialki eta asimetrikoki konformazio irekitik, 2A egoeratik, guztiz irekitako konformaziora, 3. egoerara, igarotzen da. 2A egoerak konformazio asimetrikoa eta partzialki irekia erakusten du, CD4mc anti-CoRBS eta antiCluster A antigorputzak eragin dezaketena. Irudia ⁸²-tik egokitua.

CD4rekin lotu aurretik, Env nagusiki konfigurazio itxian (“1. egoeran”) mantentzen da, non V1/V2 begiztak trimeroaren muturretik hurbil kokatzen diren. Egoera itxi honetan, Env-en dauden epitopoak konformazionalki izkutaturik daude, eta neurri handi batean antigorputzekiko erresistenteak dira ^{20,24,70}. CD4 hartzailarekin batzeak, “1. egoeratik” partzialki irekitako “2. egoerarako” trantsizioa eragiten du ⁸¹. Beste CD4 hartzailiekin lotzean, guztiz irekitako konformaziora aldatzen da Env, “3. egoerara” alegia. Azken egoera honetan, Env guztiz irekitako konformazioan egonik, CCR5/CXCR4 kohartzailleen arteko interakzioa baimentzen du, V3 begizta aldakorra guztiz agerian dagoelarik.

Bide honetatik kanpo, partzialki irekitako konformazio bat identifikatu berri da ⁸², CD4mc (ingelesetik *CD4 mimetic compounds*) eta antigorputzak sorrarazten dutena, “2A egoera” deiturikoa alegia. Konformazio honetan, Env-ek bitarteko konformazio asimetrikoa hartzen du, non protomero bakoitzak konformazio desberdinak hartzen dituzten.

“1. egoeran” agertzeko joera, dirudienez, GIB-1 azpitalde eta anduien menpekoa da. “Tier 1” edo lehenengo mailako birusek, neutralizazioarekiko sentikorragoak izanik, tarteko egoera irekiak hartzen dituzte nagusiki. Aldiz, 2. mailako (GIBaren andui zirkulatzaile gehienak) eta 3. mailako birusek, neutralizazioarekiko erresistenteagoak izanik, konformazio itxiak⁸³.

Trimeroaren irekiera iragankorrak, bnAb-en epitopo ezkutuak agerian uzten dituela dirudi, immunogenizitatea erregulatu daitekeelarik Env konformazio itxian izkutatuta dauden epitopoak agerian jarriz. Anti-MPER antigorputz askok adibidez, CD4rekin lotuta dagoen Env konformazio irekia (“3. egoera”), konformazio itxia baino eraginkorrago ezagutzen dute⁸⁴.

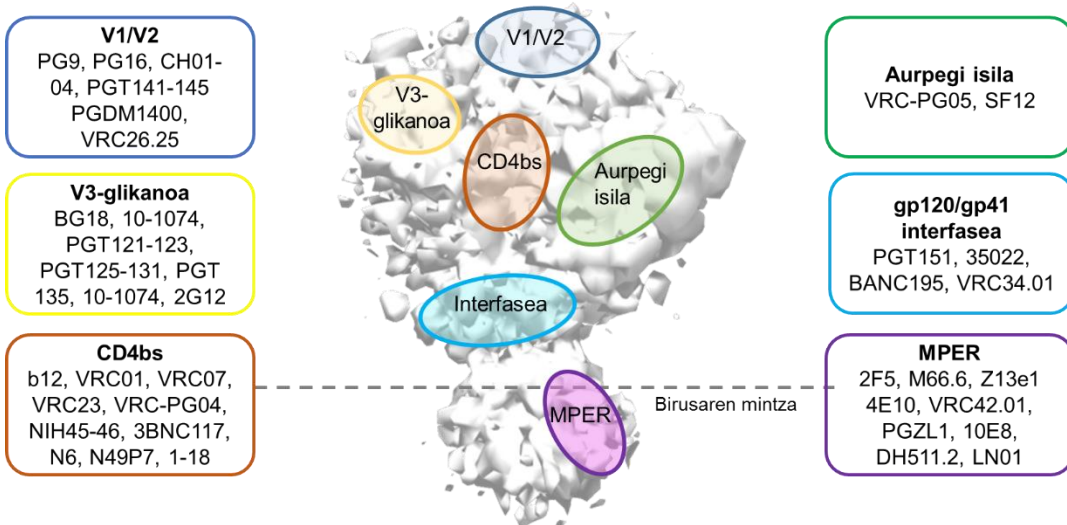
1.1.2.2 bnAb-ek ezagutzen dituzten gune zaurgarriak

Env-ek immunitate sistema saihesten du neutralizazioarekiko erresistenteark diren konformazioak bultzatzuz, non glikanoek azaleraren zatirik handiena estaltzen duten⁸⁵. Konformazio ezkutaketa honen ondorioz, Env-era zuzendutako antigorputz gehienak ez-neutralizatzailak dira. Hala eta guztiz ere, zenbait gaixok bnAb-ak garatzen dituzte, eta hauen isolamenduak, Env-en kontserbatutako gune zaurgarrien identifikazioa ahalbidetu du (1.4 irudia). Eskualde hauek, ezinbesteko funtzioka betetzen dituztela dirudi eta hurrengoak dira: V3 eta V1/V2 begiztez eta inguruko glikanoez osatutako guneak, CD4 hartzailaren lotura-gunea (CD4bs), MPER domeinua, gp41-gp120 monomeroen interfasea, FPa eta Env-aren aurpegi isila. Jarraian, hobekien karakterizatutako guneak deskribatuko dira.

V1/V2-ren gune apikalak, glikanoez eta begizta aldakorrez ezkutaturik dagoen^{86,87} epitopo glikopeptidikoa osatzen du. V1/V2ra bideratutako antigorputz espezifikoak, hala nola PG9 eta PG16, V1/V2 begiztaz eta 156 zein 160 posizioetan kokatzen diren glikanoez osaturiko epitopo kuaternarioa ezagutzen dute. Antigorputz horiek, kate astuneko osagarritasuna determinatzen duen eskualdea (CDRH3) begizta luze, zurrum, anionikoak erabiltzen dituzte glicosilazio zurruneko geruza trinkoan sartu ahal izateko⁸⁸.

V1/V2 eskualdearen antzera, V3-glikano gunea epitopo glikopeptidikoa osatzen du, CCR5 kohartzailearen batuketa guneaz eta inguruan dituen glikanoz osaturik baitago, batez ere manosa ugaridun adabaki kontserbakorrean parte hartzen duen N332 azukrea^{89,90}. Eskualde horretara zuzendutako bnAb-ak, PGT121 eta PGT128 kasu, CDRH3

begizta luzeak eta hurbiltze angelu desberdinak erabiltzen dituzte euren epitopoa gordetzen duen poltsiko kontserbakorrekin elkarrekintzak sortzeko^{89,91}.



1.4 irudia. bnAb-ek ezagutzen dituzten gune zaugarriak. V1/V2 gune apikala urdin ilunez, V3-glikanoa horiz, CD4bs-a laranjaz, gp120ren aurpegi isila berdez, gp120/g41 interfasea urdin argiz eta MPER morez. Gune bakoitzera zuzendutako bnAb esanguratsuenak kutxetan adierazi dira. (B kladoko GIB-1 JR-LF EnvCT, EM mapa EMD-3308).

CD4bs-a, funtzioko aldetik kontserbatua dagoen eta gp120 azpiunitatean glikanoez ezkutatutako gune zaugarria da. Eragozpen esterikoak medio, N49P bezalako, CD4bs-era bideratutako antigorputzek, epitopora hurbiltzeko angelu zehatzak behar izaten dute espektro zabala eta potentzia eskuratzeko^{92,93}. Eskualde honetara zuzendutako antigorputzak dira, espezifikotasun guztien artean, espektro eta potentziari dagokionez erlazio hoherena erakusten dutenak. Gune honek sekuentzia eta egitura heterogeneotasun handia erakusten badu ere, jakina da infekzio naturalean bnAb kopuru altuena eragiten duena dela⁹⁴.

Aurretiaz esan bezala, MPER eskualdea oso kontserbaturik dago eta fusio makinariaren osagai garrantzitsuenetako bat da. MPER domeinuari zuzendutako antigorputzak aurkitutakoen lehenengo artean daude, eta ondorioz, sakonki aztertuak izan dira. CDRH3 begizta luzeak erabiltzen dituzte mintzaren interfasean txertatutako aminoazidoen sekuentzia lineala ezagutzeko, eta badirudi zenbaitek, halaber, birusaren

mintzaren osagai lipidiko bat ere dutela euren epitopoan^{95,96}. Orokorean, oso espektro zabalekoak dira, baina neurriko potentzia izaten dute.

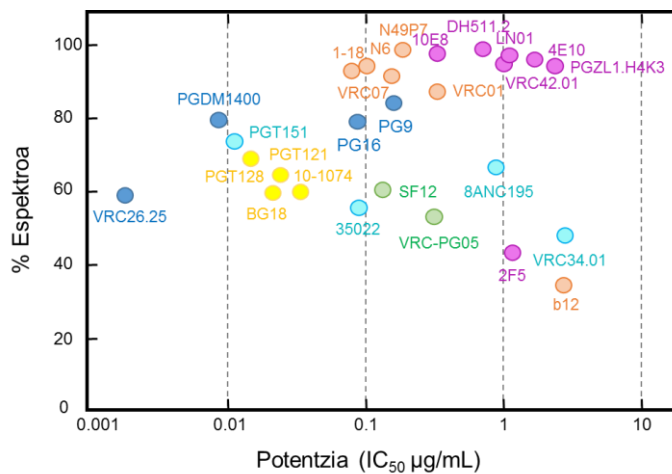
1.1.2.3 GIBaren aurkako bnAb-en aparteko ezaugarriak

GIB-1arekin infektatutako indibiduoen % 20-30 inguruk hainbat andui neutralizatzeko gai diren antigorputzak sor ditzakete infektatu eta hilabete batzuk igarotzerakoan^{97,98}; baina, soilik horien % 1ek, “elitezko neutralizatzalde” deiturikoek, garatzen ditu kaldo gehienen aurkako potentzia altuko aktibitatea duten antigorputzak⁹⁹. Hau da, bnAb-ak oso gutxitan garatzen dira prozesu naturalean eta horretarako, denbora luzez eta etengabe egon behar dute antigeno biralekin kontaktuan; horregatik, urteak igaro ondoren soilik sortzen dira⁹. Are gehiago, bnAb-ak modu pasiboan txertatuta, primateak eta gizatiartutako sanguak birusaren infekziotik babesteko gaitasuna dute^{100,101}. Gainera, horietako askok, arrakastaz egin dute aurrera gizakiekin egindako saiakuntza klinikoetan (ikus: <https://clink.gov/ct2/home>).

GIBaren aurkako bnAb-ak infekzio naturalean lortutako aparteko ezaugarri batzuk partekatzen dituzte. Lehenik, hipermutazio somatiko (ingelessez *Somatic Hypermutation*, edo SHM) maila altuak izan ohi dituzte, antigeno biral desberdinak etengabeko kontaktuaren eta heltze prozesuaren ondorioz sortuak^{10,11}. Horrez gain, bnAb-en arbasoetara jotzean, neutralizazio gaitasuna eta epitopoak batzeko espezifikotasuna murriztu eta askotan erabat galdu egiten dutela ikusi da¹⁰². Halaber, normalean ezohiko CDRH3 begizta luzeak izaten dituzte Env trimeroan sakon eta ezkutuan dauden epitopoetara heltzeko gaitasuna ematen dietenak¹⁰.

GIB-1aren aurka sortzen diren bnAb-etako batzuek, poli- edota auto-erreaktibitatea erakutsi dezakete^{103,104}. Antigorputz polierreatiboa, itxuraz zerikusirik ez duten antigeno edo autoantigeno bat baino gehiago ezagutzen dituzte. Autoerreatiboa, aldiz, autoantigeno bat edo batzuk batzen dituzte modu espezifikoan. Ezaugarri hau, B zelulen heltze prozesuan zehar lor daiteke; antigorputz poli- edota auto-erreaktiboa gehienak sistematik ezabatzen diren arren, horietako batzuk tolerantzia kontrol puntuak saihestea lortzen dute^{105,106}. CD4bs-a ezagutzen duten antigorputz batzuek, autoerreatibitate maila baxua izaten dute; adibidez b12 antigorputzak, CD4bs guneko bere epitopoa ezagutzeaz gain, erribonukleoproteina eta kate bikoitzeako DNA ere ezagutzen dute¹⁰⁷. MPER domeinuari zuzendutako zenbait antigorputzak, polierreatibitatea erakusten dute; 2F5 eta 4E10 antigorputzak adibidez, gp41ean kokatutako euren epitopoa ezagutzeaz gain, birusaren mintza ere ezagutzen dute¹⁰⁸.

BnAb-en existentziak berak frogatzen du B zelulek infekzio naturalean sortzen duten erantzuna gai dela GIB-1aren aurkako antigorputz neutralizatzailaileak sortzeko. Antigorputz hauen isolamenduak eta lotura-guneen identifikazioak, immunogenoen diseinu arrazionalerako oso baliagarria izan daitekeen informazioa eman ditzake. Gainera, antigorputz neutralizatzailleen epitopoien eta konformazio egoeren egitura eta funtzioko azterketek, aukera paregabea ematen dute antigorputz neutralizatzailaileak sorraziko dituzten txertoen diseinua burutzeko.



1.5 irudia. GIB-1aren aurkako bnAb-en konparaketa espektro vs potentzia grafikoaz. Pseudobirus saioen bitartez lortutako bnAb-en neutralizazioa, euren potentzia (antigorputz bakoitzak infekzioaren % 50a blokeatzeko beharrezko den kontzentrazioa, IC₅₀ balioa µg/mL-tan), espektroaren (panel handi bateko neutralizatutako birusen portzentaia) aurka irudikatuta. Erabilitako koloreak epitopoien espezifikotasunaren araberakoak dira, 1.4 irudian bezalaxe. Irudia, ¹⁰⁹ –tik egokitua.

1.2 ENV-EN OINARRITUTAKO IMMUNOGENOAK

Nahiz eta txertoen garapenerako metodo tradizionalek patogeno askoren aurka arrakasta handia izan duten, ez dira orain arte gai izan GIB-1aren aniztasun genetikoari aurre egiteko. Infekzio naturalaren prozesuan bnAb-ak sortzeak, baikortasuna sortzen du antigorputz hauek sorrazteko gai diren txerto eraginkorren garapenerako. BnAb horien isolamenduak, haien epitopoien identifikazioak eta Env konplexuko egituren karakterizazioak, funtsezko informazioa ematen dute immunogenoen diseinu arrazionalerako.

Env, birusaren gainazalean kokatzen den bnAb-en antigeno bakarra izanik, txertoen diseinurako itu ezin hobea da. Horrenbestez, ahalegin izugarriak egin dira txerto moduan erabili daitezkeen Env-en oinarritutako immunogenoak ekoizteko. Horien artean, SOSIP.664 trimeroa^{20,72,73,95} dago, antigenizitate profil bikaina duena; hau da, bnAb-ek modu eraginkorrean lotzen duten bitartean, antigorputz ez-neutralizatzaleek modu ahulagoan egiten dute⁷¹. Nabarmenzeko da Env-en oinarritutako lehen proteina txertoa izan zela “Tier 2” antigorputz neutralizatzairen autologoen erantzuna sortzen, animalia modeloetan eta primateetan, baina ez zen espektro zabaleko antigorputz neutralizatzairen erantzun esanguratsurik lortu¹¹⁰.

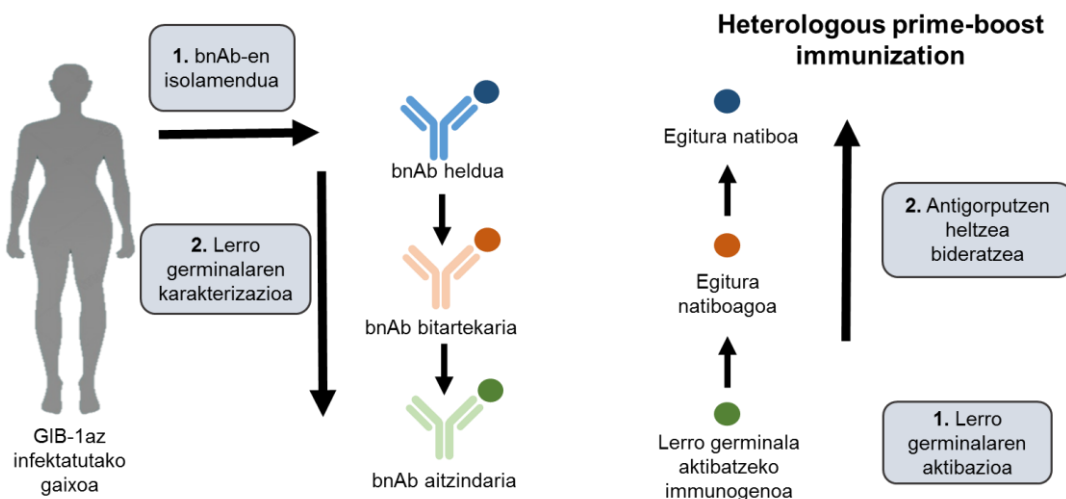
Env trimeroan oinarritutako zenbait immunogeno, 1. faseko saiakuntza klinikoetan daude, SOSIP.664 barne. Hala ere, animaliekin egindako zenbait ikerketen arabera, SOSIP-erako trimero natiboek “arnasketa” konformazionala dute, V3 begizta immunodominantearekin lotzeak adierazten duen moduan¹¹⁰⁻¹¹². Trimeroaren fusio aurreko konformazio itxia, orokorrean antigorputz neutralizatzaleek ezagutzen dutenez eta ez-neutralizatzaleek aldiz ez, zenbait saiakera burutu dira konformazio hau egonkortzeko helburuarekin¹¹³⁻¹¹⁵. Horietako bat, 4571 trimeroa da, DS-SOSIP bezala ere ezaguna. Trimero hau, egonkortu egin da eta V3 begiztaren esposizioa murriztu zaio C201-C433 disulfuro lotura gehituz¹¹⁶. Hala ere, DS-SOSIPekin egindako akurien immunizazioek, V3 begiztara zuzendutako antigorputzen erantzun maila SOSIP.664arekin lorturiko antzekoa izan zela iradokitzen dute, eta ez zen antigorputzen neutralizazio heterologorik hauteman¹¹⁷.

SOSIP-erako trimeroei buruzko beste kezka bat, andui espezifikoen immunodominantzia da; hau da, erantzun immunea batez ere, andui konkretu baten glikano zuloetara bideratuta egotea¹¹⁸⁻¹²⁰. Arazo hau gainditzeko, GIB-1aren M taldeko SOSIP.664 trimerotik eratorritako Env-en adostasun-sekuentzia bat garatu zen, ConM SOSIP.v7 deiturikoa¹²¹. Trimero honek, halaber, egonkortasun arazoak gainditzeko mutazio batzuk ere baditu. Dena dela, rhesus tximino eta untxietan egindako saio preklinikoetan ikusi da, SOSIP.v7k ez dituela 2. motako antigorputz neutralizatzailerik garatzen¹²¹.

SOSIP-erako trimeroez gain, fusio aurreko egoeran egonkortutako eta mozketa-independenteak dituzten trimeroak ere aztertu izan dira immunogeno moduan. Horien artean, Env espikularen imitazioak diren NFLak^{122,123} (ingelesetik *Cleavage-independent native flexibly linked*) eta UFO trimeroak¹²⁴ (ingelesetik *uncleaved prefusion optimized*) daude. Biek gp120 eta gp41 artean lokarri malgua dute, eta SOSIP-erako trimeroen antzera, proлина bat dute gp41eko 1. heptada errepi-korrean. Biek erakutsi dute birus

autologoak neutralizatzeko gai diren antigorputzen bidezko erantzunak sortzeko gai direla^{125,126}. C.6980 gp145 trimeroa da, fusio aurreko egitura egonkortzeko mutaziorik ez duen eta saio klinikoen 1. fasean dagoen Env trimero bakarra. Gainera, gp145 trimeroak, ukitu gabeko MPER domeinu osoa dauka, polilisina isats batera loturik dagoena. Bukatzeko, zenbait gp145 trimero erabili izan dira untxiak immunizatzeko, baina soilik 1. motako birusak neutralizatzeko gai ziren erantzunak lortu dira¹²⁷. Laburbilduz, Env trimeroa imitatzen duten immunogeno hauek egitura aldetik egonkorra diren arren, ez dute espektro zabaleko erantzun neutralizatzailerik eragitea lortu.

Azkenik, bnAb-en eta hauen epitopoen egituraren eta sekuentziaren informazioa konbinatuz, B zelula germinalak aktibatzeko gai diren Env-en oinarritutako immunogenoen diseinua garatzea lortu da¹²⁸. Antigorputzen heltze prozesua bideratzen duten antigenoen bitartekari garrantzitsuenak ezagutzeaz gain, garatzen ari den antigorputzaren leinuko bitartekari zein aitzindariak (lerro germinalean kodetzen diren aldaerak, “mutatu gabeko arbaso komuna” edo UCA) isolatza (edo inferitza) eta karakterizatzaezinbestekoa da txerto hauek diseinatzeko. Helburu hau lortu ahal izateko, GIB-1az kutsatutako pazienteen segimendua infekzioaren etapa oso goztiarretatik egin beharko litzateke, espektro zabaleko erantzun neutralizatzailera iritsi arte¹²⁹⁻¹³¹. Hala ere, bnAb-en mutazio tasa altuak eta heltze prozesu luzeak, mota honetako immunogenoen diseinua oso lan neketsua bihurtzen dute. Are gehiago, zenbait kasutan, bnAb batzuen UCA gai da Env-en aldaera goiztiarrak batu zein neutralizatzeko; beste askotan ordea, ez dute neutralizatzeko gaitasunik, eta ez dira gai Env molekularen aldaera gehienak ezagutzeko¹³²⁻¹³⁴. Hori dela eta, bnAb baten leinu espezifiko bat aktibatzeko gai izango den immunogenoa, Env trimeroarekin alderatuta, oso desberdina izan daiteke da eta sarritan, hainbat immunogeno desberdin beharko dira bnAb-en heltze prozesua bideratzeko¹³⁵.



1.6 irudia. “Egituran oinarritutako” immunizazio estrategia. Gaixoetatik isolatutako bnAb-ek Env trimeroetan kokatzen diren txertoen ituak definitzten dituzte (urdinez). Inferitutako bnAb-en aitzindariekin (berdez) ez dituzte orokorrean trimero natiboak lotzen, lerro germinalaren aktibaziorako immunogenoen diseinua ezinbestekoa delarik. BnAb-en heltze prozesua gidatzeko, baliteke immunogeno desberdinak behar izatea, epitopo natiboen antza sekuentzialki handituz joango direnak. Antigorputzen bitartez balioztatu daitezke immunogeno hauek. Irudia ¹³⁶-tik egokitua.

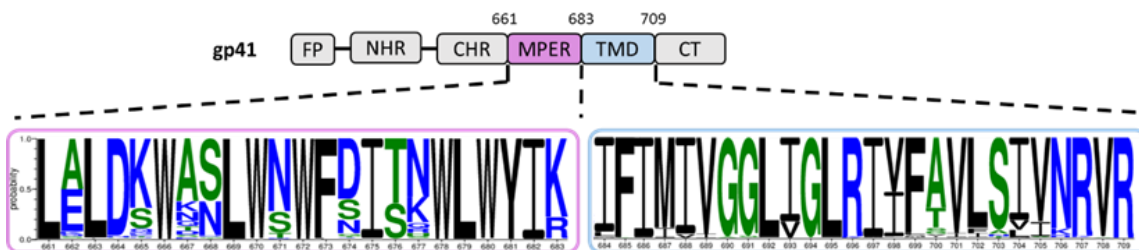
Estrategia hau jarraituz txertaketa eraginkorra izan dadin, hainbat Env desberdinez buruturiko immunizazio sekuentzia beharko litzateke B zelula aitzindarien heltze prozesua espektro zabaleko bnAb-etara bideratzeko. Beraz, *prime-boost* txertaketa heterologoa estrategia ezin hobea izango litzateke; hau da, sistema immunea immunogeno batekin piztea eta erantzuna beste batekin edo batzuekin estimulatzea. Lehenbiziko immunizazioak (*prime*), bnAb espezifikoen B zelula aitzindarien aktibazioa eta proliferazioa eragingo luke; eta hurrengo immunogenoek (*boost*) bnAb-en heltze prozesua gidatuko lukete. *Boost*-erako immunogenoak jatorrizko Env trimeroen antza handiagoa izango lukete, SOSIP-erakoak adibidez izan daitezke, edo soilik eskualde zaurgarri batean oinarritutako immunogenoak ere (1.6 irudia). Estrategia honek immunodominantzia arazoak gainditu beharko lituzke, soilik beharrezkoak diren egitura-osagaietara erantzuna zuzenduz ¹³⁶.

Lerro germinalera zuzendutako (GT, ingelesetik *germline targeting*) bi immunogeno 1. faseko saiakera klinikoetan daude gaur egun: eOD-GT8 60mer eta BG505 SOSIP GT1.1 gp140 trimeroa. eOD-GT aldagaia, inferitutako VRC01 motako antigorputz germinalak afinitate handiz lotzeko diseinatu ziren ^{133,137}. eOD-GT8 zehazki, CD4bs-a aurkezten duen immunogenoa da, kanpoaldean VRC01 motako B zelula aitzindariak espezifikoki pizteko domeinua duena ^{137,138}. Animalia modeloetan lortutako emaitzek

eraginkortasuna erakusten zutenez, eOD-GT8 saiakera klinikoetan sartzea lortu zuen, non, nanopartikula hauek gai izan ziren VRC01 motako B zelula aitzindarien erantzuna pizteko. eOD-GT8 60mer immunogenoa erabili zen 1. faseko saiakuntza klinikoko hasierako datuek, erakutsi zuten VRC01 moduko B zelula aitzindarien aktibazio indartsua ematen zela. Saiakuntza klinikoko 1. fasean dagoen bigarren GT immunogenoa, BG505 SOSIP.664 trimeroan oinarritutako Env trimero bat da, erantzuna CD4bs eta V1/V2ra zuzentzeko GT mutazio batzuk dituena. BG505 SOSIP GT1.1 trimeroarekin immunizatutako suguak, CD4bs-era zuzendutako antigorputzak garatzea lortu zuten, BG505 SOSIP trimeroarekin lortu ez zena alegia¹³⁹.

Laburbilduz, GIBaren aukako txerto eraginkor baten garapena oso urrutti badago ere, Env-en oinarritutako zenbait hautagai berri ikertzen ari dira eta azkenaldian, immunogenoen diseinurako teknika eta ikuspegi berriak sortu dira. Beraz, kontuan hartzekoa da azken urteotan egin diren aurrerakuntzak txertaketa-estategietan eta bnAb-en analisian, GIBaren aurkako txertoaren garapena eskuragarriago egotea ahalbidetu dutela.

1.3 MPER EPITOPOA



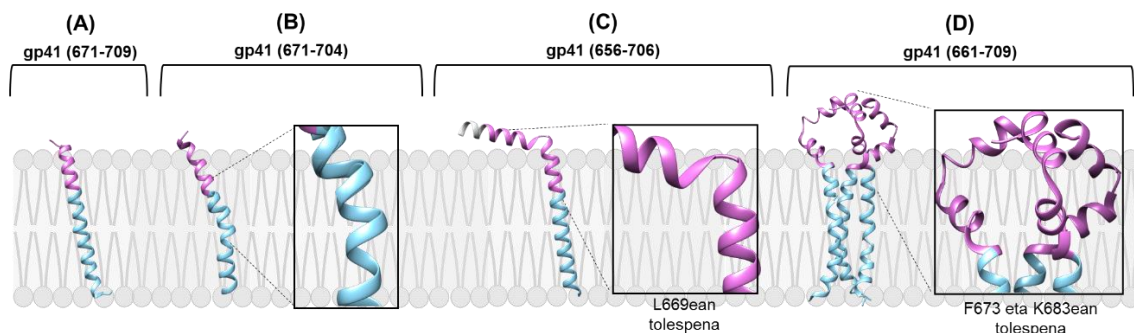
1.7 irudia. MPER-TMD domeinuko sekuentziaren kontserbazioa. GIB/SIV azpimota guztien MPER-TMDaren kontserbazio-maila, *Los Alamos National Laboratory* databasean eskuragarri dagoena. Sinbolo bakoitzaren altuerak, kokapen zehatz horretan aminoazido bakoitzak duen maiztasun erlatiboa adierazten du, eta sinboloen koloreak hidrofobizitatearen araberakoak dira: hidrofilikoak (urdinez), neutroak (berdez) eta hidrofobikoak (beltzez). MPER epitopoa osatzen duten hondarrak laukizuzen arrosaren barruan irudikatu dira, eta TMDaren sekuentzia laukizuzen urdinaren barruan.

MPER, 24 aminoazido (662-683 hondarrak) dituen triptofanoetan aberatsa den eskualde hidrofobikoa da, zeinak gp41 ektodomeinua transmintz domeinuarekin konektatzen duen¹⁴⁰ (1.7 irudia). Oso kontserbatua dagoen eskualde hau, gune zaurgarrien artean epitopo lineal bakar gisa identifikatu da^{141,142}. Horrez gain, infekzio naturalean sortzen diren espektro zabaleko zenbait antigorputz neutralizatzileen itua da; besteak beste, 2F5¹⁴³, 4E10¹⁴⁴, 10E8¹², DH511.2¹⁴⁵ eta LN01¹⁴⁶. MPER eremuuan egindako mutazio eta delezioek, domeinu honek birusaren infekzio gaitasunean eta fusio prozesuan duen garrantzia zehaztu dute^{140,147,148}. MPER eskualdearen topologia, mintzaren testuinguruaren araberakoa da; hala, Chol eta SM bezalako mintz lipidoak gai dira MPERak mintzak ezegonkortzeko duen gaitasuna modulatzeko^{149,150}. MPERan kokatzen den eta triptofanoetan aberatsa den gune hidrofobikoa da mintzarekin elkarreragiten duena eta ondorioz, mintza ezegonkortzeko gaitasuna duena^{151,152}.

Ezaugarri hauek guztiak MPER domeinua GIB-1aren aurkako txerto baten itu egokia bilakatzen duten arren, orain arte egin diren saiakera gutxiek potentzia baxuko eta espektro mugatuko antigorputzen ekoizpena soilik eragin dute¹⁵³⁻¹⁵⁶.

1.3.1. MPERen aldakortasun konformazionala

Mintzen arteko fusioan duen funtsezko zeregin dela eta, MPER oso eskualde dinamiko da eta fusio prozesuan zehar gerta daitezkeen konformazio aldaketak jasateko egokitua dago. Ondorioz, nahiz eta Env-en inguruko hainbat ikerketa funtzional eta egiturazkoak egin diren, fusio aurreko MPER domeinuaren egitura atomiko zehatza ezezaguna da oraindik. Lehen aipatu den moduan, SOSIP.664 trimero disolbagarria egonkortzeko, beste aldaketa batzuen artean, 664 hondarraren osteko MPER domeinu hidrofobikoa ezabatu zen. Hori dela eta, hondar honetatik haratagoko gunearren informazio estruktural atomikoa falta da kristalizatutako egitura horretan. Are gehiago, Lee eta lankideek⁷⁶ ebatzitako cryo-EM egituraren zoritzarrez, nahiz eta soilik domeinu zitoplasmatikoa faltan egon, MPER-TMD domeinuaren sekuentzia mizeletan integratua badago ere, desordenatuta ageri da eta ondorioz ez dago erabat ebatzita. Rantalainen eta lankideek¹⁵⁷ MPERen ezegonkortasun, malgutasun eta agregazio arazoak neurri batean konpontzea lortu zituzten Env, lipido bizeletan ainguratuz eta antigorputzen bidez egonkortuz. Mintz lipidikoetan txertatutako Env-Antigorputz konplexua, cryo-EM bitartez aztertu zen eta lortutako emaitzek Env-en malgutasuna islatu zuten, MPER domeinura zuzendutako antigorputzek Env inklinatzen zutela frogatuz. Kasu honetan ere ez zen MPER eta TMD domeinuen egitura atomikoa ebazterik lortu.



1.8 irudia. MPER-TMD domeinuaren hiru dimentsioko egitura lipido bigeruzetan. MPER-TMD domeinurako proposatu izan diren egitura desberdinaren irudikapena, MPER (661-683 hondarrak) arrosaz eta TMD (684-709 hondarrak) urdinez, 1.7 irudian bezalaxe. **A)** Helize jarraien modeloak. **B)** TMD domeinuko N-muturrearen tolespena duen eredua. **C)** MPER domeinuko N-muturrean helizearen tolespena duen eredua. **D)** Bi tolespen dituen trimero egituraren eredua. PDB kodeak hurrengoak dira: 6SNE (A), 2MG2 (671-693 hondarrak) eta 2MG1ren (671-693 hondarrak) gainjartzea (B), 7AEJ (C) eta 6E8W (D). Egiturak Chimera programa erabiliz irudikatu dira¹⁵⁸.

Eskualde hauen egitura xehetasunak, MPER eta TMD peptido isolatuetatik lortu dira, baldintza desberdinak erabiliz eta erresonantzia magnetiko nuklearra (RMN), X izpien kristalografia eta cryo-EM tekniken bitartez. Lan gehienetan arabera, MPER-TMD eskualdeak ongi definitutako konformazio α -helikoidala hartzeko joera du, baina topologia zein egoera oligomeriko desberdinak.

Lehenengo egitura modeloak, etenik gabeko helize inklinatu bat bezala deskribatzen du MPER-TMD eskualdea, zeinetan TMDa mintzean zehar zabalduko litzateke, MPER mintzaren gainazalean geldituko litzatekeen bitartean (1.8 A irudia). Zenbait taldek berresten duten modeloak da, baina peptidoak hartzen duen egoera oligomeriko desberdinak deskribatu izan dira. Alde batetik, zenbait taldek, NMR bitartez, peptidoak DPC mizeletan txertatuta¹⁵⁹ eta lipido ingurune batean, antigorputz batekin konplexua eratzen^{146,157}, MPERek egitura monomerikoa duela deskribatu dute. Bestalde, Dev eta lankideek, peptidoa bigeruza lipidikoa imitatzen duen bizeletan, trimeroa eratzen duela frogatu dute¹⁶⁰.

Bigarren egitura modeloaren arabera, MPER eta TMD domeinuaren arteko loturatik gertu helizea tolestuko litzateke (1.8 B irudia). NMRz, DPC mizeletan egindako ikerketa batean ikusi zen MPER domeinua mintzean inklinaturik kokatuko litzatekela 690. hondarrean tolestu arte¹⁶¹. Kwonek eta lankideek aldiz, Chol-dun bigeruza lipidikoan 683. hondarrean ikusi zuten tolespena, baita NMR bitartez¹⁶².

Hurrengo modeloaren arabera, helizea MPER domeinuaren N muturrean tolestuko litzateke, K665 eta N671 hondarren artean zehazki (1.8 C irudia). Berriki eginiko ikerketa batean, gp41en FP-TMD domeinua 2H10 antigorputzari lotuta ebatzi zen¹⁶³. Egitura honetan, MPER domeinuaren helizea L669 hondarrean eteten zen. Helizearen etetea eskualde berdinean zuten MPERen egiturak ebatzi ziren mintz lipidikoetan^{164,165} eta 10E8 bnAb-arekin lotuta¹².

Azkeneko egitura modeloaren arabera, MPERek L formako egitura metaegonkorra hartuko luke (1.8 D irudia); hau da, MPER kurba malgu baina itxi batez loturiko bi helizetan banatuko litzateke, non hondar hidrofobikoak mintz biralean ezkutaturik egongo liratekeen, immunitate sistemaz babestuta^{164,166,167}. Fu eta lankideek NMRz ebatzitako trimeroan, lehenengo helizea K665-N671 hondarrek osatuko lukete, eta karboxilo muturreko helizea, 683. posizioan tolestuko litzateke, TMDaren *coiled-coil* egiturarekin konektatzeko¹⁶⁸.

Ikerketa desberdinatan proposatutako egitura modeloen anitzasun hau, posizio desberdin eta ez-natiboetan etenda dauden peptidoen erabileraren, hauen luzera desberdintasunaren edota horietako bakoitzean mintza imitatzeko erabilitako lipido motaren ondorioa izan daiteke. Halaber, hainbat egitura desberdin aurkitzeak, MPER-TMD eskualdearen malgutasuna islatzen du; hain zuzen, birus eta zelularen arteko fusio prozesuaren zenbait urratsetan garrantzitsua izan daitekeena.

1.3.2. MPER domeinura zuzendutako bnAb-ak

Infektatutako indibiduoetako isolatutako MPER domeinuaren aurkako antigorputzak dira gizakion immunitate sistemak, GIBaren aurkako neutralizatzileak diren erantzun espezifikoak sortzeko gai dela frogatzen duten ebidentziarik sendoena. Azpimarragarria da gainera, MPERen aurkako bnAb-ak modu pasiboan administratuta, birusaren infekzioaren aurkako babesa ematen dutela primateetan¹⁶⁹ eta neutralizazio erantzuna handitzen dutela gizakiotan^{170,171}. Ezaggarri hauek, eskualde honek txertoen diseinurako duen potentziala azpimarratzen dute.

Lehenbizi isolatu ziren GIBaren aurkako bnAb-en artean, MPERera zuzendutako 2F5 eta 4E10 antigorputzak daude. 2F5k MPER domeinuko N muturrak osatzen duen azpieskualdea du helburu eta ez du oso espektro zabala aurkezten¹⁴³. 4E10k aldiz, triptofanoetan oso aberatsa den C muturra ezagutzen du, GIB-1aren aurkako bnAb guztien artean espektrorik zabalenetarikoa erakutsiz¹⁴⁴ (1.5 irudia ikusi).

2012. urtean 10E8a isolatu izanak, txertoen garapenerako MPER eskualdearekiko interesa piztu zuen. BnAb honen epitopoa, MPER eskualdearen C muturrean kokatzen da eta 4E10 zein 2F5k baino potentzia altuagoa eta espektro zabalagoa erakusten du¹². MPER domeinuaren C-muturrera zuzendutako hiru antigorputz berri aurkitu dira duela gutxi: VRC42, PGZL1 eta LN01^{146,172,173}.

Oro har esan daiteke, MPER domeinuaren N muturrera zuzendutako antigorputzek (2F5, Z13e1 eta M66.6) ez dutela oso espektro zabala aurkezten, C-muturrari zuzendutakoek berriz (4E10, 10E8, DH511.2, VRC42, LN01 eta PGZL1), GIB-1aren aurkako bnAb guztien artean, CD4bs-era zuzendutako antzera, espektrorik zabalena erakusten dute (1.5 irudia).

MPER, Env ektodomeinuaz birioiaren gainazalean esterikoki ezkutaturik dago, bere eskuragarritasuna murriztuz, antigorputzen iristea oztopatzetik eta eskualdearen immunogenizitatea murriztuz. Anti-MPER antigorputzek beraz, zenbait ezaugarri garatu dituzte eragozpen esterikoak gainditzeko eta mintzean kokatzen den euren epitopoa ezagutzeko. 2F5 eta 4E10 antigorputzen eta gp41-lipido konplexuaren arteko batuketa, bi pausutako prozesu sekuentzial gisa deskribatua izan da¹⁷⁴. Antigorputzak Env glikoproteinarekin eta lipidoekin dituen lehenbikiko kontaktuak, Env-en inklinazioa eragiten dute eta honekin batera, MPER mintzetik apur bat ateratzea lortzen da bere esposizioa handituz. Hasierako urrats hau, MPER aldi baterako ikusgai bihurtzen du, antigorputzaren bidezko ezagupena faboratuz.

Jatorria edozein izanda ere, anti-MPER antigorputzek afinitatea lortzeko heltze prozesu luzeak jasaten dituzte. Hori dela eta, mutazio tasa altuak izaten dituzte eta baita ezohiko CDRH3 begizta luze eta hidrofobikoak^{12,175}. Antigorputz hauek, epitopoari batu ondoren, euren CDRH3 begiztak birusaren mintz lipidikoarekin elkar eragiten dute; nabarmenki, elkarrekintza hau funtsezkoa dirudi antigorputzen neutralizazio mekanismorako¹⁷⁶⁻¹⁷⁸. Poli- edota auto-erreaktibitatea erakutsi dezakete ere zenbait anti-MPER antigorputzek^{176,179}. Bereziki, 2F5, 4E10, VRC42.N1 eta PGZL1 bnAb-ek, mintzakin interakzio ez-espezifikoak izan ohi dituzte, konkretuki, karga negatibodun zenbait lipido propiori lotzen zaizkie^{103,172,173,180}. 10E8, LN01, eta DH511.2 bnAb-ek ordea, ez dute mintzarekin lotura ez-espezifiko esanguratsurik erakusten; baina datu deigarria da, hain zuzen antigorputz hauek direla aurreneko taldearekin alderatuz, neutralizazio potentzia altuena erakusten dutenak. Honen arabera beraz, poli- edota auto-erreaktibitatea ez da MPERari zuzendutako antigorputz guztien ezinbesteko ezaugarria.

1.3.2.1 TMDa eta mintz-lipidoak MPER epitopoaren osagai gisa

Kristalografia eta cryo-EM erabiliz lortutako MPER-Fab konplexu askoren egitura atomikoak lipidoekin ebatzi izan dira^{76,96,146,157,172,173,181}, MPER epitopoaren eta lipido ezagupenaren inguruko xehetasun baliotsuak emanet.

Aurretiaz aipaturiko ohiz kanpoko CDRH3 begizta luze eta hidrofobikoa, epitopoarekin lotzeko garrantzitsua da; baina, begizta hidrofobikoenak ere, zuzenean elkarrekiten dute mintzaren lipidoekin^{180,182}. Aipatzeko da adibidez, 4E10 bnAb-aren CDRH3 eta CDRH1 begiztek interakzio espezifiko zuzena dutela glizerol fosfatoarekin, azido fosfatidikoarekin eta fosfatidil glizerolarekin⁹⁶. Horrez gain, espontaneoki mintzei batzeko gaitasunik ez duten anti-MPER antigorputzek ere (10E8 kasu), lipidoekin elkarrekiteko edo hauei egokitzenko “poltsikoak” garatu dituzte, zeinak gai diren mintz birala osatzen duten fosfolipidoen buru polarrekin elkarrekintza ez-espezifikoak ezartzeko^{96,178,181}.

Birusen TMDa, soilik mintzaren ainguraketan parte hartzen duela uste izan bada ere, osagai lipidikoaz gain, MPER epitopoaren funtsezko elementua dela ikusi da. GIB-1aren TMDa gainera, mintzeko ohiko ainguraketak baino kontserbatuago dagoela ikusi da¹⁶⁰. Eskualde honen erdialdean kokatzen den kontserbatutako eta positiboki kargatutako R696 hondarra egoteak, soilik mintzaren ainguraketa baino funtziogarrantzitsuagoak iradokitzentzu ditu¹⁶⁰. Uste da hondar honek, mintzen arteko fusio prozesuan, gp41 azpiunitateak jasaten dituen aldaketa konformativaletan, transmintz domeinuaren posizio inklinatua egonkortzen duela^{183,184}. Zenbait ikerketen bitartez ikusi izan da TMDan egindako trunkazioek eta mutazioek mintzen arteko fusioan eta birusaren infektatzeko gaitasunean eragina dutela¹⁸⁵⁻¹⁸⁷, prozesu horietan eskualde honek duen garrantzia nabarmenduz. Gainera, eginiko mutazio eta trunkazio horiek, espikularen nukleo hidrofilikoan aldaketak eragiten dituzte, Env-ekiko antigorputzen sentikortasunean eraginez eta baita TMDaren zenbait funtziotz determinatuz: ainguraketa, egonkortzea eta espikula osoaren egitura zein antigenizitatearen modulazioa. Beraz, GIB-1aren immunogenoen diseinurako, TMD eskualdea funtsezko osagaitzat hartu behar dela dirudi¹⁶⁰. Are gehiago, TMDaren presentziak eragin nabarmena du anti-MPER antigorputzek epitopoarekin duten ezagupen espezifikoan, bereziki, 10E8 eta DH511.2 antigorputzen kasuan^{178,188}.

Hori horrela izanda, transmintz domeinuaren hondarrek zein mintzeko lipidoek MPERera zuzendutako bnAb-en epitopoa osatzen dutela dirudi. Bi osagaiek, MPER-TMD egituraren konfigurazioan eta epitopoaren esposizioan parte hartzen dute, MPERen

egitura natiboa sustatuz. Halaber, mintz lipidoek immunogenizitatea areagotu ditzaketela frogatu da^{189,190}. Guzi hau kontuan hartuta, mintz ingurunea kontserbatzea eta transmintzeko hondarrak gehitza oinarrizkoa da MPER eremuan oinarritutako immunogenoen diseinurako.

1.3.3. MPER domeinuan oinarritutako txertoen saiakerak

MPER domeinuak dituen zenbait ezaugarri immunologiko, fisiko zein estrukturalek zuzenean eragiten dute bere immunogenizitatean; ezaugarri horien artean, gp120 azpiunitateak ezartzen dion ezkutaketa esterikoa, birusaren mintza eta bere hidrofobizitate altua daude. Ondorioz, MPER, soilik fusio prozesua aktibatu ostean aldi baterako ikusgai dagoela uste da, eta hala, B zelulen irisgarritasuna oso murriztuta dago. Hala eta guztiz ere, GIB-1ak eragiten duen infekzio naturalean, antigorputzen bidezko erantzun indartsua sortzen da domeinu honen aurka. Hori dela eta, nahiz eta MPER immunogeno bikaina izan, erakusten dituen zenbait ezaugarrien ondorioz, erronka handia suposatzen du GIB-1aren aurkako txertoen garapenerako itu moduan erabiltzeak.

MPERean oinarritutako txertoen garapenerako lehen saiakerak hurrengoak izan ziren: MPER epitopoa birus kimerikoetan sartzea, fusio-proteina moduan erabiltzea eta peptido txertoak garatzea¹⁹¹. Baino, saiakera guzti hauetan, immunizatutako animalietatik, soilik neutralizatzailak ez ziren MPERera zuzendutako antigorputz espezifikoak berreskuratu ziren. Fusio-proteinei dagokienez, adibidez, Hepatitis B birusaren S1 proteina MPERarekin fusionatuta erabili zen sagu eta untxiak immunizatzeko¹⁵³, baina ez zen aktibitate neutralizatzailerik berreskuratu animalien seroan. S1 proteinak nanopartikulak eratzeko gaitasuna duenez, antigorputzak hobeto elkartzeko MPERak behar duen ingurune lipidikoa ematen dio. Txerto peptidikoei dagokienez, 2F5 antigorputzaren epitopoa, toxoide tetanikoa moduko eramaile batekin konbinatu zen immunogeno moduan saguetan erabiltzeko, erantzun immune ez-neutralizatzailak eraginez¹⁹². Ikerketa horretan erabilitako sekuentzia bera, behi-gazur albuminarekin (BSA, ingelesetik *Bovine Serum Albumin*)¹⁹³ eta T linfozito laguntzaileen epitopoarekin¹⁹⁴ konbinatu ziren antzeko erantzun immuneak lortuz.

Anti-MPER bnAb-ek mintzarekin elkar eragiten dutenez, mintza imitatzen duten modeloak erabili izan dira domeinu honetan oinarrituriko txertoen garapenerako; horien artean, birusak imitatzen dituzten partikulak (VLP, ingelesetik *viral like particles*) eta

liposomak. Zenbait ikerketetan, MPER epitopoa N-muturretil moztuta, VLPetan txertatu zen eta saguak zein untxiak immunizatu ziren; berriz ere erantzun immune neutralizatzailerik lortu gabe^{154,195}.

MPER domeinura zuzendutako txertoen garapenerako, liposomen erabileraren lehen saiakeretako batean, MPER peptido sintetikoa, fosfatidil inositol-4-fosfatoarekin (PIP) (lipido antigenoa) eta A lipidoarekin (adjudantea) batera erabili zen saguak immunizatzeko¹⁵⁵. Sagu hauen serotik, MPERekiko espezifikoak ziren eta baita lipidoak batzen zituzten bi IgM antigorputz monoklonal isolatu ziren, neutralizazio ahalmen ahula erakutsi zutenak. Jarraian, formulazio antzekoarekin immunizatutako saguetatik, antigorputz monoklonal berri bat isolatu zen, MPERekiko espezifiko eta GIB-1aren klado desberdinak neutralizatzeko gaitasuna zuena¹⁹⁶.

MPER domeinura zuzendutako beste txerto hautagai bat, MPER-656 liposoma txertoa da, MPER peptidoa (656-680 hondarrak) liposometan ainguraturik duena¹⁹⁷. Rhesus tximinoetan eta akurietan egindako immunogenizazio saioetan ikusi zen MPERekiko espezifikoak ziren antigorputzak sortzen zirela, baina ez 2F5 bnAb-en antzerakoak. Hala ere, gp140 proteina oligomerikoa, lehenbizi sistema immunea pizteko erabiliz eta jarraian, MPER-656 liposoma txertoaz immunizatz, 2F5 motako erantzun immunea lortzen zela ikusi zen¹⁵⁶. Ikerketa honen jarraipenean, gp140 proteina adierazten duen *vaccinia* birusa, gp140 proteina birkonbinatua, MPER-656 liposoma txertoa eta TLR agonista adjubantetzat erabili ziren. Zoritzarrez, ez zen seroan lipidoen aurkako erantzunik aurkitu, ezta neutralizazio jarduerarik ere. Dena den, erabilitako immunizazio estrategia erabilgarria zela balioztatu zuten; hau da, Env-ekin sistema immunea piztea eta MPER duten liposomekin immunizazioa bultzatzea erabilgarria izan daitekeela ikusi zen. Are gehiago, B zelulen klon espezifikoak aktibatu, proliferatu eta heltzeko bulkada edo immunizazio gehigarriak erabakigarriak direla ikusi zen. MPER-656 liposoma gizakietan ebaluatu izan da HVTN 133 deituriko 1. faseko saiakera klinikoan. Fase hau berriki amaitu da, baina ez dago oraindik argitaratutako emaitzarik (<https://clinicaltest.gov/ct2/show/NCT03934541>).

1.4 HELBURU NAGUSIAK

Sekuentziaren kontserbazio maila altuak eta infekzio naturalean sortzen diren bnAb-en identifikazioak, 10E8 kasu, MPER-TMD eskualdearen interesa nabarmen handitu da GIB-1aren aurkako txertoen garapenerako itu gisa. Zenbait saiakera egin dira MPERera zuzendutako txertoak garatzeko, baina anti-MPER bnAb-en titulu altuen indukzioak huts egun du orain arte. Txertoek arrakasta ez izatearen arrazoietariko bat, bnAb-en indukzioa eragiten duen MPERaren egitura, oraindik ebatzia ez egotea izan daiteke. Fusio prozesuan zehar gp41 azpiunitateak izugarritzko konformazio aldaketa handiak pairatzen ditu, sistema immunea MPERaren konformazio askorekin kontaktuan egotea eragiten duena, MPER-Fab konplexuen kristal egitura anizkoitzetan ikus daitekeen bezala. Beraz, eskualde honen malgutasunak eta antigorputz neutralizatzaileak eragiten dituen konformazio zehatz ezezagunak, domeinu honetan oinarritutako immunogenoen diseinua zaildu egiten dute. Bestalde, mintzaren antzeko lipido ingurunean MPER eskualdearen konformazio egokia lortzeko sakon aztertu beharko litzateke lipidoek domeinu honen egituraren konfigurazioan, zein immunogenizitatearen modulazioan duten zeregina, baita osaera lipidiko zehatz eta adjubante egokia ere.

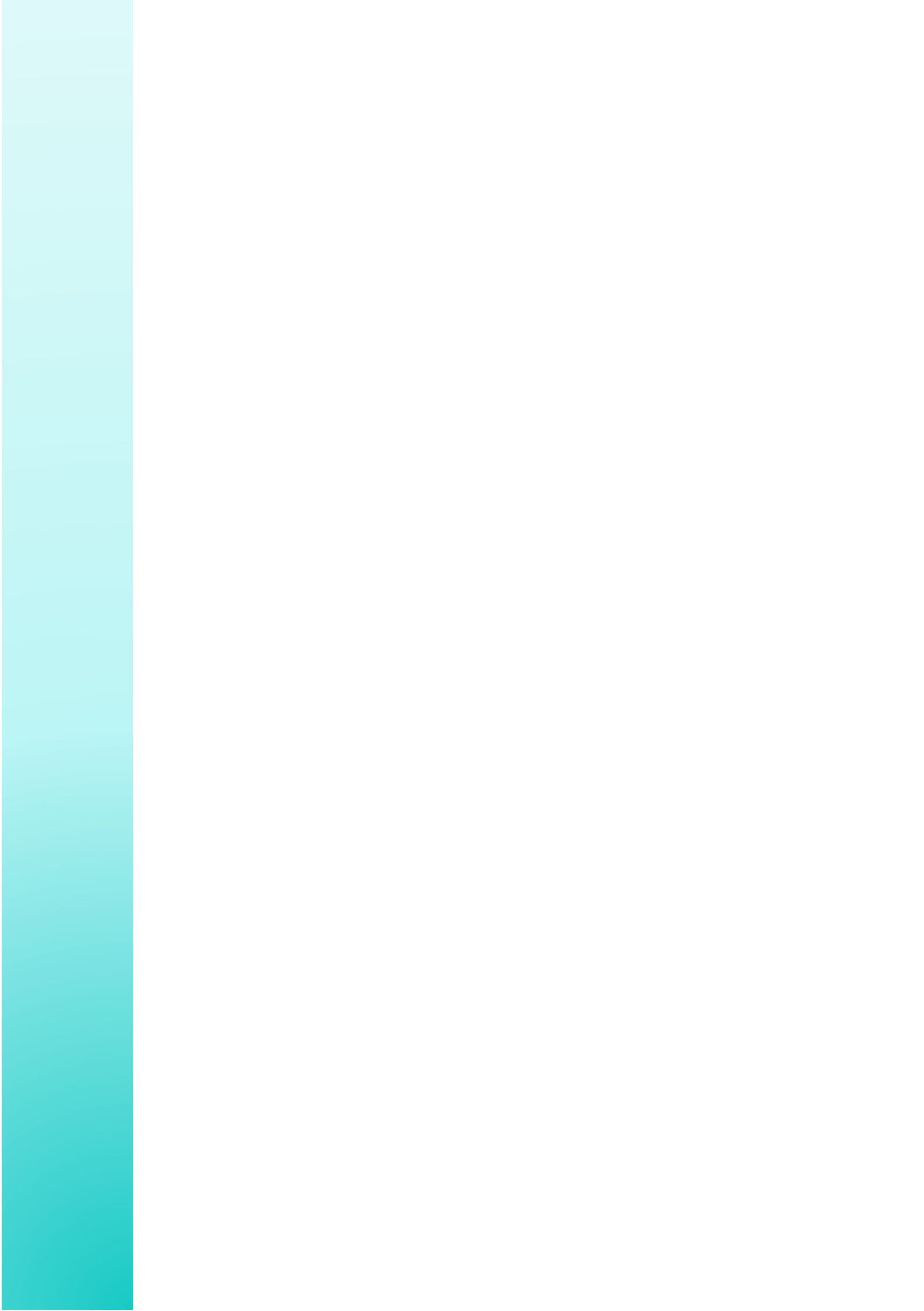
Guzti hau kontuan izanda, tesi honen helburu nagusia 10E8 erako antigorputzen bidezko erantzuna eragiten duen MPER-TMDaren egitura zehatza imitatzeko behar diren baldintza egokiak definitza litzateke, eskualde honetan oinarritutako immunogenoen diseinu arrazionalean laguntzeko.

1.4.1. Helburu zehatzak

- MPER-TMDan oinarritutako peptidoek mintzeko perturbazioak sortzeko behar duten egitura-oinarriaren zehaztapena, egitura antigenikoarekin alderatuz.
- Immunologikoki esanguratsuak diren MPER-TMDtik eratorritako peptidoen diseinua eta hauen errekonstituzioa lipido besikuletan.
- MPER epitopoaren esposizioa hobetzeko estrategien diseinua honako hauetan aldatuz: i) konposizio lipidikoa eta ii) peptidoen sekuentzia.

2.KAPITULUA

TEKNIKA ESPERIMENTALAK



2. TEKNIKA ESPERIMENTALAK

Kapitulu honetan, tesi lan honen esperimentuak egiteko erabili diren teknikak eta protokolo orokorrak deskribatu dira. Teknika horiek, kapitulu bakoitzeko *teknika experimentalen* atalean zehaztu dira.

2.1 LIPIDOETAN OINARRITUTAKO SISTEMA EREDUAK

Mintz biologikoak oso sistema konplexuak dira, lipido molekula anfipatikoen bigeruzaz osatuak daudenak eta baita proteina eta azukreak ere dituztenak. Konplexutasun altuaren ondorioz, oso zaila da mintza osatzen duten osagai bakoitzaren propietateak eta portaera aztertzea. Beraz, mintzen inguruko azterketa asko sistema ereduetan oinarritzen dira, mintz naturalen bertsio oso sinplifikatuak diren arren eta nahiz eta lortutako emaitzak ezin diren zuzenean sistema konplexuagoetara estrapolatu.

Lipidoetan oinarritutako sistema ereduak tamaina eta xafla edo lamela kopuruaren arabera sailka daitezke. Lamela bakarreko besikulak, esfera bat eratzen duen bigeruza bakar batez osatuta daude, lipido bakarrekoak edo lipido nahaste batekoak izan daitezkeelarik. Lamela anitzeko besikulak (MLV, ingelesetik *multilamellar vesicles*) aldiz, diametro desberdina izan ditzaketen eta ur geruza mehe batez bereizita dauden lamela bakarreko zenbait besikulez osaturik daude. Lamela bakarreko besikulak hiru talde nagusitan sailka daitezke: lamela bakarreko besikula erraldoiak (GUVs, ingelesetik *giant unilamellar vesicles*), lamela bakarreko besikula handiak (LUVs, ingelesetik *large unilamellar vesicles*) eta lamela bakarreko besikula txikiak (SUVs, ingelesetik *small unilamellar vesicles*).

2.1.1. Liposomen ekoizpena

Lipido besikulak, liposomak bezala ere ezagunak, bi geruzaz osatutako egitura lipidikoak dira, barnealdean soluzio urtsu bat enkapsulatzen dutenak. Modu espontaneoan sortzen dira zilindro itxurako molekula lipidiko anfipatikoak soluzio ursosuetan diluitzen direnean, eta tratamenduaren arabera, lamela bakarreko edo ugariko bigeruzak izan ditzakete.

MLVak sortzea da liposomen ekoizpenerako metodorik simpleena eta azkarrena, eta tesi honetan liposoma-peptido formulazioak (LPF) eta finkatutako lipido geruzak (SLB, ingelesetik *supported lipid bilayers*) ekoizteko erabili dira.

2.1.1.1 Lamela bakarreko besikula erraldoiak

GUVak, mintz-eredu interesgarriak dira euren tamaina handiagatik (5-100 μm inguru), zelula baten taminarekin alderagarria dena. Horri esker, mikroskopio optiko egoki baten bidez aztertu daitezke, besikula bakarrean gertatzen diren gertakarien irudia lortuz.

Tesi lan honetan, GUVak fluoreszentzia mikroskopioz aztertuta, hurrengo saioetarako erabili dira: Fab birkonbinaturek peptidoa daramaten GUVak lotzeko duten gaitasuna aztertzeko, peptidoen errekonstituzio prozesuaren ostean mintzen egonkortasuna ebalutzeko eta peptidoek lipido ordenan izan dezaketen eragina ikertzeko.

GUVak Shnirova eta lankideek ¹⁹⁸ deskribatutako berezko puztea (*spontaneous swelling*) metodoaren bitartez ekoitzu ziren. Protokolo zehatza jarraian deskribatua:

GUVak ekoizteko protokoloa

- 1) Lipido puruak kloroformoz diluitzen dira nahi den kontzentrazioan.
- 2) Behar den lipido kopurua (lipido bakarra edo nahasketa) beirazko saiodi batean gehitzen da.
- 3) Disolbatzaile organikoa, nitrogeno gasezko korronte batez lurruntzen da beirazko saiodiaren ondoan lipido geruza bat eratzen den arte.
- 4) Lagina huts ponpan lehortzen da ordu betez disolbatzaile organikoaren edozein aztarna erabat ezabatzen den arte.
- 5) Lipido lehorrez osatutako geruza 30 minutuz aurre-hidratatzen da H_2O ultrapuruaren fluxu leun batez.

- 6) Lipido geruza lehorra indargetzaile urtsu bat gehituz hidratatzen da. Jarraian, lagina irabiatu egiten da geruza lipidikoa askatzeko eta MLVen soluzio homogeneoa lortzeko. Lipidoak egoera likidoan daudela bermatzeko, lagina zein indargetzailea, lipido nagusiaren trantsizio tenperatura (T_m) baino tenperatura altuagoan mantendu behar dira.
- 7) Beharrezkoa denean, etanolez (etOH) edo 1,1,1,1,1,3,3-hexafluoro2-propanolez (HFIP) disolbatutako peptidoa, nahi den peptido-lipido erlazioan gehitzen da fase organikoan.
- 8) MLV soluzioaren 20 μL hartu eta 40 μm -ko diametroa duten silikazko mikroesferen (*bead*-ak) 5 μL -rekin nahasten dira politetrafluoroetlenozko gainazal batean. Nahasketa homogeneizatu ostean, 2-3 μL -tako tantatxotan banatzen da eta huts ponpan lehortzen da ordubetez.
- 9) Lipido-*bead* lehorrek pipeta baten punta erabiliz jaso eta A indargetzailea duen (5 mM HEPES, pH 7.4, sakarosa 3 g/L) beste punta batean murgiltzen dira. Besikulak eratzen direnean, A indargetzailea besikulen barnealdean geratuko eta behaketa-plakaren hondoan besikulak metatzea bermatuko du; izan ere, kanpo-indargetzailearekin alderatuz (5 mM HEPES, 150 mM KCl, pH 7.4), dentsitate altuagoa du. Bost minutuz, ur lurrunez asetutako ontzi batean jartzen da lipido-*bead* nahasketadun punta.
- 10) Hidratatutako lipido-besikulak kanpo-indargetzailea duen behaketa-plakara transferitzen dira.

2.1.1.2 Liposoma-peptido formulazioak (peptidoen errekonstituzioa mintzetan)

Lipidoez gain, mintzean kokatzen diren proteinak ere ezinbestekoak dira mintz biologikoen funtzioan. Proteina hauen jarduera, inguruko lipidoen egiturek modula dezakete; horrela, bigeruza lipidikoaren osaketak eragina izan dezake mintz-proteinen arteko molekulen eta baita molekula barneko elkarrekintzetan. Horrez gain, mintzean kokatzen diren proteinen azterketa burutzea oso zaila da, disoluzioan agregatzeko joera izaten baitute. Proteina hauen errekonstituzioa mintz ereduetan beraz, aukera ematen du hauen analisia jatorrizko ingurunearen antzeko ingurune batean egiteko.

Tesi honetan, peptidoak mintzetan errekonstituitzeko jarraian deskribatutako protokoloa garatu eta puntuau jarri da. Protokolo honen bidez, MPER-TMD eremutik eratorritako peptidoak errekonstituitu dira immunologikoki esanguratsuak diren formulazioak diseinatzeko. Lortutako LPFak, lipido-peptido elkarrekintzak eta peptidoek mintzean eragin ditzaketen perturbazioak aztertzeko erabili dira.

LPFak ekoizteko protokoloa (peptidoen errekonstituzioa mintzetan)

- 1) Lipido puruak kloroformoz diluitzen dira nahi den kontzentrazioan.
- 2) Peptidoak etOHean edo HFIean disolbatzen dira nahi den kontzentrazioa lortzeko.
- 3) Behar den lipido kopurua kloroformo:metanolean 1:2 (bol:bol) disolbatzen da eta aurrez disolbatutako peptidoarekin nahasten da, 1:50 edo 1:250 peptido-lipido erlazio molarrean.
- 4) Disolbatzaile organikoa, nitrogeno gasezko korronte batez lurruntzen da lipido geruza bat eratzen den arte.
- 5) Lagina huts ponpan lehortzen da ordu betez disolbatzaile organikoaren edozein aztarna erabat ezabatzen den arte.
- 6) Lipido lehorrez osatutako geruza 30 minutuz aurre-hidratatzen da H_2O ultrapuruaren fluxu leun batez.

- 7) Lagina fosfatodun indargetzailearekin (PBS, ingelesez *phosphate-buffered saline*) hidratatzen da eta nahasten da geruza lipidikoa askatzeko. Erabilitako tenperatura, nahastearen Tm-aren gainetik egon behar da (normalean 55 °C).
- 8) MLVak bainu batean ordu betez sonikatzen dira nahasketaren Tm-a baino tenperatura altuagoan.
- 9) Azkenik, 15 aldiz izotzen eta desizotzen dira LPFak lamela bakarreko besikulak lortzeko.

2.1.1.3 Finkatutako lipido geruzak (SLBak)

SLBak euskarri solidoen sortzea, oso prozedura erabilia da indar atomikozko mikroskopio (AFM, ingelesetik *atomic force microscopy*) bidezko mintzetan kokatzen diren peptidoen analisirak. Lan honetan, SLBak besikulen adsorzio metodoa jarraituz lortu dira eta AFM bidezko neurketa guztiarako erabili izan dira.

Besikulak adsorbatzeko metodoa, euskarri solido batean inkubatuz (mika hain zuen lan honetan), liposomen berezko adsorzioan oinarritzen da. Liposomak euskarri solidoen inkubatzean, adsorbatu, deformatu eta zabaldu egiten dira bigeruza lipidiko laua sortuz. Energia aldetik hain desfaboragarria den prozesu hau gertatzeko mekanismoa ez dago oraindik zehaztuta.

Lipidoen adsorzioa areagotzeko, jarraian deskribatutako zenbait jarraibide bete behar dira. Lehenik, besikula txikiak kurbadura-estres handia dutenez, hauen erabilpenak, besikulen xurgapena hobetzen du. Era honetan, besikulek mika ukitzean, mintz eredu hauen ezegonkortasun handiagatik, bigeruza egoki baten hedapena eragingo dute. Horrez gain, Mg²⁺ edo Ca²⁺ bezalako katioi dibalenteak egoteak, erraztu egiten du mintz lauen hedapena liposometatik abiaturik. Azkenik, garrantzitsua da SLBak ondo garbitzea lipido agregatuak, fusionatu gabeko besikulak eta geruza gehigarriak kentzeko.

SLBen eraketa adsortzio metodoaren bitartez

- 1) LPFak kapitulu honetan deskribatutako LPFak ekoizteko protokoloa jarraituz prestatzen dira.
- 2) Mika orri bat (1,5 x 1,5 zm) epoxi itsasgarriarekin beirazko xafla batean itsasten da.
- 3) Mikaren gainazala, zinta itsasgarri arruntarekin garbitzen da eta ioi dibalenteak dituen (normalean 1 mM Ca⁺²) indargetzailea gehitzen da gainetik.
- 4) LPFak mikara gehitzen dira eta 30 minutuz inkubatzen dira adsortzioa gertatzeko.
- 5) Geruza gehigarriak, lipido agregatuak edo kaltzioa kentzeko, 5-10 aldiz garbitzen da indargetzailearekin.
- 6) SLBak AFM bidez eskaneatzeko prest daude.

2.1.2. Lipido kontzentrazioaren determinazioa

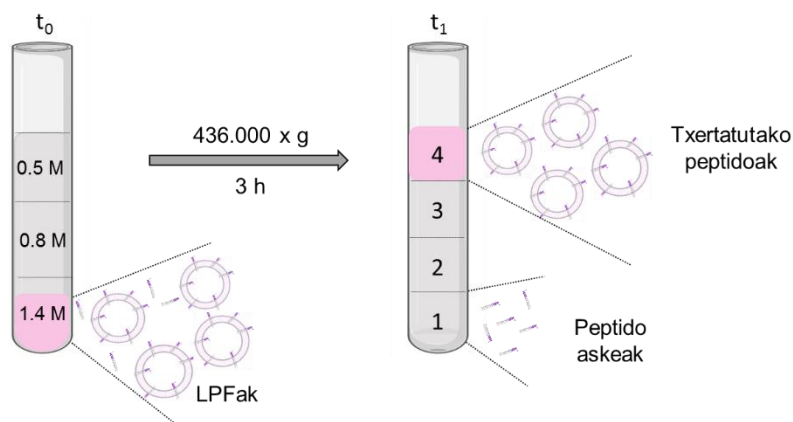
Eratutako besikulen fosfolipidoen amaierako kontzentrazioa zehazteko, fosforo ez-organikoaren kuantifikazioa erabili da. Prozedura hau, Fiskek garatu zuen 1925ean ¹⁹⁹ eta Bartlett ²⁰⁰ eta Böttcherek ²⁰¹ moldatu zuten beranduago eta fosfolipidoen hidrolisian oinarritzen den metodo kalorimetrikoa da. Fosfolipidoen hidrolisiaren ondorioz, fosfato taldea aske gelditzen da eta erreaktibo espezifiko desberdiniek erreakzionatzen du, hasierako kontzentrazioaren menpekoa izango den produktu koloredun bat emanez.

Fosfolipido kontzentrazioaren determinaziorako protokoloa

- 1) NaH_2PO_4 soluzio batetik, 0, 25, 50, 75 eta 100 nmol fosforo pipeteatzen dira, bikoitztuta, saiodi desberdinatan, lipido kontzentrazio zehatza lortzea ahalbidetuko duen kalibrazio-kurba bat eraikitzeko.
- 2) Gutxi gora behera, 50 nmol fosfato duen LPF laginaren volumen txiki bat beste saiodi batean gehitzen da.
- 3) Lagin guztiak 500 μL azido perklorikorekin (%70) nahasten dira, saiodiak irabiatu eta 205 °C -tan dagoen plakan kokatzen dira 45 minutuz fosfolipidoen hidrolisia gerta dadin.
- 4) Laginak giro temperaturan (RT, ingelesetik *room temperature*) egon arte hozten uzten dira eta hurrengo soluzioak gehitzen dira:
 - a. Amonio heptamolibdatoan oinarritutako soluzioaren 4 mL (2.2 g/L amonio heptamolibdatoa $[(\text{NH}_4)_6\text{Mo}_7\text{O}_{24} \cdot 4\text{H}_2\text{O}]$ eta 14.3 mL/L azido sulfurikoa (H_2SO_4) % 95-98.
 - b. 500 μL azido askorbikoa (% 10).
- 5) Fosfato taldeek molibdatoarekin erreakzionatzen dute lehenbizi, eta azido askorbikoarekin ondoren, produktu horixka bat sortuz. Hodiak 5 minutuz irakin ondoren, laginek kolore urdinerantz jotzen dute hasierako fosforo kantitatearen arabera.
- 6) Laginak hoztu ondoren absorbatzia neurten da 812 nm-tan.
- 7) Laginaren fosfolipido kontzentrazioa lortzeko, zuzen patroiaren absorbantziak fosforo kontzentrazioaren aurka irudikatzen dira eta lerro zuzen batera doitzen da. Zuzen honen maldatik eta laginen absorbatziak erabiliz, laginaren fosforo kontzentrazioa lortzen da.

2.1.3. Peptidoen txertaketa besikuletan: sakarosa gradiente bidezko LPFen flotazioa

LPFen flotazioa, metodo simplea da errekonstituzio prozesuaren ostean (2.1.1.2 atalean deskribatuta) peptidoen txertaketa besikuletan efizientea izan den ikusteko. Lagina, sakarosa gradiente batean ultrazentrifugatu ondoren, besikuletan txertatutako proteinak, proteina askeetatik bereizten dira.



2.1 irudia. Peptidoen txertaketaren analisia LPFen flotazioaren bitartez. Rodaminaz (Rho) markatutako LPFak 1.4 M-eko sakarosadun disoluzioarekin nahasten dira; ondoren, 0.8 M-eko sakarosa disoluzioa gainjartzen da eta azkenean, 0.5 M-eko, sakarosa gradiente bat eratuz (t_0). Lagina zentrifugatu ostean, elementu desberdinak dentsitatearen arabera bereizten dira eta lagina lau frakzioetan banatzen da (t_1). Liposomak (peptidoarekin edo peptidorik gabe) goiko frakzioan kokatuko dira eta peptidoaren txertaketa eman baldin bada, peptidoa ere besikulekin batera agertuko da. Bestalde, 1 eta SDS frakzioetan, flotatu gabeko materiala geratuko da, lotu gabeko peptidoa hain zuzen.

LPFen flotaziorako protokoloa

- 1) Sakarosa gradientearen prestaketa: Rho-z markatutako LPFen 100 μ L-ei (1.5 mM-eko lipido kontzentrazioan eta 1:50eko peptido:lipido erlazioan) sakarosadun soluzioa gehitzen zaio, 300 μ L-tan 1.4 M-ko kontzentraziora doitu arte. Jarraian, 0.8 M (400 μ L) eta 0.5 M-eko (300 μ L) sakarosa geruzak gainjartzen dira.
- 2) Prestatutako sakarosa gradientea 436.000 xg-tan zentrifugatzen da hiru orduz.

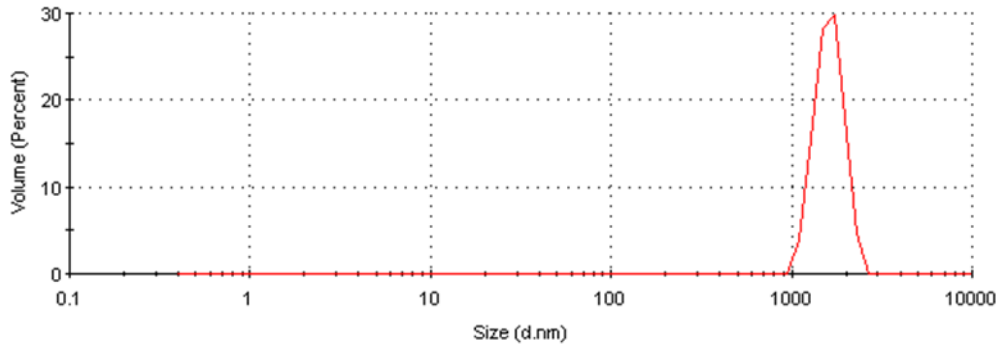
- 3) Zentrifugatu ostean, 250 µL-tako frakzioak jasotzen dira. Saiodietan itsatsita geratu den materiala berreskuratzeko, azkeneko frakzio bat jasotzen da 250 µL % 1 sodio dodezil sulfato (SDS) beroa (100 °C) gehituz.
- 4) Peptidoaren presentzia, Tris-trizina SDS-PAGE-arekin (poliakrilamidazko gelean egindako elektroforesia) banatu ondoren, Western Blot teknikaren bitartez antzeman da frakzio desberdinetan.
- 5) Rodaminadun besikulen presentzia, Rho-ren fluoreszentzian oinarrituz zehaztu da.

2.1.4. Besikulen tamainaren zehaztapena DLS bitartez

Argiaren sakabanatze dinamikoa (DLS, ingelesetik *dynamic light scattering*) esekiduretako partikulen tamaina zehazteko neurketa-teknika zehatza da. Partikulen Browndar higiduran oinarritzen da; hau da, likido batean partikula txikienak azkarrago mugitzen dira; handienak aldiz, motelago. Partikulen abiadura, erradio hidrodinamikoa (R_h) neurtzeko erabil daiteke Stokes-Einsteinen ekuazioa erabiliz (2.1 ekuazioa).

$$D = \frac{K_B T}{6\pi\rho R_h} \quad [\text{Eq 2.1}]$$

non D difusio koefizientea den, K_B Boltzmann-en konstantea, T tenperatura, ρ ingurunearen biskositatea eta R_h partikula esferikoen erradio hidrodinamikoa.



2.2 irudia. PC:eggPA-CpreTM-TMD1 LPF besikulen populazioaren tamaina banaketaren grafikoa.

DLSak, laginaren bolumen txiki batetik erauzten du informazioa, denboraren araberako sakabanatutako argiaren fluktuazioetatik hain zuen. Partikulen esekidura bati argi sorta batek eragiten dionean sortzen diren sakabanatutako argi intentsitateak neurten dira teknika honen bitartez. Intentsitate horiek, korrelazio funtziotan ematen dute, eta funtziotan horretatik abiaturik, zenbait algoritmo erabiliz, esekidurako partikulen tamaina banaketa lortu daiteke (2.2 irudia). Besikulen tamainen banaketa homogeneo edo heterogeneoari buruzko informazioa, polidispersio-indizetik (PDI) lortzen da. PDIren balioa 0 eta 1 bitarteko da, non zerotik hurbil dauden balioek soluzio homegeneoak adierazten dituzten.

Tesi honetan buruturiko DLS neurketak, Malvern Zeta-Sizer Nano ZS (Malvern Instruments, Malvern, Erresuma Batua) batean egin dira 0.6 nm eta 6 μm bitarteko tamainetarako detekzio heinarekin eta 5 mW-eko He-Ne laser izpiarekin ($\lambda = 633 \text{ nm}$). Sakabanatutako argia, laser izpiarekiko perpendikularki kokaturiko fotomultiplikatzaila batek detektatzen du. Azkenik, tresnaren software komertzialak emaitzak aztertzen ditu.

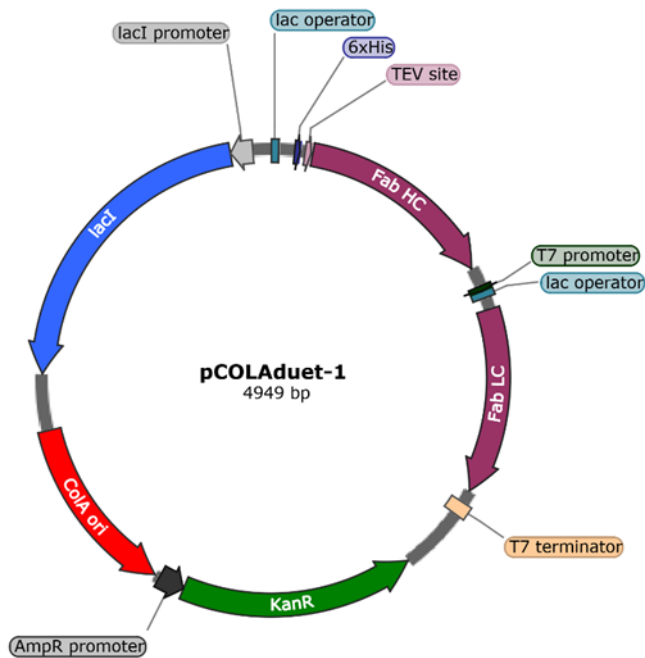
2.2 FAB-EN ADIERAZPENA, PURIFIKAZIOA ETA MARKAKETA

Intereseko proteina bat biokimikoki karakterizatzeko kopuru handia behar denez eta iturri naturaletatik lortu daitekeena gutxi denez, gainadierazpen birkonbinatua beharrezkoa izaten da. Proteinen ekoizpenerako, *E. coli* erabilienetariko adierazpen sistema da; duen kostu baxuagatik, hazkuntza zinetika azkarragatik eta lortzen den proteina etekin altuagatik, besteak beste. Hala ere, proteinen gainadirazpenerako *E. coli* erabiltzeak zenbait muga aurkezten ditu; hala nola, disulfuro zubiak edota bestelako itzulpen ondoko eraldaketak (PTM, ingelesetik *post-translational modifications*) burutzeko gaitasun eza.

2.2.1. Fab-en adierazpen eta purifikazioa bakterio zeluletan

E. coli-ren zitoplasmak ingurune erreduzitzalea du, disulfuro zubi egonkorren eraketa eragozten duena. Baino, disulfuro zubiak *E. coli*-ren periplasman eratu daitezke, non baldintza oxidatiboak bermatzen diren. Bertan daude DsbA eta DsbC deituriko entzima oxidatzaileak; lehenengoak, disulfuro Zubien eraketa katalizatzen du, bigarrena, berriz, isomerasa aktibitateaz baliatzen da proteinen toleste natiboa bermatzeko²⁰².

Disulfuro zubiek zenbait proteinen tolespen fisiologikoan eta euren funtzioan izugarrizko garrantzia dutenez, *E. coli*-ren T7 SHuffle²⁰³ anduia sortu da ingeniaritza genetikoz. Andui hau, bere zitoplasman disulfuro Zubien eraketa baimentzeko moldatuta dago; izan ere, thioerredoxin erreduktasa (trxB) eta glutathion erreduktasa (gor) entzimetan mutazioak eragin zaizkio, eta AhpC peroxidasa entzima, disulfuro zubiak erreduzitzeko gai den AhpC* erreduktasa bilakatua izan da. Azken aldaketa honek ohiko oxidoerreduktasen ibilbide metabolikoak trunkatzearen ondorioz, zelulan eragindako hazkuntza arazoak konpontzen ditu. Azkenik, DsbC isomerasa entzima gehitu zaio bakterio hauen genomari. Isomerasa honen adierazpen konstitutiboak, intereseko proteinen toleste egokia bermatzen du.



2.3 irudia. pColaDUET-1 adierazpen plasmidoa. Bektore honek bi MCS kodetzen ditu, bakoitzaz T7 sustatzaile baten ondoren kokatua, aldi berean bi gene desberdinaren (Fab-aren kate arina eta kate astuna kasu honetan) adierazpena ahalbidetzen duena. Horrez gain, lac operoia, ColA erreplikoia eta kanamizinaren erresistentzia genea kodetzen ditu.

pCola-DUET-1 plasmidoa (2.3 irudia) erabili da T7-SHuffle zelulak transformatzeko. Kopia-kopuru txikiko plasmido honek, T7 sustatzaile bakar baten menpe dauden bi klonaziorako gune anizkoitz (MCS, ingelesetik *Multiple Cloning Site*) ditu (MCS1 eta MCS2); horri esker, klonatutako Fab-aren kate astuna (HC, ingelesetik *heavy chain*) eta kate arina (LC, ingelesetik *light chain*) ratio berean adierazi daitezke. Fab-aren HCaren N muturrean, histidina isatsa gehitu da eta jarraian, Tobacco etch virusaren (TEV) proteasaren mozketa gunea jarri da.

Tesi lan honetan, T7-SHuffle anduia eta pCola-DUET-1 plasmidoa erabili dira Fab 10E8 anti-MPER antigorputza ekoizteko. Jarraitutako estrategia honen bitartez, tolespen egokia duten Fab disolbagarri guztiz aktiboak ekoitzi dira.

Fab-en purifikazio protokoloa

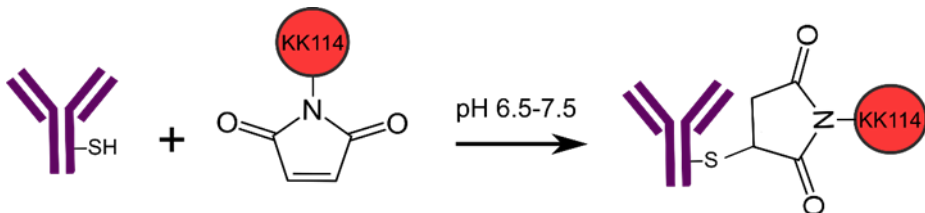
- 1) T7-SHuffle zelula elektrokonpetenteak intereseko plasmidoarekin transformatzen dira kanamizinadun LB-agarrean.
- 2) Transformatutako zelulen kolonia bat jaso eta 1:1000 Kan duen 20 mL LB-tan inokulatzen da. Hazkuntza, gau osoz (ON), 37 °C-tan eta irabiaketa konstantean ematen da.
- 3) Hazkuntzaren 1:50 diluzioa, 1:1000 Kan-dun 1 L LB-tan inokulatzen da eta Fab birkonbinatuaren adierazpena, 18 °C-tan ON (16 orduz) induzitzen da, bakterioen dentsitate optikoa (OD) 0.8 ra iritsi ondoren, 0.4 mM isopropil-D-tiogalaktosidoa (IPTG) gehituz.
- 4) Zelulak 8000 x g-tara zentrifugatzen dira eta ondoren, jalkinak bersuspenditzeko 50 mM HEPES (pH 7.5), 500 mM NaCl, 35 mM imidazol, DNasa eta proteasa inhibitzaileak (Roche, Madrid, Spainia) dituen indargetzailea gehitzen da.
- 5) Zelulak Avestin Emulsiflex C5 homogeneizatzailera apurtzen dira.
- 6) Zelula hondarrak zentrifugazioz bereizten dira eta gainjalkina nikelerako afinitate zutabetik (Ni-NTA) pasarazten da.
- 7) Histidina isatsaz zutabera itsatsitako proteinak 500 mM imidazol dituen indargetzailea erabiliz askatzen dira, kontzentratu, TEV proteasarekin (histidina isatsa ebakitzeko) nahastu eta 50 mM NaH₂PO₄ (pH 8.0), 300 mM NaCl, 1 mM DTT, eta 0.3 mM EDTA dituen soluzioan dializatzen uzten dira ON.
- 8) Fab-ak bigarren Ni-NTA afinitate zutabe bat erabiliz bereizten dira gainontzeko proteina eta TEV proteasatik. Jarraian, berriro kontzentratu eta indargetzailea aldatzen zaie (20 mM NaAc pH 5.6, % 10 glizerol) ON eta 4 °C-tan.

- 9) Azkenik, ioi trukeko kromatografia zutabe batetik pasarazten da lagina. Itsatsitako proteina berreskuratzeko, KCl gradiente bat erabiltzen da. Fab-ak 4 °C-tan eta 10 mM NaH₂PO₄ (pH 7.5), 150 mM NaCl eta % 10 glizerola dituen indargetzailean kontserbatzen dira.

2.2.2. Proteinen zuzendutako markaketa

Proteinen zuzendutako markaketa funtsezkoa da molekula bakarreko fluroszentzian oinarritutako esperimentuak burutzeko. Aminekin erreakzionatzen duten konposatuez gain, irisgarri dauden zisteinetan tiolekiko erreaktiboak diren konposatuekin eginiko markaketa prozedura ere oso erabilia da. Tiolak (-SH) zisteina aminoazidoen albo kateetan aurkitzen direnez, proteina gehienetan daude, baina ez dira amina primarioak bezain ugariak. Beraz, zisteina bidezko markaketa selektiboagoa eta zehatzagoa da.

Maleimida taldeek zisteinetan aurkitzen diren sulfidril taldeekin espezifikoki erreakzionatu dezakete pH fisiologikoetan. Prozesu honetan, aminoazidoaren sulfuro atomoak (-SH taldea) iodoa (edo beste elementu halogenatu bat) ordezkatuko du ordezkapen nukleofilikoaren bidez, tioeter lotura egonkor bat sortuz (2.5 irudia).



2.5 irudia. Maleimida eta sulfidril taldearen arteko erreakzioaren eskema. KK114, maleimida taldearekin lotutako fluoroforoa da. Magenta kolorez, -SH talde itua duen antigorputza ageri da.

Fab-etan zuzendutako markaketaren protokoloa

- 1) Zuzendutako mutagenesia erabiliz, posizio jakin bateko aminoazidoa zisteina batez ordezkatzen da.
- 2) Zisteina askea duten mutanteak 1 mM DTT-arekin 30 minutuz, 37 °C-tan inkubatzen dira disulfuro zubiak eratzen ari ez diren zsteinak erreduziteko.
- 3) Proteina eta agente erreduzitzalea banatzeko, indargetzaile aldaketa burutzen da PD-10 zutabea erabiliz.
- 4) Fab-ak, maleimida duen Abberior STAR RED (KK114) molekularekin inkubatzen dira ON 37 °C-tan.
- 5) Azkenik, lagina zentrifugatzen (14.000 x g-tan 5 minutuz) da eta konjugatu gabeko molekula kentzeko, PD-10 zutabe batean zehar pasarazten da.

Tesi lan honetan, mikroskopia konfokaleko saioetarako, Fab-aren C216HC posizioa modifikatu da maleimida duen KK114 zundarekin.

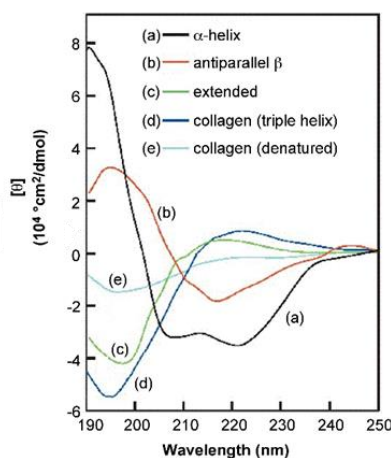
2.3 TEKNIKA ESTRUKTURALAK

2.3.1. Dikroismo zirkularreko espektroskopia (DC)

CD oso teknika sentikorra da biomolekulen egitura sekundarioa (urrutiko UB bidez) eta tertziarioa (gertuko UB bidez) zehazteko; baita biomolekulen konformazio aldaketak eta egonkortasuna aztertzeko ere balio dezake. Teknika honen abantaila nagusiak hurrengoak dira: aztertu nahi den molekula kantitate txikian erabiltzen dela eta datuen analisia erraza dela. Desanbantailarik aipagarriena, proteinak soluzioan aztertu behar direla da; muga argia izan daitekeena mintz-proteinak euren jatorrizko ingurunean ikasteko.

CD, argiaren absorbzioan oinarritzen den espektroskopia teknika bat da, zeinetan kromoforo batek, ingurune asimetriko batean modu zirkularrean ezkerralderantz eta eskuinalderantz polarizatutako argia xurgatzean ematen diren desberdintasunak neurten diren. Proteinetan agertzen diren kromoforo ohikoenak amida taldeak eta aminoazido aromatikoen albo kateak dira. Absorbzioaren ondorioz gertatzen diren trantsizio elektronikoek, uhin luzera eta intentsitate desberdina izango dute elektroiek espazioan duten kokapenaren arabera, eta honek proteinaren egituraren inguruko informazioa emango du.

Teknika hau, peptidoek mintz lipidikoak imitatzen dituen ingurune apolar batean duten egitura sekundarioa aztertzeko erabili da. Neurketak egiteko, Jasco J-810 espektrometroa erabili da, zeinaren ohiko kalibrazio prozedurak (1S)-(+)-10-azido kanforsulfonikoa eta amonio gatza erabiliz egin diren.



2.6 irudia. Proteina baten CD espektro adierazgarria. α -helize egiturek **(a)** minimo bikoitza erakusten dute 223 eta 208-210 nm-eten eta maximoa 191-193 nm artean. β egiturek **(b)** aldiz, 210 eta 225 nm arteko minimo bakarra dute, eta 190 eta 200 nm arteko maximoa, egitura paralelo edo antiparaleloaren araberakoak direnak. Ordenatu gabeko egiturek **(c)**, 200 nm inguruan dute minimoa. Irudia ²⁰⁴-tik egokitua.

CD saioetarako protokoloa

- 1) DMSO-n disolbaturiko peptidoak ON liofilizatzen dira eta indargetzaile urtsu (2 mM HEPES, 7.4 pH) batean hidratatzen dira 30 µM-eko kontzentrazioa lortzeko, HFIP kontzentrazio desberdinekin (% 2.5, % 10 edo % 25 (v/v)).
- 2) CD espektroak, 190-260 nm artean, 25 °C-tan eta 1 mm-ko ibilbide luzera duen kuartzo gelaxka batean neurten dira. Datuak, 1 nm-tako banda zabalerarekin hartzen dira, 100 nm/min-ko abiadurarekin eta 0.2 nm bakoitzeko. Baldintza bakoitzerako 20 neurketa egin dira batez beste.
- 3) Atzeko zarata kendu ondoren, lortutako eliptikotasun seinalea (ϵ), hondarren batez besteko eliptikotasun $[\theta]$ bihurtzen da 2.2 ekuazioa erabiliz:

$$[\theta] = \frac{\epsilon}{10 \cdot c \cdot l \cdot n} \quad [\text{Eq. 2.2}]$$

non c peptidoaren kontzentrazio molarra, l bide optikoa eta n peptidoen lotura kopurua diren.

2.3.2. Espektroskopia infragorria (IR)

IR materialak xurgatzen duen erradiazio elektromagnetikoan oinarritzen den teknika da; erradiazio hau lotura kimikoen araberakoa izanik. Molekula organikoek 10000 eta 100 cm^{-1} arteko erradiazio infragorria xurgatzen dute eta bibrazio-energian bihurtzen dute. Xurgapenaren uhin luzera, atomoen masa erlatiboaren, indar konstantearen eta loturen geometriaren araberakoak dira.

1950ean Elliot eta Ambrosek²⁰⁵ teknika hau erabiltzea proposatu zuten proteinen egitura zehazteko. Mintzarekin asoziaturiko proteinen egitura eta orientazioa zehazteko oso teknika erabilgarria da. Izan ere, beste teknika espektroskopiko batzuek ez bezala, bigeruza lipidikoek ez dute neurketen bereizmen edota sentikortasuna mugatzen, mintz-proteinak euren jatorrizko ingurune lipidikoan aztertzeko aukera ematen duelarik.

Proteinen kasuan, lotura peptidikoek xurgatzen duten erradiazio infragorriaren ondorioz sortzen diren xurgapen bandak aztertzen dira, amida-banda deritzenak hain zuzen. Amida maiztasunak egitura desberdinako sentikorrik diren arren, amida-I banda da proteinen konformazioa zehazteko gehien erabiltzen den bibrazio modua. Banda hau, $1600-1700\text{ cm}^{-1}$ artean kokatzen da, eta azpi-banda desberdinaren gainjarpenagatik osaturik dago. Azpi-banda horietako bakoitza, peptidoak hartzen duen bigarren mailako egitura bati dagokio. Bandaren osagai bakoitzaren kokapena ezagutzeko, prozedura matematiko desberdinak aplikatzen dira (Fourier-en transformatua). Banden esleitzea, hau da, maiztasun bakoitza bigarren mailako egitura jakin batekin korrelazionatzea, peptido sintetikoen neurketetan, kalkulu teorikoetan edo aurretiaz ezaguna den bereizmen altuko egitura tridimentsionalekin alderatuta lortzen da. Amida-I bandaren osagaien esleipen ohikoenak 1.1 taulan ageri dira.

Tesi lan honetan, IR teknika besikuletan errekonstituitu ostean peptidoek hartzen duten bigarren mailako egitura zehazteko erabili da. Neurketak eta datuen azterketa, I. de la Arada Dk.-arekin kolaborazioan egin dira.

1.1 taula. Amida-I bandaren osagaien esleipen ohikoena D₂O-tan. Esleipen hauek ez dira finkoak, tarte bat onartu behar da peptido bakoitzaren baldintzen arabera.

| Bataz-besteko maiztasunak (cm ⁻¹) | Esleitutako egitura |
|---|--|
| 1622/1685 | Luzatutako kateak/peptidoaren destolespena |
| 1630 | Helize solbatatua |
| 1640 | Coiled-coil egitura |
| 1655 | α-helizea |
| 1675 | β birak |
| 1660 | 3 ₁₀ -helizea |

IR bidezko LPFen bigarren mailako egituraren zehaztapena

- 1) LPFak 2.1.1.2 *atalean* deskribatzen den bezala prestatzen dira, 3 mg/mL-ko peptido kontzentrazioan eta 1:50eko peptido-lipido erlazioan.
- 2) LPFak liofilizatzen dira eta jarraian D₂O-n bersuspenditzen dira (H₂O-ak proteinen amida-I bandarekin gainjartzen den xurgapen banda sendoa dauka).
- 3) 25 µL-tako lagina bi CaF₂ leihoen artean jartzen da.
- 4) Espektroak, kadmio-telurido detektagailu bat eta Peltier-en oinarritutako tenperatura kontrolagailu bat duen Thermo Nicolet Nexus 5700 espektrometroan erregistratzen dira (Thermo Fisher Scientific; Waltham, MA). Lagin bakoitzerako, 370 neurketa jasotzen dira eta espektroaren datuak 2 cm⁻¹-ko bereizmen nominalarekin lortzen dira. HFIPa duten laginetan, disolbatzailearen ekarpene jatorrizko espektrotik kentzen da analizatu aurretik.
- 5) Banda kopurua eta hauen kokapena espektroaren dekonboluziotik eta Fourier-en transformatutik lortzen dira.

2.4 FLUORESZENTZIAN OINARRITUTAKO MIKROSKOPIA AURERATUA

Fluoreszentzia mikroskopia, interesko laginen handipen handiko eta kontraste handiko irudiak eskuratzeko tresna erabilgarria da. Ohiko epifluoreszentzia mikroskopio batean, argi iturri gisa lanpara bat erabiltzen da. Argia, objektiboaren aurretik aurkitzen den kitzikapen filtro batean zehar pasarazten da uhin luzera zehatz batez. Objektibo berdinak igorritako fluoreszentzia jasotzen duenez, detektagailura iritsi aurretik filtro dikroiko baten bidez kitzikapen argitik bereizten da.

Epifluoreszentzia mikroskopio baten eragozpen nagusia, laginaren plano guztiak aldi berean kitzikatzen, jasotzen eta irudikatzen direla da. Honen ondorioz, ezinezkoa da plano fokal desberdinatik ebatzitako irudiak sortzea.

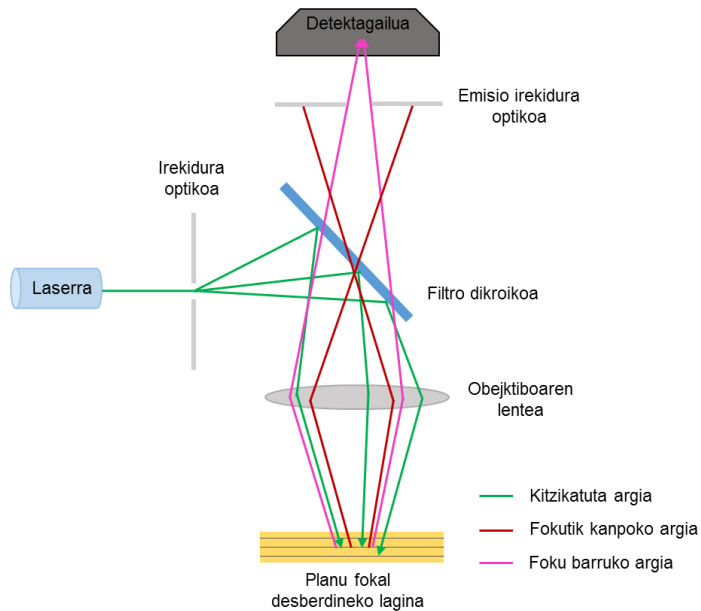
2.4.1. Mikroskopia konfokala

Mikroskopia konfokalak sekcio optikoa ahalbidetzen du, foku-plano baten bereizmen handiko irudiak eskuratz eta ondorioz, kontrastea izugarri hobetuz. Hori lortzeko, detektagailura iritsi aurretik, fokutik kanpo gelditzen den argia baztertzen du igorpen ibilbidean kokatutako irekidura optiko baten bidez. Foku-planoaren gaineko zein azpiko planoetatik datorren argia beraz, ez da jasotzen, eta honek eragin zuzena du irudiaren kontrastean. Gainera, mikroskopio optikoan argi iturri gisa erabiltzen den lanpara, laser batekin ordezkatzen da, fokoaren bolumena asko txikitzen delarik.

2.7 irudian ageri dira fluoreszentziako mikroskopio konfokal baten osagai nagusiak. Mikroskopio mota hauetan, ispilu dikroiko batera zuzendutako laser izpi batek kitzikatzen du lagina. Ispilu dikroiko honek, objektiboaren bidez laginera zuzenduko den argia aukeratzen du. Molekula fluoreszenteak kitzikatzean igortzen den fluoreszentzia, aipaturiko ispilu dikroiko horretatik bideratzen da irekidura optiko batetik igaroz. Irekidura optiko honi esker, foko barruko fluoreszentzia detektagailura pasatzea utziko du, fokutik kanpoko fluoreszentzia aldiz, blokeatuko duelarik.

Tesi lan honetan, Nikon Eclipse TE-2000 fluoreszentzia konfokaleko mikroskopioa (Nikon Instruments, Tokio, Japonia) erabili da GUV-LUV fusio heterotipikoko saioetarako, KK114 molekula fluoreszenteaz markatutako Fab-en eta peptidodun GUVen arteko lotura zehazteko eta iragazkortasun saioetarako. 63 x handipena duen olio-murgiltze objektiboa (1.2 irekidura optikoarekin (NA)) erabili da.

Azkenik, fluoreszentzia igorpenaren analisia, ImageJ softwarearekin burutu dira ²⁰⁶.



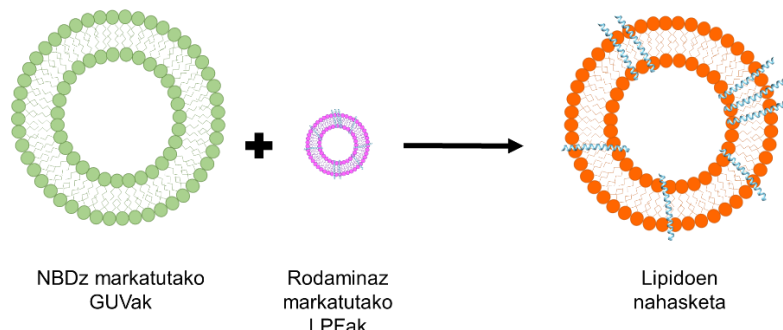
2.7 irudia. Fluoreszentzia mikroskopio konfokal baten osagai nagusiak.

2.4.1.1 GUV-FTV fusio heterotipikoa

Mintzen arteko fusio prozesu guztietan, besikulen arteko edukia nahastu aurretek zenbait urrats gertatu behar dira. Fusio prozesu guztietan presente dagoen ezinbesteko urratsa, mintzen arteko lipidoen nahasketa da.

Lan honetan, zelula plasmatikoaren kanpo-mintzaren konposizioa eta kurbadura imitatzen duten eta NBD fluoroforoaz markatuta dauden GUVak, eta MPER-TMD domeinutik eratorritako eta rodaminaz markatutako LPFak erabili dira. Bi populazioen arteko fusioa gertatuz gero, GUVen mintza LPFen zunda fluoreszentearekin homogeneoki markatuko litzateke (2.8 irudia).

Peptidoen errekonstituzioa eman ondoren, LPFen egonkortasuna aztertzeko erabili den saioa da, behean deskribatutako protokoloa jarraituz.



2.8 irudia. GUV-LPF arteko fusio heterotipikoaren saioaren adierazpen eskematikoa.
NBDaz markaturiko GUvak Rho-z LPFekin inkubatzen dira. Fusioa gertatzen bada, Rho GUVen mintzera transferitzen da.

GUV-LPF fusio heterotipikoaren protokoloa

- 1) MPER-TMDtik eratorritako peptidoak dituzten (1:50 peptido-lipido ratioan) eta Rho-z (% 0.5) markatutako LPFak, 2.1.1.2 *atalean* deskribatzen den moduan sintetizatzen dira.
- 2) POPC:Chol:SM (2:2:1 mol:mol) eta NBD-PE % 2-dun konpozioa duten GUvak 2.1.1.1 *atalean* deskribatzen den moduan sintetizatzen dira.
- 3) Behaketa-platertxoak, 0.5 g/L BSArekin, gutxienez 15 minutuz blokeatzen dira.
- 4) Irudiak hartu aurretik, GUvak eta LPFak 15 minutuz inkubatzen dira.
- 5) NBD zundarekin markatutako GUvak 476 nm-ra kitzikatzen dira, eta Rho-rekin markatutako LPFak 514 nm-ra. Iroritako fluoreszentzia bi kanaletan jasotzen da, 515/30 nm-tan eta 590/94 nm-tan, NBD eta Rho-rentzat, hurrenez hurren.
- 6) FTV-GUVen fusionatutako area erlatiboak lortzeko, Rho-ren fluoreszentzia neurten da GUVen irudien plano ekuatorialean zehar.

2.4.1.2 Molekula bakarreko iragazkortasun saioak

Mintzean aktiboak diren peptidoek, lipido mintzetan lesio zein perturbazioak eragin ditzakete. Zunda fluoreszenteak, peptidoarekin mintzak tratatu ostean, molekulen barneraketa besikuletara edo askapena neurteko erabili daitezke.

Tesi lan horretan, peptidoa daramaten NBDz markatutako GUVak eta KK114 zunda fluoreszente askea erabili dira peptidoen errekonstituzioaren osteko GU Ven egonkortasuna aztertzeko. Peptidoek, GU Ven mintza hausten badute, kanpoko soluzioan dagoen zunda GU Venetara barneratuko litzateke.

Molekula bakarreko permeabilizazio saiorako protokoloa

- 1) MPER-TMD domeinutik eratorritako peptidoak dituzten eta NBDz (% 2) markatuta dauden GUVak 2.1.1.1. atalean deskribaturik dagoen moduan sintetizatzen dira.
- 2) Behaketa-platertxoak 0.5 g/L BSArekin, gutxienez 15 minutuz blokeatzen dira.
- 3) Irudiak hartu aurretik, peptidodun GUVak eta KK114 zunda, 15 minutuz inkubatzen dira.
- 4) NBDaz markatutako GUVak 476 nm-tan kitzikatzen dira, eta KK114 zunda 637 nm-tan. Irorritako fluoreszentzia bi kanaletan jasotzen da: 515/30 nm-tan eta Long Pass 650 nm-tan, NBD eta KK114 zundentzat hurrenez hurren.
- 5) Besikula bakoitzerako iragazkortasun gradua hurrengo ekuazioa erabiliz kalkulatzen da:

$$Iragazkortasuna (\%) = \frac{F_{barruan}}{F_{kanpoan}} \cdot 100 \quad [Eq. 2.3]$$

non $F_{barruan}$ eta $F_{kanpoan}$ barneko eta kanpoko KK114ren fluoreszentzia-intentsitateen batezbestekoa diren, hurrenez hurren.

2.4.1.3 Peptidodun-GUV eta Fab-en arteko lotura saioak

Mintzeko lipidoek, mintzean kokatzen diren proteinen egitura modulatzeko gaitasuna dute; eta ondorioz, hauen funtzioan ere eragin dezakete²⁰⁷.

Lan honetan, 10E8 Fab-a eta haren aldaerak erabili dira MPER epitopoak lipido konposizio desberdinako GUVen mintzean duen irisgarritasuna aztertzeko.

Saio hauetan, Fab-ak KK114 zundarekin markaturik daude eta GUVac NBDarekin. Fab-en lotura GUVertara orduan, KK114ren igorpena neurtuz kalkulatzen da. Hau da, bien arteko lotura gertatuko balitz, GUVertaren mintza KK114 zundarekin markatuko litzateke.

GUV-Fab lotura saioetarako protokoloa

- 1) MPER-TMD domeinutik eratorritako peptidoak dituzten eta NBDz (% 2) markatuta dauden GUVac 2.1.1.1. *atalean* deskribaturik dagoen moduan sintetizatzen dira.
- 2) KK114 zundaz markatutako Fab-ak 2.2 *atalean* deskribatutako protokoloa jarraituz purifikatu eta markatzen dira.
- 3) Behaketa-platertxoak 0.5 g/L BSArekin, gutxienez 15 minutuz blokeatzen dira.
- 4) Behaketa platertxoetan 0.25 µM Fab gehitzen dira.
- 5) GUVac jadanik Fab-a daukaten behaketa platertxoetara gehitzen dira eta irudiak hartu aurretik, 15 minutuz inkubatzen dira.
- 6) NBDa 476 nm-tara kitzikatzen da eta KK114a 637 nm-tara. Igorritako fluoreszentzia bi kanaletan jasotzen da: 515/30 nm-tan eta *Long Pass* 650 nm-tan, NBD eta KK114 zudentzat hurrenez hurren.

- 7) Lagin guztien irudiak kontraste eta distira berdinarekin lortzen dira, igorpen intentsitatean egon daitekeen aldea hobeto hautemateko.
- 8) GUvetan dagoen KK114 zundak igozten duen fluoreszentziaren kuantifikazioa, ImageJ programarekin burutzen da.

2.4.1.4 Bereizmen altuko STED mikroskopioa bidezko neurketak

Fluoreszentzia mikroskopioak, difrakzioari dagokionez, sistema mugatuak dira; hala ere, badira muga hori gainditzen saiatzen diren zenbait teknika. Igorpen estimulatuaren txikiagotzean oinarritzen den mikroskopio (STED), fokuaren inguruan dauden fluoroforoen ezabaketaren bitartez, azpi-frakzioen ebazpena ematen duen teknika nanoskopikoa da. Teknika honen bitartez lortzen den bereizmen espaziala 40 nm baino baxuagokoa da, GIBaren birioien tamaina (100 nm gutxi gorabehera) baino baxuagoa alegia. Honi esker, antigorputzaren eta birus partikularen seinaleak bereiz daitezke.

STED teknika bidez neurtutako Anti-MPER antigorputzen lotura GIB-1 birioietara, P. Carravilla DK.-ak burutu zituen C. Eggeling Dk.-aren laborategian (Oxford Unibertsitatea (Erresuma Batua)). Erregistratutako fotoi kopurua zuzenki erlazionaturik dago molekula fluoreszenteen kantitatearekin; beraz, antigorputzen eta birioien arteko lotura kuantifikatzeko aukera ematen du.

Irudiak, Abberior Instrument RESOLFT QUAD-P bereizmen altuko mikroskopioarekin egin ziren. Fluoreszentziaren kitzikapena, oliotan murgildutako 100 x /1,40 NA objektiboaz egin zen (Olympus Industrial, Southend-on-Sea, Erresuma Batua). Fluoreszentzia seinalea, irekidura doigarri batetik igaro zen (Thorlabs Limited, Ely, Erresuma Batua). Datuak eskuratzeko egindako eragiketa guztiak Imspector software (Abberior Instruments) batez kontrolatu ziren.

Fab-en lotura birioietara STED mikroskopioa erabiliz

- 1) Pseudobirus fluoreszenteak (PsV), 15 µg pCHIV Env(-), 1 µg EGFP Vpr eta 2.5 µg JRCSF Env plasmidoekin HEK293T zelulak ko-transfektatz eta purifikatuz lortzen dira (2.7.1 *atalean* jarraian deskribaturik dagoen moduan).
- 2) Purifikatutako birus-partikulak, poli-L-lisinaz estalita dauden beirazko estalkietan itsasten dira 15 minutuz.
- 3) Estalkiak blokeatu egiten dira gantz-azidorik gabeko BSA (% 2) erabiliz 15 minutuz.
- 4) KK114 zundaz markatutako Fab-ak (0.5 µM) gehitzen dira eta ordu batez inkubatzen dira.
- 5) Zenbait garbiketa burutzen dira PBS-z eta jarraian STED bidezko analisia burutzen da.
- 6) KK114 zunda 640 nm-tan kitzikatzen da pultsatutako laser batekin, eta agortu 775 STED laserrarekin. EGFPa 488 nm-tan kitzikatzen da pultsatutako laserrarekin. Emisioa, 650-700 nm-tako (KK114ren seinalerako) eta 501-552 nm-tako (EGFPren seinalerako) fluoreszentzia iragazkiak dituen elektroi-oldezkotan fotodiodoarekin jaso egiten da.
- 7) Irudiak aztertzeko, Python hizkuntza erabiliz eta funtziop pertsonalizatuak dituen aurrez garatutako programa batekin burutzen dira ⁴⁴.

2.4.1.5 Laurdanen polarizazio orokorraren neurketak

Jarraian deskribatutako ezaugarriak betetzen dituzten zunda fluoreszenteak egokiak dira mintzaren ordena molekularra kuantifikatzeko. Lehenik, oinarrizko eta kitzikatutako egoeren arteko desberdintasuna handia izan behar da. Horrez gain, mintzarekin interakzionatzeko gaitasuna izan behar dute eta bigeruzaren interfasean propietate fluoreszenteak izan behar dituzte. Geruza lipidiko trinkoetan, non ura ez den mintzera iristen, giro apolarra nagusitzen da. Aitzitik, jariakortasun altuagoa duten mintzetan, non interfasea oso hidratatuta dagoen eta giro polarra nagusitzen den, fluoreszentzia igorpena gorria desplazaturik dago, mintz zurrun edo trinkoekin alderatuz. Beraz, ingurunearekiko sentikorrak diren zunden espektroaren desplazamendua, mintzaren hidratazioaren eta biskositatearen araberako da.

Laurdanek oraintxe aipaturiko propietate guztiak betetzen dituen eta naftalenoaren egituraren oinarritzen den zunda sentikorrenetako bat da. Laurdanek elektroi-emaile bat (amino alkilo taldea) eta hartzale bat (aziloak ordezkatutiko karbonilo taldea) ditu 2. eta 6. posizioetan, hurrenez hurren. Ezaugarri honek, dipolo-momentu esanguratsu bat ematen dio, disolbatzaile polarretan duen karga banaketagatik²⁰⁸. Laurdan kitzikaturik dagoenean, bere dipolo-momentua handitu egiten da eta inguruko dipoloen kokapena aldatu ditzake. Kokapen aldaketa honek murriztu egiten du kitzikatutako egoeraren energia eta ondorioz, igorpen espektroan aldaketa ikusten da.

Polarizazio orokorraren (GP, ingelesetik *general polarization*) funtzioa, Parasassik proposatu zuen 1990ean²⁰⁹ eta Laurdanen igorpen espektroaren aldaketa aztertzeko erabili ohi da. Igorpen espektroaren aldaketa hau, bigeruza oso trinkoetatik (hidratazio baxukoak) bigeruza jariakorretara (oso hidratatuak) pasatzean ematen da, edo alderantziz. 2.4 ekuazioa aplikatuz, GParen kuantifikazioa burutu daiteke, mintzaren ordenaren inguruko informazioa lortuz.

$$GP = \frac{I_B - G \times I_R}{I_B + G \times I_R} \quad [\text{Eq. 2.4}]$$

non I_B eta I_R emisio espektroaren ertz urdineko eta gorriko igorpen intentsitateak diren, hurrenez hurren eta G kalibrazio faktorea den. G faktorea, baldintza desberdineta lortutako GP balioak normalizatzeko erabiltzen da eta hurrengo ekuazioaren bidez kalkulatzen da (2.5 ekuazioa):

$$G = \frac{GP_{ref} + GP_{ref}GP_{mes} - GP_{mes} - 1}{GP_{mes} + GP_{ref}GP_{mes} - GP_{ref} - 1} \quad [\text{Eq. 2.5}]$$

non GP_{mes} Laurdan purua demetildulfoxidoan (DMSO) disolbatutakoaren GP balioa den baldintza esperimental berdineta neurrtuta, eta GP_{ref} ezarritako erreferentzia balio bat den, hain zuzen, $GP_{ref} = 0,207^{210}$.

GP neurketak P. Carra villa Dk.-arekin lankidetzen egin ziren eta MPER-TMD domeinutik eratorritako peptidoek mintz lipidikoaren ordenan eraginik duten azterzeko erabili dira.

Irudiak Leica TCS SP5 II mikroskopio batean eskuratu ziren (Leica Microsystems, Wetzlar, Alemania).

2.5 MIKROSKOPIA ELEKTRONIKOA

Mikroskopio elektronikoak (EM), ikusi nahi den objektua argiztatzeko elektroi kanoi bat erabiltzen duen mikroskopio mota bat da. Mikroskopio optikoan, argi ikuskorraren erabilera bereizmena mugatzen du, argi mota honen uhin luzeragatik hain zuzen. Zenbat eta txikiagoa izan argiaren uhin luzera, orduan eta handiagoa da haren bereizmen ahalmena. Hala, elektroi baten uhin luzera argi fotoiena baino 10000 aldiz txikiagoa izan daitekeenez, mikroskopio elektronikoek mikroskopio optikoek baino bereizmen ahalmen handiagoa dute.

Oro har, mikroskopio elektronikoek, tungstenozko harizpi bat duen elektroi kanoi batek eragindako tentsio altuko elektroi sorta bat erabiltzen dute elektro-iturri gisa. Elektroiak mugiarazteko, 100 kV eta 1000 kV bitarteko azelerazio tentsioa aplikatzen da tungsteno harizpiaren eta anodoaren artean. Elektroiak laginetik pasatzen direnean, laginaren lodieraren eta errefrakzio indizearen arabera sakabanatzen dira.

Mikroskopio elektronikoen bidez ikertu nahi diren laginek tratamendua beharko dute erradiazioa murrizteko, hutsak eragin dezakeen kalteak murrizteko eta kontrastea areagotzea. Laginen tratamendurako teknikarik erabilienak, tindaketa negatiboa eta laginaren izozte arina dira. Lehenengoan, lagina elektroidun soluzio opaku batean murgiltzen da, amonio molibdato edo uranil azetatoan adibidez. Bigarrena, kriomikroskopian erabiltzen den metodoa da, zeinetan lagina etano likidoan murgildu eta

berehala izozten den izotz beirakara sortuz (ez-kristalinoa), tindaketarik gabe lagina ikusi ahal izango delarik.

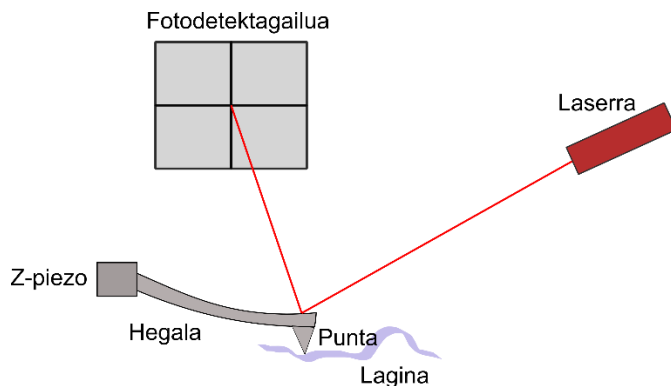
EM neurketak I. Tascón Dk.-rekin kolaborazioan egin dira. Tesi lan honetan, teknika hau MPER-TMDtik eratorritako peptidoek besikulen morfologian duten eragina aztertzeko erabili da.

EM saioetarako erabiliko den LPFen kontzentrazio optimoa zehazteko, laginak tindaketa negatiboz prestatu ziren. Laginen 8 μL kobrezko saretan adsorbatu ziren eta negatiboki tindatuak izan ziren % 1 uranilo formolarekin. Ondoren, Orius SC1000 (4008 \times 2672 pixel) kamera zuen JEM-1230 transmisio EM (JEOL Ltd., Tokio) batekin egin ziren irudiak, 20000 x handipenarekin.

Jarraian, behin laginak eta euren kontzentrazioa aukeratuta, 200 kV-ean lan egiten duen elektroien kanoi bat zuen JEM -2200FSC transmisio EM (JEOL Ltd. Tokio) baten bidez analizatu ziren. Aurretiaz, lagina beiraztatzeako, 4 μL -ko alikuotak gehitu ziren PDC-002-CE plasma garbigailuarekin 5 segunduz tratatutako Quantifoil R 2/2 eta C-flat R 1.2/1.3 kobrezko saretan. Saretak Leica EM GP2 (Leica Microsystems GmbH, Wetzlar) izozkailu automatikoaz etano likidoan sartu ziren. Irudiak dosi txikiko baldintzetan eta 4 K \times 4 K UltraScan 4000™ CCD kameraz (Gatan Inc.) 50000 x-ko handipenarekin egin ziren.

2.6 INDAR ATOMIKOKO MIKROSKOPIOA

Indar atomikoko mikroskopia (AFM, ingelesetik *atomic force microscopy*) bereizmen altuko irudi teknika bat da. Laginaren gainazala eskaneatzean oinarritzen da, honen irudi topografiko bat eratuz. Mintz biologikoen topografiaren informazioa, 1 nm baino albo bereizmen txikiagoarekin eta 0.1 eta 0.2 nm arteko bereizmen bertikalarekin lor daiteke metodo hau erabiliz. Gainera, teknika honi esker, laginaren propietate mekaniko, kimiko eta funtzionalak azter daitezke.



2.9 irudia. Indar atomikoko mikroskopio bidezko neurketen oinarrizko printzipioa.

AFM neurketetarako, lagin baten azalera eskaneatzen duen hegal batean punta fin bat eransten da. X eta y ardatzetan ematen den punta honen mugimendua, eskaner baten bidez kontrolatzen da (oinarri piezoelektrikoa). Laginaren eta puntaren arteko elkarrekintzek hegalaren mugimendua eragiten dute; mugimendu hau detektatzen duen sentsoreak, 0,1 nm baino desplazamendu txikiagoak bereiz ditzan, hegala laser argiaz argiztatu eta, argi-detektatzaile baten bidez, posizioa erregistratzen da (2.9 irudia). Beraz, lagin bat neurtzean, punta xy ardatzetan zehar eskaneatzen hasten da altuera desberdintasun bat aurkitzen duen arte; honek, hegalaren deflekzioa eragingo du z ardatzean, argi-detektatzaileak detektatuko duena. Detektagailuak jasotako seinalea, atzeraelikadurako zirkuitu batetik igarotzen da, zeinak hasierako posizioa konstante mantentzeko behar den z ardatzeko mugimendua kalkulatuko duen, eta laginaren topografiarekin erlazionatuko du hegalaren malguki konstantea eta fotodiodoaren sentikortasuna ezagututa.

AFMz lortutako datuen kalitatea bermatzeko, baldintza egokiak erabiltzea funtsezkoa da, hegal eta punta egokiaren hautaketa, pausu kritikoenetako bat delarik. Punta, lagina ukitzen duen AFMaren osagaia da eta hegalak, bultzada eta trakzio indarrak aplikatzen ditu; beraz, funtsezkoak dira. Baldintza eta lagin bakoitzerako, punta espezifiko bat hautatu behar da eta horretarako, zenbait ezaugarri hartu behar dira kontuan; horien artean, materiala, forma, estaldura, malguki-konstantea eta erresonantzia maiztasuna. Hegal komertzialak silizio edo silizio nitrurozkoak izan ohi dira eta urre-geruza mehe bateko estaldura izaten dute islapena hobetzeko. Formari dagokionez, puntak angeluzuzenak edo trianguluarrak izan daitezke eta erreflektantzia handitzeko estaldura metalikoak izaten dituzte. Lagin biologikoak aztertzerakoan, malguki konstante baxuak ($<1 \text{ N/m}$) dituzten puntak erabiltzea gomendagarriagoa da; izan ere, zenbat eta malguki

konstante baxuagoa, orduan eta txikiagoa izango da puntak laginean eragindako indarra.

Euskarri solidoa behar bezala hautatzea eta prestatzea ere oso garrantzitsua da geruza lipidikoak bezalako egitura bigunak neurtzen direnean. Hain zuen, mintz lipidikoak AFMz neurtzeko euskarririk erabiliena moscovite mica (Mica) da, karga negatibodun euskarri hidrofilikoa alegia. Irudi garbia eta egokia lortzeko, lagina inkubatu aurretik, mika atomikoki laua izan behar da; hori lortzeko, goiko orriak zatitu eta garbitu behar dira. Elementu hauez gain, eskaneatzeko abiadura, angelua, puntarekin aplikatuko den indarra zein indargetzailearen baldintzak behar bezala kontrolatu eta hautatu behar dira.

AFM bidezko neurketak bi modutan egin daitezke: ukipen moduan eta ukipena modu intermitentean izanik.

Ukipen moduan

Ukipen moduan, punta beti dago laginarekin kontaktuan. Aplikatutako indarra konstantea da piezoaren posizio bertikala etengabe zuzentzen duen atzeraelikadura-sistema baten ondorioz, era honetan laginaren topografian dauden aldaketak hautemanez. Deflexio bertikalean ematen diren aldaketa horiek, luzera unitate bihurtzen dira altueren irudia eraikitzeko. Eskaneatzeko oso modu arrunta da, baina laginarekin duen etengabeko ukipenaren ondorioz, honen hondapena gerta daiteke indar handiegiak aplikatuz gero.

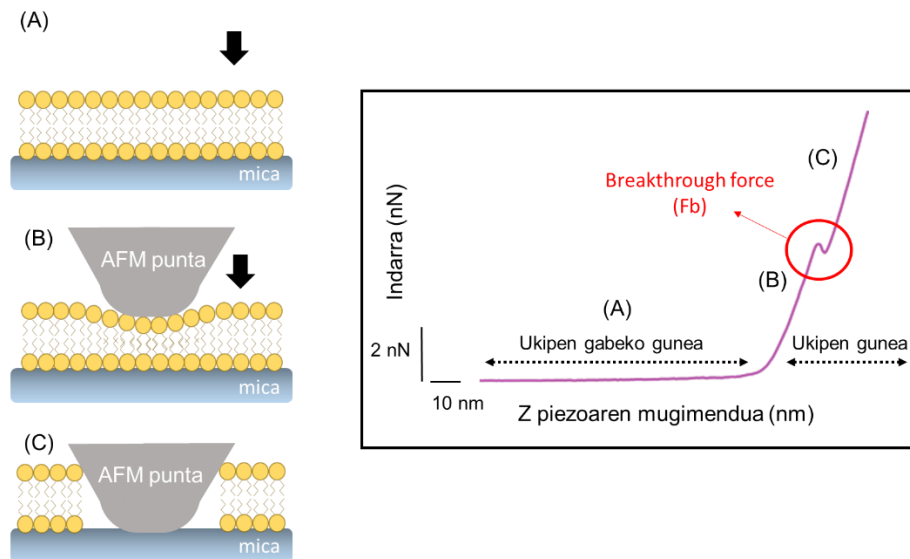
Tesi lan honetan egindako esperimentu guztieta erabili da ukipen-modua.

Ukipena modu intermitentean izanik

Eskaneatzeko modu honetan, puntak disoluzioan oszilatzen du erresonantzia maiatasun finko batekin. Hegalaren oszilazioan, puntak behin baino ez du gainazala ukitzen, eta jarraian, lehenengo posiziora bueltatzen da hurrengo oszilazio ziklorako. Puntak lagina ukitzen duenean, seinalearen amplitudean aldaketa ikusten da, eta aldaketa hauek erabiltzen dira irudi topografikoa eraikitzeko. Punta eta laginaren arteko ukipen denbora oso laburra denez, alboko marruskadura indarrak murrizten dira ukipen moduarekin alderatuz; horrela, ez da hain bortitza laginarekin eta lagin leunagoak aztertzeko aukera ematen du.

2.6.1. Indar-espektroskopia

Mintz biologikoen propietate elastiko eta mekanikoak garrantzia handia dute mintzek betetzen dituzten funtziotan. AFM bitartez irudi topografikoak lortzeaz gain, laginaren propietate mekanikoak bereizmen handiarekin ere lor daitezke; indar-espektroskopia (FS, ingelesetik *force spectroscopy*) deritzon metodoa erabiliz.



2.10 irudia. SLBen egonkortasuna aztertzeko AFM indar eta distantziaren kurba tipikoa. AFM punta laginera hurbildu ahala (A), bigeruza lipidikoarekin interakzionatu eta elastikoki deformatzen du (B) geruza hautsi eta mika substratua ukitzen duen arte (C). Grafikoan, bigeruza apurtzeko behar den indarra (F_b , ingelesetik *breakthrough force*) gorriz borobilduta ageri da.

Indar-espektroskopian, punta laginera hurbiltzen da eta indarra eragiten dio zulatzen duen arte. Amaitzeko, punta berriz atzera bueltatzen da aurretiaz zulatutako leku berdinak. Punta eta lagina kontaktuan daudenean, indar elektrostatikoak eta esterikoak gainditzen dira eta lagina deformatzen da puntak geruza bikoitza zulatzen duen arte. Bigeruza zulatzeko behar den indar honi, hau da, mintzak hautsi aurretik jasan dezakeen indarrari, F_b deritzo eta hurbilketa kurban, gailur gisa identifikatu daiteke (2.10 irudia). Geruza bikoitzaren lodiera ere, indar-kurba erabiliz neur daiteke.

Lipido geruzen propietate mekanikoak eta peptidoek mintz horien egonkortasunean duten eragina aztertzeko erabili da FSa.

AFM neurketetarako protokoloa

- 1) SLBak 2.1.1.3 atalean deskribatzen den moduan prestatzen dira, eta 1 mM Ca⁺² rekin inkubatzen dira 15 minutuz.

- 2) Mica AFM platinan kokatzen da 100 µL indargetzailearekin (TRIS 10 mM, 137 mM NaCl, 2.7 mM KCl).

- 3) Irudi topografikoak lortzeko hurrengo parametroak erabili dira:
 - a. Punta: AC-40 (Bruker, Billerica MA, AEB)
 - b. Aplikatutako indarra: 0.5 nN
 - c. Eskaneatzeko modua: Ukipen modua

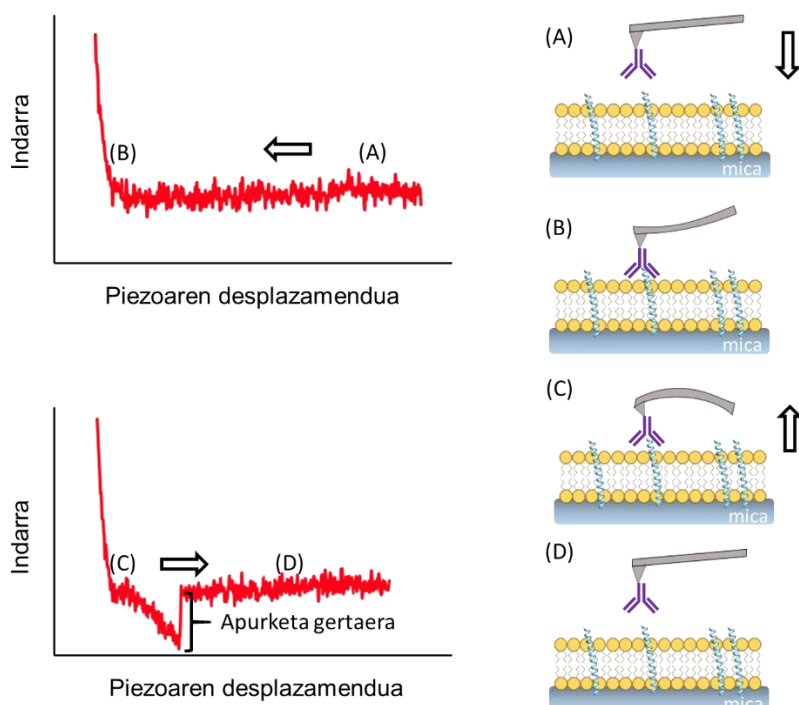
- 4) Fb-a lortzeko hurrengo parametroak erabili dira:
 - a. Punta: SNL-10 (Bruker, Billerica MA, AEB)
 - b. Aplikatutako indarra: 10 nN
 - c. Eskaneatzeko modua: Ukipen modua
 - d. Z abiadura: 0.1 µm/s, 1 µm/s eta 10 µm/s

2.6.2. Molekula bakarreko FS

FS bidezko neurketen izaera kuantitatiboa dela eta, AFMa oso tresna erabilgarria bilakatu da proteina domeinuen destolespena aztertzeko eta baita, hartzaile/ligando arteko loturak hausteko behar diren indarrak zehazteko.

Teknika honen bidez sentikortasun handiz neur daiteke bi molekulen arteko lotura hausteko behar den indarra; horietako molekula bat puntara itsatsita dagoelarik eta bestea, laginaren gainazalean txertatuta.

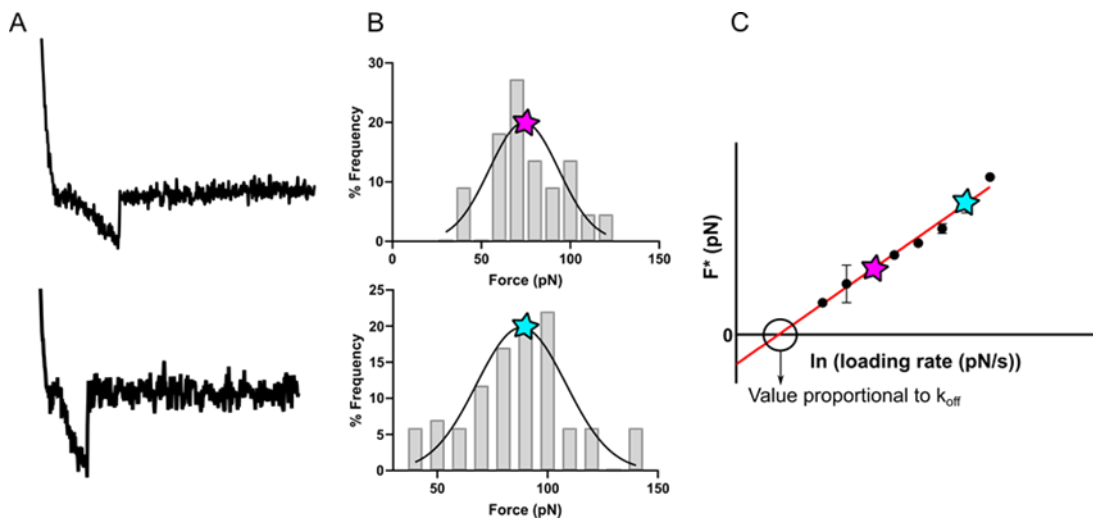
Hartzaile eta ligando baten arteko FS bidez elkarrekintzak neurtzeko ohiko saio batean, molekula batez funtzionalizatutako hegala, laginaren gainazaletik gertu kokatzen da, eta intereseko beste molekularekin funtzionalizatutako gainazaletik gertu kokatzen da bien arteko lotura ematen den arte. Orduan, indarra aplikatzen da lotura hori hautsi arte, haustura indarra lortuz.



2.11 irudia. Molekula bakarreko FS ohiko esperimentu baten eskema. AFM punta funtzionalizatua gainazalera hurbiltzen da (**A**) piezoaren laguntzarekin eta, (**B**) laginarekin kontaktuan jartzen da. Puntak laginaren gainazala ukitzean, hegala laginaren aurka bultzatzen da aldez aurretik ezarritako indar zehatz bat lortzen den arte; era honetan, molekularen arteko interakzioa edo lotura ematen dela ziurtatzen da. Aurretiaz ezarritako indarra lortzean, hegala hasierako posiziora itzultzen hasten da (**C**). Puntan funtzionalizatutako molekularen eta gainazalean txertatutako molekularen artean interakzio espezifikoa sortzen bada, hegalaren atzerapenak molekularen arteko tentsioaren handitzea eragingo du, azkenik bien arteko lotura apurtzen den arte. Apurketa gertaera honek, aldaketa nabarmena eragingo du indarraren seinalean eta azkenean, hegala jatorrizko kokapenera bueltatuko da (**D**).

Proposatu izan diren zenbait modelok aukera ematen dute bi molekularen arteko loturaren apurketa deskribatzen duten zenbati parametro erauzteko. Bell-Evans (2.6 ekuazioa) da, ziurrenik, indar espektroan profil lineala erakusten duten lotura gehienekin parametroak erauzteko erabiltzen den modeloa. Modelo hau jatorriz, Kramers-ek^{211,212} formulatutako trantsizio-egoeraren teorian oinarrituta dago, non molekularen bi egoera nahiko egonkor (lotuta eta askatuta) energia hesi aske (trantsizio-egoera) batek bereizten dituen lotura egoeratik χ_β distantzia jakin batera. Eedu horrek, beti onartu ezin daitezkeen zenbait mugak onartzen ditu.

$$F^* = \frac{k_B T}{\chi_\beta} \ln \left[\frac{r_f \chi_\beta}{k_{off} k_B T} \right] \quad [\text{Eq.2.6}]$$



2.12 irudia. Molekula bakarreko FS saioetarako datuen analisia. **A)** Loading rate desberdinatarako indar kurbak lortzen dira. **B)** Loading rate bakoitzerako haustura indarren histogramak irudikatzen dira eta funtzi Gaussiarrera doitzen dira haustura indar probableenak (F^*) lortzeko. **C)** Bell-Evans grafikoa aurreko pausuan lorturiko F^* -ekin eraikiko da. Azkeneko grafiko honetako balioak zuzen batera doitzean k_{off} and χ_β parametroak lortzen dira.

Molekulen arteko interakzioaren parametroak Bell-Evans modeloarekin erauzteko, hegalarren uzkurdura abiadura desberdinekin, indar banaketak lortzen dira (2.12 A irudia). Indar banaketa horiek, orokorrean, funtzi Gaussiarrera edo Poisson-era doitzen dira haustura-indar probableena (F^*) zehazteko (2.12 B irudia). Haustura indar probableena (F^*), loturaren *loading rate*-aren logaritmo naturalaren aurka irudikatuta, Bell-Evans grafikoa esaten zaio (2.12 C irudia). Bell-Evans grafikoa sortzeko, *loading rate* bakoitzerako haustura indarren banaketa lortu behar da. Kasurik simpleenean, non ligando eta hartzialearen lotura bakarra neurtzen den, grafikoa zuzen batera doitu daiteke, zeinak F^* -en hazkunza, *loading rate* logaritmoaren funtzioko erakusten duena. Zuzen batera doitzean lortzen den malda, 2.7 ekuazioaren berdina da, non χ_β energia minimotik trantsizio egoerara dagoen distantzia, $k_B T$ Boltzmann-en konstantea eta T tenperatura diren.

$$\text{Slope} = \frac{k_B T}{\chi_\beta} \quad [\text{Eq. 2.7}]$$

$$k_{off} = \frac{r_{F=0} \cdot \chi_\beta}{k_B T} \quad [\text{Eq. 2.8}]$$

2.6 ekuazioak, F^* , $\ln \text{loading rate}$ -ren aurka irudikatuz, F^* eta *loading rate*-aren logaritmo naturalaren arteko erlazio lineala aurreikusten du. k_{off} eta χ_β parametroak, Bell-Evans grafikotik lortutako zuzenaren ekuazioaren maldatik, jatorriko ordenatutik eta 2.8 ekuaziotik lor daitezke.

Puntaren funtzionalizaziorako protokoloa

- 1) Hegalak kloroformoaz garbitzen dira lehenbizi eta plasma-garbigailu batean oxigenoarekin ondoren (normalean, O₂ % 80ko potentzia 5-10 minutuz) edo ozono-garbigailu batean 15 minutuz.
- 2) % 5 3-aminopropildimetiletoxisilano (3-APDMES) disoluzioa etanolean (etOH) prestatzen da. Lehenik, etOH sartzen da eta gero 3-APDMES gehitzen da.
- 3) Hegalak % 5 3-APDMESeko disoluzioan sartzen dira eta 10 minutuz inkubatzen dira.
- 4) Aminofuntzionalizatutako hegalak, etOH-z eta miliQ-z (x3 bakoitza) garbitzen dira eta jarraian lehortzen dira.
- 5) Aminofuntzionalizatutako hegalak, 30 minutuz sartzen dira 80 °C-tan dagoen labean, erdi irekita dagoen Petri plaka batean.
- 6) Hegalak sodio boratozko disoluzio batean sartzen dira (pH 8.5-9), eta ordubetez inkubatzen dira RT edo ON 4 °C-tan.
- 7) Hegalak % 1eko glutaraldehidoan (amina primarioen bidezko funtzionalizaziorako) edo maleimidan (zisteina libreen bidezko funtzionalizazioarako) sartzen dira eta 30 minutuz inkubatzen dira. Ondoren, PBS-z garbitzen dira.
- 8) Hegalak lehortzen dira eta 50 µL proteina soluzioarekin (0.2 mg/mL proteina) guztiz estaltzen dira eta gutxienez ordu batez inkubatzen dira edo, 4 °C-tan gau osoz.
- 9) Hegalak % 0.01 BSA duen soluziora transferitzen dira eta 30 minutuz inkubatzen dira.

Molekula bakarreko FS AFM neurketetarako protokoloa

- 1) SLBak 2.1.1.3 atalean deskribatzen den moduan prestatzen dira, eta 1 mM Ca⁺²rekin inkubatzen dira 15 minutuz.
- 2) Mica AFM platinan kokatzen da 100 µL indargetzailearekin (TRIS 10 mM, 137 mM NaCl, 2.7 mM KCl).
- 3) Datuak lortzeko hurrengo parametroak erabiltzen dira:
 - a. Punta: MLCT-BIO-tik D eta E hegalak (Bruker, Billerica MA, AEB).
 - b. Aplikatutako indarra: 0.2 nN.
 - c. Z abiadura aldakorra: 0.1 µm/s, 2 µm/s eta 10 µm/s
 - d. Ukipen denbora aldakorra: 0.5 s, 1 s, 2 s, 5 s

Funtzionalizatutako AFM puntak ezin dira lehortu, bertan itsatsitako molekula kaltetu daitekeelako.

2.7 BIOLOGIA ZELULARRA: ZELELEN INFKEZIO ETA BIRUSEN NEUTRALIZAZIO SAIOAK

Anti-MPER antigorputzek GIBaren infekzioa inhibitzen dute birusaren eta zelula ostalariaren mintzen arteko fusioa blokeatuz. Fab 10E8ak eta bere aldaerek birusaren infekzioa blokeatzeko duten gaitasuna, gure laborategian prestatutako zelulen sarreraren inhibizioan oinarritutako saioan frogatu ziren. PsV andui desberdinak antigorputz kontzentrazio zehatzekin inkubatu ostean, CD4 eta CCR5 hartzaileak adierazten dituzten TZM-bl zelulak infektatzeko gaitasuna zehaztu zen.

2.7.1. Pseudobirusen ekoizpena

HEK293, giza enbrioaren giltzurrun (*Human Embryonic Kidney 293*) zeluletatik eratorritako hazkunza lerroa da. Zelula-lerro honen aldaera batek, 293T zelulak, SV40 T antigenoa dauka, eta SV40 jatorria, transfektatutako plasmidoen kromosomaz kanpoko erreplikazioa baimentzen duena. HEK293T zelulak, 37 °C-tan eta % 5 CO₂ kontzentrazioarekin mantentzen dira, % 10 behi fetuaren gazurrez, aminoazido ez esentzialez (1:100), sodio pirubatoz (1:100) eta penizilina/estreptomizina antibiotikoez (1:100) osatutako *Dulbecco's Modified Eagle's Medium* izeneko hazkunza medioan.

GIB-1ean oinarritutako pseudobirusak (PsV) ekoizteko, HEK293T zelulak JR-CSF-ren Env genea kodetzen duen plasmido (Jamie K. Scott irakasletik jasoa) batekin transfektatu dira kaltzio fosfatoaren metodoa erabiliz. Plasmido hau hurrengo bektoreekin batera transfektatzen da: pWPXL-GFP eta pCMV8.91 (Patricia Villacek (CSIC) emana). GFPa duen plasmidoa LTR eta Ψ sekuentziak ditu, zelularen genoman GFP-DNA txertatzeko gaitasuna ematen diotenak. pCMV8.91 plasmidoak aldiz, ez ditu bi sekuentzia horiek eta gainera, Vpu, Vpr eta Vif gene biralak mutatuak ditu infektatzeko gaitasuna duten ondorengoen eraketa eragozteko.

PsVak ekoizteko protokoloa

- 1) 4.5×10^6 HEK293T zelula erein egiten dira DMEM medioa duen hazkunza plater batean.
- 2) 20 ordu igarotakoan, hazkunza medioa, berri bategatik aldatzen da.
- 3) Hurrengo tranfekziorako soluzioak prestatzen dira eta 0.22 μM filtroetatik pasarazten dira:
 - a. A soluzioa: CaCl₂ 250 mM
 - b. B soluzioa: NaCl 140 mM, Na₂HPO₄.2H₂O 1.5 mM, HEPES 50 mM, MiliQ H₂O, pH 7.05.
- 4) Zelulak transfektatu egiten dira
 - a. 3 μg pHXB2, 10 μg pWPXL eta 18 μg pCMV8.91 nahasten dira A soluzioaren 1.3 mL-rekin.

- b. A eta DNA soluzioa duen hodia leun-leun nahasten den bitartean, B soluzioaren 1,3 mL gehitzen dira tantaz tanta. Agregatuak osatzeko minutu batez itxaroten da.
 - c. Nahasketa tantaka gehitzen da platererra gainazal osoa estali arte.
- 5) Transfekziotik 48 ordu igaro ondoren, partikula biralak gainjalkinetatik bereizten dira, medioa pipeta batez jasoz. Medioa 5 minutuz zentrifugatzen da 3.000 rpm-tako abiaduran, eta birusak dituen gainjalkina 0.45 µm-ko filtro baten bidez pasarazten da zelula-hondakinak kentzeko.
- 6) Gainjalkina 70000 xg-tan 2 orduz eta 4 °C-tan zentrifugatzen da. Zentrifuga hodien azpialdean, % 20 sakarosadun disoluzioaren 3 mL gehitzen dira, iragazki gisa jardungo dutenak eta azkenean kontzentratutako partikula biral puruak lortzen dira.
- 7) Gainjalkina bazterzen da eta 50 µL PBS hotza gehitzen zaio pelletari. Pelleta leunki bersuspenditzen da 30 minutuz 4°C –tan dagoen irabiagailu batean.
- 8) Laginak jaso eta -80°C-tan gordetzen dira.

2.7.2. Neutralizazio saioa

Birusen infekzio gaitasuna eta antigorputzen neutralizazio potentzia determinatzeko, PsVak eta TZM-bl itu zelulak erabili dira. TZM-bl zelula lerroa, HeLa zelula lerro bat da, JC.53 zelula lerrotik eratorria, zeinak CD4 eta CCR5 hartzale eta kohartzaileen kantitate handiak modu egonkorrean ekoizten dituen. TZM-bl zelula lerroa, JC.53 zelulei GIB-1aren sustatzaile baten menpe dauden luziferasa eta β -galaktosidasa geneak integratuz lortu zen eta GIB-1en andui asko eragiten dituzten infekzioaren aurrean oso sentikorrik dira. Zelula lerro berezi hau, 37 °C-tan eta % 5eko CO₂-an DMEM hazkuntza medioda modifikatuarekin (M* medioda) mantentzen dira. M* mediodari, beroaz inaktibatutako % 10eko FBSa, aminoazido ez-esentzialak (1:100), sodio pirubatoa eta penizilina/estreptomizina antibiotikoak gehitu zaizkio.

Purifikatutako PsV-en infekzio gaitasuna determinatzeko, hauen diluzio seriatuak TZM-bl zelulekin inkubatzen dira. Jarraian, 10E8 Fab-aren eta honen aldaeren neutralizazio potentzia zehazteko protokolo zehatza jarraian deskribatzen da.

Neutralizazio saioa

- 1) 50 μ L PBS antigorputz edo antigorputzik gabe, 96 putzuko plaka batean, PsV-en 50 μ L-ekin inkubatzen dira ordu batez antibiotikorik gabeko M* mediodan.
- 2) TZM-bl zelulak jaso, zentrifugatu eta % 20 antibiotikoak eta 30 μ g/mL DEAE-dextranoak dituen M* mediodan bersuspenditzen dira. 11.000 zelula putzuko gehitzen dira eta 48 orduz inkubatzen dira.
- 3) M* medioda berri batez aldatzen da.
- 4) 24 ordu igarotakoan zelulak jaso egiten dira, 100 μ L tripsina eta 200 μ L PBS putzuko gehituz.
- 5) Infektatutako zelulak kuantifikatzen dira fluxu zitometriaz.

Antigorputzen neutralizazio potentzia kalkulatzeko, fluxu zitometriaz lortutako GFP zelula positiboen (zelula infektatuen) kopuruaren murrizketa determinatzen da.

Antigorputzen potentzia konparatzeko, IC₅₀ balioa erabiltzen da, hau da, antigorputz bakoitzak infekzioaren % 50a blokeatzeko behar duen kontzentrazioa. Balio hau lortzeko, neutralizazio portzentaia, antigorputzen kontzentrazioa alderatuz eraikitako grafikoak erabili dira.

2.8 TEKNIKA IMMUNOLOGIKOAK

2.8.1. Untxien immunizazioa

Immunizazioa txerto potentzialak aztertzeko erabili ohi den metodoa da; izan ere, diseinatutako immunogeno batek antigenoa ezagutzeko eta infekzioa blokeatzeko gai diren antigorputzak sorrarazteko gai den ikusteko aukera ematen du.

Immunizazioaren ostean, ELISA, Western Blot edo beste teknika batzuk erabili ohi dira immunizatutako animalien serumetan antigenoaren aurkako erantzuna dagoen ikusteko eta horrela, txertoaren garapenerako formulazio egokia den ebaluatzeko.

Immunizazio-protokolo egokia aukeratzeko zenbait faktore hartu behar dira kontuan. Lehenik eta behin, funtsezkoa da immunogeno egokia aukeratzea, proteina zein peptidoa izan daitzekeena, antigorputzen ekoizpena eragiten duen epitopoa ordezkatuko duena. Immunogenoa orokorrean, adjubante batekin konbinatzen da, sistema immunea aktibatzen duen konposatu batekin alegia. Azkenik, oso garantzitsua da immunizatzeko erabiliko den animalia-eredua aukeratzea.

Tesi proiektu honetan, eta gure laborategiak aldez aurretik erabilitako immunizazio-protokoloa jarraituz, untxi eredua hautatu zen. Izan ere, untxien immunizazio-protokoloa oso finkatua dago eta gainera, beste animalia eredu batzuekin alderatuz, sortzen dituen antigorputzek CDRH3 begizta luzeak izaten dituzte, anti-MPER antigorputzen ezaugarri nabarmenetako bat dena ^{12,178,213}.

Lan honetan eginiko immunizazioetarako, osaketa lipidiko desberdineko liposomak erabili dira MPER-TMD domeinutik eratorritako peptidoak sistema immunera eraginkorki aurkezten direla ziurtatzeko. Horrez gain, A lipidoa gehitu da LPFetan adjubante moduan erabiltzeko, liposomak ere immunogeniko bihurtuz. A lipidoa toxikotasunik gabeko

endotoxina lipopolisakardoaren zati bat da, bakterio Gram negatiboetatik eratorritakoa. Ikusi izan da adjubante hau erabilgarria dela GIB-1aren antigorputz neutralizatzileen ezaugarriak imitatzenten dituzten antigorputz poliklonalen ekoizpenean ²¹⁴.

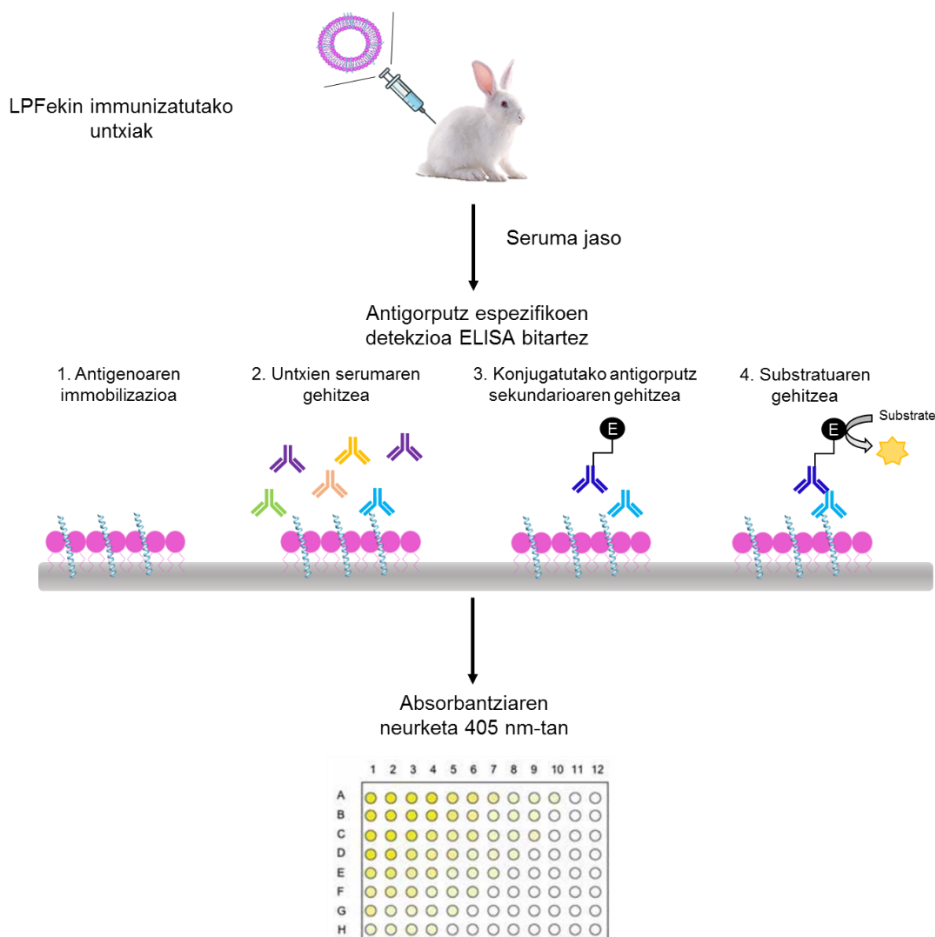
Immunizazio protokoloa

- 1) LPFak 2.1.1.2 *atalean* azaldu bezala prestatzen dira, 0.4 mg/mL-ko, 0.3 mg/mL-ko eta 0.2 mg/mL-ko peptido kontzentrazioekin eta kasu guztietaan, 1:50eko peptido-lipido erlazioarekin (mol:mol). % 0.25 A lipidoa adjuante gisa gehitzen da lipido nahastean.
- 2) LFPak gau osoz liofilizatzen dira.
- 3) Zeelanda Berriko untxi zuriak honela immunizatzen dira:
 - a. Gure immunogenoa ezagutzen duen antigorputzik ez dagoela egiazatzeko, immunizatu aurreko untxien serumaren lagin bat hartzen da, kontrol negatibo gisa erabiliko dena.
 - b. Immunogenoen laginak berhidratatzen dira 1 mL H₂O MiliQ erabiliz eta larruazalaren azpitik injektatzen dira hainbat lekutan: 0, 21 eta 42 egunetan. Lehenengo inokulazioak antigenoaren 0.4 mg ditu, bigarrenak 0.3 mg eta azkenak 0.2 mg.
 - c. Azkeneko immunizaziotik 15 egun igarotakoan, untxien odola lortzen da.
- 4) Odola ordu betez koagulatzen uzten da giro tenperaturan eta ON 4 °C-tan. Koagulatu den frakzioa baztertu egiten da eta seruma 30 minutuz 1000 xg-tan zentrifugatzen da eritrozitoak kentzeko. Gainjalkina aliquotatu egiten da eta -20 °C-tan gordetzen da.

2.8.2. ELISA ez-zuzena

ELISA (ingelesetik, *Enzyme Linked Immunosorbent Assay*), peptidoak, proteinak edo antigorputzak bezalako substantzia solugarriak detektatu eta kuantifikatzeko teknika kolorimetrikoa da. Antigenoa (itu molekula) 96 putzuko plaka bat bezalako gainazal solido batean inmobilizatzen da eta jarraian, entzima erreportari bati lotutako antigorputz bat gehitzen da. Azkenik, erreakzio kalorimetrikoa gertatzen da eta antigorputzen bidezko ezagupen espezifikoak, plaka irakurgailu batean absorbatzia neurtuz lortzen da.

Tesi honetan, ELISA saioak erabili dira untxien immunizazioaren ondoren lorturiko serumean dauden antigorputz poliklonalen espezifikotasuna aztertzeko eta 10E8 Fab-en eta honen aldaeren eta LPFen arteko ezagupena zehazteko.



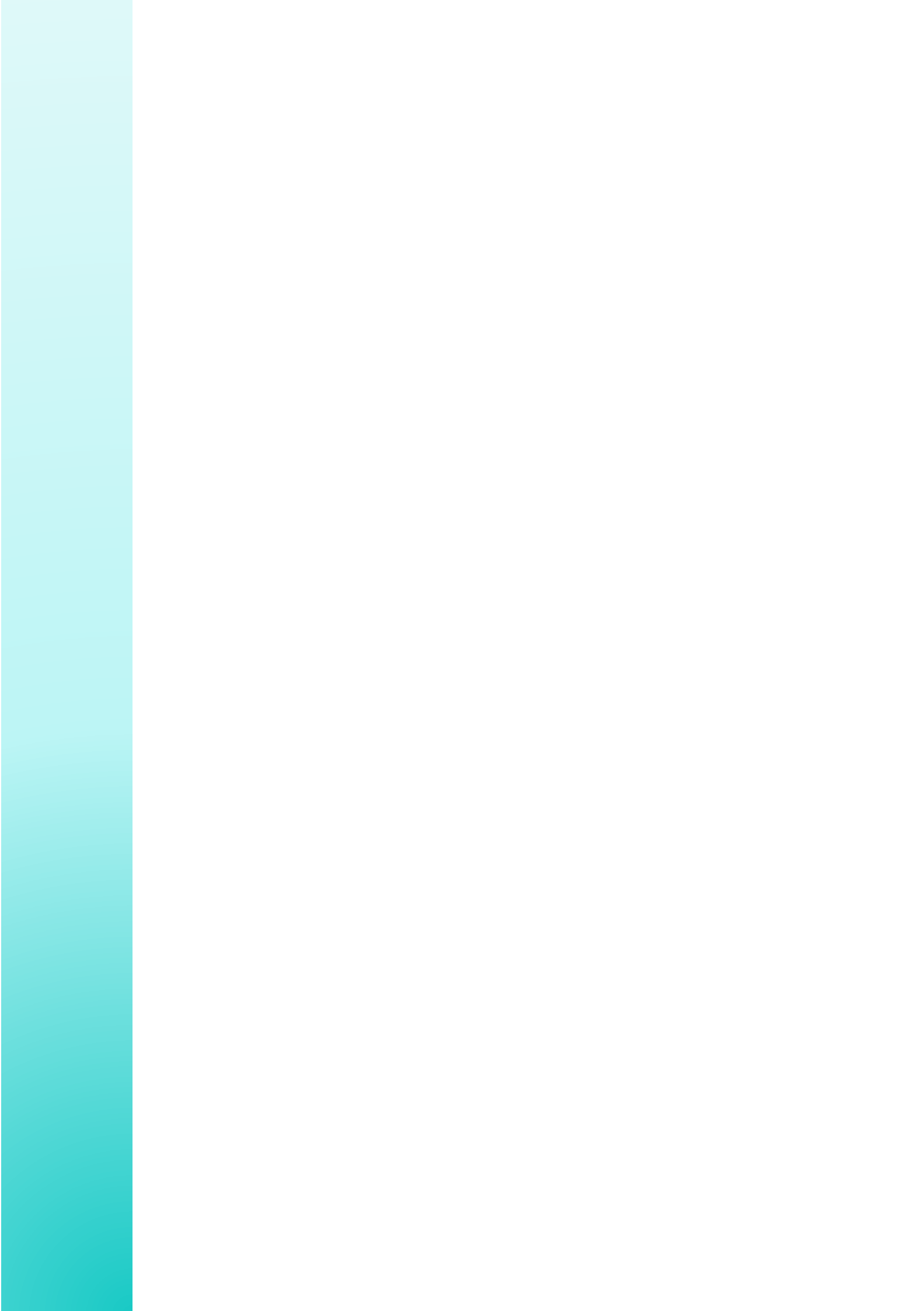
2.13 irudia. Antigorputz poliklonalen ekoizpena eta identifikazioa. Zeelanda berriko untxiak LPFekin immunizatzen dira eta antigorputz espezifikoak ekoizpena ELISA ez-zuzenaren bidez identifikatzen da.

ELISA ez-zuzeneko protokoloa

- 1) Peptidoak DMSOtan (1.37 µM) disolbatzen dira edo lipido besikuletan (0.5 mM) errekonstituitzen dira eta 96 putzuko plaketan inmobilizatzen dira (100 µL putzuko).
- 2) Putzuak PBS indargetzaileaz (200 µL/putzu) garbitzen dira eta 2 orduz % 3 BSA duen PBS-z (300 µL/putzu) blokeatzen dira.
- 3) Putzuak PBS indargetzailez (200 µL/putzu) birritan garbitzen dira.
- 4) 10E8 Fab-a eta bere aldaerak edo untxien serumaren diluzioak (100 µL/putzu) 4 orduz inkubatzen dira %1 BSA duen PBS indargetzailean.
- 5) Putzuak, PBS indargetzaileaz (200 µL/putzu) birritan garbitzen dira.
- 6) Fosfatasa alkalino entzima duen antigorputz sekundarioaren 100 µL/putzu (1:1000 diluzioan) gehitzen dira eta 50 minutuz inkubatzen da.
- 7) Putzuak PBS indargetzaileaz (200 µL/putzu) hiru aldiz garbitzen dira.
- 8) 0.1 M glizinan, 1mM MgCl₂, 1mM ZnCl₂ disolbatutako 4-nitrofenil fosfato disodio gatz hexahidratoaren 5 mg (50 µL/putzu) gehitzen dira eta 30 minutuz inkubatzen da.
- 9) Erreakzioa NaOH 3M erabiliz (50 µL/putzu) geldiarazten da eta erreakzioaren produktua, 405 nm-ko absorbantzia neurtuz kuantifikatzen da.

Chapter 3.1

***CONFORMATIONAL PLASTICITY
UNDERLIES MEMBRANE FUSION
INDUCED BY AN HIV SEQUENCE
JUXTAPOSED TO THE LIPID
ENVELOPE***



3. RESULTS

3.1 Conformational plasticity underlies membrane fusion induced by an HIV sequence juxtaposed to the lipid envelope

ABSTRACT

Envelope glycoproteins from genetically-divergent virus families comprise FPs that have been posited to insert and perturb the membranes of target cells upon activation of the virus-cell fusion reaction. Conserved sequences rich in aromatic residues juxtaposed to the external leaflet of the virion-wrapping membranes are also frequently found in viral fusion glycoproteins. These MPERs have been implicated in the promotion of the viral membrane restructuring event required for fusion to proceed, hence, proposed to comprise supplementary FPs. However, it remains unknown whether the structure–function relationships governing canonical FPs also operate in the mirroring MPER sequences. Here, we combine infrared spectroscopy-based approaches with cryo-electron microscopy to analyze the alternating conformations adopted, and perturbations generated in membranes by CpreTM, a peptide derived from the MPER of the HIV-1 Env glycoprotein. Altogether, our structural and morphological data support a cholesterol-dependent conformational plasticity for this HIV-1 sequence, which could assist cell-virus fusion by destabilizing the viral membrane at the initial stages of the process.

3.1.1. Introduction

During the early phase of the replication cycle, the HIV-1 particle fuses its lipid envelope with the plasma membrane of the CD4⁺ target cell ^{38,215}. The reaction is triggered after engagement of the Env with the cell receptor (CD4)/co-receptor (CXCR4 or CCR5), a specific recognition process that activates further refolding of the metastable native Env. Fusion activity of Env depends on the presence of the FP, a conserved sequence located at the N-terminus of the transmembrane subunit gp41 ^{216,217}. Following fusion triggering, the FP is propelled towards the target cell membrane and embeds therein due to its hydrophobic character ^{38,215}. Subsequently, helical regions within gp41 ectodomains refold into an energetically stable, trimeric 6-HB, whose formation brings together the merging membranes: the plasma membrane of the target cell, and the lipid envelope of the virus (Figure 3.1.1, see also Figure 1.2) ^{67,218,219}.

In analogy to FPs, insertion into the viral membrane of the C-terminal gp41 MPER sequence is postulated to further contribute to the overall process of membrane merger (Fig. 1, see also Figure 1.2) ^{140,147,148,151,186,220}. This sequence, sitting at the bottom of the Env complex is exceptionally enriched in aromatic residues that promote interactions with the membrane interface ^{190,191,221,222}. MPER insertion may be disruptive for the viral membrane, since peptides and constructs ^{49,223–225} derived from its sequence have been shown to exert virucidal effects ^{49,223–225}. The discovery that a number of antibodies targeting MPER can block membrane activity and infection, further underlines the importance of this region for the fusogenic function of the Env glycoprotein ^{222,226}.

There is structural evidence to support that the carboxy-terminal MPER sequence can combine with TMD residues of gp41 to form a continuous helix, at least in one of the conformational states that are accessible to the pre-fusion Env complex ^{76,146,157,159,161,178,227,228}. A peptide that spans this helix (CpreTM, Figure 3.1.1B), has been shown to induce lipid bilayer restructuring upon partitioning into Chol-enriched virus-like membranes ^{5,42,43,225}. However, it remains to be established whether structure–function relationships displayed by the standard N-terminal FP of gp41, also apply to this MPER-derived C-terminal sequence.

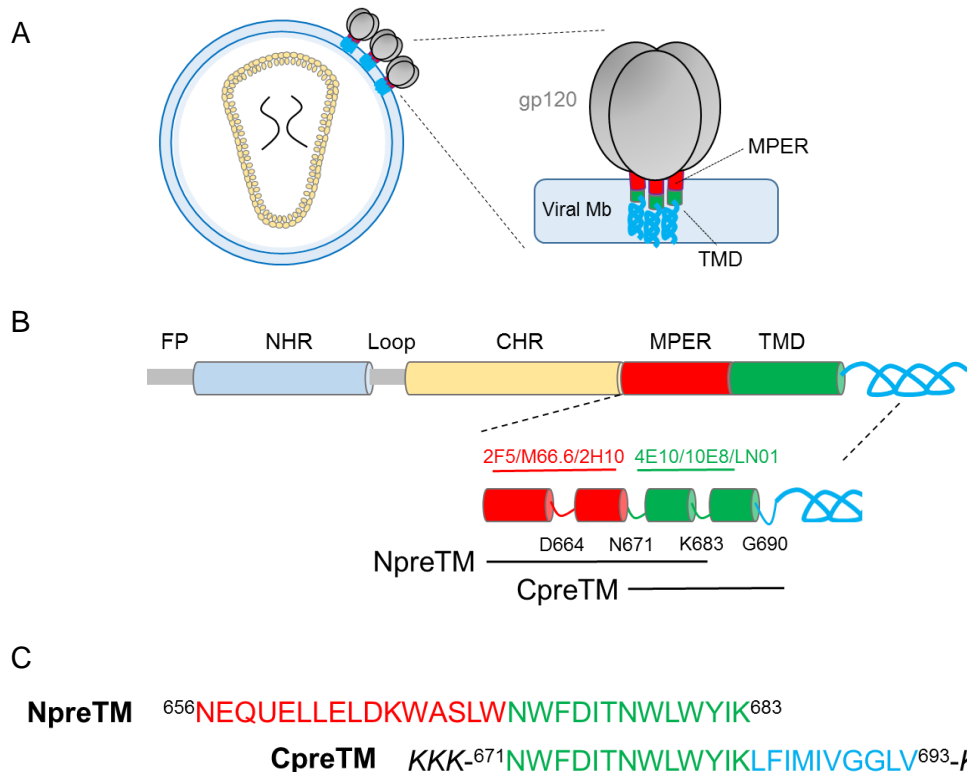


Figure 3.1.1. Designation of the HIV-1 CpreTM and NpreTM sequences used in this chapter. **(A)** Schematic displaying the general organization of the HIV-1 Env glycoprotein in virions (pre-fusion state). **(B)** Diagram showing the constituents of the gp41 subunit ectodomain and transmembrane anchor. Functional domains designated within its sequence include FP, NHR and CHR, amino- and carboxy-terminal helical regions, respectively; MPER and TMD. The MPER-TMD region contains epitopes for the recognition of several broadly neutralizing HIV antibodies as indicated. **(C)** Designation of the sequences covered by the CpreTM and NpreTM used in this chapter.

Cumulative experimental work using synthetic surrogates and model membranes has delineated physiologically relevant aspects of the FP function^{217,229,230}. High-resolution NMR studies reveal the adoption of continuous α -helical structures in membrane mimics^{231,232} whereas the combination of IR and Solid-State Nuclear Magnetic Resonance (SS-NMR) spectroscopy demonstrates that the α -helical conformation can convert into oligomeric β strand structures, a transition promoted by peptide density and the increase of the Chol concentration in the membrane²³³⁻²³⁵. Attenuated Total Reflectance (ATR)-IR studies further indicate that monomeric FP α -helices penetrate into lipid bilayers in an oblique angle^{236,237} while its oligomeric β -strand counterparts appear to associate with the main axis forming a 90° angle with respect to the membrane normal²³⁸.

Thus, regarding its conformational behavior, a hallmark of membrane-bound HIV FP appears to be its plasticity, which enables the transition from inserted α -helices, tilted

relative to the bilayer normal, into extended β -strands, lying almost parallel to the membrane plane^{216,217,234–236,238–242}. Studies in model systems suggest that these alternating conformations of the FP sequence can disrupt the lipid bilayer, breaching its permeability barrier and/or inducing aggregation and inter-bilayer mixing of lipids^{235,239,242–245}. Moreover, the membrane-inserted FP appears to modulate the elastic properties of the bilayer and facilitate the formation of the non-bilayer lipid intermediates required for fusion^{246–249}. In this context, the HR1 and HR2 helical domains within the ectodomain of gp41 are conceived as a mechanical device that brings the host-cell plasma membrane, primed for merger by the inserted FP, into contact with the viral membrane (Figure 1.2).

In this work, we combine conventional IR spectroscopy and two-dimensional correlation IR spectroscopy (2D-COS-IR), to analyze the conformation and orientation adopted by the CpreTM peptide upon reconstitution into lipid bilayers. In line with the notion that the sequences flanking the TMD anchors of fusion glycoproteins are endowed with a degree of conformational plasticity^{250–252}, our data reveal that the CpreTM helix can adopt membrane-inserted α -helical structures that convert primarily into an extended β -strand conformation in Chol-rich membranes. Occurrence of the extended conformation lying parallel to the membrane plane correlates with the induction of vesicle fusion as visualized by cryo-EM of vitrified specimens. Thus, we conclude that CpreTM bound to membranes displays structural features of canonical FPs, and propose a structure-based mechanistic model that couples CpreTM helix unfolding to membrane merger during the HIV-1 fusion cascade.

3.1.2. Methods

3.1.2.1 Reagents

The peptide sequence derived from the gp41 MPER-TMD region, KKK-NWFDITNWLWYIKLFIMIVGGLV-KK (CpreTM) (Figure 3.1.1) was produced by solid-phase synthesis using Fmoc chemistry as C-terminal carboxamides and purified by HPLC (estimated purity 97%). POPC and Chol were purchased from Avanti Polar Lipids (Birmingham, AL, USA). Rho was from Thermo Fisher Scientific (Waltham, Massachusetts, USA). HFIP was obtained from Sigma-Aldrich (St. Louis, Missouri, USA). Monoclonal antibody 4E10 (MAb4E10), kindly donated by D. Katinger (Polynum

Inc., Vienna, Austria), and rabbit anti-human-IgG-HRP (Santa Cruz Biotechnologies) were used to reveal the membrane-bound peptide.

3.1.2.2 CpreTM reconstitution in membranes

CpreTM-containing vesicles were prepared as described in 2.1.1.2 *section*. Phospholipid and cholesterol were dissolved in chloroform:methanol 1:2 (vol:vol) and mixed with CpreTM (dissolved in 100% etOH) at a peptide-to-lipid molar ratio of 1:50.

Effective incorporation of the peptide to the vesicles was ensured by peptide flotation in a sucrose gradient following 2.1.3 *protocol*.

3.1.2.3 Circular dichroism

CD measurements were carried out on a thermally-controlled Jasco J-810 circular dichroism spectropolarimeter as described in 2.3 *section*. CpreTM stock samples dissolved in DMSO, were lyophilized and subsequently dissolved in an aqueous buffer (2 mM HEPES, pH, 7.4) at 0.03 mM concentration with 2.5 %, 10 % or 25 % (v:v) HFIP. Spectra were measured in a 1 mm path-length quartz cell equilibrated at 25 °C. Data were taken with a 1 nm band-width, 100 nm/min speed, and the results of 20 scans per sample were averaged. Quantitative analysis of the spectra was carried out using the CDPro software²⁵³, as previously described²⁴⁷.

3.1.2.4 Transmission infrared spectroscopy

Infrared spectra were recorded in a Thermo Nicolet Nexus 5700 (Thermo Fisher Scientific; Waltham, MA) spectrometer equipped with a mercury-cadmium-telluride detector using a Peltier based temperature controller (TempCon, BioTools Inc., Wauconda, IL) with calcium fluoride cells (BioCell, BioTools Inc., Wauconda, IL) following 2.3.2 *protocol*. CpreTM-containing samples were lyophilized and subsequently prepared at 3 mg (peptide)/mL in D₂O buffer (PBS). Typically 370 scans were collected for each background and sample, and the spectra were obtained with a nominal resolution of 2 cm⁻¹. In the HFIP samples solvent contribution was subtracted from the original spectra before the data analysis to allow a reliable comparison between spectra.

Data treatment and band decomposition of the original amide I have been described elsewhere²⁵⁴. In brief, the number and position of bands were obtained from the

deconvolved (bandwidth = 18 and k = 2) and the Fourier derivative (power = 3 and breakpoint = 0.3) spectra. The baseline was removed before starting the fitting procedure and initial heights set at 90 % of those in the original spectrum for the bands in the wings and for the most intense component, and at 70 % of the original intensity for the rest of bands. An iterative process followed, in two stages. (i) The band position of the component bands was fixed, allowing widths and heights to approach final values; (ii) band positions were left to change. For band shape a combination of Gaussian and Lorentzian functions was used. The restrictions in the iterative procedure were needed because initial width and height parameters can be far away from the final result due to the overlapping of bands, so that spurious results can be produced. In this way, information from band position, percentage of amide I band area and bandwidth were obtained for every component. Using this procedure the result was repetitive. Mathematical accuracy was assured by constructing an artificial curve with the parameters obtained and subjecting it to the same procedure again. The number of bands was fixed on the basis of the narrowing procedures. The molar absorption coefficient for the different bands was assumed to be similar and within a + / - 3 % error.

To obtain the 2D-COS-IR maps, the Chol content was used to induce spectral fluctuations and to detect dynamic spectral variation in the secondary structure of CpreTM. Rendering of the two-dimensional synchronous and asynchronous spectra has been described previously²⁵⁵.

3.1.2.5 Electron microscopy

As initial screen to determine the optimal concentration, samples were first imaged by negative stain electron microscopy. 8 µL aliquots were adsorbed onto glow-discharged carbon coated copper grids, and negatively stained with 1% uranyl formate. Specimens were imaged with a JEM-1230 transmission electron microscope (JEOL Ltd. Tokyo) using an Orius SC1000 (4008 × 2672 pixels) cooled slow-scan CCD camera (Gatan Inc.) at the equivalent nominal magnification of 20000x, and defocus values between -2 and -5 µm. Selected samples were then vitrified and imaged using a JEM-2200FSC transmission electron microscope (JEOL Ltd. Tokyo) equipped with a field emission gun (FEG) operated at 200 kV and an in-column omega energy that helped us to record images with improved signal-to-noise ratio (SNR) by zero-loss filtering, using an energy selecting slit width of 30 eV centered at the zero-loss peak of the energy spectra. Digital images were recorded under low dose conditions using a 4 K x 4 K UltraScan 4000™ CCD camera (Gatan Inc.) at the equivalent nominal magnification of 50000x, and

defocus values between -1.5 and -4 μm . 4 μL aliquots were applied onto Quantifoil R 2/2 on 300 mesh cooper grids and C-flat R 1.2/1.3 on 400 mesh cooper grids plasma cleaned with air for 5 s using a PDC-002-CE plasma cleaner (Harrick Plasma). Grids were blotted and plunge frozen in liquid ethane with an automated Leica EM GP2 automatic plunge freezer (Leica Microsystems GmbH, Wetzlar).

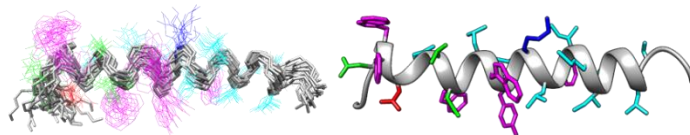
3.1.3. Results

3.1.3.1 CpreTM conformation in a low-polarity medium

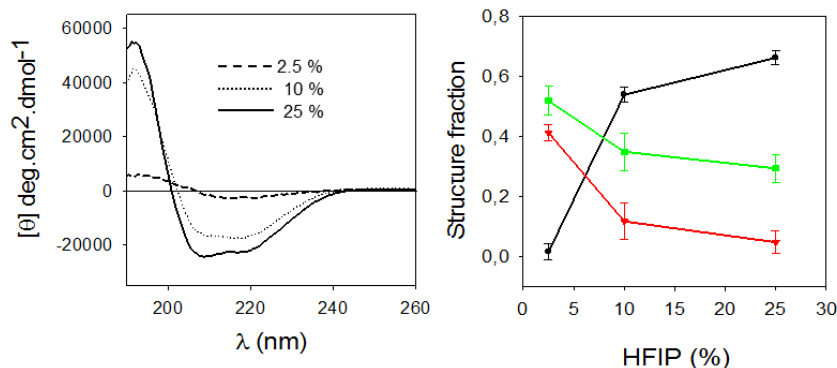
Before establishing the membrane-bound conformations of the CpreTM peptide, we analyzed the secondary structure adopted in a medium that mimics the low-polarity of lipid bilayers. As a reference, we employed the published NMR structure of monomeric CpreTM in buffer containing 25% (v/v) HFIP¹⁶¹. Figure 3.1.2A displays the superposition of the calculated models for the CpreTM structure in HFIP, and a representative single model (left and right panels, respectively). All calculated models were consistent with a predominantly α -helical geometry, with evidence for disordered regions limited to the COOH and NH₂ extremities. Panel B displays the CD spectra obtained for CpreTM in buffers with increasing HFIP content, and the quantitative analysis of the secondary structure composition (left and right panels, respectively). Consistent with peptide aggregation in solution, β -strands and turn/coil structures dominated the spectra at the lowest HFIP concentration (2.5% v/v), and diminished upon decreasing polarity. At the highest HFIP concentration where monomers are expected to be favored (25% v/v), the α -helix contribution was predominant (ca. 65%), whereas only a residual signal from peptide aggregation remained. In these samples, components attributable to the disordered conformations and turns amounted to ca. 30%.

Matching those findings, band decomposition of IR spectra obtained in 25% HFIP identified a majority of amide-I vibrational modes arising from helical conformers, with bands centered at 1665 cm^{-1} (3₁₀-helix), 1655 cm^{-1} (α -helix) and 1630 cm^{-1} (α -helix solvated)^{254,256,257} amounting to ca. 56% of the total band area (Fig. 3.1.2C). Besides, a band centered at 1642 cm^{-1} (ca. 34%) was ascribed to disordered coil structures, whereas that at 1677 cm^{-1} was attributed to turns (ca. 9%). Again, consistent with the monomeric state of the peptide (Panel A), the contribution of extended-aggregated conformations was negligible in these samples (< 1%).

A



B



C

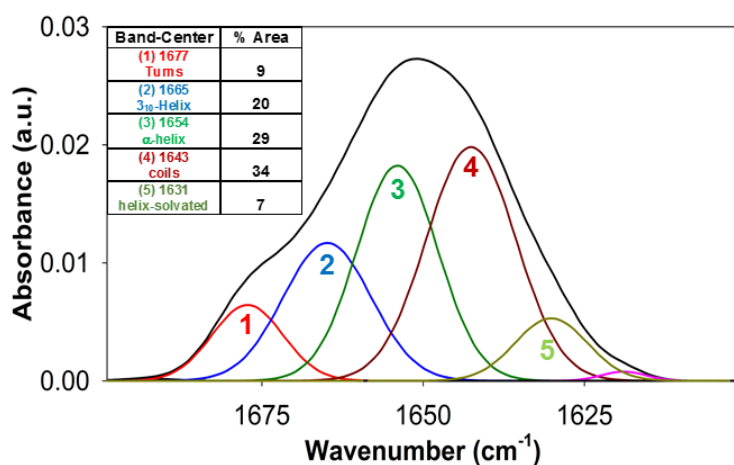


Figure 3.1.2. Structural analysis in a low-polarity medium. (A) NMR structure of the CpreTM peptide solved in 25% HFIP (v/v) (PDB code: 2MG2). (B) Left: CD spectra obtained at 25 °C in media containing increasing amounts of HFIP as indicated in the panel. Right: secondary structure fractions estimated from CDPro²⁵³. Means ± the standard deviation for the fraction values estimated with CONTIN-LL, CDSSTR, and SELCON3 are plotted. Black dots, red triangles and green squares depict the fractions of helix, strand and the sum of turns + unordered conformations, respectively. (C) IR spectrum in the amide-I region obtained in buffer containing 25 % HFIP (v/v). The absorption band was decomposed into different components. The original spectrum and the sum of the band components are superimposed and indistinguishable. The inset displays the secondary structure assignation for the main components (bands labeled with numbers 1 to 5) and the area percentages (rounded off to the nearest integer).

3.1.3.2 CpreTM conformation in lipid bilayers

We next reconstituted CpreTM in membranes by co-mixing it with lipids in organic solvent, followed by gentle evaporation and hydration (see section 2.1.1.2). Figure 3.1.3 compares the IR spectrum of CpreTM in solution with that obtained after reconstitution in lipid bilayers made of POPC (top and bottom panels, respectively). The amide-I region of the IR spectrum in solution displayed a prominent band centered at 1622 cm^{-1} , which together with high-frequency absorption in the $1680\text{--}1690\text{ cm}^{-1}$ region, denoted that a majority of peptide chains were unfolded/aggregated. In contrast, upon reconstitution in POPC bilayers, the maximum shifted to 1654 cm^{-1} , whereas the contribution of the 1620 cm^{-1} band was irrelevant. In these samples predominant helical conformers amounted to ca. 70 %. Besides, in comparison with the absorption band components measured in HFIP (Fig. 3.1.2C), the contribution of turns and disordered chains decreased, whereas the amide-I band became overall narrower. These spectral variations reflect a reduction in the conformational space accessible to the CpreTM chain upon reconstitution in lipid bilayers, consistent with the majority of the membrane-associated peptide adopting a canonical α -helical conformation.

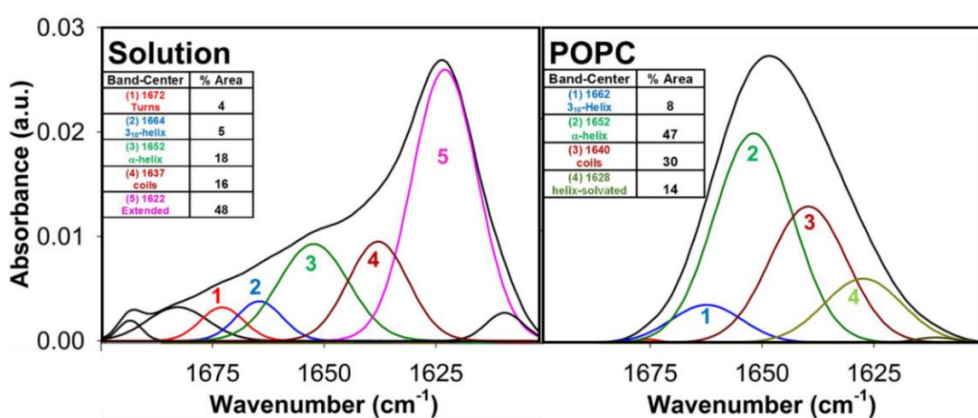


Figure 3.1.3. Reconstitution of CpreTM in lipid bilayers. Left and right IR spectra display respectively the amide-I components measured in buffer or after reconstitution of the peptide in POPC lipid bilayers (Peptide-to-lipid ratio, 1:50). Insets in both panels display the secondary structure assignation for the main band components and their area percentages.

3.1.3.3 Conformational changes in Chol-containing membranes

Chol is a major lipid of the HIV membrane required for virion infectivity^{45,47,56,258,259}. Therefore, we analyzed the conformation adopted by CpreTM reconstituted in membranes containing increasing Chol concentrations. Figure 3.1.4A displays the series of raw and deconvolved IR spectra as a function of Chol content in membranes (left and right panels, respectively). A shoulder centered at ca. 1620 cm⁻¹ could be already discerned in the samples that contained low Chol concentration, which evidenced an initial accumulation of extended chains. Samples containing the highest Chol concentrations displayed a more conspicuous band centered at 1622 cm⁻¹, consistent with a β -strand-like conformation dominating the secondary structure of the membrane-bound peptide under these conditions.

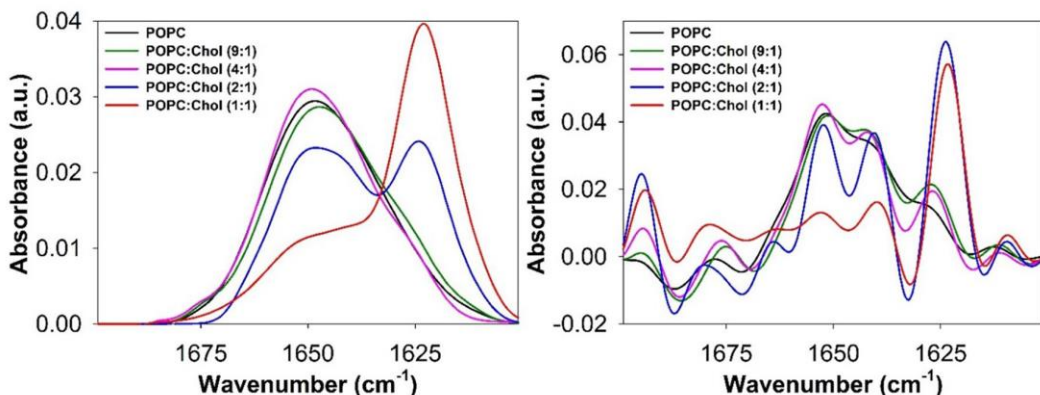
To get more insight into the CpreTM conformational changes induced by the membrane Chol concentration, we next performed the 2D-correlation analysis of the IR spectra in the corresponding amide-I band region^{260,261} (Figure 3.1.4B). We note that relevant effects detected on the 2D maps often reflect subtle changes in the relative contents of the amide-I band components. Therefore, in addition to the β -strand band that dominates in samples containing high concentrations of Chol (centered at ca. 1620 cm⁻¹), the analysis also revealed the evolution of the rest of the spectral components i.e., bands centered at ca. 1675, 1660, 1650, 1642 and 1635 cm⁻¹.

In the synchronous (Φ) 2D maps of CpreTM (Figure 3.1.4B, top panels), autopeaks indicated simultaneous changes in the bands composing the amide-I spectrum. In the 2D maps of the raw spectra (left), autopeaks were found centered at 1650 and 1620 cm⁻¹, whereas the single cross-relation negative peak 1620/1650 cm⁻¹ reflected that both vibrations were affected in-phase by Chol, the first component augmenting in intensity, the second diminishing. Higher resolution was attained using the Φ map based on the deconvolved spectra (right). Particularly, all helical components were evidenced as autopeaks centered at ca. 1635 cm⁻¹, 1655 cm⁻¹ and 1665 cm⁻¹, which could be observed together with cross-relation negative peaks 1620/1635 cm⁻¹, 1620/1655 cm⁻¹ and 1620/1665 cm⁻¹.

The corresponding asynchronous (Ψ) maps reflected the sequential order of events induced by the increase of Chol (Figure 3.1.4B, bottom panels)^{255,260,261}. The asynchronous peaks were positive (red contours) if the change in the first frequency occurred accelerated with respect to that in the second one, and negative (blue contours) if delayed. The positive correlation peak 1655/1665 cm⁻¹ detected in the raw-spectra maps, suggests the formation of less stable short regions deviating from canonical α -

helicity and adopting 3_{10} -helical geometries, whereas the negative one at 1620/1665 cm^{-1} supports the conversion of the 3_{10} -helix intermediates into extended strands.

A



B

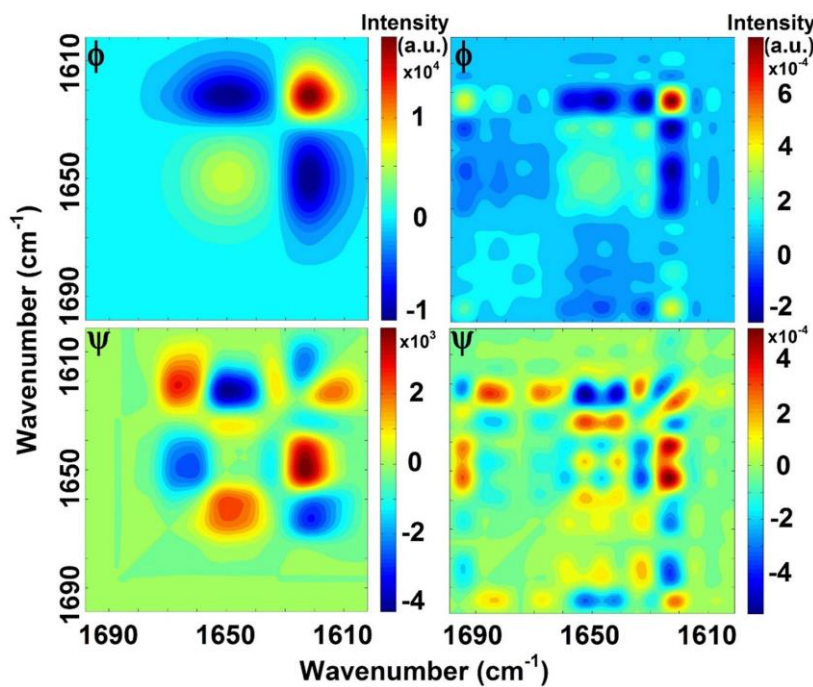


Figure 3.1.4. Conformations adopted by CpreTM as a function of the Chol content in membranes. (A) Amide I region IR spectra of CpreTM reconstituted in membranes (peptide-to-lipid ratio, 1:50) that contained increasing Chol concentrations as indicated in the panels. Raw and deconvolved spectra are shown (left and right panels, respectively). (B) 2D-COS IR analysis. Synchronous (top) and asynchronous (bottom) correlation map contours of the raw (left) and deconvolved (right) IR spectra obtained with increasing Chol concentrations are shown. Red peaks correspond to positive correlations and blue peaks to negative ones.

This pathway was also apparent in the Ψ map based on deconvolved spectra. In this case, an additional positive correlation peak was found for the pair 1635/1665 cm^{-1} . It is known that partial solvation of α -helical structures can give rise to low-frequency bands centered at ca. 1635–1630 cm^{-1} because of the cross-hydrogen bonds that can be formed with water^{45,256} (see also Figure 3.1.2C). Thus, we attribute the CpreTM absorption mode at 1635 cm^{-1} to a fraction of the helical structure not buried in the membrane, i.e., exposed to solvent and/or in contact with interfacial polar moieties. The positive correlation found at 1635/1665 cm^{-1} suggests that these solvated helices also unfold adopting 310-helical geometries, whereas the negative one at 1635/1655 cm^{-1} would be consistent with the buried helical fraction unfolding more readily than the solvent-exposed one upon increasing the Chol concentration.

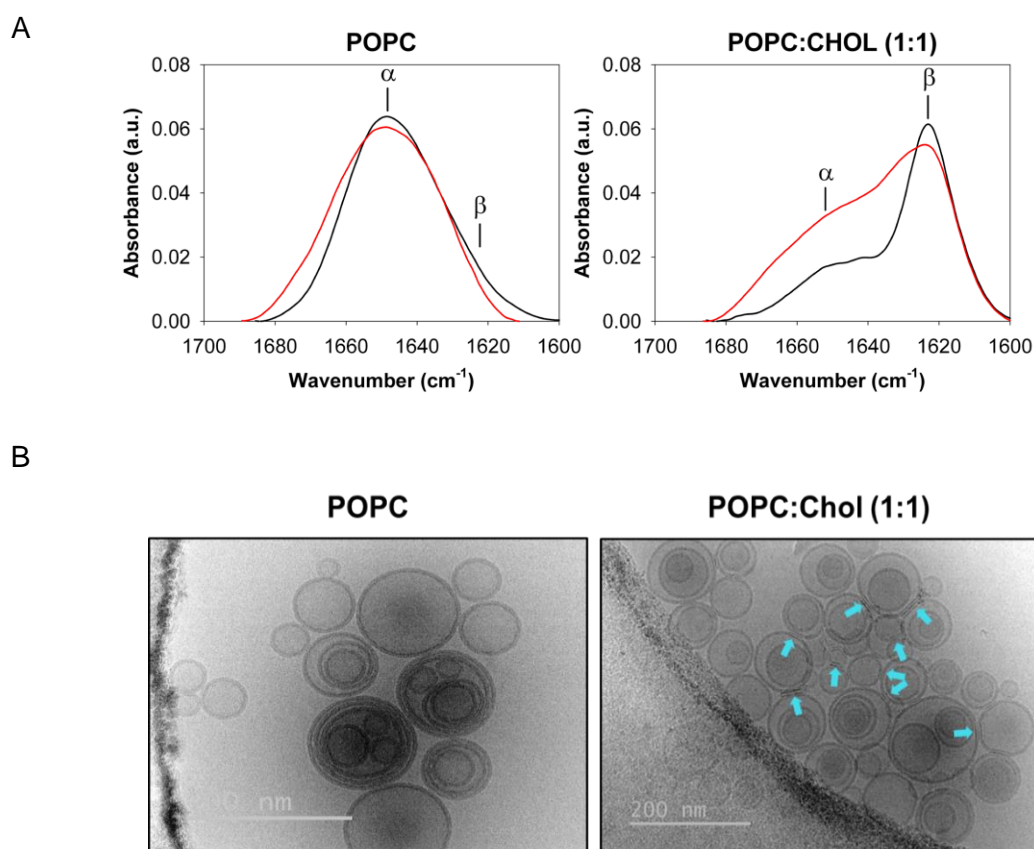


Figure 3.1.5. Conformations adopted in membranes by the NpreTM peptide and changes induced on vesicle morphology. (A) IR spectra (red lines) in the amide-I region obtained after reconstitution of NpreTM in POPC (left) or POPC:Chol 1:1 (right) membranes. Spectra of CpreTM measured under similar conditions have been added for comparison (black lines). (B) Cryo-EM images of POPC (left) and POPC:Chol 1:1 (right) vesicles containing NpreTM peptide. Arrows in the POPC:Chol sample indicate flat vesicle-vesicle contacts displaying a trilayer appearance, which are absent in the POPC samples. The peptide-to-lipid mole ratio was 1:50 in both panels.

Additional positive peaks were observed at 1655/1675 cm⁻¹ and 1635/1675 cm⁻¹, and a negative peak found at 1620/1675 cm⁻¹. This indicates that β -turns can also act as intermediates of the helix-to-strand unfolding process. In conclusion, upon increasing the Chol content in the membrane, β -turns/3₁₀-helical regions seem to be produced at the expense of the canonical α -helical conformations, and these intermediates appear to convert into extended strands.

To establish whether the C-terminal region accounted for the tendency of MPER to adopt extended conformations in membranes, we also analyzed the effect of Chol on the conformation adopted by NpreTM, a peptide overlapping with the aromatic-rich N-terminal stretch of CpreTM, but lacking its TMD residues (Figure 3.1.1). Following CpreTM's trend, NpreTM reconstituted in POPC membranes adopted a main helical conformation (Figure 3.1.5A). However, when reconstituted in POPC:Chol (1:1) membranes, β -strands did not dominate the overall conformation of the NpreTM peptide, supporting the implication of the membrane-buried CpreTM TMD residues in the conformational conversion promoted by Chol.

3.1.3.4 Changes in vesicle morphology induced by CpreTM reconstituted in membranes

Despite the differences in the attained conformation, the reconstituted CpreTM peptide incorporated to the same extent and quantitatively into vesicles containing different concentrations of Chol (Figure 3.1.6A). In contrast, Cryo-EM images revealed different morphologies for the peptide-containing vesicles, suggesting that the adopted conformations induced distinct patterns of membrane destabilization (Figure 3.1.6B,C and 3.1.7). Untreated control samples displayed spherical vesicles with heterogeneous sizes ranging in mean diameter from ca. 100 to 200 nm (Figure 3.1.6, B,C bottom panels). The α -helical peptide did not alter the overall morphology or size of POPC vesicles when incorporated at a 1:50 peptide-to-lipid dose (Figure 3.1.6B,C, top left panels). In contrast, an increase of extended conformations in the peptide-treated samples (Chol-containing membranes) correlated with a significant increase of the mean vesicle size (Figure 3.1.6B,C, top center and right panels). Particularly, in peptide-containing POPC:Chol (1:1) samples, massive aggregation and vesicle sizes in the range of 500 nm could be observed.

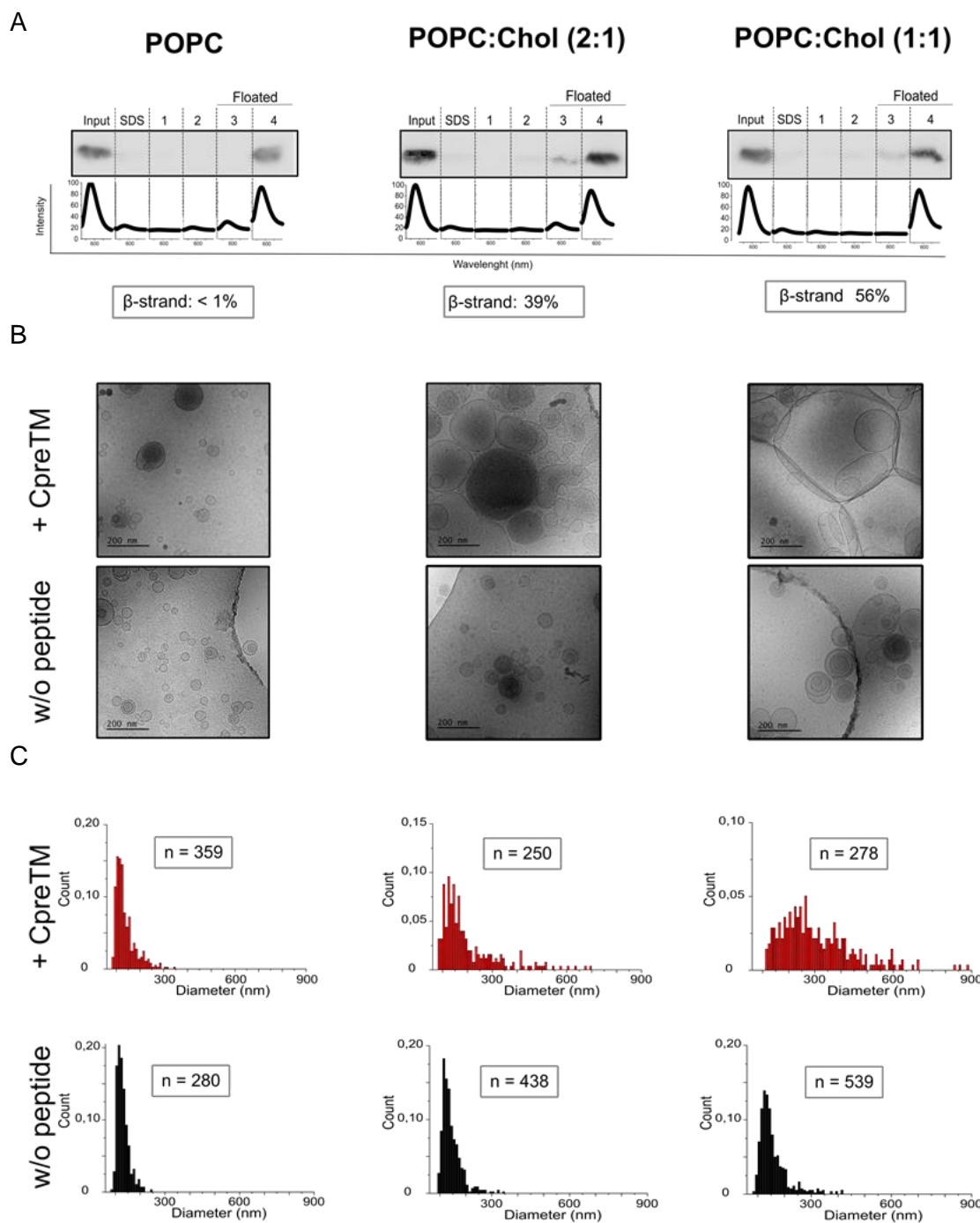
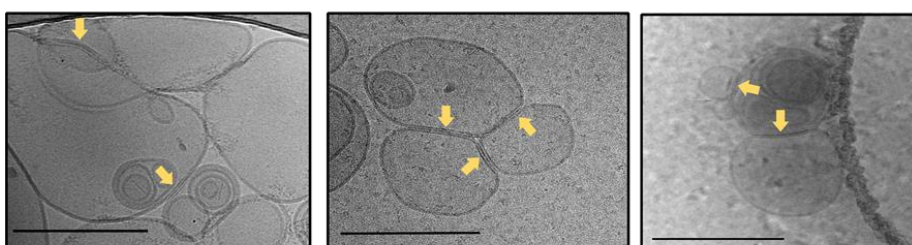


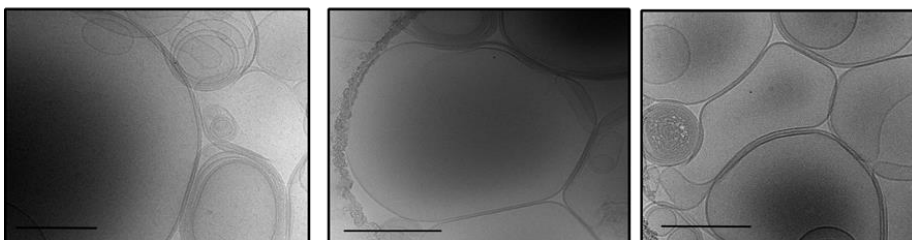
Figure 3.1.6. Vesicle morphology changes induced by the different conformations adopted by CpreTM in membranes. (A) Vesicle flotation analysis. Incorporation to vesicles of CpreTM was verified after ultracentrifugation in a sucrose gradient (peptide-to-lipid mole ratio, 1:50). The presence of the peptide in the floated and non-floated fractions of the gradient and in the original sample (input) was revealed by Western Blot analysis after Tris-Tricine SDS-PAGE separation. Fluorescence emission spectra below reveal the presence of Rhodamine-labeled vesicles in the collected fractions. The amount of extended β -strand adopted by the peptide in the samples is indicated below the panels (values determined in the spectra of Figure 3.1.5A after band decomposition). (B) Vesicle morphology by cryo-EM. Images obtained for vesicles containing reconstituted peptide are shown in the top-panels. Bottom panels display images of vesicles devoid of peptide. (C) Vesicle size distribution as determined from the diameters measured in cryo-EM images. The sizes of oval-shaped vesicles were determined by measuring their major axes. Conditions as those in the previous panel.

Figure 3.1.7 displays more detailed views of the effects exerted by CpreTM on vesicle morphology. The peptide reconstituted in POPC membranes did not affect the stability of the vesicle samples, whereas its inclusion into POPC:Chol membranes induced tight vesicle-vesicle contacts (lipid bilayer aggregation) and increased the mean diameter of the vesicles (membrane fusion). Notably, POPC:Chol (1:1) vesicles containing the reconstituted NpreTM control peptide displayed a pattern of tight bilayer aggregation, which did not result in an increase of the mean vesicle size (Figure 3.1.5B). Thus, it appears that completion of the fusion process required the presence of the CpreTM-TMD residues.

Aggregation



Fusion



Restructuring

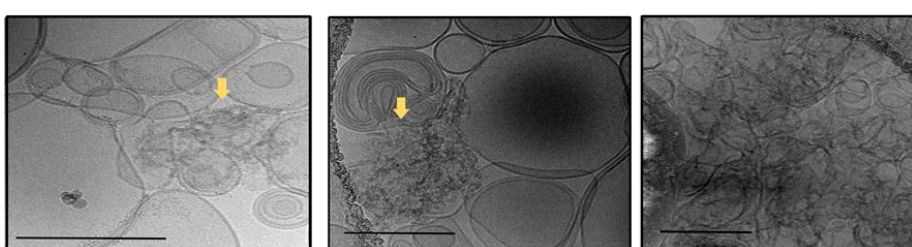


Figure 3.1.7. Morphological changes induced by CpreTM reconstituted in Chol containing vesicles as determined by cryo-EM. In images illustrating the aggregation pattern, flat zones of tight bilayer-bilayer contact are indicated by the yellow arrows. Lipid aggregates with spongy morphology are also indicated by yellow arrows. The peptide was incorporated at a peptide-to-lipid ratio of 1:50 (mol:mol). Scale bars: 200 nm.

Lipid aggregates with spongy morphology also accumulated sporadically in certain areas of CpreTM-containing POPC:Chol vesicles (Figure 3.1.7, bottom panels). The occurrence of lipid aggregates reminiscent of non-lamellar arrangements suggested that, following an FP-like fashion^{217,246–249}, the CpreTM peptide could also facilitate the formation of highly curved lipid structures involved in membrane merger²³⁰. Moreover, an inspection by AFM of SBLs containing reconstituted peptide revealed that CpreTM disrupted the lipid continuity of the solvent-accessible membrane monolayer, and increased the amount of force required to break the bilayer (Figure 3.1.8). Thus, it appears that inclusion of CpreTM at doses leading to vesicle fusion did not facilitate membrane deformation by increasing curvature or reducing bilayer stiffness²³⁰.

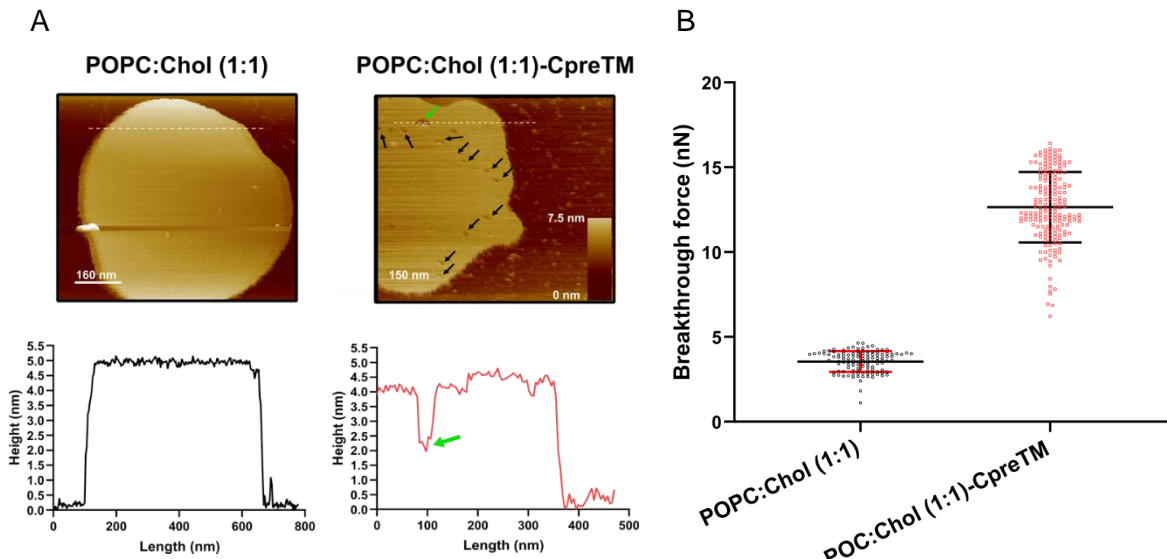


Figure 3.1.8. Atomic Force Microscopy characterization of supported lipid bilayers. A) Image and cross section of POPC:Chol (1:1) lipid bilayers without (left) and with CpreTM (right). The presence of the reconstituted peptide modifies the membrane producing holes (black arrows). The cross section, white dotted-line, shows that only the outer layer is affected (green arrow). **B)** Breakthrough force of POPC:Chol and POPC:Chol + CpreTM bilayers. The control bilayer without peptide shows a significantly lower breakpoint force (3.5455 ± 0.6151 , Mean \pm SD) than that containing the reconstituted peptide (12.65 ± 2.077 , Mean \pm SD). In both panels, the peptide-to-lipid mole ratio was 1:50 in the samples containing CpreTM.

3.1.4. Discussion

Studies in model systems support a predominant α -helical conformation for monomeric forms of the membrane-bound HIV FP, which appear to insert tilted relative to the membrane normal^{237–239,243,262}. In addition, the membrane-inserted FP helix can undergo conformational changes leading to the formation of extended β -strands, which have been associated with the perturbation of the lipid bilayer architecture and the promotion of lipid mixing during membrane fusion^{235,238,239,243–245,263,264}. Such conformational plasticity would be at odds with the stagnant α -helical conformation generally assumed for the MPER-TMD sequences of gp41 in the context of the Env glycoprotein^{146,157,159–162,265}. However, challenging the existence of a single MPER conformation after biogenesis, several studies support that a substantial portion of the membrane-embedded MPER can exist in an extended conformation during the gp41 refolding process that accompanies fusion activation (Figure 3.1.9 A)^{161,164,219}. Epitope peptides resolved in complex with antibody fragments, also suggest that partly extended MPER chains can be targeted by certain antibodies^{95,266}. In a more general sense, it has been argued that sequences flanking viral glycoprotein TMD helices might unfold adopting β -strand conformations, and contribute to the promotion of the fusion process by imparting negative curvature to the bilayer²⁵⁰.

Here, we employed IR spectroscopy approaches to analyze the conformations accessible to the membrane proximal CpreTM sequence reconstituted in membranes. Together, the spectroscopy results confirm that the reconstitution process results in a membrane-inserted CpreTM α -helix, which is partially exposed to solvent. Chol appears to induce conformational changes leading to the formation of β -strands. The occurrence of CpreTM extended chains is associated with the destabilization of the lipid bilayers, as suggested by cryo-EM imaging and AFM characterization.

The model displayed in Figure 3.1.9 B integrates these findings in a general model of HIV-1 gp41-induced membrane fusion. The prefusion Env complex may alternate compact (1) with more open conformations (2), and it is likely that in these structures the helices spanning the MPER-TMD sequence could kink at different positions. Recent structural studies support that, at least in one of those conformational states, a straight and continuous CpreTM helix inserted in a subtle angle would be the target to antibodies exerting broad and potent neutralization^{157,228}.

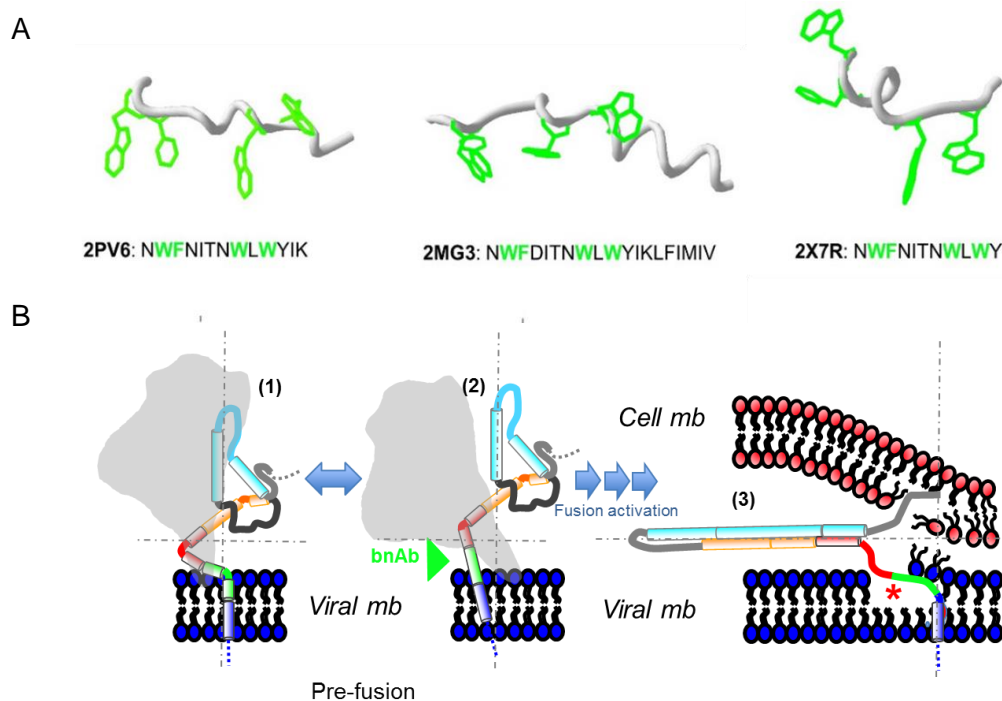


Figure 3.1.9 Proposed role for CpreTM sequence in an extended conformation during the process of Env-mediated HIV fusion. **A)** High-resolution structures of MPER sequences displaying sections of extended chain conformation. PDB accession numbers used to render the panel together with the sequence ranges covered are displayed below. **B)** Mechanistic model: Compact (1) and open (2) conformations of the Env glycoprotein are postulated to interchange spontaneously before engagement with receptor/co-receptor (one Env monomer is depicted for simplicity). The cartoon representing the gp41 subunit is based on the pre-fusion X-ray structure (PDB accession code: 4TVP) and illustrates the relative positions of the most important constituents in the ectodomain (same color code as in previous Fig. 3.1.1). Upon activation of the fusion cascade, helical regions reposition to interact with each other initiating the assembly of the 6-HB, whereas the main axis of the complex align with the membrane plane (3). This process is proposed to be facilitated by the extension of the MPER chain connecting the enlarging 6-HB to the TMD. Insertion of the MPER connection into the viral membrane in an extended conformation may prime it for fusion (*), creating poorly solvated spots to facilitate initial interbilayer contacts and/or generating a lipid bridge between the merging membranes.

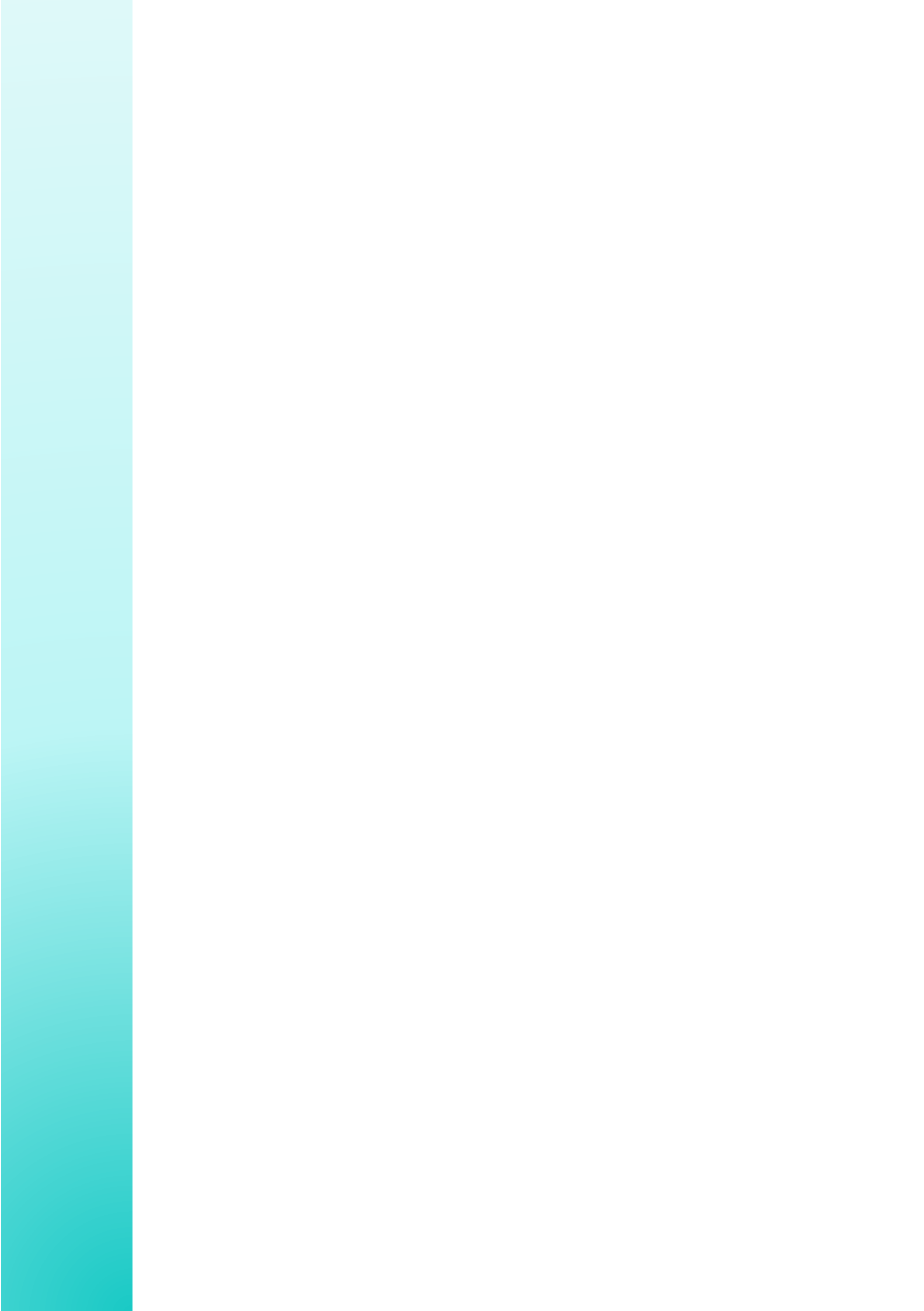
Subsequent activation of the fusion process involves the refolding of the gp41 helical domains HR1 and HR2 (depicted in cyan and yellow colors, respectively) to initiate the formation of a compact 6-HB. Establishment of the extensive helix-helix hydrophobic interactions between HR1 and HR2 implies the relocation of the helical sections and the reorientation of the complex main axis with respect to the membrane (3). We infer that the initial formation of the 6-HB likely requires extension of the C_α chain at sections joining the emerging complex to the membrane-inserted sequences. These extended hydrophobic chains, most prominently at FP and MPER areas, could associate with membrane surfaces helping to overcome repulsive hydration and electrostatic forces, as the cell and viral membranes approach pulled by the growing 6-HB hairpin. Furthermore,

our data suggest that the CpreTM sequence could also break lipid continuity of the viral membrane external monolayer (Figure 3.1.8), generating poorly solvated hydrophobic spots where the initial contacts could be established between the approaching bilayers.

Overall, the experimental data presented in this study support the notion that a similar conformational plasticity underpins the membrane activity of the FP and CpreTM region during the initial (and transient) stages of HIV-1 fusion, but caution that effects of these sequences on the elastic properties of membranes involved in the process might be different. In this regard, we note that the present work provides no hints as to how the membrane-inserted structures of the FP or MPER evolve at later stages of the fusion process. It has been argued that the FP could first assemble as β -sheets on membrane surfaces, but later convert into α -helices to complete fusion²³³. Thus, at least theoretically, it is possible that at later stages of the fusion process the CpreTM sequence also attains secondary structures and membrane topologies that differ from those described in this work. Such alternative conformations might allow completion of the 6-HB structure and/or modulate the elastic properties of the membrane to facilitate fusion²⁴⁹.

Chapter 3.2

***CHOLESTEROL CONSTRAINS THE
ANTIGENIC CONFIGURATION OF
THE MEMBRANE-PROXIMAL
NEUTRALIZING HIV-1 EPITOPE***



3.2 Cholesterol constrains the antigenic configuration of the membrane-proximal neutralizing HIV-1 epitope

ABSTRACT

The Env enables HIV-1 cell entry through fusion of host-cell and viral membranes induced by the transmembrane subunit gp41. Antibodies targeting the C-terminal sequence of the membrane-proximal external region (C-MPER) block the fusogenic activity of gp41 and achieve neutralization of divergent HIV-1 strains and isolates. Thus, recreating the structure that generates broadly neutralizing C-MPER antibodies during infection is a major goal in HIV vaccine development. Here, we have reconstituted a peptide termed CpreTM-TMD1 in a membrane environment. This peptide contains the C-MPER epitope and the minimum TMD residues required for the anchorage of the Env glycoprotein to the viral membrane. In addition, we have used antibody 10E8 variants to gauge the antigenic configuration attained by CpreTM-TMD1 as a function of the membrane Chol content, a functional determinant of the HIV envelope and liposome-based vaccines. Differential binding of the 10E8 variants and the trend of the IgG responses recovered from rabbits immunized with LPFs, suggested that Chol may restrict 10E8 accessibility to the C-MPER epitope. Our data ruled out the destabilization of the lipid bilayer architecture in CpreTM-TMD1-containing membranes, and pointed to the perturbation of the helical conformation by lipid packing as the cause of the antigenic configuration loss induced by cholesterol. Overall, our results provide additional insights into the structural basis of the Env complex anchoring to membranes, and suggest new approaches to the design of effective immunogens directed against the near pan-neutralizing HIV-1 epitope C-MPER.

3.2.1. Introduction

Fusion with the target host-cell membrane marks the beginning of the HIV-1 replication cycle^{3,38,215,267}. The transmembrane subunit gp41 of the Env promotes the process by the concerted action of two types of structural elements: (i) two highly conserved membrane-inserting regions, one at the free N-terminus and the other proximal to the viral membrane²¹⁷ and (ii) helical domains or HRs that refold forming an energetically favorable, trimeric 6-HB⁶⁷. The membrane-inserting sequence at the N-terminus constitutes the FP (reviewed in ref²¹⁷). After fusion triggering by receptor (CD4)/coreceptor engagement (CXCR4 or CCR5), the FP is propelled toward the cell membrane and embeds therein due to its hydrophobic character^{38,215,267}. However, the tip of the FP remains exposed to the solvent in one of the conformational states of the prefusion Env complex^{34,268}, and is accessible to antibodies that neutralize HIV-1 with modest potency and breadth^{269,270}.

The sequence inserting into the viral membrane, also known as MPER, is exceptionally enriched in aromatic residues that promote interactions with the membrane interface^{140,151,162,190}. Structural analyses suggest that the C-MPER residues (Env residues 671–683, HXB2 numbering), can combine with N-terminal residues of the TMD (Env residues 684–690) into a single continuous helix^{76,146,159–161,178,227}. CpreTM, a peptide spanning this region can induce lipid bilayer restructuring upon partitioning into Chol-enriched virus-like membranes^{42,43,225}. Thus, the membrane activity of this sequence, unleashed after fusion activation, is postulated to help the fusion process proceed by perturbing the highly rigid HIV lipid envelope⁵.

Importantly, the conserved C-MPER sequence is immunogenic during infection^{12,172,271} which underscores the existence of a structurally stable state of this Env region accessible to B-cell receptors, at least within one of the conformational states visited by the prefusion complex^{77,78}. Further supporting the existence of a structurally defined C-MPER epitope common to diverse prefusion Env variants, all anti-C-MPER bnAbs that have been isolated so far (e.g., 4E10, 10E8, or LN01), recognize the same surface of the C-MPER helix, and consistently display the broadest coverage among the HIV-1 bnAb classes^{12,141,145,146,170,172,173}. Using superresolution microscopy we have recently demonstrated that C-MPER is indeed accessible to the bnAbs 4E10 and 10E8 on the surface of intact virions⁵¹.

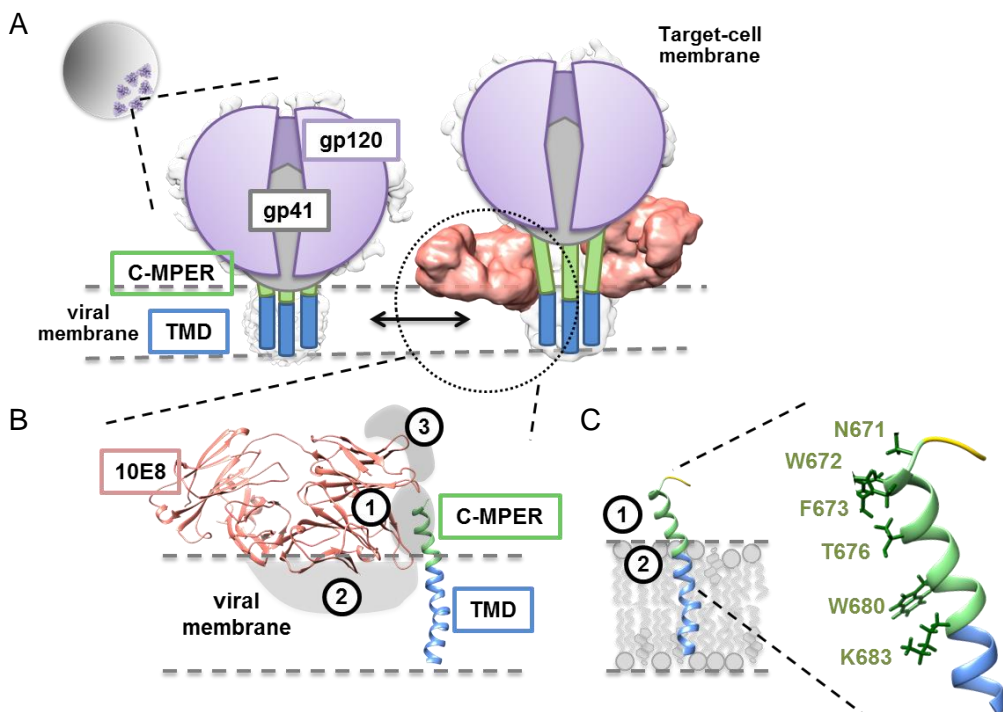


Figure 3.2.1. Schematics depicting the accessibility of the HIV-1 neutralizing epitope MPER at the viral membrane interface. A) Model for accessibility of C-MPER based on cryo-EM reconstructions of native Env complexes⁷⁶. Back contours are derived from detergent-solubilized Env trimers, without (left, EMDB-3308) or with 10E8 bound (right, EMDB-3312). Transition between both states would result in accessibility to MPER helix in native Env (green). **B)** Structural model for 10E8 recognition of the helical C-MPER epitope inserted in membranes. The position of the TMD residues (blue) was rendered by superimposing residues N671–V689 of MPER in complex with Fab 10E8 (PDB ID: 5GHW) onto structures of MPER-TMD peptides (PDB ID: 2MG1, 2MG2). Numbers denote the interaction-accommodation surfaces in the Fab after binding to C-MPER epitope (see main text). **C)** Schematics of the LPF vaccines used in this study, which contain the reconstituted CpreTM-TMD1 peptide (in ribbon representation, lysine tag depicted in yellow). Left panel: numbers denote the attempt to recover through vaccination antibodies that bind to C-MPER epitope (1); and develop a surface to accommodate the membrane interface (2). Right panel: antigenic face of the C-MPER helix. Main epitope residues that interact with the 10E8 paratope are depicted in stick representation.

Atomic structure resolution of bnAbs 4E10, 10E8, and LN01 in complex with lipids^{96,146,181} or with epitope-peptides elongated to include TMD residues^{146,178} in combination with cryo-EM reconstructions of Env-Fab complexes^{76,173}, has provided a model for the molecular recognition of C-MPER at the virus membrane surface (Figure 3.2.1). According to this model, monomers of continuous helices spanning the MPER-TMD region stick out the membrane with similar topologies, with angles ranging from slightly tilted to almost perpendicular to the membrane plane, and antibodies nonspecifically adsorbed to the interfacial region of the membrane approach, the C-MPER epitope laterally. However, in analogy with the dynamic conformation of the prefusion Env ectodomain^{34,77,78,268}, cumulative evidence supports the conformational pliability of

MPER-TMD helices, which, depending on the sequence range considered, membrane dose, and lipid composition, may adopt in the unbound conformation membrane structures differing in oligomeric state, insertion angle, or C-MPER epitope exposure^{159,160,162,168,190,227,272}. Interestingly, recent studies report a transmembrane helix tilt angle of ca. 45° for a TMD peptide elongated at its C-terminus¹⁵⁹ or the total occlusion of C-MPER antigenic face into the membrane when a peptide is elongated to contain the full MPER sequence at its N- terminus¹⁶². Thus, the membrane-inserted states adopted by these peptides appear to be incompatible with the proposed mechanism of lateral Env docking of anti-C-MPER antibodies^{76,96,178,181}.

In an attempt to mimic the membrane-inserted MPER structure that elicits anti-C-MPER antibodies, in this study we have addressed the reconstitution of the C-MPER epitope recognized by bnAb 10E8 in liposome vaccines. To that end, we employ peptides that combine the C-MPER epitope with the minimal TMD anchor of Env previously described by Yue et al.¹⁸⁷. In addition, we have generated bnAb 10E8 mutants that can be used as reference standards to measure the antigenicity profile of the reconstituted peptides. We demonstrate that the C-MPER epitope can attain a correct configuration in membranes, but that high concentration of Chol induces its concealment. We propose a model that, besides providing new insights into the molecular basis of Env-anchoring to the viral membrane, may inform the design of immunogenic formulations aimed at boosting anti-C-MPER bnAb production.

3.2.2. Methods

3.2.2.1 Reagents

The peptide sequences derived from the gp41 MPER-TMD region, KKK-NWFDITNWLWYIKLFIMIVGGLV-KK (see *peptides derived from gp41 MPER-TMD region*, CpreTM) and KKK-NWFDITNWLWYIKLFIMIVGGLVGLRIVFA-KKKK (CpreTM-TMD1) were produced by solid-phase synthesis using Fmoc chemistry as C-terminal carboxamides and purified by HPLC. POPC, phosphatidic acid (egg, chicken) (PA), Chol, SM (egg, chicken), and Lipid A detoxified (*Salmonella Minnesota R595*) were purchased from Avanti Polar Lipids (Birmingham, AL, USA). NBD, Rho, and Laurdan fluorescent probes were from Thermo Fisher Scientific (Waltham, Massachusetts, USA). Abberior STAR RED (KK114) was obtained from Abberior (Göttingen, Germany). Goat anti-Human IgG (Fab specific)-AP was obtained from Invitrogen (Carlsbad, California, USA)

and goat anti-Rabbit IgG-AP from Thermo Fisher Scientific (Waltham, Massachusetts, USA).

3.2.2.2 Production of Fab 10E8 and its variants

Fab 10E8 antibody sequence was cloned in the plasmid pColaDuet and expressed in *Escherichia coli* T7-shuffle strain as previously described in 2.2.1 section. For the preparation of mutant Fabs, the KOD-Plus mutagenesis kit (Toyobo, Osaka, Japan) was employed following the instructions of the manufacturer. For confocal microscopy experiments, position C216_{HC} of the Fabs was modified in vitro with a sulfhydryl-specific iodacetamide derivative of the KK114 probe.

3.2.2.3 Functional Characterization of Fab 10E8 and its variants

Pseudovirus Production

HIV-1 PsVs were produced as described in 2.7.1 section.

Super-Resolution STED Microscopy

EGFP Vpr-labeled virions were immobilized on 0.1% poly-L-lysine coated coverslips after 10 minutes of incubation. Coverslips were then blocked with 2 % BSA and antibodies incubated in blocking buffer for 1 hour at a concentration of 25 µg/mL (ca. 0.5 µM). In the case of unlabeled Fabs, the samples were incubated for an extra hour with donkey antihuman STAR RED antibodies (1/200 dilution). Finally, samples were fixed with 2% PFA and mounted in Mowiol//DABCO mounting medium. Imaging was performed using an Abberior STEDYCON system. STAR RED was excited using a 640 nm pulsed laser line and depleted with using a 775 STED laser. EGFP was excited with a 488 nm pulsed laser line. Emission was collected using avalanche photodiodes. The emission filters were 650–700 nm for the super-resolved STAR RED signal and 501–552 nm for the confocal EGFP signal. Pixel size was fixed at 20 nm pixel, dwell time was 10 µs, and line accumulation was set to 5. Only samples prepared in parallel and imaged within the same session were compared. To allow for comparison of independent experiments, intensity was normalized to the median 10E8 intensity after background noise subtraction. Image analysis was performed using the Python code developed previously^{51,273}. The software automatically identified EGFP.Vpr positive particles using an intensity-maximum finding algorithm on a Gaussian smoothed image ($\sigma = 2.0$), and

quantified the number of collected photons in a circular region of interest of 14 pixels (280 nm) in diameter. It performed the same quantification in a random region presenting no Vpr.EGFP signal, which was used as a reference background signal.

Cell Entry Assays

HIV entry was determined using TZM-bl target cells as described in 2.7.2 section. Neutralization levels after 72 hours were inferred from the reduction in the number of GFP positive cells as determined by flow cytometry using a BD FACSCalibur Flow Cytometer (BD Biosciences, San Jose, California, USA).

3.2.2.4 LPF production

To prepare CpreTMTMD1 containing LPFs at peptide-to-lipid molar ratio of 1:50, lipids and the CpreTM-TMD1 dissolved in etOH were mixed in organic solvent prior to the production of the liposomes as explained in 2.1.1.2 section.

3.2.2.5 Rabbit immunization and response analysis by ELISA

New Zealand White rabbits were immunized at the antibody production service from the CID-CSIC (Barcelona, Spain) as detailed in 2.8.1 section. LPFs were prepared including 0.25 mol % Lipid A as adjuvant²¹⁴ and were lyophilized. Two rabbits were inoculated intradermally following 2.8.1 protocol.

Antibody response was analyzed by ELISA. LPFs were dissolved in PBS at a concentration of 500 µM and 1:50 CpreTM-TMD1:lipid (mol:mol ratio) and immobilized (100 µL/well) ON onto C96 Maxisorp microplate wells (Nunc, Denmark). The plates were blocked for 2 h with 3% (w/v) BSA in PBS and incubated with either the Fabs or rabbit sera for 4 hours. The binding of the Fabs or sera IgGs was detected by incubation for 50 min with 1:1000 dilution of alkaline phosphatase-conjugated goat antihuman IgG F(ab)2 (Invitrogen, Carlsbad, CA, USA) or goat anti-Rabbit IgG (Thermo Fisher Scientific (Waltham, MA, USA) respectively, which then catalyzed a color reaction for 30 minutes with 1 mg/mL p-nitrophenyl phosphate substrate (VWR International, Radnor, Pennsylvania, USA) in 0.1 M glycine, 1 mM MgCl₂, 1 mM ZnCl₂, pH 10.4, that could be measured by absorbance at a wavelength of 405 nm in a Synergy HT microplate reader (Bio-TEK Instruments Inc., VT, USA).

3.2.2.6 Single-vesicle assays for membrane stability

GUVs were produced by spontaneous swelling as described in 2.1.1.1 section. In brief, 0.125 mg lipid was codissolved in 100 μ L CHCl₃:CH₃OH (9:1) with the fluorescent probes Laurdan (1 mol %) or NBD (2 mol %). When required, CpreTM-TMD1 peptide (dissolved in 100% etOH) was included in organic phase at 1:50 peptide-to-lipid ratio.

GUV-Fab binding experiments

For binding experiments, NBD-labeled GUVs with increasing concentrations of Chol and with or without the CpreTM-TMD1 peptide (1:50 peptide-to-lipid molar ratio) were used. The GUVs were added to a bovine serum albumin (BSA)-blocked microscope chamber that already included 250 nM of 10E8-based Fabs conjugated with the KK114 probe at residue C216_{HC}, and were incubated for 15 min prior to imaging.

GUV-LUV heterotypic fusion experiments

NBD-labeled POPC:Chol:SM (2:2:1 mol:mol) GUVs devoid of peptide were added to a suspension of Rho-labeled LUVs previously incubated with the CpreTM peptide or to a suspension of Rho-LPFs bearing CpreTM-TMD1, both at 1:50 peptide-to-lipid molar ratio, and were incubated for 15 minutes prior to imaging.

GUV permeabilization assays

NBD-labeled CpreTMTMD1 bearing GUVs were added to a BSA-blocked microscope chamber that already included the unconjugated and soluble KK114 dye, and were incubated for 15 minutes prior to imaging.

Images for these three assays were acquired and quantified as described in sections 2.4.1.3, 2.4.1.1 and 2.4.1.2 respectively. Relative extents of Fab-GUV binding or LUV-GUV fusion were obtained by measuring the fluorescence intensity of KK114 or Rhodamine, respectively, along the equatorial plane of the GUV images. Extents of permeabilization were calculated for each vesicle after 15 minutes of incubation with KK114 following Equation 2.3.

Membrane Packing Analysis by Multiphoton Fluorescence Microscopy

Images were acquired on a Leica TCS SP5 II microscope (Leica Microsystems GmbH, Wetzlar, Germany) as described in 2.4.1.5. *section*. For multiphoton excitation, the sample was illuminated with a 780 nm beam from a femtosecond-pulsed titaniumsapphire Mai-Tai Deepsee (Spectra-Physics, Berlin, Germany) laser. GUVs were imaged through a $\times 63$ water-immersion objective (NA = 1.2) and 512 \times 512 pixel images were acquired at 400 Hz per scanning line. Fluorescence emission was collected by nondescanned (NDD) hybrid detectors, as they offer higher sensitivity compared to photomultipliers. NDD 1 collected the blue edge of the emission spectrum at 435 ± 20 nm and NDD 2 collected the red edge at 500 ± 10 nm. For GP measurements unilamellar GUVs were selected and imaged at the equatorial plane to avoid photoselection. GP values were calculated as described in *section 2.4.1.5* following Equation 2.4.

3.2.2.7 Infrared Spectroscopy

Infrared spectra were recorded in a Bruker Tensor 27 spectrometer equipped with a mercurycadmium-telluride detector using a Peltier-based temperature controller (TempCon, BioTools Inc., Wauconda, IL) with calcium fluoride cells (BioCell, BioTools Inc., Wauconda, IL) and following *protocol 2.3.2*. Data treatment and band decomposition of the original amide I as described in²⁵⁴.

3.2.3. Results

3.2.3.1 Design of a C-MPER epitope peptide with a membrane anchor.

The model in Figure 3.2.1 A reflects the capacity of the native Env trimer for sampling different conformational states⁷⁸ with the C-MPER epitope becoming accessible to the bnAb 10E8 within one of such states⁵¹. Figure 3.2.1 B displays a detailed view of 10E8 docking to Env in the prefusion state^{76,178,181}. From this model one can infer that 10E8 binding to Env would freeze the CpreTM region in an upright position, preventing further interaction with the viral membrane and, hence, fusion to proceed. Figure 3.2.1 B highlights the three elements of the Fab 10E8 involved in the efficient engagement with the C-MPER epitope at membranes, namely, (1) the specificity binding pocket, (2) an

accommodation surface with the membrane interface, and (3) an area in contact with the Env complex ectodomain^{12,178,181}. As explained in the diagram depicted in Figure 3.2.1 C, in this study we seek to reproduce the components (1) and (2) of the interaction by reconstituting in liposome vaccines the peptide CpreTM-TMD1 (Env residues 671–700, HXB2 numbering). This peptide encompasses the full 10E8 epitope and a minimal membrane anchor of Env¹⁸⁷. In addition, it contains Lys-tags to increase solubility at both ends of the molecule¹⁶¹. In contrast to the shorter CpreTM peptide that destabilizes the membrane architecture^{5,42,225} or longer peptides that seem to conceal the C-MPER epitope^{159,162,272}, we expected the CpreTM-TMD1 peptide to span the lipid bilayer without affecting its integrity, and to expose the antigenic face of the C-MPER helix accessible for its engagement with antibodies and B-cell receptors (Figure 3.2.1 C, right). Thus, in our approach we reasoned that a scaffold peptide with a minimal TMD would force the upright orientation of the helix and ensure at the same time an efficient exposure of the C-MPER epitope at the membrane interface.

3.2.3.2 Functional Characterization of bnAb 10E8 variants used to assess C-MPER exposure

Fab 10E8 binding to membranes containing CpreTM-TMD1 reflects the accessibility to the C-MPER epitope at the membrane surface. As explained above, Fab binding implies not only the adequate fitting of the specificity pocket of the antibody to its MPER epitope, but also the correct positioning of the antibody at the membrane interface. Thus, in our approach we assumed that alteration of the Fab surface that accommodates the membrane interface might promote or diminish the capacity of 10E8 to bind its epitope. Following this rationale we generated two Fab 10E8 variants that, along with the WT Fab, were used as standard references to gauge the correct membrane topology of the C-MPER epitope (Figure 3.2.2 A). The LC.S65W mutation added a Trp at the Fab surface that accommodates the viral membrane, and was expected to enhance the binding of the Fab to Env by increasing its affinity for the membrane interface^{51,274}. Conversely, the HC.W100bD mutation was designed to interfere with the membrane insertion of the CDRH3 of the Fab^{178,213}.

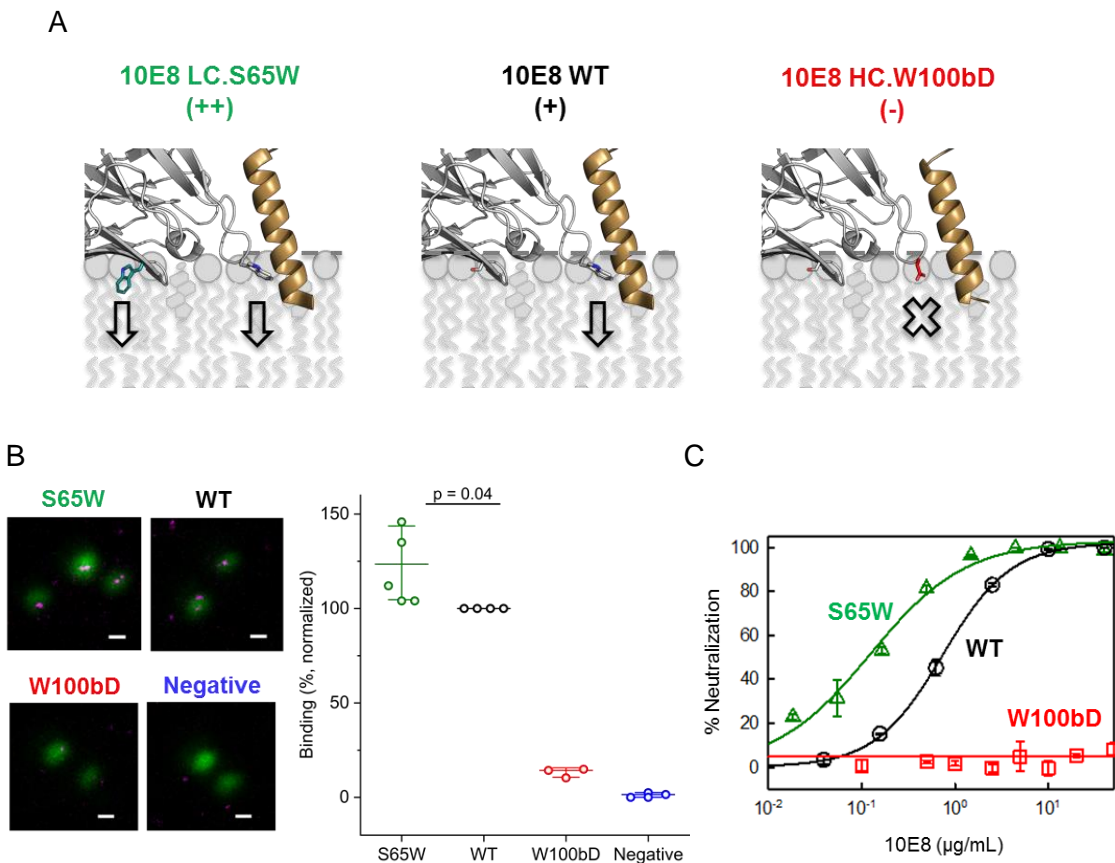


Figure 3.2.2. Functional properties of Fab 10E8 variants. **A)** Structural model of gp41 C-MPER at the membrane interface in complex with Fab 10E8 WT (PDB ID: 5GHW, middle panel). LC.S65W and HC.W100bD variants are depicted in left and right panels, respectively. HC.W100b residue and mutated residues LC.S65W and HC.W100bD are displayed in stick representation. Arrows indicate the potential capacity of each Fab to anchor to the membrane. **B)** Binding of Fab 10E8 WT and its mutants to native Env, measured by quantitative STED microscopy. Left: micrographs of HIV virions (EGFP.Vpr confocal signal, green) and 10E8 variants (STAR RED, magenta). Scale bar is 200 nm. Right: STED intensity signals (sum of collected photons) detected on single virions for each antibody were normalized to the signal of Fab WT after background subtraction. Each point is an independent experiment, middle horizontal bar represents the median, and whiskers the SD. The number of individual virions analyzed in every experiment was at least 150 and typically around 400 for every. Negative corresponds to viruses untreated with Fabs. **C)** Neutralization potency of 10E8 Fab variants. Dose-response curves follow cell entry inhibition measured against HIV-1 JR-CSF Env PsVs. Data for WT, LC.S65W and HC.W100bD are shown with circles (black), triangles (green), and squares (red), respectively, and correspond to mean values (\pm SD) from two replicate wells in a representative experiment.

Super-resolution fluorescence microscopy experiments confirmed the differential binding of the 10E8-based Fabs to native Env on intact virions⁵¹. STED microscopy offers a spatial resolution of <40 nm, below the size of HIV virions (around 125 nm), which allowed us to unequivocally identify the antibody signal coming from viral particles and resolve features within them²⁷⁵. Moreover, due to the linear nature of STED microscopy, the number of photons recorded is directly proportional to the amount of fluorescent

molecules, which permitted quantification of antibody binding⁵¹. Figure 3.2.2 B displays microscopy images of individual Vpr.EGFP-labeled viral particles incubated with Fab 10E8 WT or its variants, LC.S65W and HC.W100bD (left panels), whose binding to Env on the particles was visualized by directly labeling Fabs with the STED-able Aberior STAR RED (also known as KK114) dye and also using a STAR RED-labeled secondary antibody. As hypothesized, quantitative analysis of the antibody signal in individual virions followed the trend: 10E8-LC.S65W > 10E8-WT > 10E8-HC.W100bD, with an average 24 % increased binding of the LC.S65W variant to Env as compared to the WT version, and an 87% binding decrease of the HC.W100bD mutant (Figure 3.2.2 B right panels). The capacity of these Fab 10E8 variants to bind to MPER on intact virions further correlated with their neutralization potency (Figure 3.2.2 C). Therefore, we conclude that this binding pattern has to be reproduced by any relevant peptide epitope proposed as a vaccine candidate targeting 10E8-like antibody responses.

3.2.3.3 C-MPER accessibility in LPFs containing reconstituted CpreTM-TMD1

Chol acts as modulator of the structure–function of integral membrane proteins, thereby affecting the exposure of cell surface/membrane anchored therapeutic targets such as GPCRs, ion channels, transporters, or growth factor receptors^{276,277}. Folding of the gp41 MPER-TMD region also takes place in the Chol-enriched environment of the viral membrane^{47,49}; hence, this compound is assumed to play a role in C-MPER immunogenicity and its molecular recognition by 10E8. Furthermore, the stability and immunogenicity of liposome-based vaccine formulations are customarily enhanced by inclusion of Chol in the lipid composition¹⁹⁰. Using the Fab 10E8 variants described in the previous section, we next determined the exposure of the C-MPER epitope in LPFs proposed as vaccines, which consisted of the CpreTM-TMD1 peptide reconstituted into liposomes composed of POPC:PA and 0, 20, 40, or 50 % Chol (Figure 3.2.3). LPFs were generated by mixing the CpreTM-TMD1 peptide with POPC:PA:Chol lipids in organic phase prior to generation of the liposome particles. Sucrose density gradient ultracentrifugation proved full incorporation of CpreTM-TMD1 to membranes after the reconstitution procedure (Figure 3.2.4 A). Moreover, the resulting LPFs did not differ significantly in size as measured by DLS.

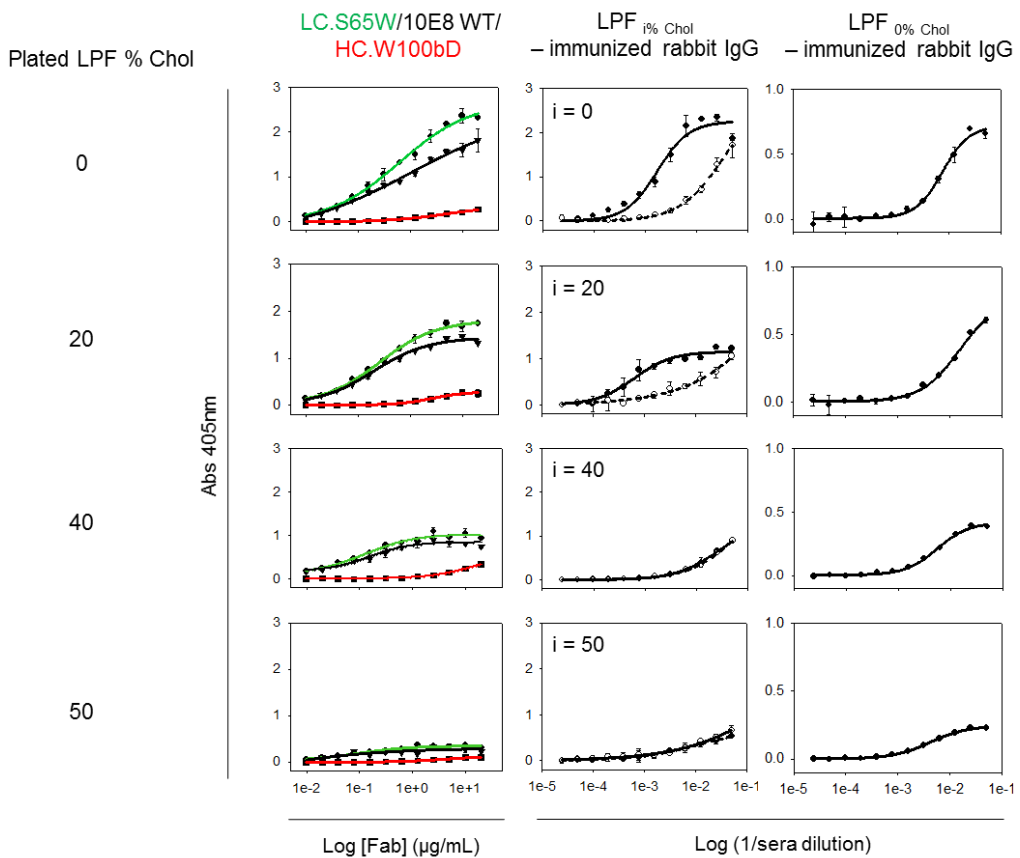


Figure 3.2.3. Antigenic profile and immunogenicity of liposome-peptide formulations. ELISAs were performed with LPFs containing CpreTM-TMD1 (peptide-to-lipid mole ratio, 1:50) that were coated on plates at a concentration of 500 µM and containing increasing concentrations of Chol as indicated in the panels. Plotted absorbance values are means (\pm SD) from two replicate wells. Left panels: comparative binding of Fab 10E8 variants WT (black line and filled triangles), LC.S65W (green line and filled circles) and HC.W100bD (red line and filled squares). Middle panels: immunogenicity of LPFs, as measured by the presence of IgG antibodies in the sera of two different rabbits after immunization. Signal of the pre-immune sera was subtracted. Right panels: cross-reactivity of IgG produced in sera of rabbits immunized with LPFs devoid of cholesterol, against LPFs with increasing cholesterol concentration. Sera from the two animals were pooled and the IgG levels in the mixture subsequently detected by ELISA. In all cases, experimental values were adjusted to sigmoid dose-response curves.

Binding of Fab 10E8 variants to LPFs coated on ELISA plates followed in all instances the expected trend for a correctly exposed epitope: 10E8-LC.S65W > 10E8-WT >10E8-HC.W100bD, but the binding levels decreased greatly in samples containing the highest Chol concentrations (Figure 3.2.3 left panels). Thus, high doses of Chol seemed to conceal the 10E8 epitope of the reconstituted CpreTM-TMD1 peptide. Similar results were obtained for KK114-labeled 10E8 variants interacting with CpreTM-TMD1 peptide GUVs made of the same lipid mixtures (Figure 3.2.4).

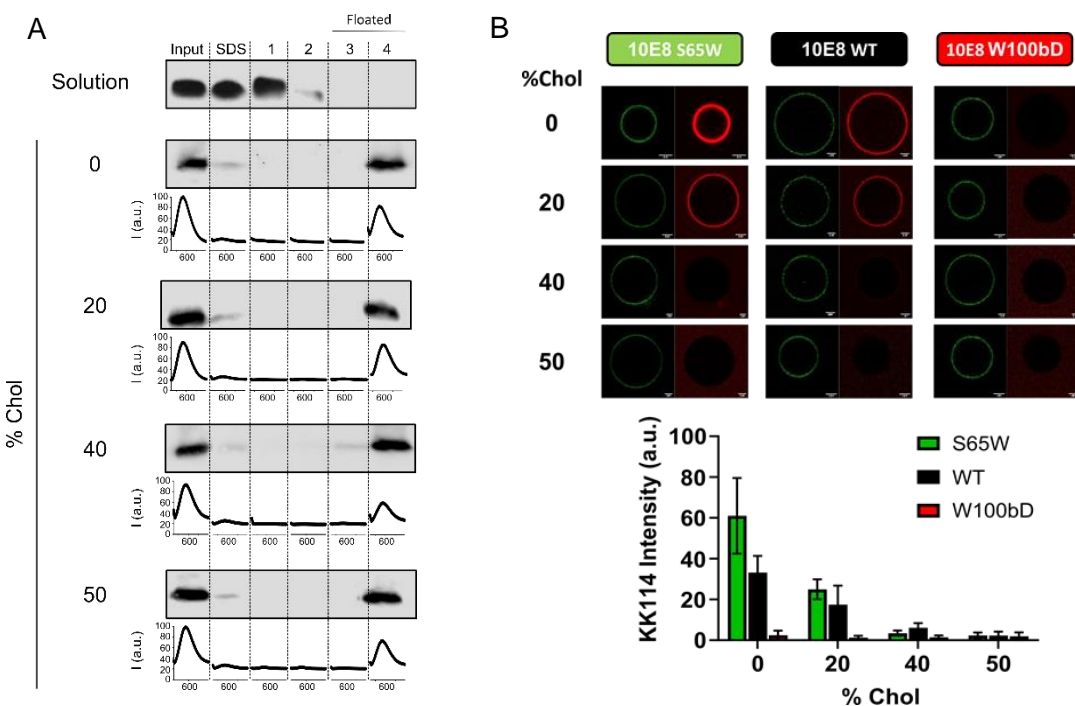


Figure 3.2.4. Incorporation and single vesicle approach of CpreTM-TMD1 liposomes containing increasing cholesterol concentrations. **A)** To rule out inefficient/differential incorporation of the peptide, LPFs were subjected to ultracentrifugation in a sucrose gradient after the reconstitution process. The presence of CpreTM-TMD1 peptides in the floated and non-floated fractions of the gradient and in the original sample (input) was revealed by Western Blot analysis after Tris-Tricine SDS-PAGE separation. Line plots below the panels display the fluorescence emission of the Rhodamine probe, revealing the presence of liposomes. Negative control sample containing the peptide in solution without liposomes is shown on the top. **B)** Binding of Fab 10E8 variants to GUVs containing CpreTM-TMD1 and increasing concentrations of Chol. Binding of fluorescently labeled KK114-10E8 LC.S65W (left), KK114-10E8 WT (middle) and KK114-10E8 HC.W100bD Fabs (right), rendered in red, to NBD labelled GUVs (green) containing increasing cholesterol concentrations. Micrographs display confocal images of GUVs at the equatorial plane and all were rendered with equal contrast and brightness to best appreciate the difference in emission intensity. The bottom plot displays KK114 fluorescence intensity quantification at the equatorial plane of the GUVs in each sample.

A similar trend was observed for the serum IgG produced after immunization of rabbits with the LPF vaccines. Thus, the amount of IgG that bound to LPF immunogens also decreased with the content of Chol present in the formulations (Figure 3.2.3, center panels). Interestingly, IgG produced in rabbits immunized with the LPF devoid of Chol, also trended to lower binding to the LPFs containing increasing concentrations of Chol (Figure 3.2.3, right panels). Thus, Chol may have restricted the accessibility of B-cell receptors to C-MPER, and also that of the IgGs produced upon immunization with LPFs bearing an accessible C-MPER epitope.

3.2.3.4 Stability of liposome vaccines with reconstituted CpreTM-TMD1

Membrane-active peptides can generate fusion-related perturbations in lipid bilayers²¹⁷. We have previously reported that preloading Chol-enriched vesicles with CpreTM rendered them competent for subsequent lipid mixing with target vesicles^{5,43}. Therefore, CpreTM can alter the membrane integrity of Chol-enriched membranes to make them competent for fusion.

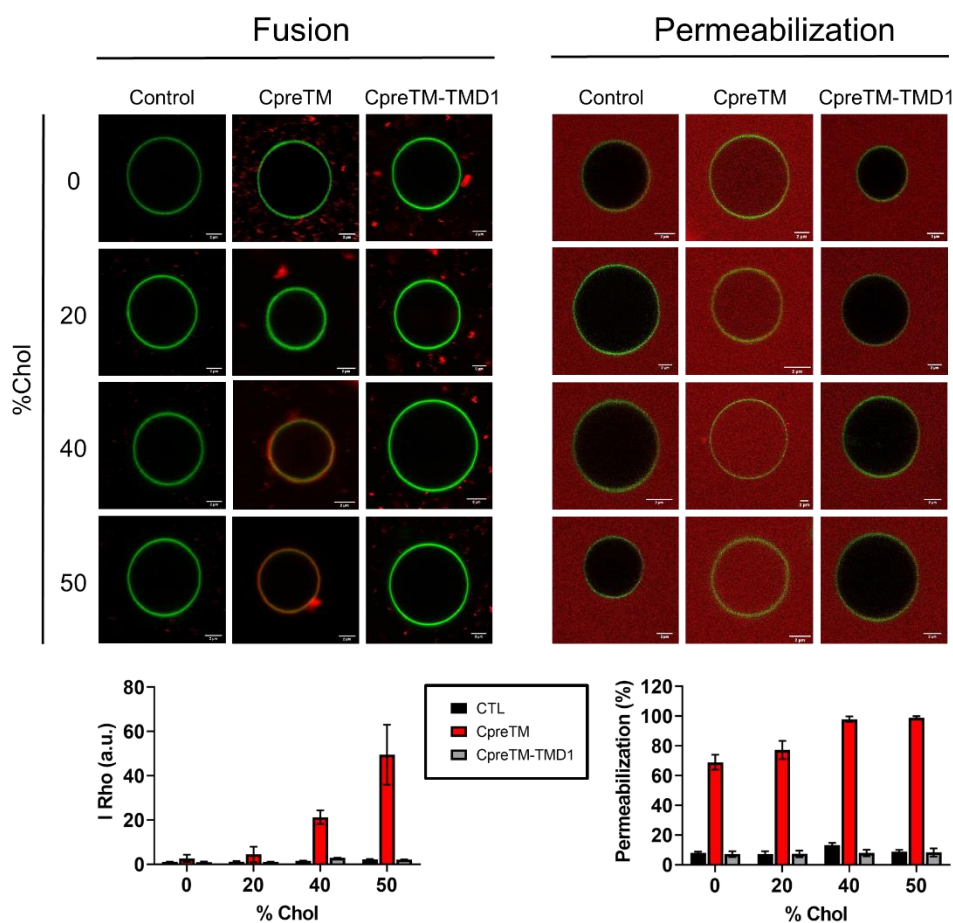


Figure 3.2.5. Stability of CpreTM-TMD1-containing lipid bilayers measured in single-vesicle assays. In the left panel, channel-merged confocal fluorescence microscopy images of a heterotypic fusion assay between NBD-labeled GUVs mimicking the outer leaflet of cell plasma membrane (green) and Rho-labeled LPFs of varying cholesterol concentrations (red) in the absence (control, CTL) or presence of CpreTM or CpreTM-TMD1 peptides (1:50 peptide-to-lipid mole ratio) is shown. Rho dye transfer to GUV membranes is indicative of lipid-mixing. The bottom plot shows the relative extents of fusion obtained by measuring the fluorescence intensity of the Rho dye at the membrane of each GUV after co-incubation with LUVs for 60 min (mean fluorescence values \pm SD of 5 different vesicles per composition). In the right panel, channel-merged micrographs of single GUV permeabilization assays are shown. NBD-labeled GUVs matching the lipid composition of the LPFs (green circumferences) and containing CpreTM, CpreTM-TMD1, or without peptide (CTL), were immersed in a solution containing the water-soluble KK114 fluorescent probe (red background). The presence of KK114 inside the vesicles indicates effective permeabilization. The bottom plot shows relative permeabilization levels after 60 minutes of incubation (mean fluorescence values \pm SD of 5 different vesicles per composition).

Since vesicle fusion with cellular membranes might diminish the fraction of C-MPER epitope accessible for engagement with the components of the immune system, we next analyzed whether CpreTM-TMD1-containing liposome vaccines were also inherently unstable and prone to fusion (Figure 3.2.5 left, panel). To test this, we used a heterotypic fusion assay, in which GUVs that mimicked the composition and curvature of the cell plasma membrane external leaflet were the targets for LPFs primed for fusion by incubation with C-MPER containing peptides. Incubation of GUVs with CpreTM-primed LPFs led to the homogeneous labeling of the GUV membranes with the fluorescent LPF label, indicative of LPFs mixing their membrane lipids with those of GUVs. Consistent with previously published bulk measurements^{5,43}, this effect was only observed when CpreTM was administered together with vesicles containing high concentrations of Chol. Conversely, incubation of fluorescently labeled CpreTM-TMD1 liposome vaccines with target GUVs did not lead to dye transfer under any condition, demonstrating that CpreTM-TMD1-containing LPFs are not prone to fusion, not even when they contain a high proportion of Chol.

To inquire whether the non-fusogenic CpreTM-TMD1 peptide reconstituted in Chol-containing membranes could still perturb locally the integrity of the lipid bilayer, we next determined the permeability of the membranes composing the different LPF vaccines also using a single-vesicle approach⁴¹. Confocal micrographs of GUVs matching the lipid composition of the LPFs, and containing CpreTM-TMD1 are depicted in Figure 3.2.5. In addition, vesicles lacking peptide (CTL) or vesicles treated with the peptide CpreTM were used as a control for negative permeabilization or effective permeabilization, respectively^{41,42}. Both untreated and CpreTM-TMD1-containing GUVs were viewed as dark (empty) spheres surrounded by the NBD-labeled lipid bilayer (depicted in green color), against a background containing the permeant and soluble KK114 fluorescent probe, (rendered in red color). In contrast, incubation with the CpreTM peptide resulted in the red labeling of the internal compartments, consistent with the permeabilization of the lipid bilayer to the dye in the external solution⁴¹.

Even though the absence of bilayer perturbations in samples that contained CpreTM-TMD1 was apparent after microscopic examination, we also performed quantitative measurements of fluorescence in selected GUVs (lower panels of Figure 3.2.5). These data further illustrate the absence of peptide-induced effects (i.e., ground-like levels of Rho or KK114 fluorescence in membrane or lumen, respectively).

3.2.3.5 Lipid packing changes and peptide conformational transitions in LPFs

Overall, the previous results demonstrate that the reconstituted CpreTM-TMD1 peptide is devoid of the membrane activity of the CpreTM section, suggesting that membrane restructuring is not the cause of the C-MPER epitope concealment observed in Chol-rich LPFs. Chol also induces a dose-dependent lipid packing increase when incorporated into lipid bilayers²⁷⁸. It has been suggested that the “cholesterol recognition/interaction amino acid consensus” motif⁶⁷⁹ LWYIK/R⁶⁸³ present in CpreTM-TMD1 could sequester Chol^{225,279}, and interfere with lipid packing, making bilayers more fluid, a biophysical effect that may condition immunogenicity of the LPFs¹⁹⁰. Thus, we next performed two-photon fluorescence imaging of Laurdan-stained GUVs to quantitatively determine lipid packing in the liposome-based vaccines that contained different amounts of Chol^{49,225}. The emission spectrum of Laurdan changes in response to polarity. In a membrane context, changes in polarity are ascribed to differences in lipid packing, which influences water accessibility. The GP ratiometric parameter quantifies Laurdan’s emission spectral shift from tightly packed bilayers (high GP value) to loosely packed membranes (low GP value), thus providing an *in situ* estimation of membrane packing.

Figure 3.2.6 A displays GP images of POPC:PA GUVs containing increasing Chol concentrations. The bottom panels include vesicles that incorporated the reconstituted CpreTM-TMD1 peptide. Mean average GP values increased with Chol concentration in the samples, as expected from the ordering effect exerted by this compound in lipid bilayers. Besides, the measured GP values demonstrated that incorporation of the peptide had little effect on membrane order levels, ruling out that the reconstitution process and/or potential specific interactions with Chol could affect lipid packing in LPFs.

It has been additionally argued that lipid packing augmented by Chol can affect the accommodation of the transmembrane helices^{278,280}. Thus, we next established the influence of Chol on the conformation adopted by CpreTM-TMD1 in LPF vaccines (Figure 3.2.6 B). Infrared spectra in the amide-I region of CpreTMTMD1 reconstituted in POPC:PA LPFs exhibited absorption centered at 1654 cm⁻¹, indicative of a main α -helical conformation adopted by the peptide²⁵⁴. Appearance of a shoulder could be discerned in LPF samples that contained increasing amounts of Chol, which was evidenced as a band centered at ca. 1620 cm⁻¹ at the highest concentration of the compound. The growth of this band component reflected accumulation of extended chains, a product of peptide partial unfolding. Spectral changes could also be observed within the 1670–1660 cm⁻¹ range, ascribed to absorption by conformers rich in 3₁₀-helix and turns. A relative contribution of the different conformations to the overall CpreTM-

TMD1 structure in membranes was obtained after band decomposition of the LPF spectra.

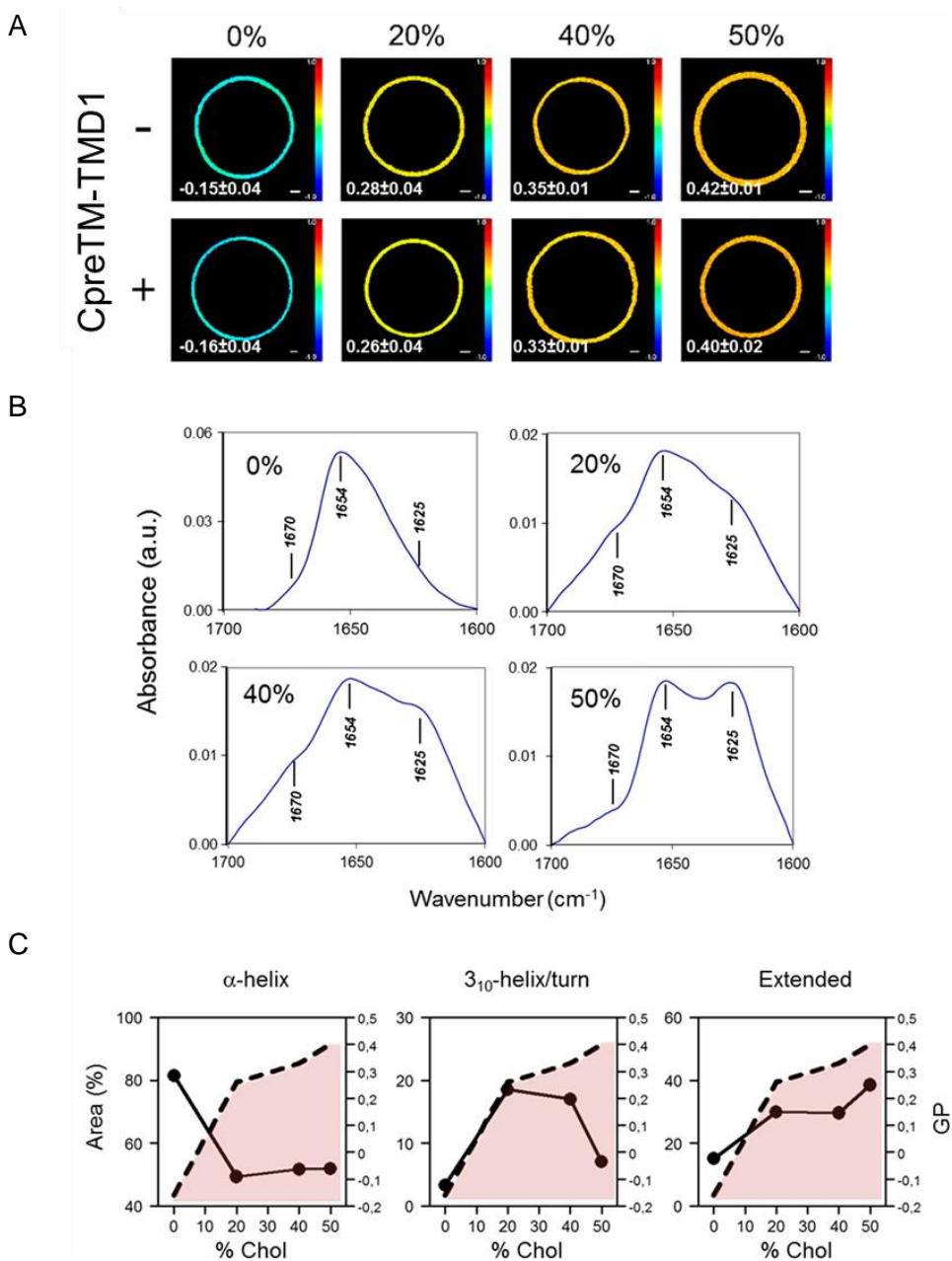


Figure 3.2.6. Lipid packing and structure of CpreTM-TMD1 in LPFs. **A)** Laurdan GP images of single GUVs containing increasing Chol concentrations (0, 20, 40, or 50 mol %) with reconstituted CpreTM-TMD1 or in the absence of the peptide. High GP values (red) correspond to high molecular packing as opposed to lower GP values (blue) corresponding to more loosely packed membranes. Mean GP values \pm SD of more than 30 GUVs of two independent experiments are shown in the panels. Scale bars are 1 μ m. **B)** IR spectra in the amide-I region of CpreTM-TMD1 reconstituted in LPFs containing increasing Chol concentrations. **C)** Correlation between changes in CpreTM-TMD1 conformation (% Area), and lipid packing degree (Laurdan GP values). Contribution of the secondary structure components was calculated after IR amide-I band decomposition.

Figure 3.2.6 C illustrates the evolution of the different structural components (percentage of amide-I band area) as a function of the Chol content and lipid packing (GP value). The data suggest that an initial sharp increase in lipid packing correlates with a reduction of the α -helix content and an increment in the contribution of 3_{10} -helix and turns, consistent with the partial destabilization of the main helical conformation in the samples. Further addition of Chol resulted in accumulation of extended structures and reduction of 3_{10} -helix and turns. Together, the IR results suggest that Chol can alter gradually the conformation of the CpreTM-TMD1 helix inducing its partial unfolding.

3.2.3.6 Model for Chol-induced C-MPER epitope disruption

It has been recently described that TMDs with smaller solvent accessible surface areas accommodate more efficiently in highly packed membranes than those rich in bulkier residues²⁸⁰. Consequently, most of the TMD helices found to reach the plasma membrane in eukaryote cells tend to segregate amino acids asymmetrically in two regions²⁸¹: residues containing short and less bulky side chains locate in the section that passes through the highly packed exoplasmic leaflet, whereas those with the more voluminous side chains tend to remain in contact with the internal monolayer, where the disorder of the acyl chains is higher. This trend is reflected by the Surface Area_{exoplasmic}/Surface Area_{endoplasmic} parameter, which measures the ratio of exoplasmic to cytoplasmic lipid-accessible surface areas of the helix²⁸¹. The value of this parameter is significantly less than 1 in the TMDs anchored to the plasma membrane.

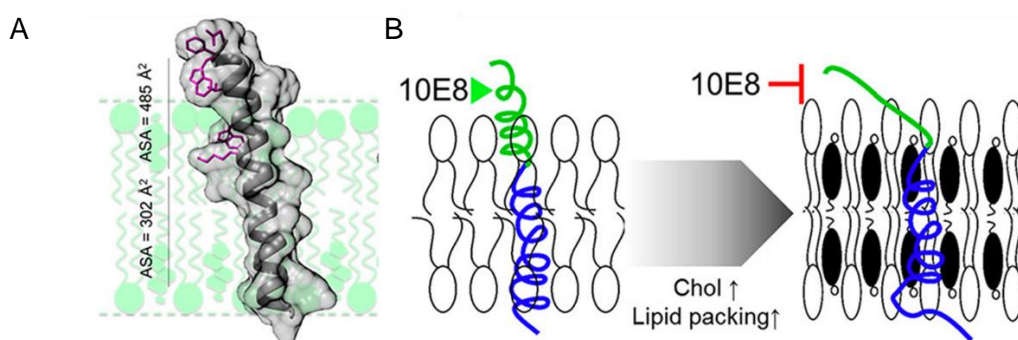


Figure 3.2.7. Model for restricted accessibility to C-MPER epitope in Chol-enriched membranes. **A)** Asymmetry of CpreTM-TMD1 transmembrane helix surface area between halves of the lipid bilayer. Accessible surface areas (ASA) were calculated as described^{280,282}. **B)** Cartoon illustrating unfolding of the CpreTM-TMD helix section containing the C-MPER epitope upon lipid-packing increase. Note that the model does not exclude chain extension also occurring at the C-terminal side of the helix, as previously proposed¹⁶².

Remarkably, as shown in Figure 3.2.7 A, the Surface Area_{exoplasmic}/Surface Area_{endoplasmic} parameter calculated for the helix spanning the CpreTM-TMD1 region of HIV-1 is ca. 1.6, i.e., significantly higher than 1. Therefore, the CpreTM-TMD1 section rich in bulky residues is more prone to unfold in tightly packed lipid bilayers than the rest of the TMD region due to its comparatively larger surface area. We surmise that the increase in lipid packing causes the conformational changes of the MPER-TMD helix that result in the disruption of the C-MPER epitope (Figure 3.2.7 B).

3.2.4. Discussion

The relevance of the C-MPER epitope as a target for vaccine design is highlighted by the discovery that broad and potent HIV-1 neutralizing activity of sera collected from chronically infected individuals can be in part mapped to this subregion^{12,283–289}. Despite the interest in developing effective immunogenic formulations, as a general rule, vaccines against this site are poorly immunogenic¹⁹⁰. The available structural information on the mechanism of HIV bnAb binding to native C-MPER suggests that an effective vaccine should elicit antibodies that (i) engage with the integral membrane antigen Env, (ii) develop the ability to recognize specifically residues exposed on the accessible face of the C-MPER helix, and (iii) develop a surface to accommodate the viral membrane interface (Figure 3.2.1).

To formulate properly the C-MPER sequence at membrane surfaces, in this work we have followed a new strategy. First, to focus immune responses to a single epitope, the selected CpreTM-TMD1 peptide contains only the C-terminal subdomain of MPER, which is followed by a minimal Env TMD that can effectively anchor the protein in the membrane¹⁸⁷. We note that peptides containing the full MPER sequence appear to occlude the C-MPER sequence in the membrane interface^{162,290}, and tend to raise responses focused on the N-terminal subdomain when formulated as LPFs (i.e., produce antibodies against the 2F5 epitope, but not against the 10E8 epitope)²⁹⁰.

Second, we have generated functional variants of 10E8 and used them to gauge the correct presentation of 10E8 epitope in LPFs. Our data indicate that LPFs containing CpreTM-TMD1 are recognized by 10E8 variants following their functional profile. Furthermore, these formulations are immunogenic in rabbits, demonstrating their capacity to engage with B-cell receptors.

Third, we have altered the lipid composition of the membrane and evaluated its effect on the antigenicity and immunogenicity of LPFs. It has been argued that a virus-like membrane environment should be preserved in the conception of peptide vaccines targeting the C-terminal region of MPER^{96,227}. Thus, we used increasing concentrations of Chol in the lipid mixtures in order to mimic the tight lipid packing of the viral membrane⁴⁹. The antibody-based experiments revealed that C-MPER gets occluded in the Chol-rich membranes, in line with the trend revealed by the immunogenicity assays. Consistent with this notion, recently published data indicate that the 10E8 epitope is more accessible in cyclodextrin-treated virions, which purportedly contain lower amounts of Chol²⁹¹.

Given the crucial importance of the lipid composition in the development of a LPF MPER vaccine, we further investigated the molecular basis for the Chol-induced 10E8 epitope occlusion. Our data demonstrate that the lipid bilayers containing the reconstituted CpreTM-TMD1 peptide are stable in all compositions. However, the increase in lipid packing induced by Chol appears to directly affect C-MPER helix accommodation, provoking its unfolding and the loss of antigenicity.

Under the assumption that to ensure reproducibility and lower cost, simple lipid compositions would be preferred over complex lipid mixtures to manufacture liposome-based vaccines^{214,227}, in this work we have used a single lipid, Chol, to adjust lipid packing. Nevertheless, other components of the HIV membrane such as sphingomyelin (SM) and aminophospholipids (phosphatidylserine/phosphatidylethanolamine)⁴⁷ can increase membrane packing as determined by the Laurdan GP value⁴⁹. Thus, although their ordering effects are less pronounced than those of Chol, in principle these lipids could also interfere with MPER exposure at membrane surfaces. However, it is well established that under certain conditions complex lipid mixtures that combine Chol with low melting T^a phospholipids, and high melting T^a SM, can undergo lateral segregation generating Chol-rich (rigid) and Chol-depleted (fluid) domains in membranes (see ref 292). Therefore, despite the high Chol content of the HIV membrane and the presence of other lipids that enhance packing, it cannot be excluded that an effective recognition of the MPER epitope by antibodies and BCRs occurs within the segregated fluid domains.

Finally, we can speculate on whether the structures observed, and the effect of Chol, provide some insight into the structure–function of Env. In this respect, a crystal structure of the 6-HB containing the full MPER sequence supports the adoption of an extended conformation by MPER residues within an Env fusion intermediate²¹⁹. Thus, we surmise that a tendency for alternating the helical conformation of the MPER-TMD region with

more flexible and extended structures might help complete the structural changes undergone by the gp41 ectodomains upon fusion activation of the Env trimer.

Chapter 3.3

***ANTIBODY ACCESSIBILITY TO THE
NEARLY PAN-NEUTRALIZING HIV-1
MPER EPITOPE MODULATED BY
THE LENGTH OF THE ENV
GLYCOPROTEIN MEMBRANE
SPANNING SCAFFOLD AND THE
BILAYER THICKNESS***

3.3 Antibody accessibility to the nearly-pen-neutralizing HIV-1 MPER epitope modulated by the length of the Env glycoprotein membrane-spanning scaffold and the bilayer thickness

ABSTRACT

HIV-1 antibodies that engage with the highly-conserved carboxy-terminal section of the membrane-proximal external region (C-MPER) are among the broadest neutralizing antibodies discovered so far. Therefore, a pursued goal in the HIV vaccine field is to resolve the Env structures and the mechanisms that underpin the production of antibodies with C-MPER specificity. The MPER sequence is rich in hydrophobic-at-interface aromatic residues allowing its stable insertion as an interfacial helix with its main axis almost parallel to the membrane plane. However, high-resolution structural data suggest that a protuberant C-MPER helix followed by the TMD and oriented closely perpendicular to the viral membrane represents better the structure targeted by C-MPER bnAbs and hence, the one that is potentially recognized by B-cell receptors. Here, to delineate more precisely the requirements for C-MPER molecular recognition in the membrane environment, we have reconstituted C-MPER-TMD helices that differed in length in lipid bilayers with variable thicknesses, and compared their binding to the C-MPER antibody 10E8. We found that adding a helical turn within the membrane-spanning sequence not only did not destabilize the overall fold of the C-MPER-TMD constructs reconstituted in membranes, but enhanced significantly and consistently 10E8 epitope recognition as a function of the bilayer thickness. Thus, our data support a ‘pole’-like model for the optimal C-MPER recognition, according to which, epitope exposure depends on the membrane-buried scaffold length. We surmise that membrane-spanning scaffold engineering can open up unexplored avenues for the optimization of MPER-based vaccines.

3.3.1. Introduction

The HIV-1 Env sequence juxtaposed with the external leaflet of the viral membrane, also known as the MPER, is the target for a class of bnAbs^{109,191,221,226,293}. In particular, those that target the highly conserved C-terminal MPER section preceding the TMD (C-MPER, Env residues 671-683, HXB2 numbering) are found to steadfastly exert the broadest levels of neutralization among identified HIV-1 bnAbs, and are considered as nearly pan-neutralizing^{12,141,145,146,170,172,173}. Production through vaccination of antibodies with comparable neutralization breadth would potentially confer full protection against infection by the tremendous diversity of circulating HIV-1 variants, a consideration that justifies the interest in elucidating the mechanisms that underlie the generation and antiviral activity of C-MPER bnAbs^{191,221,226,293}.

Taken together, the fact that the immune system is capable of eliciting bnAbs with C-MPER specificity during infection, and that the isolated bnAbs share comparable modes of C-MPER helix recognition, demonstrates the existence of one stable MPER ensemble recognized by BCRs^{12,172,271,293}. However, the composition and structure of that hypothetical ensemble is still a matter of debate. The abundance, periodicity and conservation degree of aromatic residues within the sequence can theoretically stabilize a mainly helical conformation of MPER upon membrane interface contact^{140,151,162,164,190,222,290}. Assumed from this arrangement, anti-MPER bnAbs would dock onto a partially buried MPER helix and extract it from the membrane interface^{164,166,188,222,294}. Based on recent structural work, it has long been assumed that the peptide chain may kink at the position where the C-terminal end of the MPER helix, adsorbed in parallel onto the interface, connects with the N-terminus of the TMD helix, which traverses the lipid bilayer perpendicular to the membrane surface¹⁶². Interestingly, Chol would readily bind to this interfacial helix-turn-transmembrane helix conformation adopted by the MPER-TMD sequence in membranes²⁹⁵.

A different view derives from the identification of a chain kink located at an upstream position, which establishes two helical subregions within MPER, i.e., N-MPER and C-MPER^{12,76,146,159–161,178,227,296}. Resolution of the structure by X-ray diffraction of different Fabs with bound lipids and epitope-peptides^{96,146,173,181}, in combination with cryo-EM reconstructions of Env-Fab complexes^{76,157,173}, suggest that the C-MPER helix would compose the N-terminus of the TMD and stick out with its main axis almost perpendicular to the membrane plane in a ‘pole’-like fashion. In this arrangement, the C-MPER epitope would become accessible for recognition by the Fabs, which would engage laterally with the helix pole, making extensive contacts with the membrane through an accommodating

surface^{146,157,173,178,181}. Supporting this model of molecular recognition, mutations and chemical modifications that enhance Fab-membrane interactions through the accommodating surfaces, also increase both the affinity towards native Env and the neutralization potency of C-MPER bnAbs^{51,173,228,274,297}.

Here, we sought to gain further insight into the mechanisms underlying molecular recognition of the pan-neutralizing HIV-1 C-MPER epitope at membrane surfaces. Based on the ‘pole’-like model, we analyze the effects of the TMD scaffold length and the membrane thickness on the binding capacity of the 10E8 antibody. Our data indicate that longer TMDs and thinner lipid bilayers facilitate the accessibility to the 10E8 epitope. In contrast, inclusion of Chol in the membrane composition inhibited 10E8 binding, independently of the TMD length. Thus, our observations may inform procedures for the optimal exposure of the pan-neutralizing HIV-1 C-MPER epitope on the surface of membrane-based vaccine formulations.

3.3.2. Methods

3.3.2.1 Reagents

The peptide sequences derived from the gp41 MPER-TMD region, *KKK-NWFDITNWLWYIKLFIMIVGGLVGLRIVFA-KKKK* (CpreTM-TMD1), *NWFDITNWLWYIKLFIMIVGGLVGLRIVFAVLSVVNRVR* (CpreTM-TMD2) and *NWFDITNWLWYIKLFIMIVGGLVGLRIVFALLAVLSVVNRVR* (CpreTM-TMD3) were produced by solid-phase synthesis using Fmoc chemistry as C-terminal carboxamides and purified by HPLC. POPC, 1,2-dimyristoleyl-sn-glycero-3-phosphocholine (diC14:1-PC), 1,2-erucoyl-sn-glycero-3-phosphocholine (diC22:1-PC) were purchased from Avanti Polar Lipids (Birmingham, AL, USA). NBD and Rho fluorescent probes were from Thermo Fisher Scientific (Waltham, Massachusetts, USA). Abberior STAR RED (KK114) was obtained from Abberior (Göttingen, Germany).

3.3.2.2 Production of Fab 10E8

Fab 10E8 antibody sequence was cloned in the plasmid pColaDuet and expressed in Escherichia coli T7-shuffle strain as previously described in 2.2.1 section. For confocal microscopy experiments, position C216_{HC} of the Fabs was modified in vitro with a sulphydryl-specific iodacetamide derivative of the KK114 probe.

3.3.2.3 LPF production

To prepare peptide containing LPFs at peptide-to-lipid molar ratio of 1:50, lipids and CpreTM-TMD1, CpreTM-TMD2 or CpreTM-TMD3 dissolved in HFIP were mixed in organic solvent prior to the production of the liposomes as explained in *2.1.1.2 section*.

Effective incorporation of the peptide to the vesicles was ensured by peptide flotation in a sucrose gradient following *2.1.3 protocol*.

3.3.2.4 GUV-Fab binding assays

NBD-labeled GUVs were produced by spontaneous swelling as described in *section 2.1.1.1*, co-dissolving lipids with NBD (2 mol %). When required, peptide dissolved in HFIP was included in organic phase at 1:250 peptide-to-lipid ratio.

For binding experiments, NBD-labeled GUVs with peptide (1:250 peptide-to-lipid molar ratio) were used. The GUVs were added to a bovine serum albumin (BSA)-blocked microscope chamber that already included 250 nM of 10E8 Fab conjugated with the KK114 probe at residue C216_{HC}, and were incubated for 15 min prior to imaging.

Images were acquired on an inverted confocal fluorescence microscope (Nikon Eclipse TE-2000, Nikon, Nikon Instruments, Tokyo, Japan) as described in *section 2.4.1.3*. In brief, NBD-stained GUVs and Fabs conjugated with the KK114 probe were excited at 476 nm and 637 nm, respectively. The band pass filters used were 515/30 and Long Pass 650 nm. The objective used was a 63X oleo immersion with a NA of 1.2.

Relative extents of Fab-GUV binding were obtained by measuring the fluorescence intensity of KK114 along the equatorial plane of the GUV images. Fluorescence emission analyses were carried out with ImageJ software (rsb.info.nih.gov/ij/).

3.3.2.5 Infrared spectroscopy

Infrared spectra were recorded in a Bruker Tensor 27 spectrometer equipped with a mercurycadmium-telluride detector using a Peltier-based temperature controller (TempCon, BioTools Inc., Wauconda, IL) with calcium fluoride cells (BioCell, BioTools Inc., Wauconda, IL) and following *protocol 2.3.2*. LPFs of different compositions were lyophilized and subsequently prepared at 3 mg/mL in D₂O buffer. Data treatment and band decomposition of the original amide-I as described in ²⁵⁴.

3.3.3. Results

3.3.3.1 C-MPER epitope anchoring to membranes through TMD scaffolds differing in length

Models displayed in Figure 3.3.1 illustrate the design of the different synthetic peptides derived from the HIV-1 C-MPER-TMD sequence that have been employed in this study and the rationale behind their application. Based on the ‘pole’-like model proposed for 10E8 docking to Env in the pre-fusion state (Figure 3.3.1 A)^{76,178,181}, we hypothesized that the length of the membrane-spanning scaffold would modulate epitope accessibility and, hence, antibody affinity (Figure 3.3.1 B). To test the hypothesis, we employed the three synthetic peptides displayed in Figure 3.3.1 C, which combined the C-MPER helix with increasingly longer TMD moieties, namely: i) CpreTM-TMD1 (Env residues 671-700, HXB2 numbering), containing a minimal TMD anchor and Lys-tags to increase solubility at both ends of the molecule^{161,187,297}; ii) CpreTM-TMD2 (Env residues 671-709, HXB2 numbering), which included a sequence representing the nominal Env TMD sequence (Env residues 684-709); and iii) CpreTM-TMD3, a sequence based on the previous peptide, which was elongated by adding an additional helical turn to the section spanning the hydrophobic membrane core.

3.3.3.1 Reconstitution of C-MPER-TMD helices in membranes

To test our hypothesis we first sought to reconstitute MPER-TMD helices in lipid bilayers made of POPC, and then measure C-MPER epitope recognition by the antibody 10E8. In addition, we compared the recognition in POPC with that in lipid bilayers made of equimolar mixtures of POPC and Cholesterol (POPC:Chol; 1:1). This comparison was carried out for two reasons: on the one hand, Chol has been shown to bind to MPER-TMD helix-turn-helix structures in membranes^{162,295}; on the other hand, this compound stiffens the lipid bilayer and increases its thickness²⁷⁸, alterations that may restrict epitope accessibility, more critically in the case of the shortest construct CpreTM-TMD1

²⁹⁷

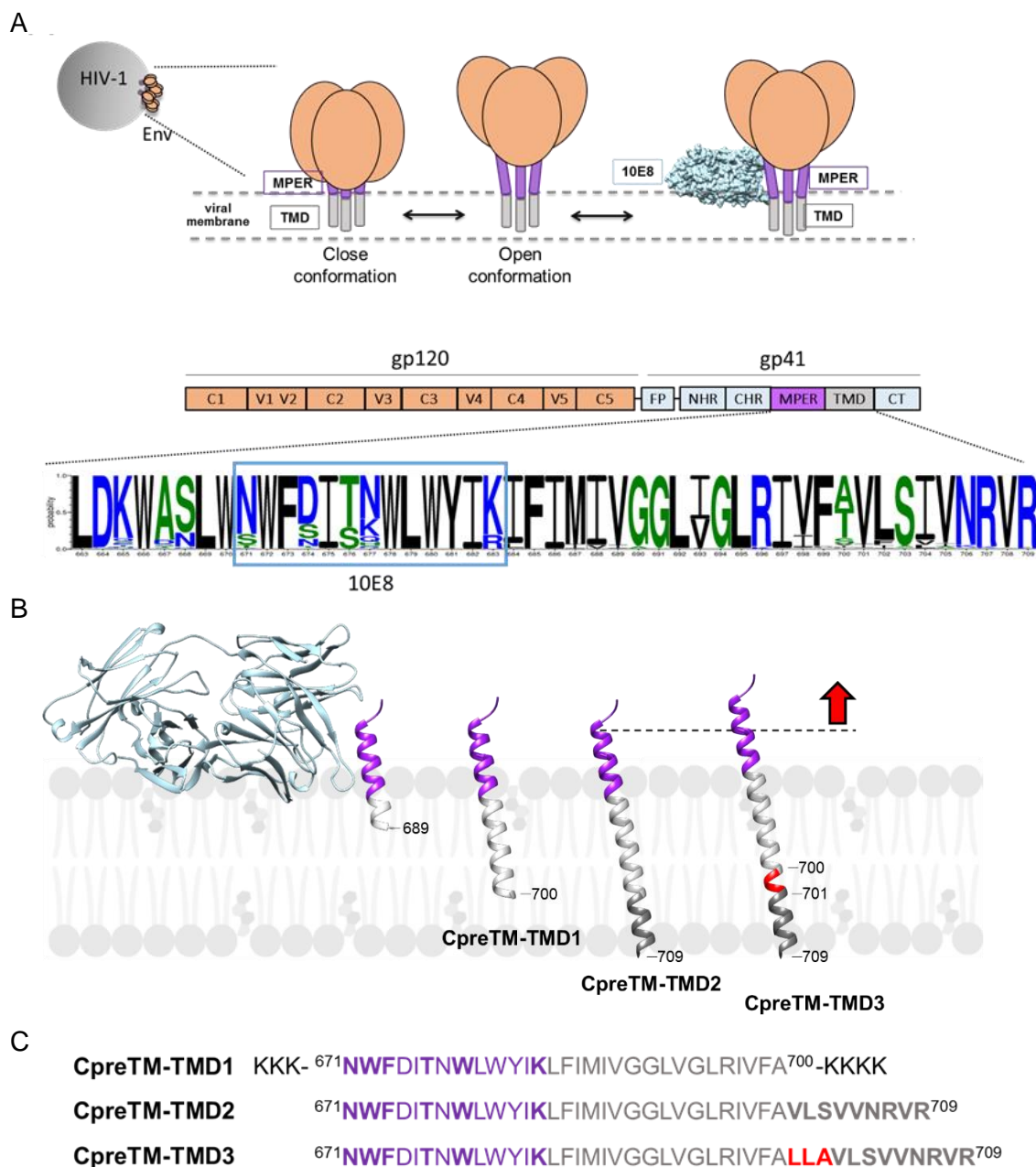


Figure 3.3.1. Design of C-MPER-containing peptides with membrane-spanning sequences of different lengths. A) Proposed model for 10E8 antibody binding to Env and designation of the epitope sequence within the conserved MPER. The binding mode is based on cryo-EM reconstructions of native Env-Fab complexes^{76,157}. The degree of conservation of MPER sequence of all HIV/SIVcpz subtype genomes available at the Los Alamos National Laboratory HIV Sequence Database is represented by a WebLogo. The height of each symbol indicates relative frequency of each amino acid at that position, and symbols are color-coded for hydrophobicity: hydrophilic (blue), neutral (green) and hydrophobic (black). **B)** Left: Binding of 10E8 (PDB ID: 5GHW) to the helical C-MPER epitope inserted in membranes through the TMD. The MPER (residues 671-683) and the TMD (residues 684-709) are colored in purple and gray respectively. Extra turn in CpreTM-TMD3 is red colored. Right: Increasing the length of the membrane-spanning scaffold is postulated to facilitate exposure of the C-MPER helix (purple stretch). The models were constructed by superposition of MPER-TMD structure (PDB ID: 5GHW), residues 671-689, with residues 690-709 of the TMD (PDB code: 6B3U). The structures were rendered using Chimera. **C)** Sequences of the synthetic peptides used in the study and their designation.

In our previous work, we showed that the CpreTM-TMD1 helix could be readily reconstituted into membranes after dissolving the peptide in etOH and then co-mixing it with lipids in organic solvent²⁹⁷. However, the same procedure yielded peptide aggregation and poor incorporation into vesicles in the case of the longer CpreTM-TMD2. This was not the case when we turned to HFIP as the primary solvent for the peptides. Thus, when peptides were first dissolved in HFIP and then mixed in organic solvent with the lipids, efficient reconstitution was attained after gentle evaporation and hydration (see *Experimental techniques 2.1.1.2*).

Results displayed in Figure 3.3.2 confirmed the efficacy of this procedure. Detection of peptides in the liposome fraction floated after ultracentrifugation in a sucrose gradient indicated that peptide incorporation levels in both, POPC and POPC:Chol liposomes, were comparable and almost maximum (Figure 3.3.2 A). Moreover, analyses of the IR amide-I region of the different LPFs denoted bands centered at ca. 1650 cm⁻¹, consistent with the three peptides adopting main helical conformations after their reconstitution in membranes (Figure 3.3.2 B).

However, upon closer inspection of the results by deconvolution of the IR spectra, resulting band components evidenced differences between the conformations attained in POPC and POPC:Chol membranes (Figure 3.3.2 C). In line with previous results obtained for the peptide reconstituted from an etOH solution²⁹⁷, in the presence of Chol, CpreTM-TMD1 displayed a prominent band at ca. 1622 cm⁻¹, and simultaneous reduction of the components at 1656 and 1642 cm⁻¹, indicative of partial unfolding-aggregation of the helix. We interpreted these changes as the fraying undergone by the TMD helix edges in the tightly packed-and-thicker membranes containing Chol²⁹⁷.

In contrast, components centered at ca. 1620 cm⁻¹ contributed little to the amide-I bands of the CpreTM-TMD2 and CpreTM-TMD3, suggesting that the overall helical conformation was preserved in these peptides in the presence of Chol. The most remarkable change observed in these samples was an increase of absorption by the low-frequency helical component centered at ca. 1630 cm⁻¹, which has been assigned to solvent-exposed helical amides^{256,257,290} (see also insets).

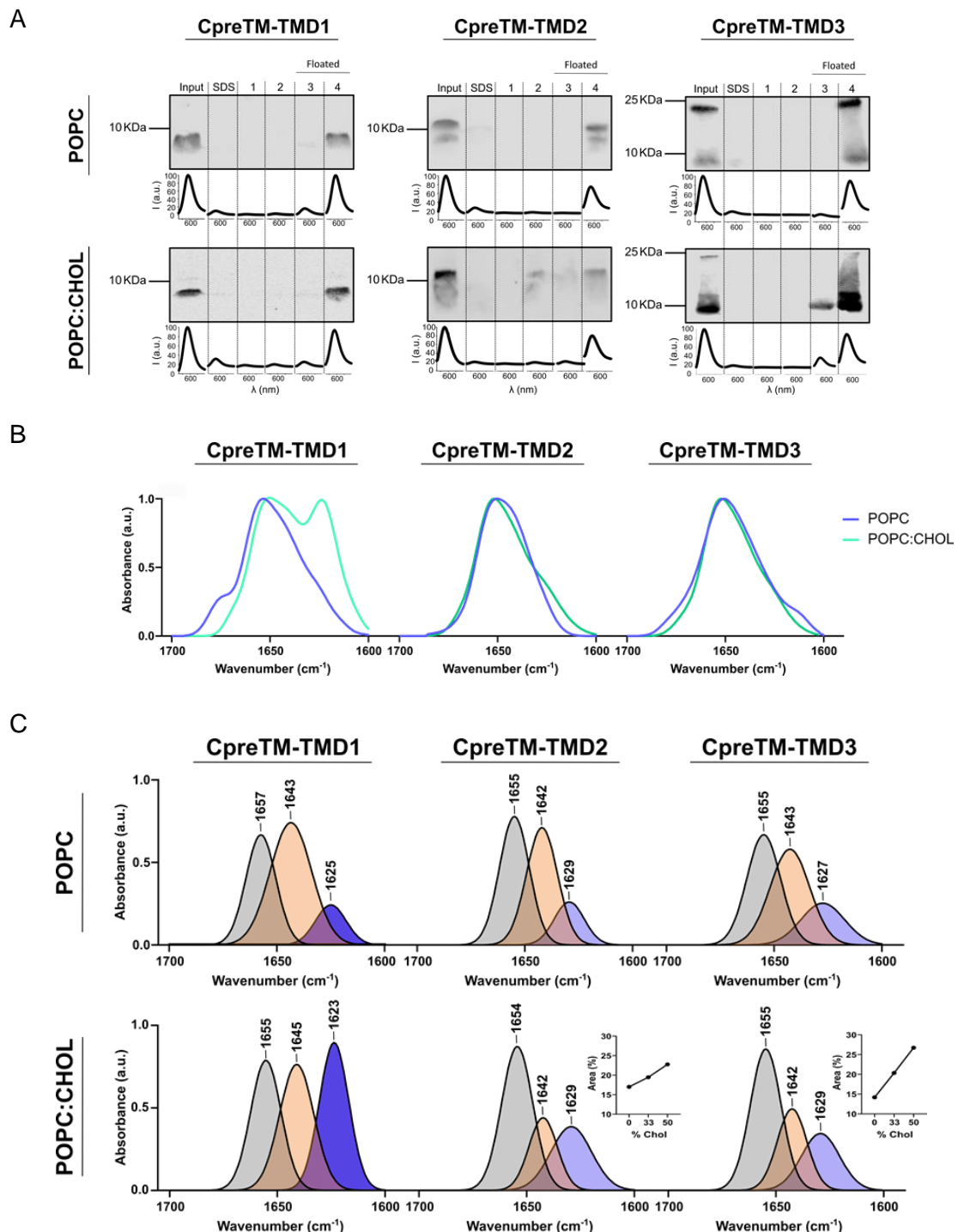


Figure 3.3.2: Reconstitution of MPER-TMD helices in lipid bilayers. (A) Full incorporation of CpreTM-TMD1, CpreTM-TMD2 and CpreTM-TMD3 to POPC and POPC:Chol (1:1) lipid bilayers. Liposome-peptide complexes were subjected to ultracentrifugation in a sucrose gradient after the reconstitution process. The presence of peptides in the floated and non-floated fractions of the gradient and in the original sample (input) was revealed by Western Blot analysis after Tris-Tricine SDS-PAGE separation. Line plots below the panels display the fluorescence emission of the Rhodamine probe, revealing the presence of liposomes. (B) Amide-I region IR spectra of the peptides reconstituted in POPC and POPC:Chol (1:1) membranes (peptide-to-lipid ratio, 1:50), colored in blue and green respectively. (C) Components of the amide-I band measured after reconstitution of the peptides in POPC or POPC:Chol (1:1) lipid bilayers (top and bottom panels)

respectively). Insets in CpreTM-TMD2 and CpreTM-TMD3 panels denote the evolution of the band centered 1630 cm^{-1} (area percentages) upon increasing Chol.

3.3.3.2 10E8 epitope accessibility in membranes containing reconstituted C-MPER-TMD peptides

We next determined by quantitative confocal microscopy the degree of 10E8 epitope exposure on membranes containing the different C-MPER-TMD peptides. To perform these experiments KK114-labeled Fab 10E8 was incubated with GUVs that contained the reconstituted peptides (Figure 3.3.3 A). The level of antibody binding was then estimated by measuring the fluorescence intensity of the KK114 label in single vesicles (Figure 3.3.3b).

The data revealed that Fab binding followed two general trends. On the one hand, the amount of the Fab bound increase upon increasing lengthening of the membrane-spanning sequence (i.e., CpreTM-TMD3>CpreTM-TMD2>CpreTM-TMD1). On the other hand, the presence of Chol seemed to conceal the 10E8 epitope in all instances, as previously described for the case of the CpreTM-TMD1 peptide reconstituted from an EtOH solution²⁹⁷.

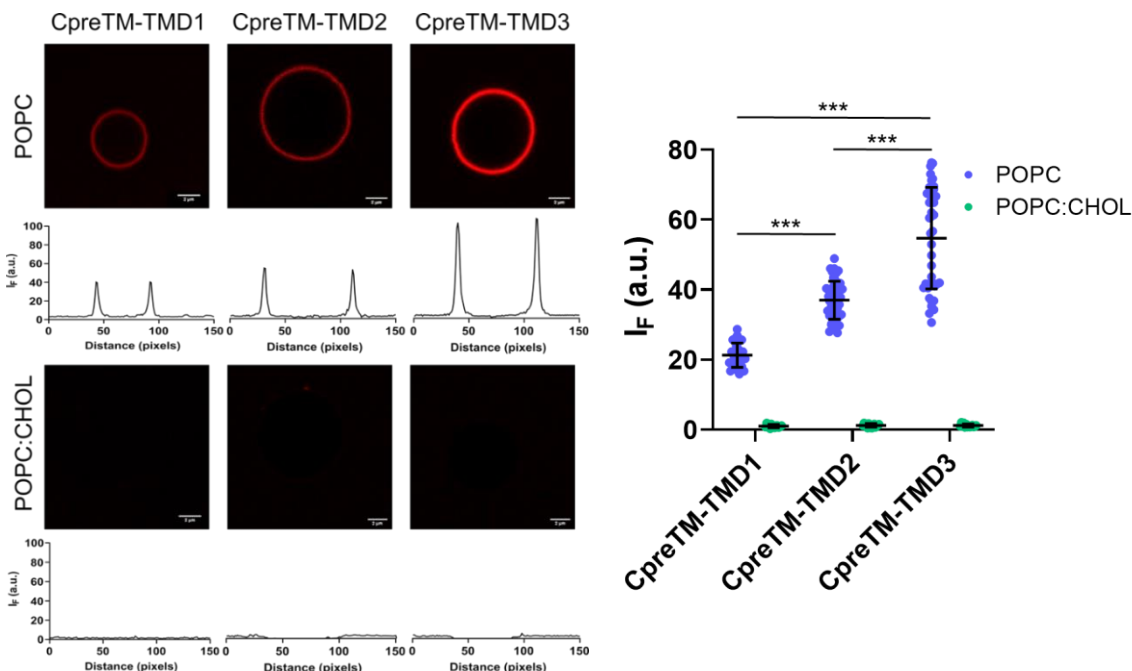


Figure 3.3.3. Binding of Fab 10E8 to GUVs containing MPER-TMD helices reconstituted. Micrographs on the left display confocal images of peptide-containing POPC and POPC:Chol (1:1) GUVs, which were incubated with fluorescently labeled KK114-10E8 Fab (rendered in red). Traces below follow the changes in fluorescence intensity at the equatorial plane. All micrographs were rendered with equal contrast and brightness to better appreciate the difference in emission intensity. The plot on the right shows KK114 fluorescence intensity quantification at the equatorial plane of individual GUVs. The statistical significance was assessed by Mann-Whitney test, ***p < 0.001; **p < 0.01, *p < 0.05, n.s. ≥ 0.05.

3.3.3.3 10E8 epitope recognition on lipid bilayers of different thickness

The previous results suggest that for comparable C-MPER conformations adopted in lipid bilayers without Chol, the longer membrane-spanning scaffolds may expose more efficiently the 10E8 epitope to solution. Molecular Dynamic simulation studies suggest that 50 mol % of Chol can increase the POPC lipid bilayer thickness by ca. 7 Å^{298,299}. Thus, deeper insertion of the C-MPER helix into thicker POPC:Chol lipid bilayers cannot be discarded as the cause for the lack of Fab binding.

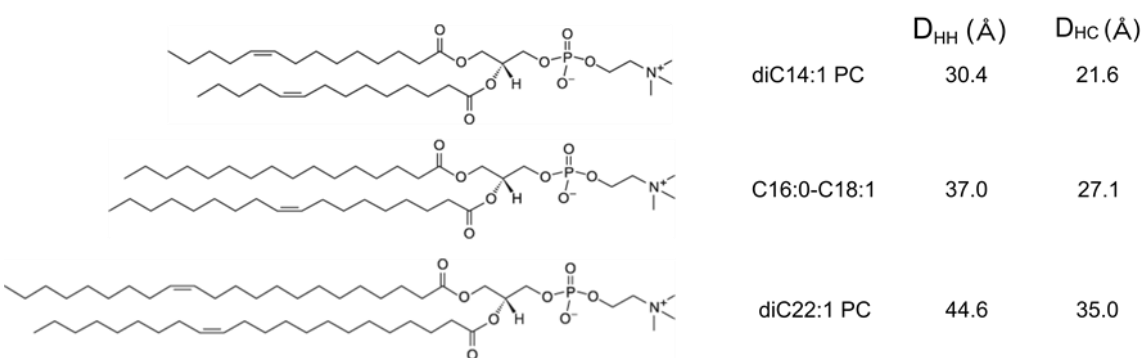


Figure 3.3.4. diPCs of different lengths used in this study. Comparison of monounsaturated phosphatidylcholines diC14:1PC and diC22:1PC with POPC (C16:0-C18:1PC). Values measured in lipid bilayers for the headgroup-to-headgroup distance, D_{HH} , and the hydrocarbon thickness, D_c have been taken from^{299,300}.

To confirm that the bilayer thickness is a critical factor that restrains epitope accessibility, we next sought to investigate the effect of varying this parameter systematically. To that end, the three C-MPER-TMD peptides were reconstituted in membranes composed of diacyl PCs (diPCs) containing monounsaturated acyl chains of different lengths. The diC14:1PC and diC22:1PC specimens give rise to lipid bilayers that are respectively thinner and thicker than that of POPC (C16:0-C18:1PC)^{300,301} (Figure 3.3.4). Moreover, the thickness of diC22:1PC bilayers would approximate that estimated for POPC:Chol (1:1) bilayers^{298,299}.

Following their reconstitution from HFIP, flotation experiments confirmed that the peptides are also fully incorporated into vesicles made of these lipids (Figure 3.3.5 A). IR measurements in the amide-I region revealed comparable helical conformations adopted by the three peptides in the thinnest and thickest bilayers (Figure 3.3.5 B). Interestingly, the shortest peptide CpreTM-TMD1 did not display bands attributable to unfolding-aggregation under any condition.

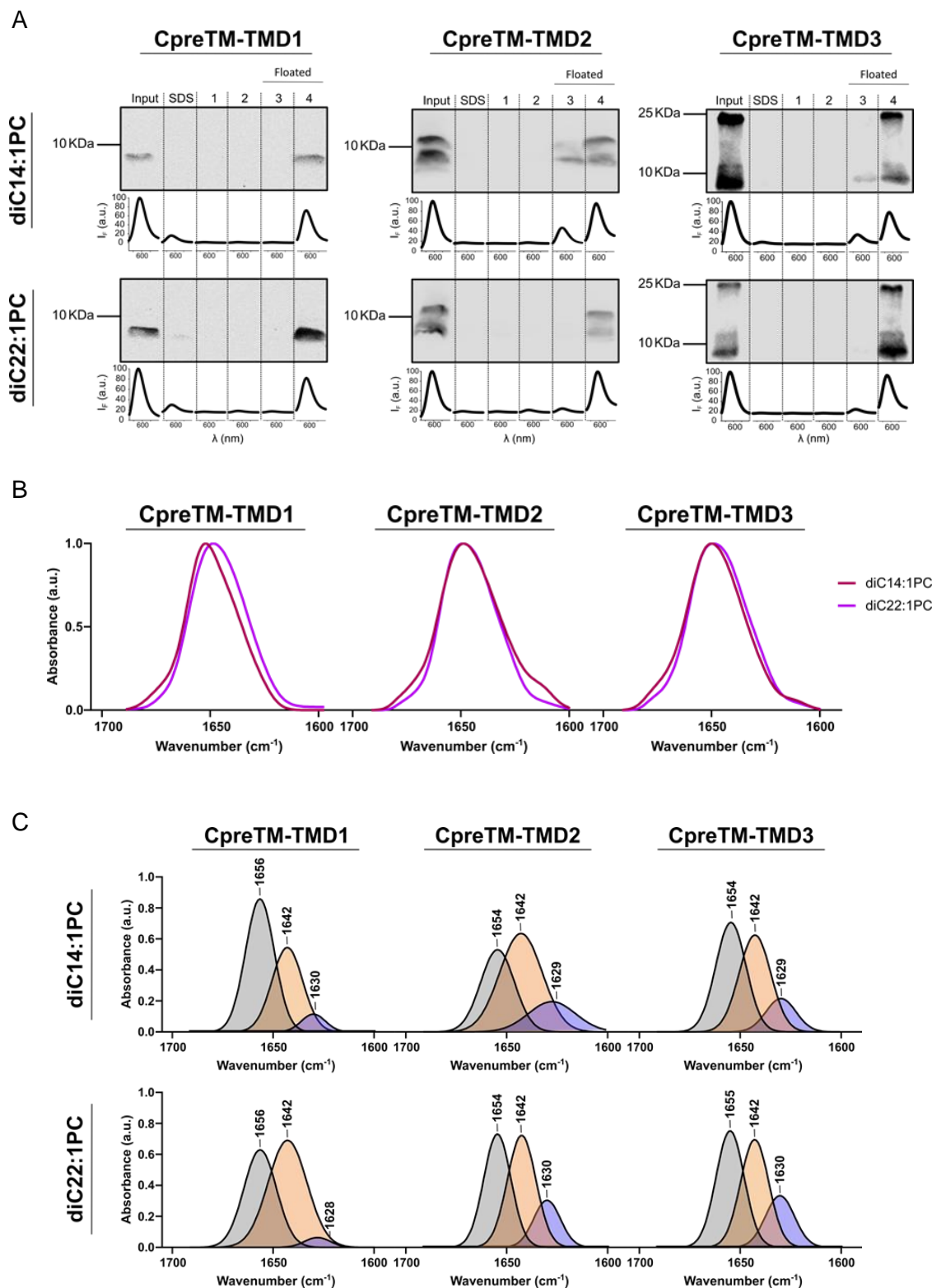


Figure 3.3.4. Reconstitution of MPER-TMD helices in ‘thin’ and ‘thick’ lipid bilayers. **A)** Flotation assays to demonstrate full incorporation of CpreTM-TMD1, CpreTM-TMD2 and CpreTM-TMD3 to diC14:1PC and diC22:1PC lipid bilayers. Conditions otherwise as in previous figure 3.3.2 A. **B)** Amide-I region IR spectra of the peptides reconstituted in diC14:1PC (red) and diC22:1PC (purple) lipid bilayers (peptide-to-lipid ratio, 1:50). **C)** Components of the amide-I band attributable to helical conformations (measured after reconstitution of the peptides).

The lipid bilayer distance covered by the hydrocarbon acyl chains (D_C) strongly conditions the favorable interactions between TMDs and lipids, so that a mismatch between this distance and the TMD length can give rise to alterations in the structure and function of the integral membrane proteins. Therefore, to get a more detailed view of the D_C effect on the conformations adopted by the reconstituted peptides, we performed IR experiments and varied this parameter systematically utilizing a complete series of monounsaturated PCs (i.e., diC14:1PC, diC16:1PC, diC18:1PC, diC20:1PC and diC22:1PC)³⁰². Figure 3.3.6 displays the changes in peptide conformation (areas of the amide-I band components) as a function of the hydrocarbon section thickness. Again, we observed no remarkable changes in the conformations adopted by any of the peptides reconstituted in systematically thicker lipid bilayers.

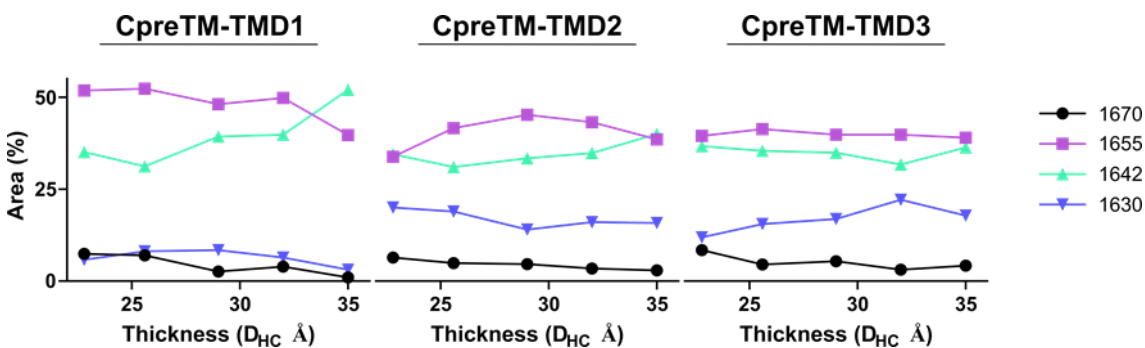


Figure 3.3.6. Effect of hydrocarbon thickness on the conformation adopted by MPER-TMD helices reconstituted in lipid bilayers. The evolution of the different structural components (percentage of amide-I band area) are displayed as a function of the D_C parameter estimated by Gallová et al.³⁰² for the series of monounsaturated PCs.

Having determined the stability of the helical conformations adopted by the peptides, we next established the influence of the bilayer thickness on the accessibility to the 10E8 epitope (Figure 3.3.7). Again, results of Fab 10E8 binding to GUVs containing the peptides followed two different trends. In the one hand, at a defined thickness, binding augmented upon increasing the TMD length of the peptide (i.e., CpreTM-TMD3>CpreTM-TMD2>CpreTM-TMD1). On the other hand, for a defined peptide, binding improved for the thinner membranes in comparison with the thicker ones (i.e., diC14:1PC>diC22:1PC). In conclusion, the extent of the helix fraction accessible from the solution modulates the degree of antibody binding to the 10E8 epitope.

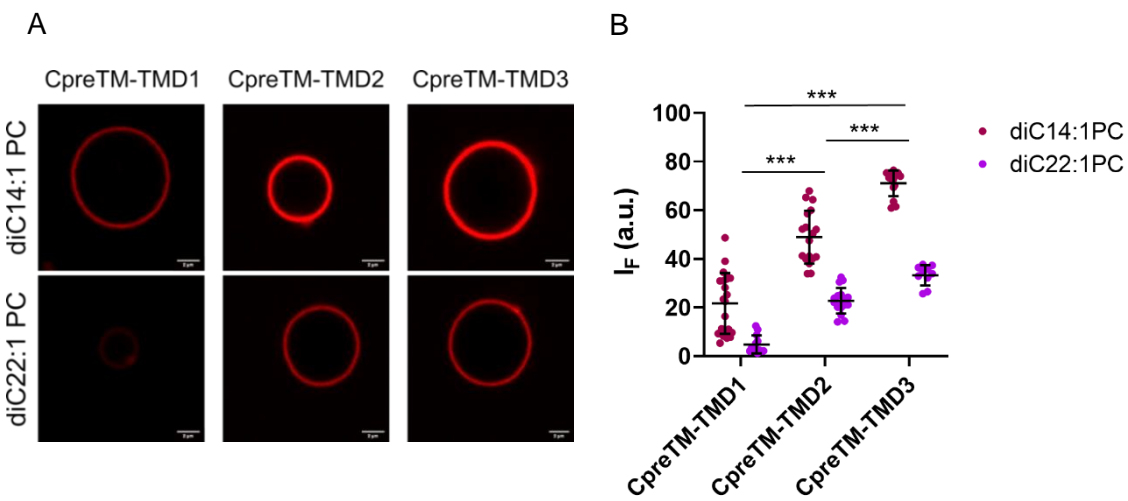


Figure 3.3.7: Binding of Fab 10E8 to MPER-TMD helices reconstituted in GUVs made of ‘thin’ and ‘thick’ lipid bilayers. **A)** Confocal images at the equatorial plane of peptide-containing diC14:1PC and diC22:1PC GUVs, after incubation with fluorescently labeled KK114-10E8 Fab (rendered in red). **B)** KK114 fluorescence intensity quantification at the equatorial plane of individual GUVs in each sample. Mann-Whitney Test: ***p < 0.001; **p < 0.01, *p<0.05, n.s. ≥0.05).

3.3.4. Discussion

HIV-1 neutralizing activity of sera collected from some infected individuals map to the highly conserved MPER sequence^{12,283–289}. Binding profiles of isolated bnAbs and structural studies further support the division of this vulnerability Env site into two sub-regions, the N-terminal helix containing epitopes recognized by the bnAbs 2F5, M66.6 and 2H10; and the C-terminal helix, which contains the epitope sequences for bnAbs such as 4E10, 10E8, DH511.1, LN01, VRC42.N1 or PGZL.1^{226,293}. Experimental vaccines tested so far appear to successfully elicit antibodies against the N-terminal epitopes¹⁹⁰. In contrast, producing antibodies against the C-terminal epitopes through vaccination remains anecdotic¹⁶¹. In our previous approach based on CpreTM-TMD1 (see Chapter 3.2), we reasoned that a peptide with a minimal TMD scaffold would force the upright orientation of the C-MPER helix thereby facilitating the optimal exposure of the 10E8 epitope at the membrane interface²⁹⁷. Here, based on the ‘pole’-like model, we have investigated the effects of the scaffold length spanning the membrane on C-MPER recognition at the membrane surface.

As a general rule, PC-based lipid bilayers containing reconstituted MPER-TMD helices appeared to expose 10E8 epitope efficiently, the degree of exposure being a function of the length of the membrane-spanning sequence and the bilayer thickness (Figure 3.3.7). The almost linear correlation observed between the values of these parameters and

extents of Fab binding (Figure 3.3.7 A), allowed inferring from simple geometrical considerations the basis supporting the similar degrees of epitope exposure occurring in CpreTM-TMD1/diC14:1PC and CpreTM-TMD2/diC22:1PC systems (Figure 3.3.7 B).

However, we found that POPC:Chol (1:1) lipid bilayers containing the reconstituted peptides deviated from this behaviour. In our previous work (see *Chapter 3.2*) we described that Chol increased lipid packing and partially unstructured the helical conformation of CpreTM-TMD1, two effects that correlated with restrained access to the 10E8 epitope. Reconstitution from an HFIP solution reproduced the effects of Chol on this peptide's conformation and epitope presentation.

Furthermore, we found that longer CpreTM-TMD2 and CpreTM-TMD3 sequences, which presented the epitope efficiently at POPC surfaces, also lost this capacity upon reconstitution in POPC:Chol (1:1) lipid bilayers, even though they retained their predominantly helical conformation. The explanation that a thicker POPC:Chol (1:1) lipid bilayer would conceal the 10E8 epitope by simply burying C-MPER helix is difficult to reconcile with the experimental observations (Figure 3.3.7 A).

In the one hand, the TMD in CpreTM-TMD2 is longer than that in CpreTM-TMD1 by approximately 15 Å. Since both peptides expose 10E8 epitope in POPC, and Chol increases the bilayer thickness by ca. 7 Å, it is unlikely that C-MPER immersion occurred by effect of this increase in thickness in the case of the CpreTM-TMD2 (or CpreTM-TMD3). On the other hand, even if lipid bilayers composed of diC22:1PC and POPC:Chol (1:1) are comparable in terms of thickness, CpreTM-TMD2 and CpreTM-TMD3 presented an accessible 10E8 epitope in the former case (Figure 3.3.7 A), but not in the latter (Figure 3.3.3, lower panels).

Thus, we infer that, besides the unfolding effects scored in the conformation of the short CpreTM-TMD1 peptide, Chol must induce additional structural rearrangements that translate into 10E8 epitope inaccessibility also in the case of the longer CpreTM-TMD2 and CpreTM-TMD3 sequences reconstituted in membranes. One possibility is that Chol interacts with the MPER-TMD sequence as recently proposed by SS-NMR studies^{162,295}. This interaction might favor immersion of a section of the C-MPER helix into the interface with residues Phe673 and Thr676 critical for 10E8 epitope binding facing the membrane core¹². Thus, the 10E8 epitope would not be accessible from solution in this arrangement, as put forward in the model displayed in Figure 3.3.8 B (left panels).

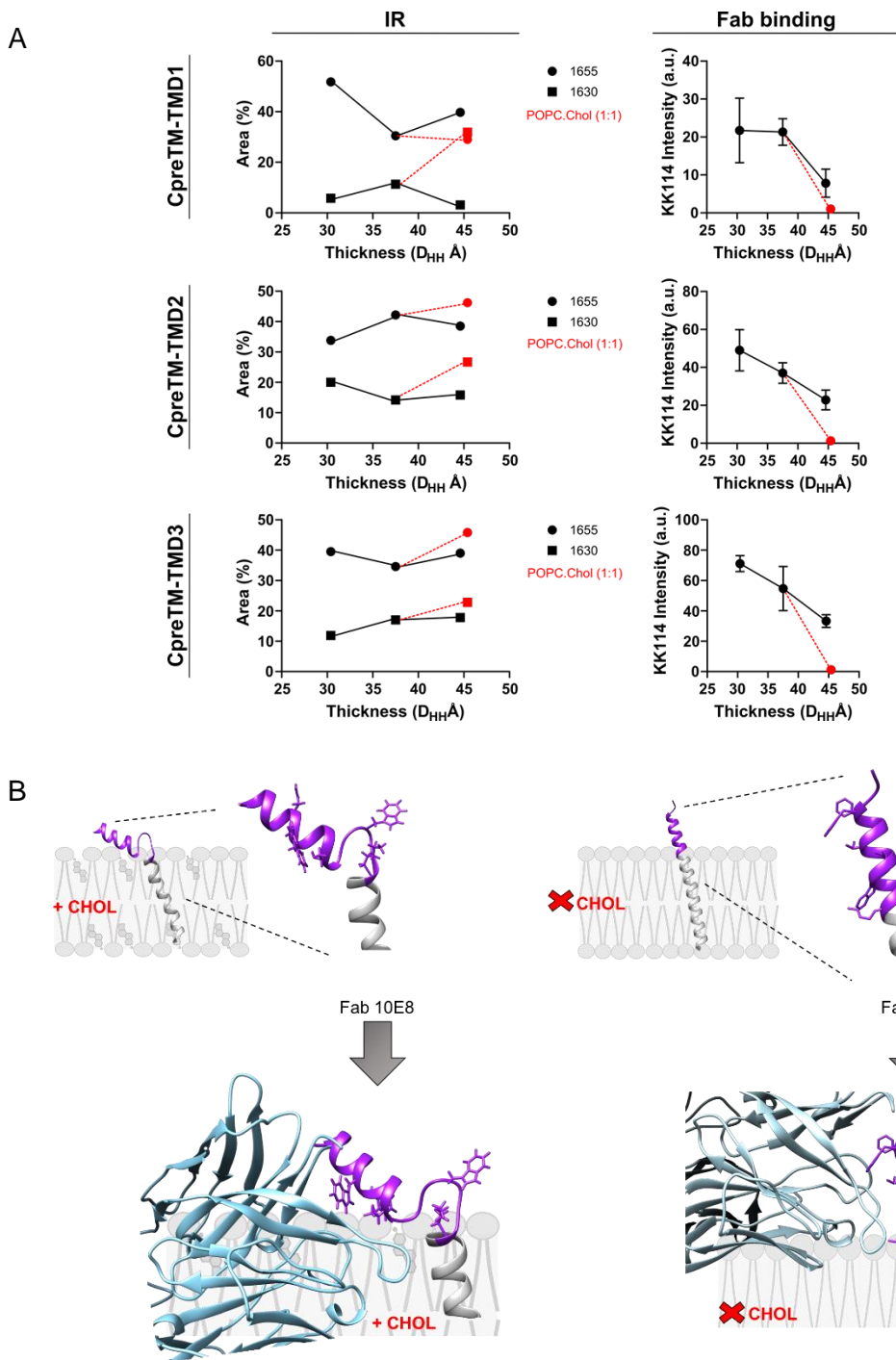


Figure 3.3.7. Models for the modulation of C-MPER helix accessibility at the surface of membranes. (A) Comparison of the effects exerted by lipid bilayer thickness (DHH) on conformation and epitope accessibility measured by IR and Fab binding assays. (B) Differential effects of Chol and membrane thickness on 10E8 epitope accessibility. Cartoon illustrating unfolding of the CpreTM-TMD helix section containing the C-MPER epitope upon lipid-packing increase (left panel). On the top, disposition of the peptide in membranes with and without cholesterol, left and right respectively. Panels below show the angle of approach of Fab 10e8. On the left, the epitope is occluded in the membrane and the Fab would have steric hindrance for efficient binding. On the contrary, on the right side, the residues of the epitope are accessible for efficient binding. The models on the left were constructed by superposition of MPER-TMD structure (PDB code: 6DLN) with Fab 10E8 (PDB code: 5GHW). The models on the right were constructed by superposition of MPER-TMD structure, residues 671-689(PDB code: 5GHW), with residues 690-709 of the TMD (PDB code: 6B3U). The structures were rendered using Chimera

Chapter 3.4

***ANCHORING OF HIV-1 10E8 EPITOPE
THROUGH THE TRANSMEMBRANE
DOMAIN REVERSES MPER EFFECTS
ON THE MECHANICAL STABILITY OF
THE LIPID BILAYER AND AUGMENTS
ANTIBODY BINDING AFFINITY.
IMPLICATIONS FOR LIPOSOME
BASED MPER VACCINE DESIGN***

3.4 Anchoring of HIV-1 10E8 epitope through the transmembrane domain reverses MPER effects on the mechanical stability of the lipid bilayer and augments antibody binding affinity. Implications for liposome-based MPER vaccine design.

ABSTRACT

Current models postulate that the HIV-1 MPER inserts into, and destabilizes the viral membrane during the dynamic process of virus-cell fusion. At the same time, supporting the existence of at least one stable structure engaged by BCRs and antibodies, MPER is the target epitope for a class of antibodies that exert broad and potent neutralization against the HIV-1. Thus, determining the steady structure of MPER that is competent in the production of bnAbs remains a critical goal in the field of HIV-1 vaccine development. Here, to better define the sequence and structural requirements that underlie molecular recognition of MPER by antibodies, we have presented the neutralizing HIV-1 10E8 epitope in a membrane environment in two formats: i) as the C-terminal section of an interfacial helix (NpreTM peptide), i.e., emulating constructs that are profusely utilized as components of experimental MPER vaccines; and ii) reconstituted in membranes as the N-terminus of the Env TMD helix (CpreTM-TMD2 peptide). Through AFM in its force spectroscopy mode, we have compared their capacity for altering the mechanical properties of the lipid bilayer and for supporting binding to the Fab 10E8. Characterization of SLBs containing the reconstituted peptides revealed mechanical destabilization of the bilayer by the interfacial NpreTM helix, an effect which mostly reversed upon anchoring the 10E8 epitope sequence through the TMD helix. Single-molecule measurements of 10E8 interaction with SLBs loaded with the peptides scored more frequently Fab binding and stronger unbinding forces in CpreTM-TMD2-containing than in NpreTM-containing SLBs. These observations and approaches may help the rational design of more stable anti-MPER immunogens and molecular baits useful to produce/identify effective antibodies against the pan-neutralizing HIV-1 MPER epitope.

3.4.1. Introduction

In spite of the intense research efforts made during the last four decades, a vaccine efficient at preventing infection by HIV-1 is not available as yet, a deficit hampering the control of a pervasive AIDS pandemic that still affects millions of people around the globe¹⁰⁹. However, the discovery that some individuals can produce bnAbs upon infection proves the feasibility of raising protective immune responses against the HIV-1^{109,303}. Furthermore, structures of these isolated bnAbs are currently applied to the rational development of new immunotherapeutic agents with the capacity of preventing and treating infection by the immense number of circulating variants of the virus³⁰⁴.

Among the identified HIV-1 bnAbs, members belonging to the class that recognize a helical epitope within the MPER of the Env glycoprotein, exhibit an extremely broad coverage^{12,141,145,146,170,172}. Under the assumption that production of MPER bnAbs through vaccination could protect against infection by virtually all variants of the virus, a variety of MPER-based vaccines have been developed and tested (see for a review¹⁹⁰). Therefore, to elucidate the native structure responsible for MPER bnAb generation, and to define with molecular detail the mechanisms of MPER epitope recognition are of outmost importance in the AIDS vaccine research field.

Opposite to the view of a structurally stable epitope region engaged by the components of the immune system, insertion of MPER-based peptides into lipid bilayers appears to generate the type of perturbations required for the promotion of membrane fusion^{5,6,150,225,305,306}. This static (antigen) vs. dynamic (fusogen) behavior may reflect the existence of swapping structures and modes of MPER interactions with membranes, which are different in the pre-fusion states of the Env glycoprotein^{146,157,159,161,162,168,227}, upon fusion activation³⁰⁷, or after the completion of the process^{163,217}. Therefore, discerning the conditions that ensure the stable presentation of MPER epitopes to the immune system from the ones that promote bilayer perturbations is incumbent to develop HIV-1 MPER vaccines.

Here, we tackle this issue by analyzing SLBs through AFM in its force spectroscopy format^{308–310}. The SLBs subjected to study contained two different MPER-based peptides reconstituted, namely: i) NpreTM (Env residues 656-683), comprising the full MPER sequence that inserts as an interfacial helix; thus, this peptide places the neutralizing 10E8 epitope at its C-terminus; and ii) CpreTM-TMD2 (Env residues 671-709), assumed to display the 10E8 epitope at the N-terminal extremity of a TMD helix. These SLBs were first challenged by force spectroscopy to obtain information at the

nanoscopic level on the effects exerted by NpreTM and CpreTM-TMD2 on the mechanical stability of the lipid bilayer. Furthermore, to establish the differences on 10E8 epitope recognition, we performed single-molecule measurements of unbinding forces using AFM tips functionalized with Fab 10E8 molecules. In conjunction, our data support that the 10E8 epitope is exposed more efficiently when membrane-anchored through TMD residues. We conclude that different approaches of MPER-based helix reconstitution in membranes may affect the performance as immunogens of liposome-based formulations.

3.4.2. Methods

3.4.2.1 Reagents

The peptide sequences derived from the gp41 MPER-TMD region, ⁶⁵⁶NEQELLELDKWASLWNWFDTNWLWYIK⁶⁸³ (NpreTM) and ⁶⁷¹NWFDTNWLWYIKLFIMIVGGLVGLRIVFAVLSVVNRVR⁷⁰⁹ (CpreTM-TMD2) were produced by solid-phase synthesis using Fmoc chemistry as C-terminal carboxamides and purified by HPLC. POPC and Chol were purchased from Avanti Polar Lipids (Birmingham, AL, USA). NBD and Rho fluorescent probes were from Thermo Fisher Scientific (Waltham, Massachusetts, USA). Abberior STAR RED (KK114) was obtained from Abberior (Göttingen, Germany).

3.4.2.2 Production of Fab 10E8

Fab 10E8 antibody sequence was cloned in the plasmid pColaDuet and expressed in Escherichia coli T7-SHuffle strain as previously described in 2.2.1 section. For confocal microscopy experiments, position C₂₁₆HC of the Fabs was modified in vitro with a sulphydryl-specific iodacetamide derivative of the KK114 probe.

3.4.2.3 LPF production

To prepare peptide containing LPFs at peptide-to-lipid molar ratio of 1:50, lipids and NpreTM or CpreTM-TMD2 dissolved in HFIP were mixed in organic solvent prior to the production of the liposomes as explained in 2.1.1.2 section.

Effective incorporation of the peptide to the vesicles was ensured by peptide flotation in a sucrose gradient following 2.1.3 protocol.

3.4.2.4 GUV-Fab binding assays

NBD-labeled GUVs were produced by spontaneous swelling as described in section 2.1.1.1, co-dissolving lipids with NBD (2 mol %). When required, NpreTM or CpreTM-TMD2 peptides are dissolved in HFIP and included in organic phase at 1:250 peptide-to-lipid ratio.

For binding experiments, NBD-labeled GUVs with peptide (1:250 peptide-to-lipid molar ratio) were used. The GUVs were added to a BSA-blocked microscope chamber that already included 250 nM of 10E8 Fab conjugated with the KK114 probe at residue C₂₁₆HC, and were incubated for 15 min prior to imaging.

Images were acquired on an inverted confocal fluorescence microscope (Nikon Eclipse TE-2000, Nikon, Nikon Instruments, Tokyo, Japan) as described in section 2.4.1.3. In brief, NBD-stained GUVs and Fabs conjugated with the KK114 probe were excited at 476 nm and 637 nm, respectively. The band pass filters used were 515/30 and Long Pass 650 nm. The objective used was a 63X oleo immersion with a NA of 1.2.

Relative extents of Fab-GUV binding were obtained by measuring the fluorescence intensity of KK114 along the equatorial plane of the GUV images. Fluorescence emission analyses were carried out with ImageJ software (rsb.info.nih.gov/ij/).

3.4.2.5 Infrared spectroscopy

Infrared spectra were recorded in a Bruker Tensor 27 spectrometer equipped with a mercurycadmium-telluride detector using a Peltier-based temperature controller (TempCon, BioTools Inc., Wauconda, IL) with calcium fluoride cells (BioCell, BioTools Inc., Wauconda, IL) and following protocol 2.3.2. LPFs of different compositions were lyophilized and subsequently prepared at 3 mg/mL in D₂O buffer. Data treatment and band decomposition of the original amide-I as described in ²⁵⁴.

3.4.2.6 SLB production

To produce SLBs, the vesicle adsorption method was followed as described in *section 2.1.1.3*. LPFs were prepared at a peptide-to-lipid molar ratio of 1:50, mixing lipids and NpreTM or CpreTM-TMD2 dissolved in HFIP.

3.4.2.7 AFM measurements

SLBs topographical images were performed using a Nanowizard III AFM (JPK Instruments) under contact mode AFM scanning and following protocol in *2.6.1 section*. AC-40 Si₃N₄ cantilevers (Bruker, Billerica, MA, USA) with a nominal spring constant of 0.9 N/m were used for bilayer imaging with 0.5 nN of force applied.

Force spectroscopy data were collected following step 4 of *2.6.1 section* and using SNL-10 Si₃N₄ cantilever (Bruker, Billerica MA, USA) with a nominal spring constant of 0.35 N/m, at a speed of 1 μm/s and applying 10 nN of force. Force steps were determined for each of the indentation curves as reproducible jumps within the extended traces.

For single molecule force spectroscopy, MLCT-BIO probes (Bruker, Billerica MA, USA) were functionalized with Fab 10E8 as described in *section 2.6.2*. Force maps were recorded using a maximum applied force of 0.2 nN, a varying contact time of 0.5, 1, 2 and 5 s and varying retraction speeds of 0.1 μm/s, 2 μm/s and 10 μm/s. Data were analyzed with the data processing software from JPK Instruments (Berlin, Germany).

Prior to imaging cantilevers were individually calibrated in a lipid free mica substrate in buffer, using the thermal noise method ³¹¹ after having correctly measured the piezo sensitivity (V/m).

3.4.3. Results

3.4.3.1 Reconstitution in membranes of NpreTM and CpreTM-TMD2 helices

Atomic structure resolution of Fab 10E8 in complex with soluble MPER-based peptides and protein scaffolds revealed a binding surface onto the C-terminal MPER helix comprising residues $^{671}\text{NWFDITNWLWYIK}^{683}$, which precedes the TMD of the Env glycoprotein (residues 684-709, Figure 3.4.1 A) ^{12,178,181}. In the structure of the Fab 10E8 published by Huang et al.¹², the sequence of the bound peptide spans the complete MPER (residues 656-683) whereas its structure displays two well-defined helices joined by a flexible hinge at position 669-671. An earlier epitope recognition model proposed that the C-terminal helix (residues 671-683) containing the 10E8 epitope submerges into the membrane interface, while the Fab settles on top of the bilayer (Figure 3.4.1 B, left)^{164,188,312}. According to this tenet, MPER would be connected to the TMD through an elbow at position 683-684 that changes the direction of the chain ¹⁶². In a later study, Rujas et al. ¹⁷⁸ described a structure of the Fab in complex with a peptide that included residues derived from the TMD (residues 664-690). In the structure of this Fab-peptide complex, no connecting elbows were observed between the C-terminal helix of MPER and the N-terminal end of the TMD, but both sequences combined to form a continuous helix spanning residues 671-690 (Figure 3.4.1 B, right). Furthermore, the presence and position of bound phosphates suggested that the Fab approaching laterally to the MPER helix, could accommodate the viral membrane through a defined paratope surface. Subsequent experimental evidence, including the precise positioning of phospholipid moieties in the atomic structures of Fab-peptide complexes ^{96,146,181}, cryo-EM studies ^{76,157} and superresolution optical microscopy ⁵¹ data gave further support to this arrangement of Fab and MPER helix on membrane surfaces. Thus, according to this model of MPER recognition, the 10E8 epitope would actually project into the solution as a continuation of a TMD helix inserted perpendicular to the plane of the bilayer, and the membrane surface would be a component of the antigen structure.

To compare these models, in this study we employ two different peptides that contain the 10E8 epitope sequence, one at its C-terminus (NpreTM: $^{656}\text{NEQELLELDKWASLWNWFNITNWLWYIK}^{683}$), the other at its N-terminus (CpreTM-TMD2: $^{671}\text{NWFDITNWLWYIKLFIMIVGGLVGLRIVFAVLSVVNRVR}^{709}$) (Figure 3.4.1 A and B, bottom panels). Hence, we expect these peptides to expose the 10E8 epitope with different topologies when reconstituted in membranes, the former as part of an

interfacial helix, the latter as the initial section of a continuous helix that spans the membrane.

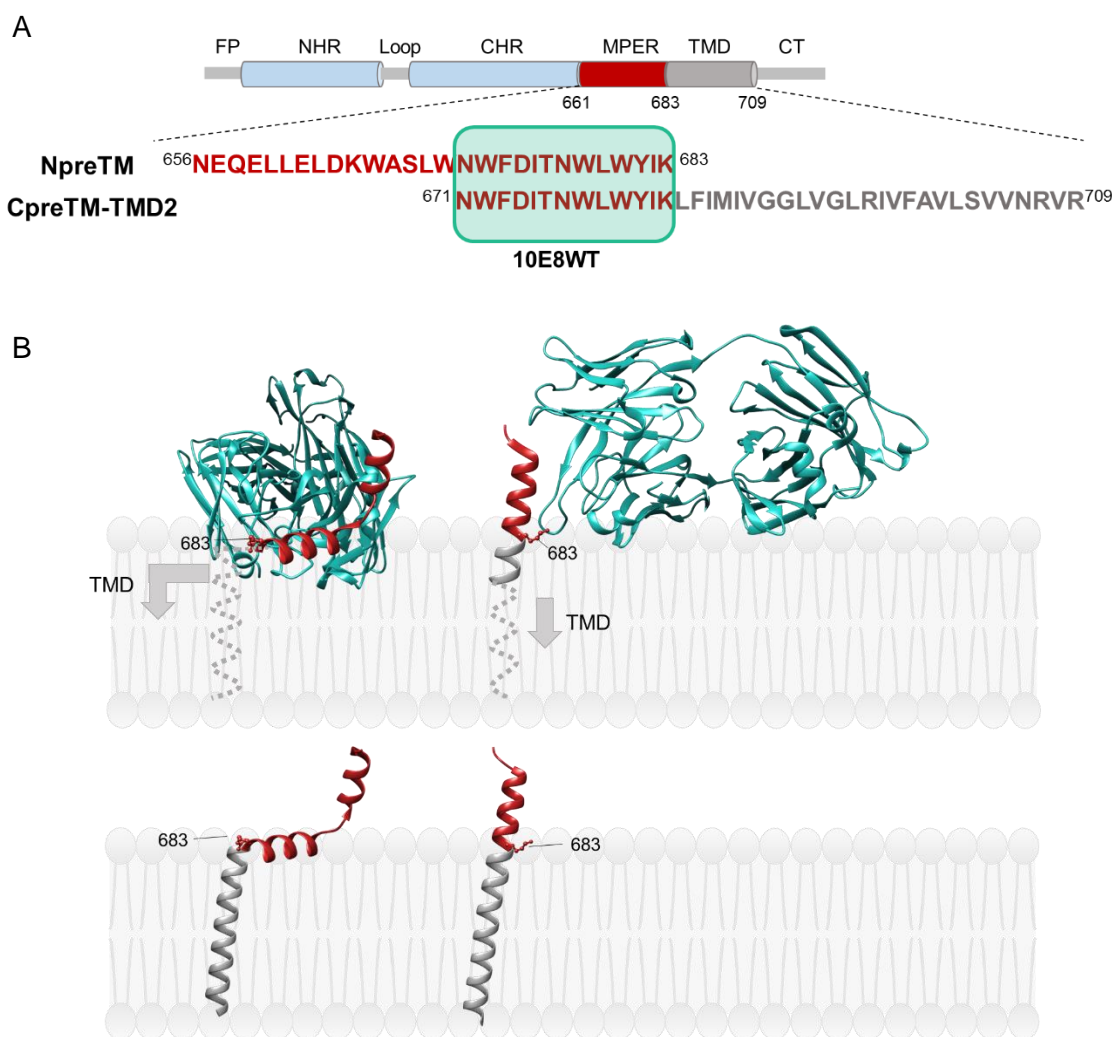


Figure 3.4.1. Models of binding to the HIV-1 neutralizing epitope 10E8 at the viral membrane interface. A) Sequence range and designation of the epitope-peptides used in this study. **B)** Two different modes of 10E8 epitope recognition are compared according to solved structures of the Fab in complex with different MPER-based peptides. Left: Fab solved in complex with 656-683 MPER peptide (PDB entry: 4G6F). Right: Fab solved in complex with 664-690 MPER-TMD peptide (PDB entry: 5GHW). The bottom panels display models for insertion into the membrane based on the structures on top superposing with residues 683-709 of the TMD (PDB entry: 6B3U).

For their reconstitution in POPC membranes, the peptides dissolved in an HFIP solution were mixed with lipids in organic solvent and desiccated (as previously described in section 2.1.1.2). The peptide-to-lipid mole ratio was 1:50, approaching the peptide membrane densities previously used in liposome-peptide MPER vaccine formulations¹⁹⁰.

The resulting peptide-lipid films were subsequently subjected to gentle hydration²⁹⁷. The vesicle-flootation experiments shown in Figure 3.4.2 A corroborated total incorporation of both peptides into membranes following this reconstitution procedure. The electrophoretic mobility of the peptide bands also suggested the formation of SDS-resistant homo-oligomers in the case of the CpreTM-TMD2 peptide reconstituted in the membrane.

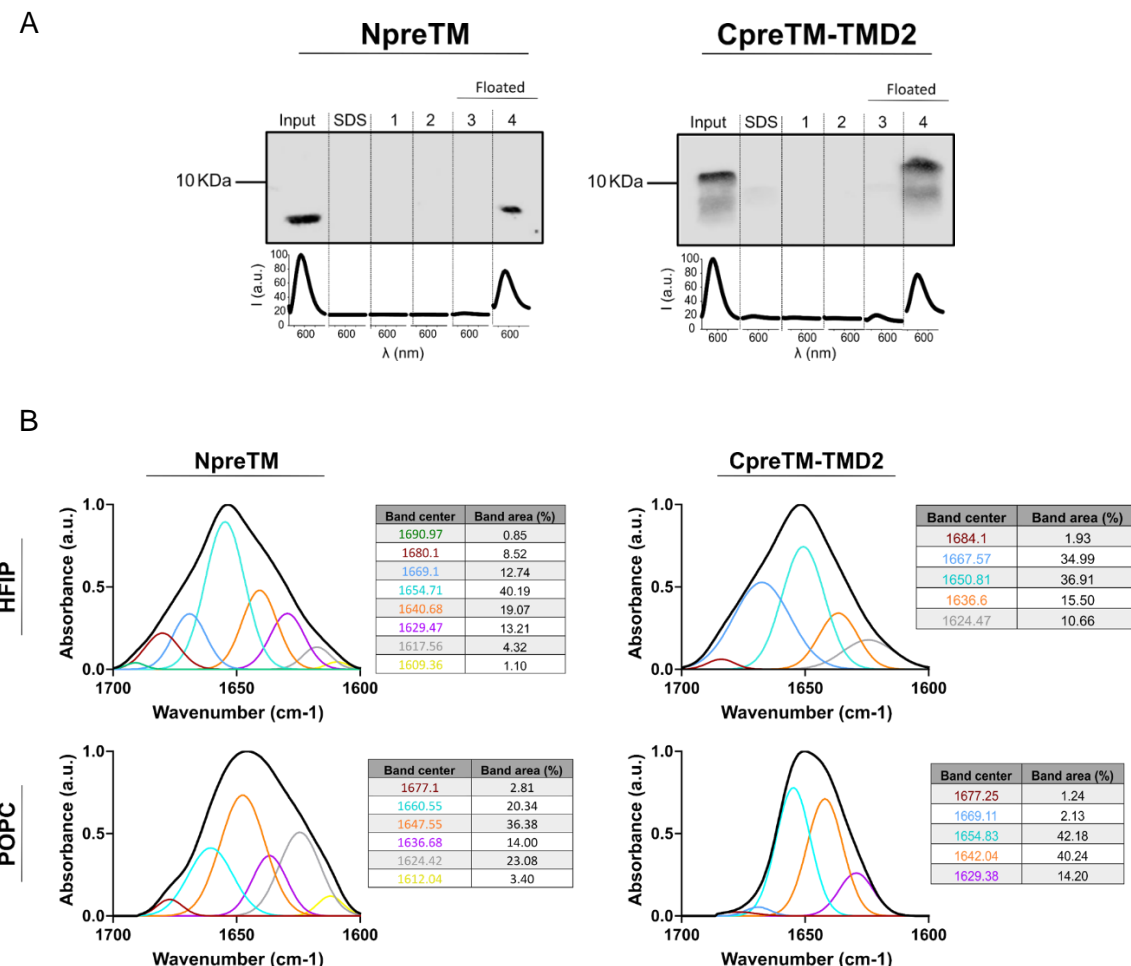


Figure 3.4.2. Reconstitution of NpreTM and CpreTM-TMD2 peptides in POPC membranes. **A)** Flootation experiments. Vesicles incorporating the peptides were subjected to ultracentrifugation in a sucrose gradient and the presence of peptides in the floated and non-floated fractions of the gradient and in the original sample (input) revealed by Western Blot analysis. Fluorescence emission spectra of the Rhodamine probe are displayed below to reveal the presence of vesicles in the floated fractions. **B)** IR absorption bands in the amide-I region obtained for peptides in 50 % HFIP (vol:vol) or after reconstitution in POPC membranes (top and bottom panels, respectively). Percentages contributed by the band components are displayed in the side Tables. In both panels the peptide-to-lipid ratio was 1:50 (mol:mol).

The secondary structure determination by IR spectroscopy confirmed absorption maxima around 1650 cm^{-1} in the amide-I regions of the spectra, consistent with the efficient reconstitution of both peptides adopting main α -helical conformations in POPC bilayers (Figure 3.4.2 B). However, as judged from the width of the bands, when compared with the spectra obtained in 50 % HFIP (Figure 3.4.2 B top panels), a more pronounced reduction of conformational flexibility (i.e., lower number of absorption modes) could be discerned in the case of the reconstituted CpreTM-TMD2 peptide. Moreover, the significant contribution of a band centered at 1642 cm^{-1} to absorption in the amide-I region, was consistent with a tendency to self-oligomerization of the CpreTM-TMD2 helices in the membrane^{313,314}.

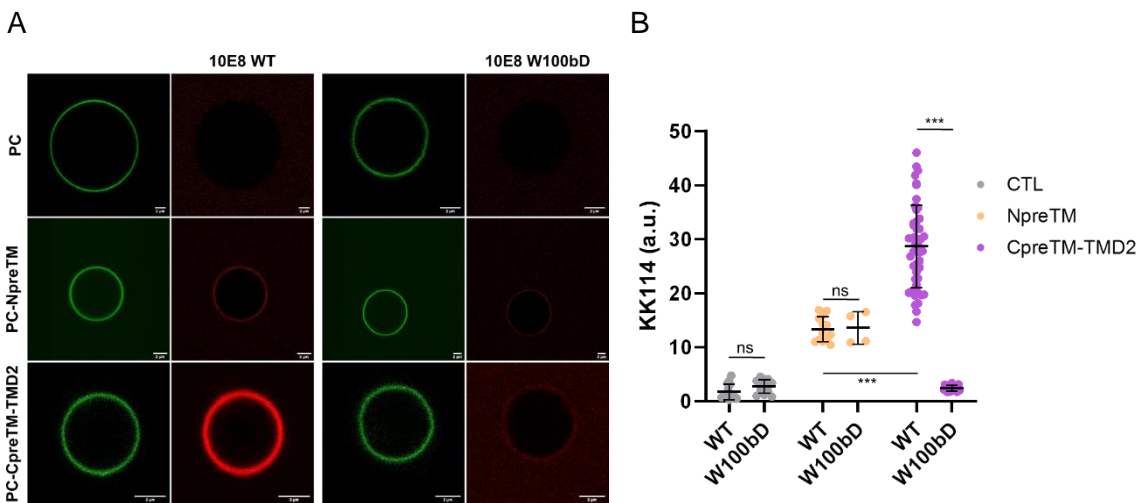


Figure 3.4.3. Binding of 10E8 to POPC GUVs containing MPER peptides reconstituted. **A)** Confocal microscopy images of single POPC vesicles (green label) incubated with KK114-Fab 10E8 (red label). In samples containing peptide the peptide-to-lipid ratio was 1:250 (mol:mol). **B)** KK114 intensity quantitation at the equatorial plane of the different GUV samples. (Mann-Whitney Test: ***p < 0.001; **p < 0.01, *p<0.05, n.s. ≥0.05).

We next compared the accessibility to the 10E8 epitope after reconstitution of NpreTM and CpreTM-TMD2 α -helices in membranes (Figure 3.4.3). To that end we quantified binding to single vesicles by confocal microscopy of GUVs incubated with fluorescently labeled Fab 10E8^{274,297}. According to the scored intensities, the Fab 10E8 appeared to bind more efficiently to CpreTM-TMD2-containing vesicles than to NpreTM-containing ones. Moreover, emphasizing the specificity of the process, the non-neutralizing Fab 10E8 bearing the W100bD mutation at the combining site¹⁷⁸ did not bind appreciably to the reconstituted CpreTM-TMD2 peptide. Conversely, this Fab mutant seemed to display

an affinity degree toward the reconstituted NpreTM that was comparable to that displayed by the WT for the same peptide in these assays. Consistent with an epitope recognition-dependent phenomenon, label KK114 was not detected in association with the membranes of GUVs devoid of peptide upon incubation with the Fab-s.

3.4.3.2 Topography of SLBs containing reconstituted peptides probed by AFM

Having demonstrated the efficient reconstitution of both peptides and the accessibility of the 10E8 epitope at the surface of the POPC membrane, we next analyzed the nanoscopic structure of peptide-containing membranes by AFM. Topographical characterization of SLBs with and without peptides were first carried out to ensure that the surfaces were homogeneous and defect-free. AFM images displayed in Figure 3.4.4 A compare the topography of POPC SLBs devoid of peptide with those containing NpreTM or CpreTM-TMD2 reconstituted at 1:50 peptide-to-lipid mole ratios. In all instances, the heights of the flat membrane patches adhered to the mica substrate were consistent with the thickness of a single lipid bilayers (ca. 4 nm). In the case of NpreTM-containing samples, the SLB covered the measured surface except for some circular holes that accumulated material at their edges. This material protruded approximately 1 nm from the bilayer plane.

Nonetheless, a detailed statistical analysis revealed a significant increase of the lipid bilayer thickness in the case of the SLBs containing CpreTM-TMD2 peptide reconstituted (Fig. 3.4.4B)

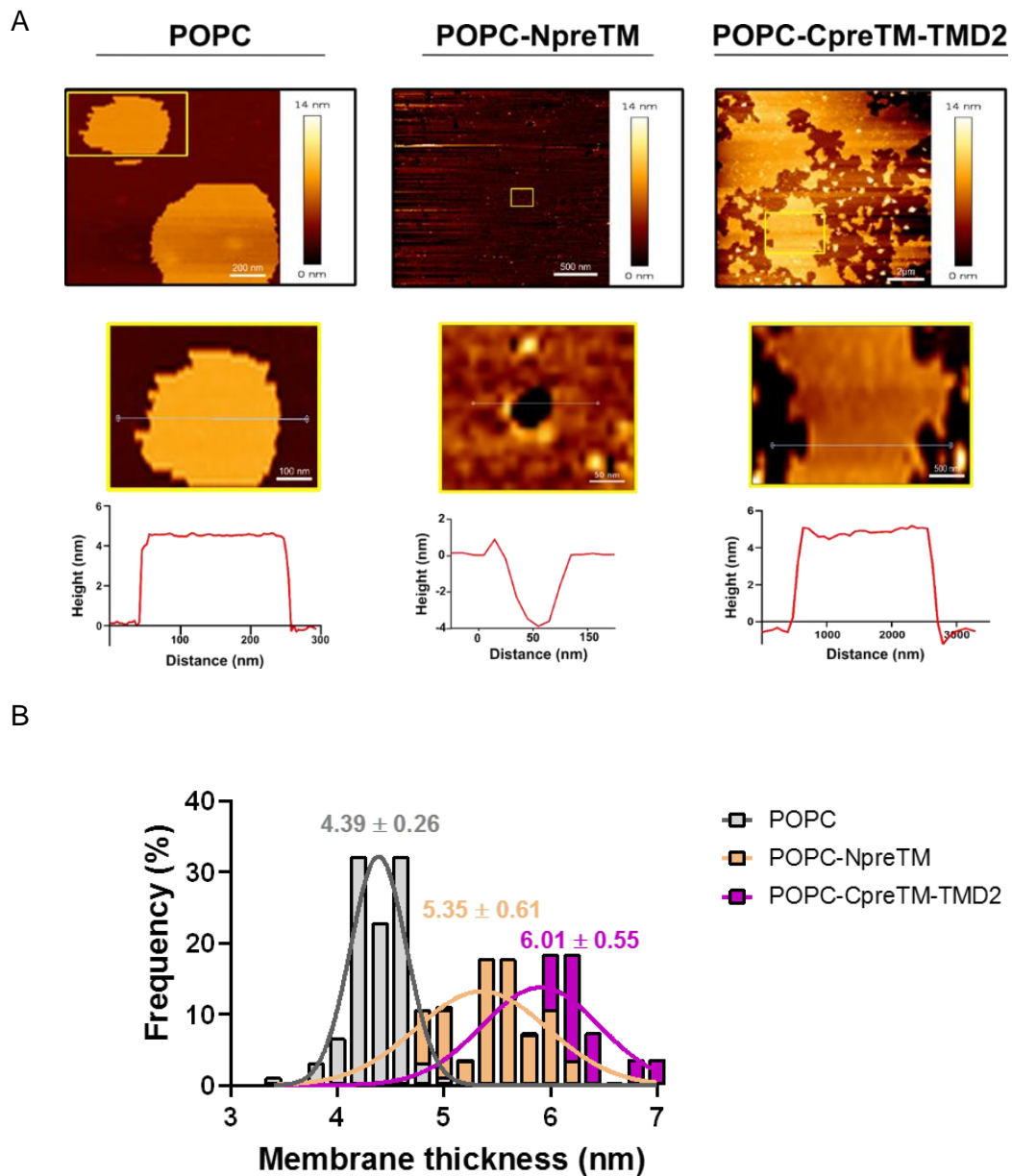


Figure 3.4.4. Topographical analysis by AFM of POPC SLBs containing MPER derived peptides reconstituted. A) AFM images taken from POPC SLBs with or without peptide as indicated in the panels. Plots below images display the height profiles for the trajectories indicated by the white lines. **B)** Frequency distribution of the height profiles of the SLBs. The curves indicate the fitted Gaussian functions and the peaks of the distributions (\pm S.D.) are indicated above.

3.4.3.3 Effect of the reconstituted peptides on the nanomechanical stability of SLBs

To discern effects of the reconstituted peptides in a quantitative way, we next turned to FS-AFM³⁰⁸ (Figure 3.4.5 A). Thus, we measured the breakthrough forces (Fb) of the different SLBs to determine effects of the peptides on the nanomechanical resistance to membrane rupture (Figure 3.4.5 B). The obtained values indicated that reconstitution of NpreTM reduced the force required to break the POPC lipid bilayer, consistent with a reduction on its mechanical stability. This softening effect would be in line with the roles proposed for MPER-membrane interactions during the fusion process^{140,151,166,217,305,313}. Interestingly, inclusion of CpreTM-TMD2 increased the values of the forces at which rupture was observed. This increase was even larger than that observed in an SLB-containing 50 mol % Chol, which was added as a control sample to the analysis. Thus, in contrast to NpreTM, CpreTM-TMD2 appeared to stiffen the lipid bilayer following the trend displayed by cholesterol. This different behavior could arise from effects on lipid packing modulated by the distinct topologies adopted by the peptides in the membrane, interfacially adsorbed the former, and integrated as a membrane-spanning moiety the latter (see Discussion below).

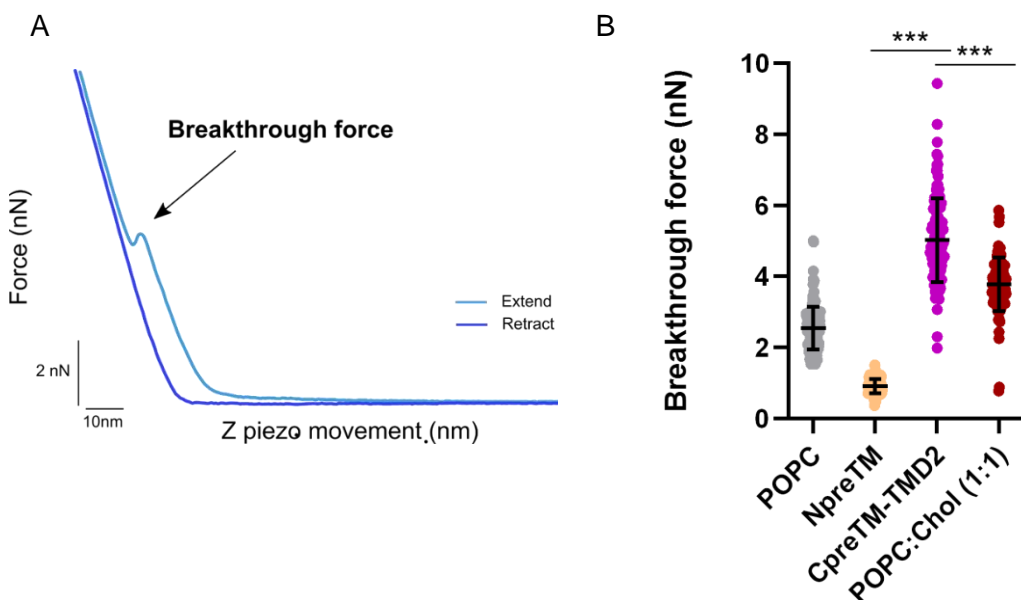


Figure 3.4.5. Effects of peptide reconstitution on the breakthrough force of POPC SLBs. A) Experimentally measured approaching and retraction force curves performed on a sample showing the jump in distance of ca. 4 nm with an applied force of 10 nN. **B)** Mean breakthrough force values measured in the different samples. The NpreTM-containing SLBs displayed significantly lower breakthrough forces than those containing CpreTM-TMD2 (Mann-Whitney Test: ***p < 0.001; **p < 0.01, *p < 0.05, n.s. ≥ 0.05). The peptide-to-lipid mole ratio was 1:50 in the samples containing peptide. The POPC:Chol (1:1) sample was included as a control of membrane stiffening.

3.4.3.4 Determination of SLB antigenicity by Single-molecule force spectroscopy

To probe the different antigenicity of the samples by AFM, FS was finally applied in an effort to measure antibody-MPER interactions at the single molecule level. Single-molecule FS is a useful strategy to obtain information about the unbinding process of receptor-ligand interactions and has been used for a wide range of different biological systems, including antibody-antigen interactions^{315–319}. Single molecule AFM is based on the fact that k_{off} is increased when an external force is applied. Thus, measuring the rupture forces of a receptor-ligand interaction at different loading rates permits the extrapolation to the dissociation rate at zero force, which represents the k_{off} of the binding reaction (for data analysis see section 2.6.2.). Furthermore, this method provides additional information, the potential width ($\chi\beta$), which could be useful for analysing changes in the binding site or other conformational rearrangements of the molecules.

Figure 3.4.6 A illustrates the force-extension experimental approach followed. To evaluate antibody-epitope binding strengths, antibody 10E8 was first attached to an AFM tip, and SLBs loaded with peptides are attached to mica surfaces. During the procedure, the functionalized AFM tip is cyclically brought into contact with the surface, until formation of an antibody-epitope complex takes place. In such case, the retraction of the tip from the surface translates into an increasing force that applies continuously to the formed intermolecular complex until the Fab-epitope connection breaks apart at a critical force, called the unbinding force.

To perform these experiments we turned to a recombinant form of the antigen-binding fragment (Fab) of the antibody 10E8, which was covalently tethered via a crosslinker to the AFM probe. Since the Fab contained a single titratable Cys residue at position 216 of the HC, through the free thiol we first tried to link the Fab 10E8 to an previously amino-functionalized AFM tip treated with maleimide, which reacts specifically with thiol groups (Figure 3.4.6 B, top). Unfortunately, in force-distance measurements using these tips we were unable to detect binding events in a number of trials. Thus, we turned to treat the amino-functionalized tip with glutaraldehyde that enable covalent coupling to AFM-tips through accessible amine groups on the Fab surface (Figure 3.4.6 B, bottom). In this case, after probing SLBs containing the peptides we confirmed empirically the occurrence of binding events as exemplified by the force-extension experiment displayed in the rectangle at the bottom of Figure 3.4.6.

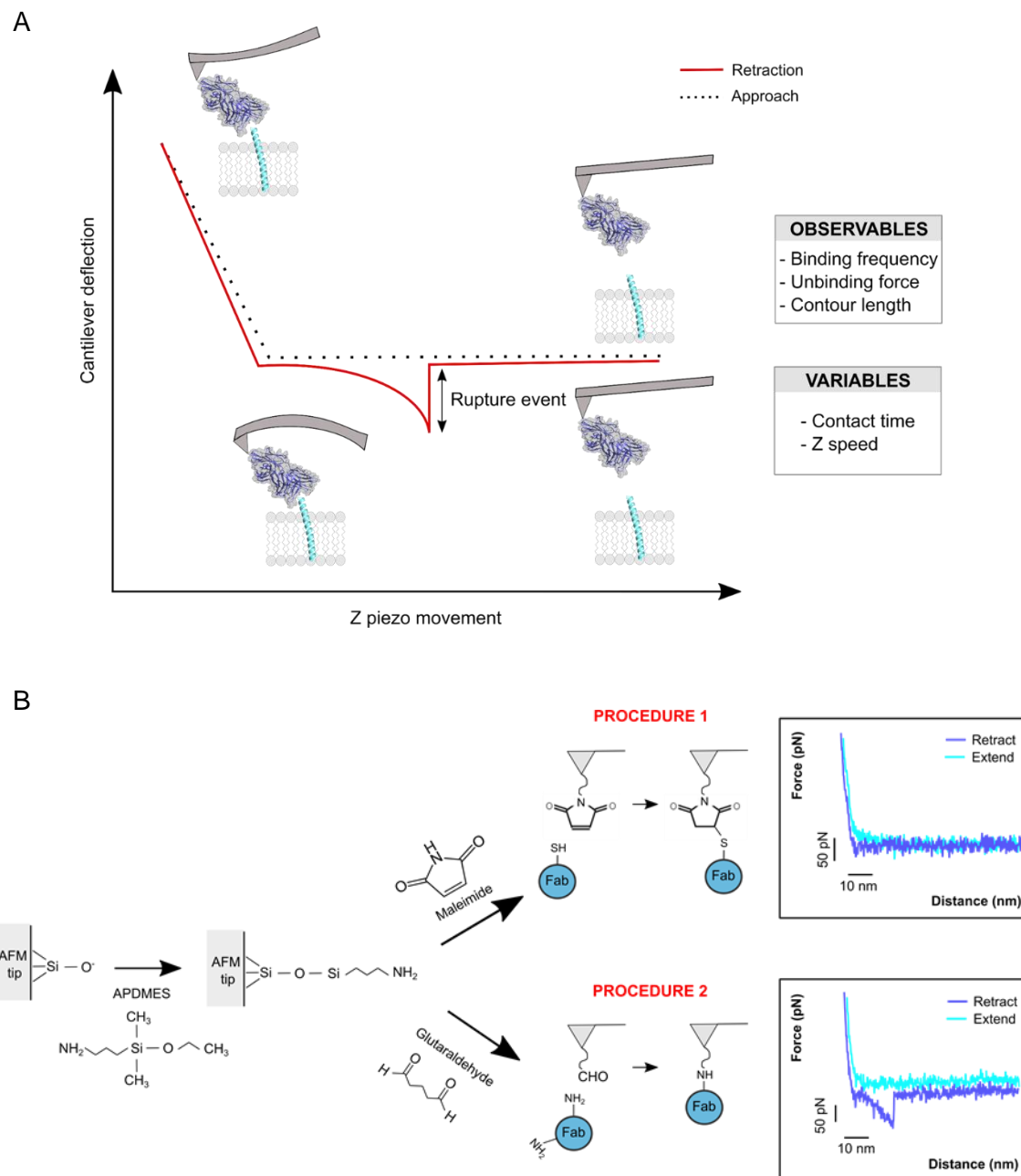


Figure 3.4.6. Force-extension approach followed to detect single-Fab binding to MPER in SLBs. **A)** Diagram depicting a theoretical force-extension curve using AFM tips with Fab 10E8 covalently tethered via a crosslinker, and the parameters that can be inferred as a function of the measuring conditions. **B)** Diagram on the left illustrates the first step of cantilever functionalization, the treatment with APDMES to silanize the surfaces with amine groups. Then, the two procedures used are depicted on the right. In procedure 1 (on the top) the Fab is linked through free Cys thiol, whereas that on the bottom (procedure 2) depicts linking through free amines. Rectangles on the right show force-distance cycles with no binding event using procedure 1 of functionalization on the top; and revealing an unbinding event in POPC SLBs loaded with the CpreTM-TMD2 peptide and using a tip functionalized with Fab 10E8 following procedure 2 on the bottom.

Figure 3.4.7 illustrates experiments detecting the number of events as a function of the tip-SLB contact time. In the presence of peptides, a fraction of the retraction curves (<20 %) was observed to display unbinding events as those illustrated in Figure 3.4.7 A (left). In contrast, unbinding events were hardly discernable when SLBs devoid of peptide were probed. Moreover, these events appeared to exhibit higher unbinding forces in the case of CpreTM-TMD2-containing SLBs (Figure 3.4.7 A right). The frequency of occurrence as a function of the contact time also appeared to indicate higher frequency of binding in the case of CpreTM-TMD2 peptide (Figure 3.4.7 B).

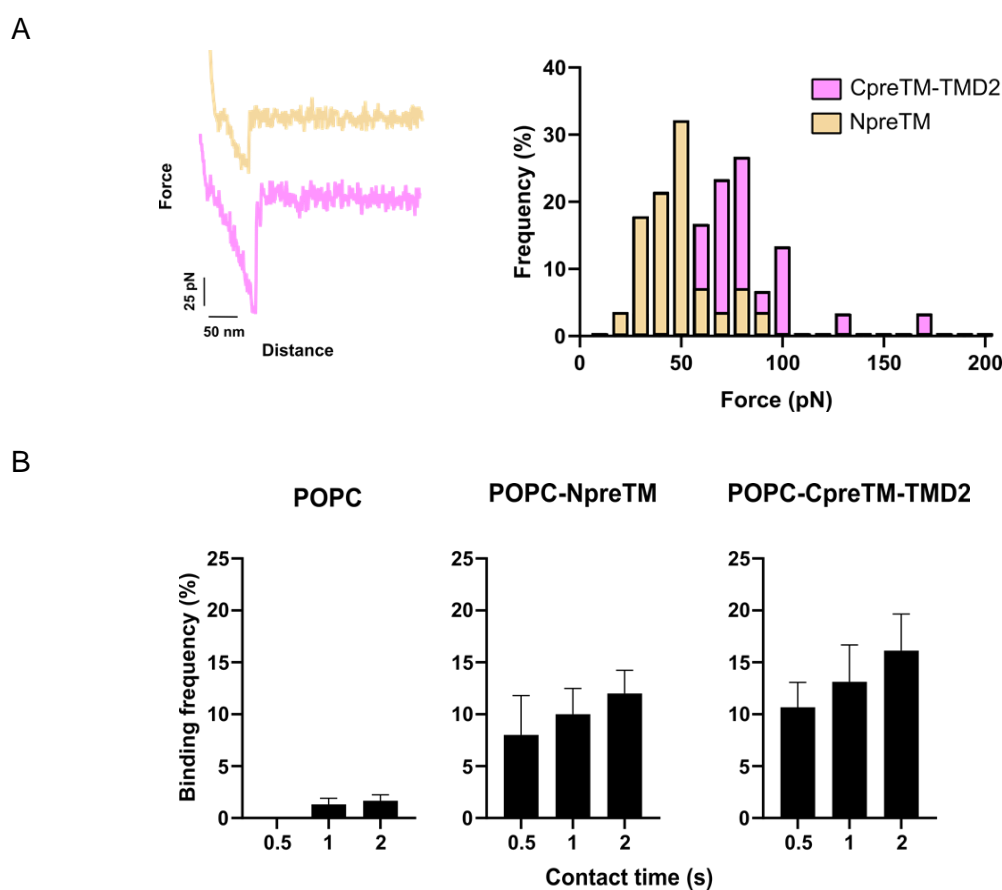


Figure 3.4.7. Unbinding events scored as a function of the contact time. **A)** Representative force curves on the left display single unbinding events and a force histogram for SLBs containing peptides. **B)** Plots comparing the binding frequencies after probing the different SLBs at different contact times. The retraction velocity was fixed in these experiments ($2 \mu\text{m}\cdot\text{s}^{-1}$).

To obtain measurements over a broad range of different loading rates, several experiments were performed, each at a different retract velocity ranging from $0.1 \mu\text{m}/\text{s}$ to $10 \mu\text{m}/\text{s}$. Thus, we determined single-molecule unbinding forces (the force at which

the antibody-antigen complex ruptures) as a function of the loading rate. The loading rate describes how much force was applied to the bond at a certain time shortly before the rupture event occurs.

Data obtained in this way were treated as described in section 2.6.2^{320,321}. Briefly, to determine the F^* at a given loading rate the frequency histograms of the measured forces were fitted to a Gaussian distribution and its maximum calculated. As an example, Figure 3.4.8 A compares force histograms obtained for SLBs loaded with NpreTM or CpreTM-TMD2 (Contact time: 0.5 s, loading rate 41 nN·s⁻¹). F^* is a function of the loading rate as defined by Eq. 3.4.1.

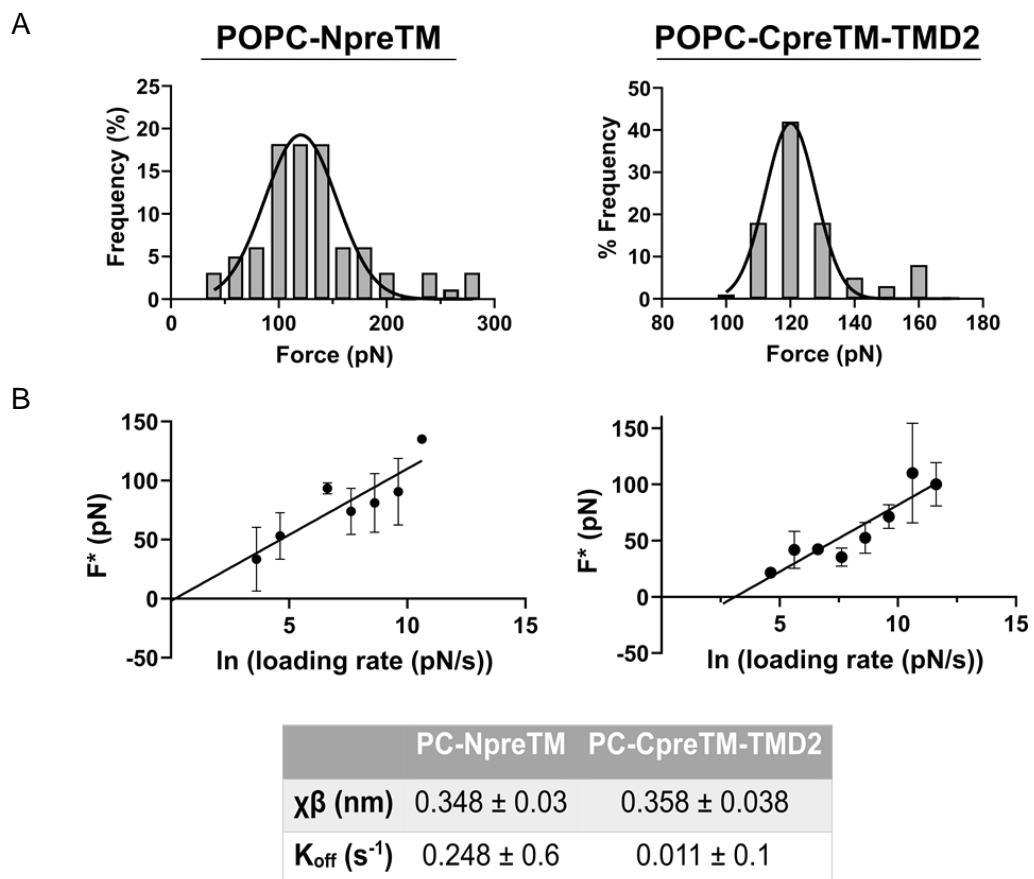


Figure 3.4.8. Single-molecule force spectroscopy assays to evaluate Fab 10E8 binding strength. A) Comparison of F^* s obtained in SLBs loaded with NpreTM or CpreTM-TMD2 peptides. Contact time: 0.5 s; Loading rate: 41 nNs⁻¹. B) Semi-logarithmic Bell-Evans plots. Means (\pm SD; $n > 150$) of the experimental F^* values measured with distinct loading-rates were fitted to linear regressions. Inferred $\chi\beta$ and K_{off} values are displayed in the Table below.

$$F^* = \frac{k_\beta \cdot T}{\chi_\beta} \ln \frac{r_f \cdot \chi_\beta}{K_{off} \cdot k_\beta \cdot T} \quad [\text{Eq. 3.4.1}]$$

where k_B is Boltzmann constant, T is the temperature, k_{off} is the natural dissociation rate at zero force and r_f is the loading rate.

This equation represents the Bell-Evans model, which establishes that a linear increase of the unbinding forces with respect to a logarithmically increasing of loading rate denotes the existence of a single-energy barrier in the thermally activated regime^{322,323}. To produce the Bell-Evans plots displayed in Figure 3.4.8 B, F^* determinations were repeated several times at each retract velocity and mean values plotted against the natural logarithm of the loading rate. A linear fit of the force vs. logarithm of the loading rate according to Eq. 3.4.1 reveals the natural dissociation rate at zero force (K_{off}) and the distance of the unbinding energetic barrier from the equilibrium position ($\chi\beta$). These parameters can be obtained from the slope of the linear fit of the data, and the off-rate K_{off} deduced by linearly extrapolating the experimental data to zero external force (i.e., conditions of thermal energy alone). The values obtained for SLB-s containing NpreTM and CpreTM-TMD2 confirmed comparable $\chi\beta$ values for unbinding in both peptides, but 20-fold slower dissociation rate for the Fab-CpreTM-TMD2 complex, in comparison with the Fab-NpreTM complex (Figure 3.4.8 B, Table).

3.4.4. Discussion

Anti-MPER antibodies bind to their target helical epitope in the environment of the membrane^{96,146,178,180,181}. It has been suggested that the natural maturation process of these antibodies requires the development of an accommodation surface to the membrane to increase their affinity and acquire sufficient potency to neutralize HIV^{96,178,181}. Therefore, it follows that MPER peptides must be presented in a membrane-inserted state to emulate an antigen relevant for virus neutralization. The efficiency of a liposome-based MPER vaccine formulation is expected to depend on the stability of the membrane scaffold. It can also be expected that the different topologies that peptides can spontaneously adopt will directly affect their degree of antigenicity, that is, their ability to efficiently expose the MPER epitope.

The results of this work based on the use of AFM-spectroscopy, show that two peptides derived from MPER, namely, NpreTM and CpreTM-TMD2, reconstituted in the membrane with a similar helical conformation, but adopting different topologies, affect the nanomechanical properties of the bilayer in opposite ways. A first indication of their

dissimilar effects could be obtained after measuring the lipid bilayer thicknesses of the SLBs.

Thus, NpreTM incorporated at a dose of 1:50 (peptide to lipid mole ratio) significantly reduced the Fb of the bilayer, while no obvious effects were observed on the overall thickness. Being its location eminently interfacial, this behavior could reflect the lipid packing defects generated by its insertion into a single monolayer. If we calculate its approximate insertion area from its DPC-resolved NMR structure (PDB ID: 2M8O)²⁹⁰, the value would amount to approximately 540 Å², and about 25 POPC molecules would be needed to encircle its perimeter. That is, approximately half of the phospholipids in the bilayer would be directly affected by the inclusion of this peptide.

In contrast, the inclusion of the CpreTM-TMD2 helix exerted a clear effect of mechanical stabilization of the bilayer consistent with a higher degree of lipid packing, also reflected by the increase of the lipid bilayer thickness observed after reconstitution. A CpreTM-TMD2 monomer in its thickest section, close to the interface and rich in aromatic amino acids, could occupy an area of about 130 Å². In this case, the phospholipid layer in contact with the peptide would be occupied by about 20 molecules (10 POPC molecules/monolayer), which is equivalent to 40 % of the total in the bilayer. However, its electrophoretic mobility suggested that this peptide could assemble trimers in membranes (Figure 3.4.2 A). Thus, in the case of considering a trimer (about 580 Å² of occupied area), the number of phospholipids directly in contact with the peptide would amount to 30, but the effective trimer:lipid dose would be reduced to 1:150, so the percentage of the total lipid in contact with the peptide would be cut in half (20 %). It is therefore likely that the packing effect induced by the membrane-spanning helices spreads beyond the perimeter of the peptide in either monomers or trimers.

Single-molecule FS provided additional information on the degree of antigenicity of the different SLBs containing peptides. Contact time experiments gave first an idea of the degree of specificity of the measured process. The specificity of the unbinding events was supported by two observations in these assays: (i) the relatively low frequency at which the events were scored in the series of force-distance cycles; and (ii) the fact that virtually no events were detected when POPC SLBs devoid of peptide were probed. Also in line with measurements pertaining to intermolecular Fab-antigen interactions, it can be mentioned the fact that tips functionalized following procedure 1 detected no events under the most favorable conditions (i.e., contact times of 2 s, and loading rates as high as 50 nN · s⁻¹). Thus, this observation ruled out the capacity of tips devoid of functional

Fabs to engage with and extract directly non-specifically adsorbed membrane-associated MPER helices³²⁴.

Furthermore, contact time experiments suggested higher affinity of the Fab for the CpreTM-TMD2 peptide. The calculation of the most probable distance between accessible epitopes in a monolayer gives us values of approximately 6 nm for the case of monomeric NpreTM and CpreTM-TMD2 (antigen to lipid mole ratio 1:100), and 10 nm for trimeric CpreTM-TMD2 (antigen to lipid mole ratio 1:300). It is therefore unlikely that the differences in the epitope dose in the membrane caused the differences between both peptides in the frequency of detected events.

In experiments carried out increasing the loading rate, the need to apply a greater force to break the Fab-peptide complex was also invariably observed in the case of CpreTM-TMD2 peptide-containing samples. The data derived from the Bell-Evans diagram seem to indicate that indeed the rate of dissociation is slower in this case. However, the fact that the distance to the activation barrier is essentially the same in both complexes would be consistent with interaction processes mediated at the molecular level by very similar structures. Together with the values of the measured F*-s (mostly below 100 pN, see reference³²⁴), that observation adds to the notion that the unbinding events scored in our experiments pertain to the Fab-antigen complex rupture and not to membrane-spanning helix extraction.

In summary, most liposome-based vaccine approaches have assumed until now that synthetic peptides representing the MPER sequence (i.e., bending at position K/R683) can expose neutralizing epitopes in a fixed position when attached to the surface of vesicles^{190,290,325,326}. However, even in cases where the overall stability of vesicles remains uncompromised, the material properties of the lipid bilayer scaffold can change by effect of peptide insertion into the interface, which in turn can modulate peptide insertion modes and conformations. Our evaluation based on the use of AFM spectroscopy suggests that MPER peptides anchored through the TMD scaffold, stabilize the membrane mechanically and engage more efficiently with antibodies. As such, we believe they should be considered in future liposome-peptide formulations aimed at the production of MPER antibodies.

4.KAPITULUA

EZTABIDA OROKORRA



4. EZTABAIDA OROKORRA

GIB-1aren aurkikuntza eman zenetik, komunitate zientifikoak ikerketa ugari eta ahalegin handiak egin dituen arren, ez dago egun HIESaren pandemiarekin amaituko lukeen txerto profilaktiko eraginkorrik¹³⁶. Hala ere, kutsatutako zenbait indibiduoen serumetatik lortutako antigorputzak GIB-1aren andui desberdinak neutralizatzeko gai direnaren aurkikuntzak, birus honen aukako erantzun immune babeslea sor daitekeela frogatzen du³⁰³. Beraz, infekzioan zehar sortzen diren bnAb-ek ezagutzen dituzten epitopoen egitura antzeratzea, funtsezkoa da Env-en oinarritutako immunogenoen garapen arrazionalerako¹³⁶.

MPER domeinua, mintza zeharkatzen duen gp41 azpiunitatean kokatua dago, kontserbazio maila oso altua du eta funtzio kritikoa betetzen du GIB-1aren fusio prozesuan mintza ezegonkortuz¹⁹¹. Halaber, orain arte isolatutako bnAb-en artean, MPERaren C muturrera zuzenduta daudenak, gp41 azpiunitatearen jarduera fusogenikoa blokeatzen dute eta gainera, GIB-1aren espektro oso zabala neutralizatzeko gai dira^{12,145,170}. 10E8 antigorputza, MPERera zuzendutako bnAb aztertuenetako bat denez, MPERean oinarritutako peptidoen antigenizitatea ebaluatzeko eredu gisa erabili da tesia lan honetan. Anti-MPER antigorputzek mintzarekin kontaktuan dagoen sekuentzia bat ezagutzen dutenez^{96,146,178,181}, MPER domeinuan oinarritutako antigenoa sortzeko mintz ingurune hori mantentzea garrantzitsua dela argudiatu da.

Horrez gain, C-MPER sekuentzia immunogenikoa izateak¹⁷², gutxienez BCRenzako eskuragarri dagoen eta erantzun neutralizatzalea eragiten duen egitura egonkor bat badagoela iradokitzen du.

Ezaugarri guzti hauek kontuan izanda, ondoriozta daiteke MPER domeinua immunogenoen diseinurako itu ezin hobea dela; izan ere, espero da txertaketa bidez sor daitezkeen anti-MPER antigorputzek GIB-1aren infekzioaren aurrean erabateko babes ematea. Hala ere, oso eskualde dinamikoa da eta ez dago beti immunitate sistemarentzako ikusgai, ondorioz, babes-erantzuna sortzeko behar den egitura hipotetikoa identifikatzea erronka izugarria da eta horrek, asko zaitzen du domeinu honetan oinarritutako txertoen garapena.

Tesi lan honek, espektro zabaleko eta potentzia altuko antigorputzak sortzeko gai den MPERaren egitura egonkorra imitatzen duten LPFen diseinuari buruzko ezagutza berriak eman ditu (4.1 irudia). Hau lortzeko, lipido mintzak MPER epitopoaren egitura

immunologikoan duen eginkizuna eta beharrezko den sekuentzia sakon aztertu eta deskribatu da kapituluetan zehar.

LPFetan erabiliko den MPERaren sekuentzia zehaztean, kontuan izan behar da GIB-1aren eta itu zelulen arteko mintzen arteko fusioan parte hartzen duen sekuentzia dela^{140,148,151,187} eta ondorioz, mintz lipidikoa perturbatzeko gaitasuna duela ²²⁵. LPFen egonkortasuna, hau da, mintza perturbatzeko eta fusionatzeko gaitasunik ez izatea, peptido txertoak diseinatzerakoan kontuan hartu beharreko funtsezko ezaugarriarik bat da. Egonkortasun honek, immunitate sistemarentzako epitopoaren etengabeko eskuragarritasuna bermatuko du mintzen gainazalean. Beraz, LPFen diseinurako lehen urratsa, txerto formulazioetan erabiliko den MPER epitopoaren egitura eta sekuentzia adierazgarriak zehaztea izango litzateke.

3.1 kapituluan, CpreTM peptidoa lipido besikuletan errekonstititu da eta peptidoak mintzean hartutako egitura eta mintzen perturbazioetan duen eragina, IR eta cryo-EM bidez aztertu da. CpreTM peptidoak, erantzun immunea MPER domeinuaren alde C-terminalera bideratzeko helburuarekin, ez du zonalde N-terminala, 2F5 bezalako espektro ertaineko erantzunak eragiten dituena ¹⁴³. Aurreko ikerketek iradokitzen dute CpreTM peptidoak mintzen berregituratzea eragiten duela GIB-1aren mintza bezalako Chol kantitate handia duten lipido besikuletan ^{6,41,43}. Emaitza hauekin bat etorri, 3.1 kapituluko espektroskopia datuek (3.1.4 A irudia) iradokitzen dute, CpreTM-a kolesterolik gabeko mintzetan, soluzioan eskuragarri dagoen α -helize egitura hartzen duela errekonstituzio prozesuaren ostean. Aldiz, lipido besikuletan Chol-a gehitzean, peptidoaren konformazio aldaketa gertatzen da, honen helizeen luzapena hain zuzen. Egitura berri honek mintza desegonkortzen ditu besikulen arteko fusioa eraginez, cryo-EM bidez ikus daitekeen bezala (3.1.6 B irudia). Ondorioz, 3.1 kapituluan aurkeztutako datuetatik abiatuta, ondoriozta daiteke C-MPER domeinuaren egitura oso malga dela eta mintzaren konposizioaren araberakoa. Aurkikuntza horiek, azpimarratzen dute LPFen gainazalean kokatuko den MPER epitopoaren aurkezpena sistema immunera modu egonkorrean gertatzeko, ezinbestekoa dela peptido sekuentzia eta osaera lipidiko egokiak identifikatzea.

Peptido sekuentziaren optimizazioaren eragina

Besikula lipidikoen gainazalean kokatuko den epitopoaren aurkezpena era egonkor batean gerta dadin behar den peptido sekuentziaren optimizaziorako, aldamio moduan jokatuko lukeen transmintz domeinuaren gehipena ikertu da. Hau ikertu ahal izateko, mintza zeharkatzen duten sekuentziaren luzera desberdinako bi peptido diseinatu dira

Yue eta lankideek¹⁸⁷ lorturiko mutagenesi emaitzetan oinarritutik: CpreTM-TMD1, mintzera ainguratzeko behar den TMDaren sekuentzia minimoa duena (3.2 eta 3.3 kapituluetan deskribatua) eta CpreTM-TMD2, transmintz sekuentzia osoa duena (3.3 eta 3.4 kapituluetan deskribatua). 3.2 kapituluan aurkeztutako datuek erakusten dute, etOH-ean disolbatutiko CpreTM-TMD1 peptidoa POPC-dun mintzetan eraginkorki errekonstituitu daitekeela, 10E8 Fab-ak gainazalean kokatutako epitopoa lotzeko duen gaitasunean (3.2.4 irudia) eta peptidoak mintzean hartzen duen alfa helize konformazioan ikus daitekeen moduan (3.2.6 B irudia). Gainera, peptidoaren errekonstituzioak ez du mintzeko lipidoen ordena aldatzen (3.2.5). Hala ere, Chol-aren gehitzeak peptidoaren agregazioa eta destolespena eragiten du (3.2.6 irudia), eta ondorioz, epitopoaren ezkutaketa ematen da, LPFen antigenizitatea galtzen delarik (3.2.5 irudia). 3.3 Kapituluan, errekonstituzio prozesurako, peptidoa disolbatutako HFIPa erabili da etOH-a erabili beharrean, eta 3.2 kapituluan lorturiko emaitzen antzera, Chol-ak peptidoaren agregazioa (3.3.2 irudia) eta epitopoaren ezkutaketa eragiten ditu (3.3.3 irudia). Aitzitik, CpreTM-TMD2 peptidoak egitura helikoidalara hartzen du POPC mintzetan, Chol-a gehitzean ere mantentzen dena. Chol-dun lipido bigeruzetan peptido honek aipaturiko egitura egokia hartzen duen arren, 10E8ren irisgarritasuna epitopora nahiko murrizten da, kolesterolak, 10E8 epitopoaren oklusioa eragiten duten peptidoaren egituraren berrantolaketa gehigarriak sorrarazten dituela iradokiz. Hala ere, POPC bigeruzetan soilik arreta jarriz, 3.3 Kapituluan aurkeztutako datuek erakusten dute 10E8 Fab-aren epitopoa lotzeko gaitasuna, nabarmenki handitzen dela mintza zeharkatzen duen sekuentzia luzatuz (3.3.3 irudia); hau da, CpreTM-TMD2 peptidoa era eraginkorrago batean ezagutzen du antigorputzak.

Epitopoaren irisgarritasun arazoa gainditzeko, CpreTM-TMD2an oinarritutako beste peptido bat diseinatu da, CpreTM-TMD3 alegia. Peptido berri honi, errekonstituzio prozesu ostean, epitopoa mintzetik apur bat altxatzeko nahiarekin, bira helikoidal gehigarri bat erantsi zaio mintza zeharkatzen duen domeinuan. 3.3 Kapituluan lortutako datuen arabera ondoriozta daiteke, MPER-TMD-tik eratorritako peptidoak kolesterolik gabeko geruza lipidikoetan eraginkortasunez aurkezten dutela epitopoa eta mintza zeharkatzen duen sekuentziaren luzerarekin batera handitzen dela epitopoaren esposizio-maila (3.3.3 irudia). Gainera, CpreTM-TMD3 peptidoari gehitutako helize bira honek ez du peptidoaren egitura ezegonkortzen, α -helizea mantentzen delarik konformazio nagusi gisa (3.3.2 irudia).

3.4 Kapituluan, transmintz domeinuaren gehikuntzak, peptidoak mintzean hartzen duen egituraren, gainazalean epitopoak duen esposizio-mailan eta mintzak desegonkortzeko duen gaitasunean dituen efektuak aztertu dira. Horretarako, NpreTM, MPER

domeinuaren N-muturra duen eta interfasean kokatzen den peptidoa, eta CpreTM-TMD2, transmintz domeinuaz ainguratutako MPERaren C-muturra duen peptidoak, AFMz aztertu dira. TMDa epitopoaren aldamio gisa erabiltzearen alde eginez, 3.4 Kapituluan aurkeztutako emaitzek, TMDaren gehipenak bigeruzaren egonkortasun mekanikoa nabarmen hobetzen duela erakusten dute (3.4.5 B irudia). Gainera, molekula bakarreko AFM neurketen arabera, transmintz domeinuaren bidezko ainguraketak epitopoaren disposizioa hobetzen du, CpreTM-TMD2 peptidoa antigorputzen bidez hobeto ezagutzen dela frogatzen duenez.

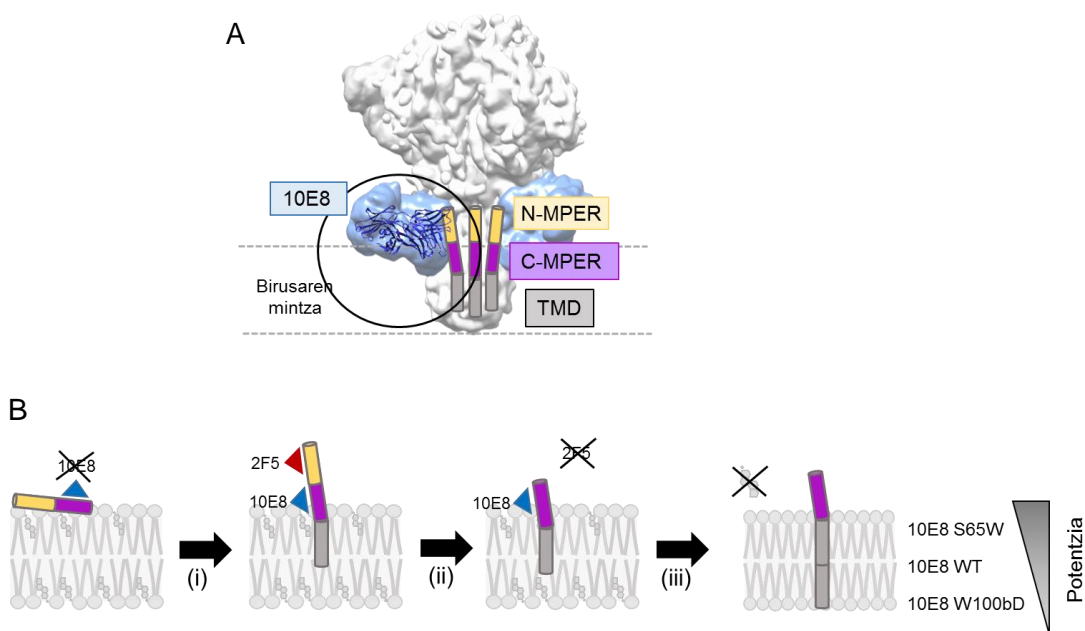
Lipido konposizioa optimizatzearren eragina

Aurretiaz aipatu moduan, lipido konposizioa funtsezko elementua da MPER-TMD domeinuan oinarritutako peptido-lipido txertoen diseinuan. Izan ere, lipidoek peptidoen egitura modulatzeko gaitasuna dute eta ondorioz, epitopoa sistema immunera eraginkortasunez aurkezteko kapazidadea daukate. GIB-1aren mintza zelula ostalariaren mintz plasmatikotik eratorria den arren, espektroskopia bidez bi mintzen arteko desberdintasun esanguratsuak hauteman dira⁴⁷. Desberdintasun nabarmenena, birusaren lipido geruza Chol eta SM-z aberasturik dagoela da; Chol-a birusaren lipido geruzaren lipidoen ia % 50a osatzen duelarik. Gainera, Chol-a birusaren lipido-bilgarritik ezabatzeak, honen infekzio gaitasuna murrizten duela ikusi da⁵⁶, fusio prozesuan ezinbesteko elementua dela iradokiz. C-MPER domeinuan oinarritutako peptido-lipido txertoen garapenerako, birusean dagoen mintz ingurune bat kontserbatu behar dela proposatu denez²²⁶, 3.2 Kapituluan, birusaren mintzaren trinkotasuna imitatzeako helburuarekin, CpreTM-TMD1 peptidoa errekonstituitu da Chol kontzentrazio desberdineko lipido mintzetan. Kapitulu honetan aurkeztutako datuen arabera, peptidoak Chol-ik gabeko besikuletan α -helize egitura hartzen du (3.2.6 B irudia) eta C-MPER epitopoa eraginkorki azalarazten da mintzen gainazalean. Ostea, besikulen Chol edukia handitzeak, zuzenean eragiten du peptidoaren egituraren, honen destolespena eraginez. Ondorioz, GIB-1aren mintza imitatzen duten, eta Chol-ean aberatsak diren mintzetan C-MPER epitopoa ezkutatzen dela dirudi, 10E8 antigorputzen aldaeren bitartez antigenizitatearen galera gertatu dela ikus daitekeen moduan (3.2.4 B irudia). Kapitulu hau beraz, C-MPER domeinuan oinarritutako txertoak ekoizteko birusaren mintza imitatzearen ideiarekin kontra dago.

Era berean, CpreTM-TMD2 eta CpreTM-TMD3 peptido luzeak ere, nahiz eta Chol-dun mintzetan egitura helikoidal mantentzen duten, epitopoa modu eraginkorrean aurkezteko gaitasuna galtzen dutela ikusi da (3.3.2 B eta 3.3.3 irudiak). Beraz,

ondoriozta daiteke Chol-ak peptido luzeagotan ere, egitura berrantolaketa gehigarriak eragiten dituela, 10E8 antigorputzak C-MPER epitopora iristeko ezintasuna eragiten dituztenak hain zuzen. Hipotesi bat izan liteke Chol-ak peptidoarekin elkarrekin dezakeela, 10E8 epitopoaren hondar kritikoak mintzean murgiltzea eragingo lukeena.

4.1 ONDORIOA



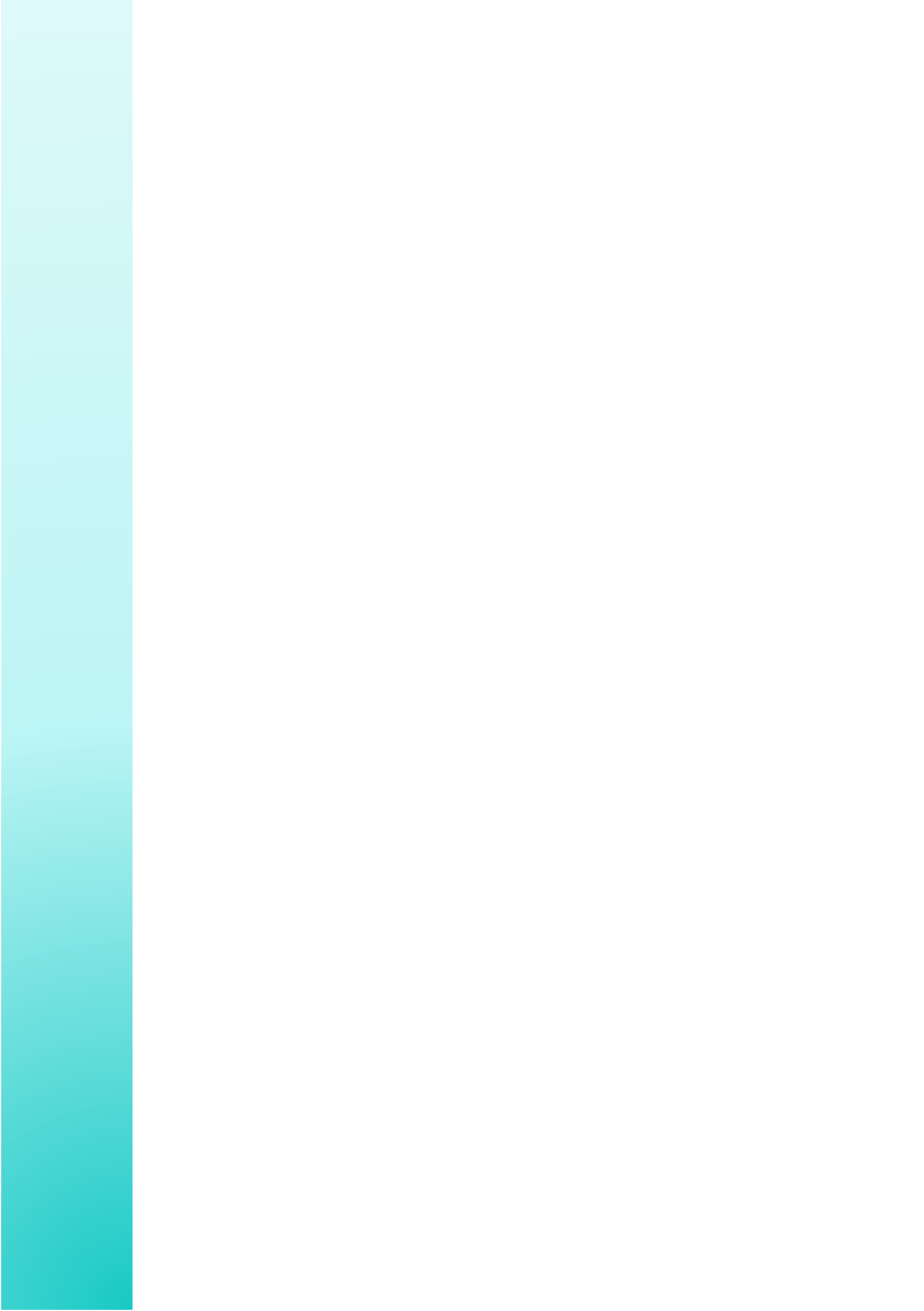
4.1 irudia. MPER domeinuan oinarritutako immunogenoak ekoizteko jarraitutako estrategia. A) cryo-EM berreraikuntzan oinarritutako 10E8 MPERari lotutako eredua (EMDB-3312). B) 10E8 antigorputzak ezagutzen duen MPER epitopoaren egitura imitatzeko jarraitutako estrategia. i) Epitopoaren gainazaleko aurkezpen egonkorra TMDa ainguraketa moduan erabiliz. ii) Erantzun immunea C-MPERera zuzentzeko, N-MPER domeinu immunogenikoaren ezabaketa. iii) LPF-en formulazioen optimizazioa 10E8 eta honen aldaerak erreferentzia gisa erabiliz. Peptidoaren aurkezpena hobetzen da transmintz domeinuaren sekuentziaren luzera handitz eta besikula lipidikoen kolesterola ezabatuz.

MPER-TMD domeinuak jatorrizko Env-ean duen bereizmen handiko egitura atomikoaren informazioa oraindik faltan dagoen arren, eta zenbait antigorputzei lotutako epitopoaren egiturari buruz dugun ezagutza osatu gabe dagoen arren, tesi lan honetan jarraituriko estrategiak (4.1 B irudia) eta lorturiko datuek, 10E8 bezalako antigorputz neutralizatzailak sortzeko gai diren immunogenoen diseinu arrazionalean lagundu dezakete.

Etorkizunean, MPERera zuzendutako txertoen formulazioetan sartu daitekeen peptidoaren deseinuari dagokionez, ondoriozta daiteke MPER domeinuaren N-amaiera kentzeak, antigorputzen erantzuna 10E8aren epitopora bideratzen duela. Horrez gain, lan honetan deskribaturiko errekonstituzio prozesuak eta transmintz domeinuaren bidezko peptidoen ainguraketak, C-MPERean oinarritutako immunogeno egonkorren diseinurako ikuspegi berriak eman dituzte. Halaber, txerto formulazioetan erabilitako mintza zeharkatzen duen sekuentziaren luzerak, epitopoaren irisgarritasuna eta honekin batera antigorputzen afinitatea modula dezake.

Azkenik, epitopoak mintzen gainazalean ahalik eta hoheren aurkezteko, eta aurreko usteen kontra, anti-MPER antigorputzak sortzeko LPF-en formulazioak Chol-ik gabe diseinatu behar dira; lipido horrek, C-MPER epitoporako 10E8 antigorputzaren eskuragarritasuna murrizten baitu.

REFERENCES



REFERENCES

1. Barré-Sinoussi F, Chermann JC, Rey F, et al. Isolation of a T-lymphotropic retrovirus from a patient at risk for acquired immune deficiency syndrome (AIDS). *Science*. 1983;220(4599):868-871. doi:10.1126/science.6189183
2. Buzón MJ, Massanella M, Llibre JM, et al. HIV-1 replication and immune dynamics are affected by raltegravir intensification of HAART-suppressed subjects. *Nat Med*. 2010;16(4):460-465. doi:10.1038/nm.2111
3. Wyatt R, Sodroski J. The HIV-1 envelope glycoproteins: fusogens, antigens, and immunogens. *Science*. 1998;280(5371):1884-1888. doi:10.1126/science.280.5371.1884
4. Frey G, Peng H, Rits-Volloch S, Morelli M, Cheng Y, Chen B. A fusion-intermediate state of HIV-1 gp41 targeted by broadly neutralizing antibodies. *Proc Natl Acad Sci U S A*. 2008;105(10):3739-3744. doi:10.1073/pnas.0800255105
5. Apellániz B, Rujas E, Carravilla P, et al. Cholesterol-Dependent Membrane Fusion Induced by the gp41 Membrane-Proximal External Region–Transmembrane Domain Connection Suggests a Mechanism for Broad HIV-1 Neutralization. *J Virol*. 2014;88(22):13367-13377. doi:10.1128/JVI.02151-14
6. Apellániz B, García-Sáez A, Nir S, Nieva JL. Destabilization exerted by peptides derived from the membrane-proximal external region of HIV-1 gp41 in lipid vesicles supporting fluid phase coexistence. *Biochim Biophys Acta*. 2011;1808(7):1797-1805. doi:10.1016/j.bbapm.2011.02.005
7. Zhu P, Chertova E, Bess J, et al. Electron tomography analysis of envelope glycoprotein trimers on HIV and simian immunodeficiency virus virions. *Proc Natl Acad Sci U S A*. 2003;100(26):15812-15817. doi:10.1073/pnas.2634931100
8. Preston BD, Poiesz BJ, Loeb LA. Fidelity of HIV-1 reverse transcriptase. *Science*. 1988;242(4882):1168-1171. doi:10.1126/science.2460924
9. Burton DR, Mascola JR. Antibody responses to envelope glycoproteins in HIV-1 infection. *Nat Immunol*. 2015;16(6):571-576. doi:10.1038/ni.3158
10. Landais E, Moore PL. Development of broadly neutralizing antibodies in HIV-1 infected elite neutralizers. *Retrovirology*. 2018;15(1):61. doi:10.1186/s12977-018-0443-0

11. Scheid JF, Mouquet H, Feldhahn N, et al. Broad diversity of neutralizing antibodies isolated from memory B cells in HIV-infected individuals. *Nature*. 2009;458(7238):636-640. doi:10.1038/nature07930
12. Huang J, Ofek G, Laub L, et al. Broad and potent neutralization of HIV-1 by a gp41-specific human antibody. *Nature*. 2012;491(7424):406-412. doi:10.1038/nature11544
13. Gallo RC, Salahuddin SZ, Popovic M, et al. Frequent detection and isolation of cytopathic retroviruses (HTLV-III) from patients with AIDS and at risk for AIDS. *Science*. 1984;224(4648):500-503. doi:10.1126/science.6200936
14. Coffin J, Haase A, Levy JA, et al. What to call the AIDS virus? *Nature*. 1986;321(6065):10. doi:10.1038/321010a0
15. Finzi D, Blankson J, Siliciano JD, et al. Latent infection of CD4+ T cells provides a mechanism for lifelong persistence of HIV-1, even in patients on effective combination therapy. *Nat Med*. 1999;5(5):512-517. doi:10.1038/8394
16. Levy JA. HIV pathogenesis and long-term survival. *AIDS*. 1993;7(11):1401-1410. doi:10.1097/00002030-199311000-00001
17. Gilbert PB, McKeague IW, Eisen G, et al. Comparison of HIV-1 and HIV-2 infectivity from a prospective cohort study in Senegal. *Stat Med*. 2003;22(4):573-593. doi:10.1002/sim.1342
18. Korber B, Muldoon M, Theiler J, et al. Timing the ancestor of the HIV-1 pandemic strains. *Science*. 2000;288(5472):1789-1796. doi:10.1126/science.288.5472.1789
19. Reeves JD, Doms RW. Human immunodeficiency virus type 2. *J Gen Virol*. Published online 2002:1253-1265.
20. Julien JP, Cupo A, Sok D, et al. Crystal structure of a soluble cleaved HIV-1 envelope trimer. *Science*. 2013;342(6165):1477-1483. doi:10.1126/science.1245625
21. Ganser-Pornillos BK, Yeager M, Sundquist WI. The structural biology of HIV assembly. *Curr Opin Struct Biol*. 2008;18(2):203-217. doi:10.1016/j.sbi.2008.02.001
22. Starcich BR, Hahn BH, Shaw GM, et al. Identification and characterization of conserved and variable regions in the envelope gene of HTLV-III/LAV, the retrovirus of AIDS. *Cell*. 1986;45(5):637-648. doi:10.1016/0092-8674(86)90778-6

23. Chen L, Kwon YD, Zhou T, et al. Structural basis of immune evasion at the site of CD4 attachment on HIV-1 gp120. *Science*. 2009;326(5956):1123-1127. doi:10.1126/science.1175868
24. Kwong PD, Doyle ML, Casper DJ, et al. HIV-1 evades antibody-mediated neutralization through conformational masking of receptor-binding sites. *Nature*. 2002;420(6916):678-682. doi:10.1038/nature01188
25. Briggs JAG, Kräusslich HG. The molecular architecture of HIV. *J Mol Biol*. 2011;410(4):491-500. doi:10.1016/j.jmb.2011.04.021
26. Checkley MA, Luttge BG, Freed EO. HIV-1 envelope glycoprotein biosynthesis, trafficking, and incorporation. *J Mol Biol*. 2011;410(4):582-608. doi:10.1016/j.jmb.2011.04.042
27. Rand RP, Parsegian VA. Physical force considerations in model and biological membranes. *Can J Biochem Cell Biol*. 1984;62(8):752-759. doi:10.1139/o84-097
28. Harrison SC. Viral membrane fusion. *Virology*. 2015;479-480:498-507. doi:10.1016/j.virol.2015.03.043
29. Weissenhorn W, Dessen A, Calder LJ, Harrison SC, Skehel JJ, Wiley DC. Structural basis for membrane fusion by enveloped viruses. *Mol Membr Biol*. 1999;16(1):3-9. doi:10.1080/096876899294706
30. Yang X, Kurteva S, Ren X, Lee S, Sodroski J. Stoichiometry of envelope glycoprotein trimers in the entry of human immunodeficiency virus type 1. *J Virol*. 2005;79(19):12132-12147. doi:10.1128/JVI.79.19.12132-12147.2005
31. Klasse PJ. Modeling how many envelope glycoprotein trimers per virion participate in human immunodeficiency virus infectivity and its neutralization by antibody. *Virology*. 2007;369(2):245-262. doi:10.1016/j.virol.2007.06.044
32. Brandenberg OF, Magnus C, Rusert P, Regoes RR, Trkola A. Different infectivity of HIV-1 strains is linked to number of envelope trimers required for entry. *PLoS Pathog*. 2015;11(1):e1004595. doi:10.1371/journal.ppat.1004595
33. Liu J, Bartesaghi A, Borgnia MJ, Sapiro G, Subramaniam S. Molecular architecture of native HIV-1 gp120 trimers. *Nature*. 2008;455(7209):109-113. doi:10.1038/nature07159

34. Ozorowski G, Pallesen J, de Val N, et al. Open and closed structures reveal allostery and pliability in the HIV-1 envelope spike. *Nature*. 2017;547(7663):360-363. doi:10.1038/nature23010
35. Rizzuto CD, Wyatt R, Hernandez-Ramos N, Sung Y, Kwong PD, Sodroski J. A Conserved HIV gp120 Glycoprotein Structure Involved in Chemokine Receptor Binding. *Science*. 1998;280(5371):1949-1953. doi:10.1126/science.280.5371.1949
36. Maddon PJ, Dalgleish AG, McDougal JS, Clapham PR, Weiss RA, Axel R. The T4 gene encodes the AIDS virus receptor and is expressed in the immune system and the brain. *Cell*. 1986;47(3):333-348. doi:10.1016/0092-8674(86)90590-8
37. Klasse PJ. The molecular basis of HIV entry. *Cell Microbiol*. 2012;14(8):1183-1192. doi:10.1111/j.1462-5822.2012.01812.x
38. Blumenthal R, Durell S, Viard M. HIV entry and envelope glycoprotein-mediated fusion. *J Biol Chem*. 2012;287(49):40841-40849. doi:10.1074/jbc.R112.406272
39. Chernomordik LV, Kozlov MM. Membrane hemifusion: crossing a chasm in two leaps. *Cell*. 2005;123(3):375-382. doi:10.1016/j.cell.2005.10.015
40. Apellániz B, Nir S, Nieva JL. Distinct mechanisms of lipid bilayer perturbation induced by peptides derived from the membrane-proximal external region of HIV-1 gp41. *Biochemistry*. 2009;48(23):5320-5331. doi:10.1021/bi900504t
41. Apellániz B, Nieva JL, Schwille P, García-Sáez AJ. All-or-none versus graded: single-vesicle analysis reveals lipid composition effects on membrane permeabilization. *Biophys J*. 2010;99(11):3619-3628. doi:10.1016/j.bpj.2010.09.027
42. Apellániz B, Ivankin A, Nir S, Gidalevitz D, Nieva JL. Membrane-proximal external HIV-1 gp41 motif adapted for destabilizing the highly rigid viral envelope. *Biophys J*. 2011;101(10):2426-2435. doi:10.1016/j.bpj.2011.10.005
43. Apellániz B, Nieva JL. Fusion-competent state induced by a C-terminal HIV-1 fusion peptide in cholesterol-rich membranes. *Biochim Biophys Acta*. 2015;1848(4):1014-1022. doi:10.1016/j.bbamem.2015.01.011
44. Sundquist WI, Kräusslich HG. HIV-1 assembly, budding, and maturation. *Cold Spring Harb Perspect Med*. 2012;2(7):a006924. doi:10.1101/cshperspect.a006924
45. Aloia RC, Tian H, Jensen FC. Lipid composition and fluidity of the human immunodeficiency virus envelope and host cell plasma membranes. *Proc Natl Acad Sci U S A*. 1993;90(11):5181-5185. doi:10.1073/pnas.90.11.5181

46. Gordon LM, Jensen FC, Curtain CC, Mobley PW, Aloia RC. Thermotropic lipid phase separation in the human immunodeficiency virus. *Biochim Biophys Acta*. 1988;943(2):331-342. doi:10.1016/0005-2736(88)90565-2
47. Brügger B, Glass B, Haberkant P, Leibrecht I, Wieland FT, Kräusslich HG. The HIV lipidome: a raft with an unusual composition. *Proc Natl Acad Sci U S A*. 2006;103(8):2641-2646. doi:10.1073/pnas.0511136103
48. Lorizate M, Brügger B, Akiyama H, et al. Probing HIV-1 membrane liquid order by Laurdan staining reveals producer cell-dependent differences. *J Biol Chem*. 2009;284(33):22238-22247. doi:10.1074/jbc.M109.029256
49. Huarte N, Carra villa P, Cruz A, et al. Functional organization of the HIV lipid envelope. *Sci Rep*. 2016;6:34190. doi:10.1038/srep34190
50. Lorizate M, Sachsenheimer T, Glass B, et al. Comparative lipidomics analysis of HIV-1 particles and their producer cell membrane in different cell lines. *Cellular Microbiology*. 2013;15(2):292-304. doi:10.1111/cmi.12101
51. Carra villa P, Chojnacki J, Rujas E, et al. Molecular recognition of the native HIV-1 MPER revealed by STED microscopy of single virions. *Nat Commun*. 2019;10(1):78. doi:10.1038/s41467-018-07962-9
52. Soares MM, King SW, Thorpe PE. Targeting inside-out phosphatidylserine as a therapeutic strategy for viral diseases. *Nat Med*. 2008;14(12):1357-1362. doi:10.1038/nm.1885
53. Mücksch F, Citir M, Lüchtenborg C, et al. Quantification of phosphoinositides reveals strong enrichment of PIP2 in HIV-1 compared to producer cell membranes. *Sci Rep*. 2019;9(1):17661. doi:10.1038/s41598-019-53939-z
54. Ono A, Freed EO. Role of lipid rafts in virus replication. *Adv Virus Res*. 2005;64:311-358. doi:10.1016/S0065-3527(05)64010-9
55. Nguyen DH, Hildreth JE. Evidence for budding of human immunodeficiency virus type 1 selectively from glycolipid-enriched membrane lipid rafts. *J Virol*. 2000;74(7):3264-3272. doi:10.1128/jvi.74.7.3264-3272.2000
56. Campbell SM, Crowe SM, Mak J. Virion-associated cholesterol is critical for the maintenance of HIV-1 structure and infectivity. *AIDS*. 2002;16(17):2253-2261. doi:10.1097/00002030-200211220-00004

57. Ono A, Freed EO. Plasma membrane rafts play a critical role in HIV-1 assembly and release. *Proc Natl Acad Sci U S A.* 2001;98(24):13925-13930. doi:10.1073/pnas.241320298
58. Lee JH, Crotty S. HIV vaccinology: 2021 update. *Semin Immunol.* Published online July 13, 2021:101470. doi:10.1016/j.smim.2021.101470
59. McCune JM, Rabin LB, Feinberg MB, et al. Endoproteolytic cleavage of gp160 is required for the activation of human immunodeficiency virus. *Cell.* 1988;53(1):55-67. doi:10.1016/0092-8674(88)90487-4
60. Cao L, Diedrich JK, Kulp DW, et al. Global site-specific N-glycosylation analysis of HIV envelope glycoprotein. *Nat Commun.* 2017;8:14954. doi:10.1038/ncomms14954
61. Kwong PD, Wyatt R, Majeed S, et al. Structures of HIV-1 gp120 envelope glycoproteins from laboratory-adapted and primary isolates. *Structure.* 2000;8(12):1329-1339. doi:10.1016/s0969-2126(00)00547-5
62. Kwong PD, Wyatt R, Robinson J, Sweet RW, Sodroski J, Hendrickson WA. Structure of an HIV gp120 envelope glycoprotein in complex with the CD4 receptor and a neutralizing human antibody. *Nature.* 1998;393(6686):648-659. doi:10.1038/31405
63. Chen B, Vogan EM, Gong H, Skehel JJ, Wiley DC, Harrison SC. Structure of an unliganded simian immunodeficiency virus gp120 core. *Nature.* 2005;433(7028):834-841. doi:10.1038/nature03327
64. Huang C chin, Tang M, Zhang MY, et al. Structure of a V3-containing HIV-1 gp120 core. *Science.* 2005;310(5750):1025-1028. doi:10.1126/science.1118398
65. Pancera M, Majeed S, Ban YEA, et al. Structure of HIV-1 gp120 with gp41-interactive region reveals layered envelope architecture and basis of conformational mobility. *Proc Natl Acad Sci U S A.* 2010;107(3):1166-1171. doi:10.1073/pnas.0911004107
66. Kwon YD, Finzi A, Wu X, et al. Unliganded HIV-1 gp120 core structures assume the CD4-bound conformation with regulation by quaternary interactions and variable loops. *Proc Natl Acad Sci U S A.* 2012;109(15):5663-5668. doi:10.1073/pnas.1112391109
67. Weissenhorn W, Dessen A, Harrison SC, Skehel JJ, Wiley DC. Atomic structure of the ectodomain from HIV-1 gp41. *Nature.* 1997;387(6631):426-430. doi:10.1038/387426a0

68. Tan K, Liu J, Wang J, Shen S, Lu M. Atomic structure of a thermostable subdomain of HIV-1 gp41. *Proc Natl Acad Sci U S A.* 1997;94(23):12303-12308. doi:10.1073/pnas.94.23.12303
69. Yang ZN, Mueser TC, Kaufman J, Stahl SJ, Wingfield PT, Hyde CC. The crystal structure of the SIV gp41 ectodomain at 1.47 Å resolution. *J Struct Biol.* 1999;126(2):131-144. doi:10.1006/jsb.1999.4116
70. Lyumkis D, Julien JP, de Val N, et al. Cryo-EM structure of a fully glycosylated soluble cleaved HIV-1 envelope trimer. *Science.* 2013;342(6165):1484-1490. doi:10.1126/science.1245627
71. Sanders RW, Derking R, Cupo A, et al. A next-generation cleaved, soluble HIV-1 Env trimer, BG505 SOSIP.664 gp140, expresses multiple epitopes for broadly neutralizing but not non-neutralizing antibodies. *PLoS Pathog.* 2013;9(9):e1003618. doi:10.1371/journal.ppat.1003618
72. Binley JM, Sanders RW, Clas B, et al. A recombinant human immunodeficiency virus type 1 envelope glycoprotein complex stabilized by an intermolecular disulfide bond between the gp120 and gp41 subunits is an antigenic mimic of the trimeric virion-associated structure. *J Virol.* 2000;74(2):627-643. doi:10.1128/jvi.74.2.627-643.2000
73. Sanders RW, Vesanen M, Schuelke N, et al. Stabilization of the soluble, cleaved, trimeric form of the envelope glycoprotein complex of human immunodeficiency virus type 1. *J Virol.* 2002;76(17):8875-8889. doi:10.1128/jvi.76.17.8875-8889.2002
74. Schommers P, Gruell H, Abernathy ME, et al. Restriction of HIV-1 Escape by a Highly Broad and Potent Neutralizing Antibody. *Cell.* 2020;180(3):471-489.e22. doi:10.1016/j.cell.2020.01.010
75. Henderson R, Lu M, Zhou Y, et al. Disruption of the HIV-1 Envelope allosteric network blocks CD4-induced rearrangements. *Nat Commun.* 2020;11(1):520. doi:10.1038/s41467-019-14196-w
76. Lee JH, Ozorowski G, Ward AB. Cryo-EM structure of a native, fully glycosylated, cleaved HIV-1 envelope trimer. *Science.* 2016;351(6277):1043-1048. doi:10.1126/science.aad2450
77. Munro JB, Gorman J, Ma X, et al. Conformational dynamics of single HIV-1 envelope trimers on the surface of native virions. *Science.* 2014;346(6210):759-763. doi:10.1126/science.1254426

78. Lu M, Ma X, Castillo-Menendez LR, et al. Associating HIV-1 envelope glycoprotein structures with states on the virus observed by smFRET. *Nature*. 2019;568(7752):415-419. doi:10.1038/s41586-019-1101-y
79. Herschhorn A, Sodroski J. An entry-competent intermediate state of the HIV-1 envelope glycoproteins. *Receptors Clin Investig*. 2017;4(1):e1544. doi:10.14800/rcl.1544
80. Bruel T, Schwartz O. HIV-1 Envelope FRETted Over by Antibodies. *Cell Host Microbe*. 2019;25(6):767-768. doi:10.1016/j.chom.2019.05.009
81. Ma X, Lu M, Gorman J, et al. HIV-1 Env trimer opens through an asymmetric intermediate in which individual protomers adopt distinct conformations. *eLife*. 2018;7:e34271. doi:10.7554/eLife.34271
82. Alsahafi N, Bakouche N, Kazemi M, et al. An Asymmetric Opening of HIV-1 Envelope Mediates Antibody-Dependent Cellular Cytotoxicity. *Cell Host Microbe*. 2019;25(4):578-587.e5. doi:10.1016/j.chom.2019.03.002
83. Montefiori DC, Roederer M, Morris L, Seaman MS. Neutralization tiers of HIV-1. *Curr Opin HIV AIDS*. 2018;13(2):128-136. doi:10.1097/COH.0000000000000442
84. Chakrabarti BK, Walker LM, Guenaga JF, et al. Direct antibody access to the HIV-1 membrane-proximal external region positively correlates with neutralization sensitivity. *J Virol*. 2011;85(16):8217-8226. doi:10.1128/JVI.00756-11
85. Scanlan CN, Offer J, Zitzmann N, Dwek RA. Exploiting the defensive sugars of HIV-1 for drug and vaccine design. *Nature*. 2007;446(7139):1038-1045. doi:10.1038/nature05818
86. McLellan JS, Pancera M, Carrico C, et al. Structure of HIV-1 gp120 V1/V2 domain with broadly neutralizing antibody PG9. *Nature*. 2011;480(7377):336-343. doi:10.1038/nature10696
87. Julien JP, Lee JH, Cupo A, et al. Asymmetric recognition of the HIV-1 trimer by broadly neutralizing antibody PG9. *Proc Natl Acad Sci U S A*. 2013;110(11):4351-4356. doi:10.1073/pnas.1217537110
88. Walker LM, Phogat SK, Chan-Hui PY, et al. Broad and potent neutralizing antibodies from an African donor reveal a new HIV-1 vaccine target. *Science*. 2009;326(5950):285-289. doi:10.1126/science.1178746

89. Kong, Lee JH, Doores KJ, et al. Supersite of immune vulnerability on the glycosylated face of HIV-1 envelope glycoprotein gp120. *Nat Struct Mol Biol.* 2013;20(7):796-803. doi:10.1038/nsmb.2594
90. Walker LM, Huber M, Doores KJ, et al. Broad neutralization coverage of HIV by multiple highly potent antibodies. *Nature.* 2011;477(7365):466-470. doi:10.1038/nature10373
91. Pejchal R, Doores KJ, Walker LM, et al. A potent and broad neutralizing antibody recognizes and penetrates the HIV glycan shield. *Science.* 2011;334(6059):1097-1103. doi:10.1126/science.1213256
92. Ryu SE, Hendrickson WA. Structure and design of broadly-neutralizing antibodies against HIV. *Mol Cells.* 2012;34(3):231-237. doi:10.1007/s10059-012-0104-4
93. Sajadi MM, Dashti A, Tehrani ZR, et al. Identification of near pan-neutralizing antibodies against HIV-1 by deconvolution of plasma humoral responses. *Cell.* 2018;173(7):1783-1795.e14. doi:10.1016/j.cell.2018.03.061
94. Zhou T, Lynch RM, Chen L, et al. Structural Repertoire of HIV-1-Neutralizing Antibodies Targeting the CD4 Supersite in 14 Donors. *Cell.* 2015;161(6):1280-1292. doi:10.1016/j.cell.2015.05.007
95. Ofek G, Tang M, Sambor A, et al. Structure and mechanistic analysis of the anti-human immunodeficiency virus type 1 antibody 2F5 in complex with its gp41 epitope. *J Virol.* 2004;78(19):10724-10737. doi:10.1128/JVI.78.19.10724-10737.2004
96. Irimia A, Sarkar A, Stanfield RL, Wilson IA. Crystallographic Identification of Lipid as an Integral Component of the Epitope of HIV Broadly Neutralizing Antibody 4E10. *Immunity.* 2016;44(1):21-31. doi:10.1016/j.immuni.2015.12.001
97. Doria-Rose NA, Klein RM, Manion MM, et al. Frequency and phenotype of human immunodeficiency virus envelope-specific B cells from patients with broadly cross-neutralizing antibodies. *J Virol.* 2009;83(1):188-199. doi:10.1128/JVI.01583-08
98. Hraber P, Seaman MS, Bailer RT, Mascola JR, Montefiori DC, Korber BT. Prevalence of broadly neutralizing antibody responses during chronic HIV-1 infection. *AIDS.* 2014;28(2):163-169. doi:10.1097/QAD.0000000000000106
99. Simek MD, Rida W, Priddy FH, et al. Human immunodeficiency virus type 1 elite neutralizers: individuals with broad and potent neutralizing activity identified by using a high-throughput neutralization assay together with an analytical selection algorithm. *J Virol.* 2009;83(14):7337-7348. doi:10.1128/JVI.00110-09

100. Gautam R, Nishimura Y, Pegu A, et al. A single injection of anti-HIV-1 antibodies protects against repeated SHIV challenges. *Nature*. 2016;533(7601):105-109. doi:10.1038/nature17677
101. Julg B, Sok D, Schmidt SD, et al. Protective Efficacy of Broadly Neutralizing Antibodies with Incomplete Neutralization Activity against Simian-Human Immunodeficiency Virus in Rhesus Monkeys. *J Virol*. 2017;91(20):e01187-17. doi:10.1128/JVI.01187-17
102. Xiao X, Chen W, Feng Y, et al. Germline-like predecessors of broadly neutralizing antibodies lack measurable binding to HIV-1 envelope glycoproteins: implications for evasion of immune responses and design of vaccine immunogens. *Biochem Biophys Res Commun*. 2009;390(3):404-409. doi:10.1016/j.bbrc.2009.09.029
103. Haynes BF, Fleming J, St Clair EW, et al. Cardiolipin polyspecific autoreactivity in two broadly neutralizing HIV-1 antibodies. *Science*. 2005;308(5730):1906-1908. doi:10.1126/science.1111781
104. Verkoczy L, Diaz M. Autoreactivity in HIV-1 broadly neutralizing antibodies: implications for their function and induction by vaccination. *Curr Opin HIV AIDS*. 2014;9(3):224-234. doi:10.1097/COH.0000000000000049
105. Mouquet H, Nussenzweig MC. Polyreactive antibodies in adaptive immune responses to viruses. *Cell Mol Life Sci*. 2012;69(9):1435-1445. doi:10.1007/s0018-011-0872-6
106. Wardemann H, Yurasov S, Schaefer A, Young JW, Meffre E, Nussenzweig MC. Predominant autoantibody production by early human B cell precursors. *Science*. Published online September 5, 2003. Accessed September 14, 2021. <https://pubmed.ncbi.nlm.nih.gov/12920303/>
107. Burton DR, Pyati J, Koduri R, et al. Efficient neutralization of primary isolates of HIV-1 by a recombinant human monoclonal antibody. *Science*. 1994;266(5187):1024-1027. doi:10.1126/science.7973652
108. Yang G, Holl TM, Liu Y, et al. Identification of autoantigens recognized by the 2F5 and 4E10 broadly neutralizing HIV-1 antibodies. *J Exp Med*. 2013;210(2):241-256. doi:10.1084/jem.20121977
109. Burton DR, Hangartner L. Broadly Neutralizing Antibodies to HIV and Their Role in Vaccine Design. *Annu Rev Immunol*. 2016;34:635-659. doi:10.1146/annurev-immunol-041015-055515

110. Sanders RW, van Gils MJ, Derking R, et al. HIV-1 VACCINES. HIV-1 neutralizing antibodies induced by native-like envelope trimers. *Science*. 2015;349(6244):aac4223. doi:10.1126/science.aac4223
111. Havenar-Daughton C, Carnathan DG, Torrents de la Peña A, et al. Direct Probing of Germinal Center Responses Reveals Immunological Features and Bottlenecks for Neutralizing Antibody Responses to HIV Env Trimer. *Cell Rep*. 2016;17(9):2195-2209. doi:10.1016/j.celrep.2016.10.085
112. Hu JK, Crampton JC, Cupo A, et al. Murine Antibody Responses to Cleaved Soluble HIV-1 Envelope Trimers Are Highly Restricted in Specificity. *J Virol*. 2015;89(20):10383-10398. doi:10.1128/JVI.01653-15
113. Pauthner M, Havenar-Daughton C, Sok D, et al. Elicitation of Robust Tier 2 Neutralizing Antibody Responses in Nonhuman Primates by HIV Envelope Trimer Immunization Using Optimized Approaches. *Immunity*. 2017;46(6):1073-1088.e6. doi:10.1016/j.jimmuni.2017.05.007
114. Kulp DW, Steichen JM, Pauthner M, et al. Structure-based design of native-like HIV-1 envelope trimers to silence non-neutralizing epitopes and eliminate CD4 binding. *Nat Commun*. 2017;8(1):1655. doi:10.1038/s41467-017-01549-6
115. Torrents de la Peña A, Sanders RW. Stabilizing HIV-1 envelope glycoprotein trimers to induce neutralizing antibodies. *Retrovirology*. 2018;15(1):63. doi:10.1186/s12977-018-0445-y
116. Do Kwon Y, Pancera M, Acharya P, et al. Crystal structure, conformational fixation and entry-related interactions of mature ligand-free HIV-1 Env. *Nat Struct Mol Biol*. 2015;22(7):522-531. doi:10.1038/nsmb.3051
117. Chuang GY, Geng H, Pancera M, et al. Structure-Based Design of a Soluble Prefusion-Closed HIV-1 Env Trimer with Reduced CD4 Affinity and Improved Immunogenicity. *J Virol*. 2017;91(10):e02268-16. doi:10.1128/JVI.02268-16
118. McCoy LE, van Gils MJ, Ozorowski G, et al. Holes in the glycan shield of the native HIV envelope are a target of trimer-elicited neutralizing antibodies. *Cell Rep*. 2016;16(9):2327-2338. doi:10.1016/j.celrep.2016.07.074
119. Yang YR, McCoy LE, van Gils MJ, et al. Autologous Antibody Responses to an HIV Envelope Glycan Hole Are Not Easily Broadened in Rabbits. *J Virol*. 2020;94(7):e01861-19. doi:10.1128/JVI.01861-19

120. Crooks ET, Osawa K, Tong T, et al. Effects of partially dismantling the CD4 binding site glycan fence of HIV-1 Envelope glycoprotein trimers on neutralizing antibody induction. *Virology*. 2017;505:193-209. doi:10.1016/j.virol.2017.02.024
121. Sliepen K, Han BW, Bontjer I, et al. Structure and immunogenicity of a stabilized HIV-1 envelope trimer based on a group-M consensus sequence. *Nat Commun*. 2019;10(1):2355. doi:10.1038/s41467-019-10262-5
122. Sarkar A, Bale S, Behrens AJ, et al. Structure of a cleavage-independent HIV Env recapitulates the glycoprotein architecture of the native cleaved trimer. *Nat Commun*. 2018;9(1):1956. doi:10.1038/s41467-018-04272-y
123. Yang L, Sharma SK, Cottrell C, et al. Structure-Guided Redesign Improves NFL HIV Env Trimer Integrity and Identifies an Inter-Protomer Disulfide Permitting Post-Expression Cleavage. *Front Immunol*. 2018;9:1631. doi:10.3389/fimmu.2018.01631
124. Kong, He L, de Val N, et al. Uncleaved prefusion-optimized gp140 trimers derived from analysis of HIV-1 envelope metastability. *Nat Commun*. 2016;7:12040. doi:10.1038/ncomms12040
125. Dubrovskaya V, Tran K, Ozorowski G, et al. Vaccination with Glycan-Modified HIV NFL Envelope Trimer-Liposomes Elicits Broadly Neutralizing Antibodies to Multiple Sites of Vulnerability. *Immunity*. 2019;51(5):915-929.e7. doi:10.1016/j.immuni.2019.10.008
126. He L, Kumar S, Allen JD, et al. HIV-1 vaccine design through minimizing envelope metastability. *Sci Adv*. 2018;4(11):eaau6769. doi:10.1126/sciadv.aau6769
127. Wieczorek L, Krebs SJ, Kalyanaraman V, et al. Comparable Antigenicity and Immunogenicity of Oligomeric Forms of a Novel, Acute HIV-1 Subtype C gp145 Envelope for Use in Preclinical and Clinical Vaccine Research. *J Virol*. 2015;89(15):7478-7493. doi:10.1128/JVI.00412-15
128. Stamatatos L, Pancera M, McGuire AT. Germline Targeting Immunogens. *Immunol Rev*. 2017;275(1):203-216. doi:10.1111/imr.12483
129. Liao HX, Lynch R, Zhou T, et al. Co-evolution of a broadly neutralizing HIV-1 antibody and founder virus. *Nature*. 2013;496(7446):469-476. doi:10.1038/nature12053
130. Bonsignori M, Zhou T, Sheng Z, et al. Maturation Pathway from Germline to Broad HIV-1 Neutralizer of a CD4-Mimic Antibody. *Cell*. 2016;165(2):449-463. doi:10.1016/j.cell.2016.02.022

131. MacLeod DT, Choi NM, Briney B, et al. Early Antibody Lineage Diversification and Independent Limb Maturation Lead to Broad HIV-1 Neutralization Targeting the Env High-Mannose Patch. *Immunity*. 2016;44(5):1215-1226. doi:10.1016/j.jimmuni.2016.04.016
132. Hoot S, McGuire AT, Cohen KW, et al. Recombinant HIV envelope proteins fail to engage germline versions of anti-CD4bs bNAbs. *PLoS Pathog*. 2013;9(1):e1003106. doi:10.1371/journal.ppat.1003106
133. Jardine J, Julien JP, Menis S, et al. Rational HIV immunogen design to target specific germline B cell receptors. *Science*. 2013;340(6133):711-716. doi:10.1126/science.1234150
134. Sliepen K, Medina-Ramírez M, Yasmeen A, Moore JP, Klasse PJ, Sanders RW. Binding of inferred germline precursors of broadly neutralizing HIV-1 antibodies to native-like envelope trimers. *Virology*. 2015;486:116-120. doi:10.1016/j.virol.2015.08.002
135. Escolano A, Steichen JM, Dosenovic P, et al. Sequential Immunization Elicits Broadly Neutralizing Anti-HIV-1 Antibodies in Ig Knockin Mice. *Cell*. 2016;166(6):1445-1458.e12. doi:10.1016/j.cell.2016.07.030
136. Burton DR. Advancing an HIV vaccine; advancing vaccinology. *Nat Rev Immunol*. 2019;19(2):77-78. doi:10.1038/s41577-018-0103-6
137. Jardine JG, Kulp DW, Havenar-Daughton C, et al. HIV-1 broadly neutralizing antibody precursor B cells revealed by germline-targeting immunogen. *Science*. 2016;351(6280):1458-1463. doi:10.1126/science.aad9195
138. Havenar-Daughton C, Sarkar A, Kulp DW, et al. The human naive B cell repertoire contains distinct subclasses for a germline-targeting HIV-1 vaccine immunogen. *Sci Transl Med*. 2018;10(448):eaat0381. doi:10.1126/scitranslmed.aat0381
139. Whitaker N, Hickey JM, Kaur K, et al. Developability Assessment of Physicochemical Properties and Stability Profiles of HIV-1 BG505 SOSIP.664 and BG505 SOSIP.v4.1-GT1.1 gp140 Envelope Glycoprotein Trimers as Candidate Vaccine Antigens. *J Pharm Sci*. 2019;108(7):2264-2277. doi:10.1016/j.xphs.2019.01.033
140. Salzwedel K, West JT, Hunter E. A Conserved Tryptophan-Rich Motif in the Membrane-Proximal Region of the Human Immunodeficiency Virus Type 1 gp41 Ectodomain Is Important for Env-Mediated Fusion and Virus Infectivity. *Journal of Virology*. 1999;73(3):2469-2480. doi:10.1128/JVI.73.3.2469-2480.1999

141. Cardoso RMF, Brunel FM, Ferguson S, et al. Structural basis of enhanced binding of extended and helically constrained peptide epitopes of the broadly neutralizing HIV-1 antibody 4E10. *J Mol Biol.* 2007;365(5):1533-1544. doi:10.1016/j.jmb.2006.10.088
142. Huang J, Kang BH, Pancera M, et al. Broad and potent HIV-1 neutralization by a human antibody that binds the gp41-gp120 interface. *Nature.* 2014;515(7525):138-142. doi:10.1038/nature13601
143. Buchacher A, Predl R, Strutzenberger K, et al. Generation of human monoclonal antibodies against HIV-1 proteins; electrofusion and Epstein-Barr virus transformation for peripheral blood lymphocyte immortalization. *AIDS Res Hum Retroviruses.* 1994;10(4):359-369. doi:10.1089/aid.1994.10.359
144. Zwick MB, Labrijn AF, Wang M, et al. Broadly neutralizing antibodies targeted to the membrane-proximal external region of human immunodeficiency virus type 1 glycoprotein gp41. *J Virol.* 2001;75(22):10892-10905. doi:10.1128/JVI.75.22.10892-10905.2001
145. Williams LD, Ofek G, Schätzle S, et al. Potent and broad HIV-neutralizing antibodies in memory B cells and plasma. *Sci Immunol.* 2017;2(7):eaal2200. doi:10.1126/sciimmunol.aal2200
146. Pinto D, Fenwick C, Caillat C, et al. Structural Basis for Broad HIV-1 Neutralization by the MPER-Specific Human Broadly Neutralizing Antibody LN01. *Cell Host Microbe.* 2019;26(5):623-637.e8. doi:10.1016/j.chom.2019.09.016
147. Muñoz-Barroso I, Salzwedel K, Hunter E, Blumenthal R. Role of the membrane-proximal domain in the initial stages of human immunodeficiency virus type 1 envelope glycoprotein-mediated membrane fusion. *J Virol.* 1999;73(7):6089-6092. doi:10.1128/JVI.73.7.6089-6092.1999
148. Vishwanathan SA, Hunter E. Importance of the membrane-perturbing properties of the membrane-proximal external region of human immunodeficiency virus type 1 gp41 to viral fusion. *J Virol.* 2008;82(11):5118-5126. doi:10.1128/JVI.00305-08
149. Huarte N, Lorizate M, Kunert R, Nieva J. Lipid modulation of membrane-bound epitope recognition and blocking by HIV-1 neutralizing antibodies. *FEBS letters.* 2008;582:3798-3804. doi:10.1016/j.febslet.2008.10.012
150. Sáez-Cirión A, Nir S, Lorizate M, et al. Sphingomyelin and cholesterol promote HIV-1 gp41 pretransmembrane sequence surface aggregation and membrane restructuring. *J Biol Chem.* 2002;277(24):21776-21785. doi:10.1074/jbc.M202255200

151. Suárez T, Gallaher WR, Agirre A, Goñi FM, Nieva JL. Membrane Interface-Interacting Sequences within the Ectodomain of the Human Immunodeficiency Virus Type 1 Envelope Glycoprotein: Putative Role during Viral Fusion. *J Virol.* 2000;74(17):8038-8047.
152. Suárez T, Nir S, Goñi FM, Saéz-Cirión A, Nieva JL. The pre-transmembrane region of the human immunodeficiency virus type-1 glycoprotein: a novel fusogenic sequence. *FEBS Lett.* 2000;477(1-2):145-149. doi:10.1016/s0014-5793(00)01785-3
153. Phogat S, Svehla K, Tang M, et al. Analysis of the human immunodeficiency virus type 1 gp41 membrane proximal external region arrayed on hepatitis B surface antigen particles. *Virology.* 2008;373(1):72-84. doi:10.1016/j.virol.2007.11.005
154. Benen TD, Tonks P, Kliche A, Kapzan R, Heeney JL, Wagner R. Development and immunological assessment of VLP-based immunogens exposing the membrane-proximal region of the HIV-1 gp41 protein. *J Biomed Sci.* 2014;21(1):79. doi:10.1186/s12929-014-0079-x
155. Matyas GR, Wieczorek L, Beck Z, et al. Neutralizing antibodies induced by liposomal HIV-1 glycoprotein 41 peptide simultaneously bind to both the 2F5 or 4E10 epitope and lipid epitopes. *AIDS.* 2009;23(16):2069-2077. doi:10.1097/QAD.0b013e32832faea5
156. Dennison SM, Sutherland LL, Jaeger FH, et al. Induction of Antibodies in Rhesus Macaques That Recognize a Fusion-Intermediate Conformation of HIV-1 gp41. *PLoS One.* 2011;6(11):e27824. doi:10.1371/journal.pone.0027824
157. Rantalainen K, Berndsen ZT, Antanasićević A, et al. HIV-1 Envelope and MPER Antibody Structures in Lipid Assemblies. *Cell Rep.* 2020;31(4):107583. doi:10.1016/j.celrep.2020.107583
158. Pettersen EF, Goddard TD, Huang CC, et al. UCSF Chimera--a visualization system for exploratory research and analysis. *J Comput Chem.* 2004;25(13):1605-1612. doi:10.1002/jcc.20084
159. Chiliveri SC, Louis JM, Ghirlando R, Baber JL, Bax A. Tilted, uninterrupted, monomeric HIV-1 gp41 transmembrane helix from residual dipolar couplings. *J Am Chem Soc.* 2018;140(1):34-37. doi:10.1021/jacs.7b10245
160. Dev J, Park D, Fu Q, et al. Structural basis for membrane anchoring of HIV-1 envelope spike. *Science.* 2016;353(6295):172-175. doi:10.1126/science.aaf7066

161. Apellániz B, Rujas E, Serrano S, et al. The Atomic Structure of the HIV-1 gp41 Transmembrane Domain and Its Connection to the Immunogenic Membrane-proximal External Region. *J Biol Chem.* 2015;290(21):12999-13015. doi:10.1074/jbc.M115.644351
162. Kwon B, Lee M, Waring AJ, Hong M. Oligomeric Structure and Three-Dimensional Fold of the HIV gp41 Membrane-Proximal External Region and Transmembrane Domain in Phospholipid Bilayers. *J Am Chem Soc.* 2018;140(26):8246-8259. doi:10.1021/jacs.8b04010
163. Caillat C, Guilligay D, Torralba J, et al. Structure of HIV-1 gp41 with its membrane anchors targeted by neutralizing antibodies. *eLife.* 2021;10:e65005. doi:10.7554/eLife.65005
164. Sun ZYJ, Oh KJ, Kim M, et al. HIV-1 broadly neutralizing antibody extracts its epitope from a kinked gp41 ectodomain region on the viral membrane. *Immunity.* 2008;28(1):52-63. doi:10.1016/j.jimmuni.2007.11.018
165. Kim M, Sun ZYJ, Rand KD, et al. Antibody mechanics on a membrane-bound HIV segment essential for GP41-targeted viral neutralization. *Nat Struct Mol Biol.* 2011;18(11):1235-1243. doi:10.1038/nsmb.2154
166. Huarte N, Lorizate M, Maeso R, et al. The broadly neutralizing anti-human immunodeficiency virus type 1 4E10 monoclonal antibody is better adapted to membrane-bound epitope recognition and blocking than 2F5. *J Virol.* 2008;82(18):8986-8996. doi:10.1128/JVI.00846-08
167. Kim M, Song L, Moon J, et al. Immunogenicity of Membrane-bound HIV-1 gp41 Membrane-proximal External Region (MPER) Segments Is Dominated by Residue Accessibility and Modulated by Stereochemistry. *J Biol Chem.* 2013;288(44):31888-31901. doi:10.1074/jbc.M113.494609
168. Fu Q, Shaik MM, Cai Y, et al. Structure of the membrane proximal external region of HIV-1 envelope glycoprotein. *Proc Natl Acad Sci U S A.* 2018;115(38):E8892-E8899. doi:10.1073/pnas.1807259115
169. Ferrantelli F, Rasmussen RA, Buckley KA, et al. Complete protection of neonatal rhesus macaques against oral exposure to pathogenic simian-human immunodeficiency virus by human anti-HIV monoclonal antibodies. *J Infect Dis.* 2004;189(12):2167-2173. doi:10.1086/420833

170. Stiegler G, Kunert R, Purtscher M, et al. A potent cross-clade neutralizing human monoclonal antibody against a novel epitope on gp41 of human immunodeficiency virus type 1. *AIDS Res Hum Retroviruses.* 2001;17(18):1757-1765. doi:10.1089/08892220152741450
171. Trkola A, Kuster H, Rusert P, et al. Delay of HIV-1 rebound after cessation of antiretroviral therapy through passive transfer of human neutralizing antibodies. *Nat Med.* 2005;11(6):615-622. doi:10.1038/nm1244
172. Krebs SJ, Kwon YD, Schramm CA, et al. Longitudinal Analysis Reveals Early Development of Three MPER-Directed Neutralizing Antibody Lineages from an HIV-1-Infected Individual. *Immunity.* 2019;50(3):677-691.e13. doi:10.1016/j.jimmuni.2019.02.008
173. Zhang L, Irimia A, He L, et al. An MPER antibody neutralizes HIV-1 using germline features shared among donors. *Nat Commun.* 2019;10(1):5389. doi:10.1038/s41467-019-12973-1
174. Alam SM, Morelli M, Dennison SM, et al. Role of HIV membrane in neutralization by two broadly neutralizing antibodies. *Proc Natl Acad Sci U S A.* 2009;106(48):20234-20239. doi:10.1073/pnas.0908713106
175. Zwick MB, Komori HK, Stanfield RL, et al. The long third complementarity-determining region of the heavy chain is important in the activity of the broadly neutralizing anti-human immunodeficiency virus type 1 antibody 2F5. *J Virol.* 2004;78(6):3155-3161. doi:10.1128/JVI.78.6.3155-3161.2004
176. Chen J, Frey G, Peng H, et al. Mechanism of HIV-1 Neutralization by Antibodies Targeting a Membrane-Proximal Region of gp41. *J Virol.* 2014;88(2):1249-1258. doi:10.1128/JVI.02664-13
177. Julien JP, Huarte N, Maeso R, et al. Ablation of the Complementarity-Determining Region H3 Apex of the Anti-HIV-1 Broadly Neutralizing Antibody 2F5 Abrogates Neutralizing Capacity without Affecting Core Epitope Binding. *J Virol.* 2010;84(9):4136-4147. doi:10.1128/JVI.02357-09
178. Rujas E, Caaveiro JMM, Partida-Hanon A, et al. Structural basis for broad neutralization of HIV-1 through the molecular recognition of 10E8 helical epitope at the membrane interface. *Sci Rep.* 2016;6:38177. doi:10.1038/srep38177

179. Doyle-Cooper C, Hudson KE, Cooper AB, et al. Immune tolerance negatively regulates B cells in knock-in mice expressing broadly neutralizing HIV antibody 4E10. *J Immunol.* 2013;191(6):3186-3191. doi:10.4049/jimmunol.1301285
180. Alam SM, McAdams M, Boren D, et al. The Role of Antibody Polyspecificity and Lipid Reactivity in Binding of Broadly Neutralizing Anti-HIV-1 Envelope Human Monoclonal Antibodies 2F5 and 4E10 to Glycoprotein 41 Membrane Proximal Envelope Epitopes. *J Immunol.* 2007;178(7):4424-4435.
181. Irimia A, Serra AM, Sarkar A, et al. Lipid interactions and angle of approach to the HIV-1 viral membrane of broadly neutralizing antibody 10E8: Insights for vaccine and therapeutic design. *PLoS Pathog.* 2017;13(2):e1006212. doi:10.1371/journal.ppat.1006212
182. Lutje Hulsik D, Liu Ying, Strokappe NM, et al. A gp41 MPER-specific llama VHH requires a hydrophobic CDR3 for neutralization but not for antigen recognition. *PLoS Pathog.* 2013;9(3):e1003202. doi:10.1371/journal.ppat.1003202
183. Schibli DJ, Weissenhorn W. Class I and class II viral fusion protein structures reveal similar principles in membrane fusion. *Mol Membr Biol.* 2004;21(6):361-371. doi:10.1080/09687860400017784
184. Long Y, Meng F, Kondo N, Iwamoto A, Matsuda Z. Conserved arginine residue in the membrane-spanning domain of HIV-1 gp41 is required for efficient membrane fusion. *Protein Cell.* 2011;2(5):369-376. doi:10.1007/s13238-011-1051-0
185. Owens RJ, Burke C, Rose JK. Mutations in the membrane-spanning domain of the human immunodeficiency virus envelope glycoprotein that affect fusion activity. *J Virol.* 1994;68(1):570-574. doi:10.1128/JVI.68.1.570-574.1994
186. Shang L, Yue L, Hunter E. Role of the membrane-spanning domain of human immunodeficiency virus type 1 envelope glycoprotein in cell-cell fusion and virus infection. *J Virol.* 2008;82(11):5417-5428. doi:10.1128/JVI.02666-07
187. Yue L, Shang L, Hunter E. Truncation of the membrane-spanning domain of human immunodeficiency virus type 1 envelope glycoprotein defines elements required for fusion, incorporation, and infectivity. *J Virol.* 2009;83(22):11588-11598. doi:10.1128/JVI.00914-09
188. Wang Y, Kaur P, Sun ZYJ, et al. Topological analysis of the gp41 MPER on lipid bilayers relevant to the metastable HIV-1 envelope prefusion state. *Proc Natl Acad Sci U S A.* 2019;116(45):22556-22566. doi:10.1073/pnas.1912427116

189. Hanson MC, Abraham W, Crespo MP, et al. Liposomal vaccines incorporating molecular adjuvants and intrastructural T-cell help promote the immunogenicity of HIV membrane-proximal external region peptides. *Vaccine*. 2015;33(7):861-868. doi:10.1016/j.vaccine.2014.12.045
190. Apellániz B, Nieva JL. The Use of Liposomes to Shape Epitope Structure and Modulate Immunogenic Responses of Peptide Vaccines Against HIV MPER. *Adv Protein Chem Struct Biol*. 2015;99:15-54. doi:10.1016/bs.apcsb.2015.03.002
191. Montero M, van Houten NE, Wang X, Scott JK. The Membrane-Proximal External Region of the Human Immunodeficiency Virus Type 1 Envelope: Dominant Site of Antibody Neutralization and Target for Vaccine Design. *Microbiol Mol Biol Rev*. 2008;72(1):54-84. doi:10.1128/MMBR.00020-07
192. Decroix N, Hocini H, Quan CP, Bellon B, Kazatchkine MD, Bouvet JP. Induction in mucosa of IgG and IgA antibodies against parenterally administered soluble immunogens. *Scand J Immunol*. 2001;53(4):401-409. doi:10.1046/j.1365-3083.2001.00894.x
193. Liao M, Lu Y, Xiao Y, Dierich MP, Chen Y. Induction of high level of specific antibody response to the neutralizing epitope ELDKWA on HIV-1 gp41 by peptide-vaccine. *Peptides*. 2000;21(4):463-468. doi:10.1016/s0196-9781(00)00179-0
194. Decroix N, Pamonsinlapatham P, Quan CP, Bouvet JP. Impairment by Mucosal Adjuvants and Cross-Reactivity with Variant Peptides of the Mucosal Immunity Induced by Injection of the Fusion Peptide PADRE-ELDKWA. *Clin Diagn Lab Immunol*. 2003;10(6):1103-1108. doi:10.1128/CDLI.10.6.1103-1108.2003
195. Toukam DK, Tenbusch M, Stang A, et al. Targeting Antibody Responses to the Membrane Proximal External Region of the Envelope Glycoprotein of Human Immunodeficiency Virus. *PLOS ONE*. 2012;7(5):e38068. doi:10.1371/journal.pone.0038068
196. Matyas GR, Jobe O, Wieczorek L, et al. Cross-clade neutralization of HIV-1 by a monoclonal antibody obtained by immunization with liposomes containing lipid A and a synthetic MPER peptide. *Retrovirology*. 2012;9(Suppl 2):P4. doi:10.1186/1742-4690-9-S2-P4
197. Dennison SM, Stewart SM, Stempel KC, Liao HX, Haynes BF, Alam SM. Stable Docking of Neutralizing Human Immunodeficiency Virus Type 1 gp41 Membrane-Proximal External Region Monoclonal Antibodies 2F5 and 4E10 Is Dependent on the

- Membrane Immersion Depth of Their Epitope Regions. *J Virol.* 2009;83(19):10211-10223. doi:10.1128/JVI.00571-09
198. Shnyrova AV, Bashkirov PV, Akimov SA, et al. Geometric catalysis of membrane fission driven by flexible dynamin rings. *Science.* 2013;339(6126):1433-1436. doi:10.1126/science.1233920
199. Fiske CH, Subbarow Y. The colorimetric determination of phosphorus. *Journal of Biological Chemistry.* 1925;66(2):375-400. doi:10.1016/S0021-9258(18)84756-1
200. Bartlett GR. Phosphorus assay in column chromatography. *J Biol Chem.* 1959;234(3):466-468.
201. van Gent, C.M., Böttcher, C.J.F. A rapid and sensitive sub-micro phosphorus determination. *Anal Chim Acta.* 1961;24:203-204.
202. Collet JF, Bardwell JCA. Oxidative protein folding in bacteria. *Mol Microbiol.* 2002;44(1):1-8. doi:10.1046/j.1365-2958.2002.02851.x
203. Lobstein J, Emrich CA, Jeans C, Faulkner M, Riggs P, Berkmen M. SHuffle, a novel Escherichia coli protein expression strain capable of correctly folding disulfide bonded proteins in its cytoplasm. *Microb Cell Fact.* 2012;11:56. doi:10.1186/1475-2859-11-56
204. Greenfield NJ. Using circular dichroism spectra to estimate protein secondary structure. *Nat Protoc.* 2006;1(6):2876-2890. doi:10.1038/nprot.2006.202
205. Elliott A, Ambrose EJ. Structure of Synthetic Polypeptides. *Nature.* 1950;165(4206):921-922. doi:10.1038/165921a0
206. Schindelin J, Arganda-Carreras I, Frise E, et al. Fiji: an open-source platform for biological-image analysis. *Nat Methods.* 2012;9(7):676-682. doi:10.1038/nmeth.2019
207. Bogdanov M, Mileykovskaya E, Dowhan W. Lipids in the assembly of membrane proteins and organization of protein supercomplexes: implications for lipid-linked disorders. *Subcell Biochem.* 2008;49:197-239. doi:10.1007/978-1-4020-8831-5_8
208. Sanchez S, Tricerri A, Gunther G, Gratton E. *Laurdan Generalized Polarization: From Cuvette to Microscope.* Vol 2.; 2007.
209. Parasassi T, De Stasio G, d'Ubaldo A, Gratton E. Phase fluctuation in phospholipid membranes revealed by Laurdan fluorescence. *Biophys J.* 1990;57(6):1179-1186. doi:10.1016/S0006-3495(90)82637-0

210. Gaus K, Zech T, Harder T. Visualizing membrane microdomains by Laurdan 2-photon microscopy. *Mol Membr Biol.* 2006;23(1):41-48. doi:10.1080/09687860500466857
211. Kramers HA. Brownian motion in a field of force and the diffusion model of chemical reactions. *Physica.* 1940;7(4):284-304. doi:10.1016/S0031-8914(40)90098-2
212. Hänggi P, Talkner P, Borkovec M. Reaction-rate theory: fifty years after Kramers. *Rev Mod Phys.* 1990;62(2):251-341. doi:10.1103/RevModPhys.62.251
213. Scherer EM, Leaman DP, Zwick MB, McMichael AJ, Burton DR. Aromatic residues at the edge of the antibody combining site facilitate viral glycoprotein recognition through membrane interactions. *Proc Natl Acad Sci U S A.* 2010;107(4):1529-1534. doi:10.1073/pnas.0909680107
214. Alving CR, Rao M, Steers NJ, Matyas GR, Mayorov AV. Liposomes containing lipid A: an effective, safe, generic adjuvant system for synthetic vaccines. *Expert Review of Vaccines.* 2012;11(6):733-744. doi:10.1586/erv.12.35
215. Melikyan GB. Membrane fusion mediated by human immunodeficiency virus envelope glycoprotein. *Curr Top Membr.* 2011;68:81-106. doi:10.1016/B978-0-12-385891-7.00004-0
216. Epand RM. Fusion peptides and the mechanism of viral fusion. *Biochim Biophys Acta.* 2003;1614(1):116-121. doi:10.1016/s0005-2736(03)00169-x
217. Apellániz B, Huarte N, Largo E, Nieva JL. The three lives of viral fusion peptides. *Chem Phys Lipids.* 2014;181:40-55. doi:10.1016/j.chemphyslip.2014.03.003
218. Eckert DM, Kim PS. Mechanisms of viral membrane fusion and its inhibition. *Annu Rev Biochem.* 2001;70:777-810. doi:10.1146/annurev.biochem.70.1.777
219. Buzon V, Natrajan G, Schibli D, Campelo F, Kozlov MM, Weissenhorn W. Crystal Structure of HIV-1 gp41 Including Both Fusion Peptide and Membrane Proximal External Regions. *PLOS Pathogens.* 2010;6(5):e1000880. doi:10.1371/journal.ppat.1000880
220. Vishwanathan SA, Thomas A, Brasseur R, Epand RF, Hunter E, Epand RM. Hydrophobic substitutions in the first residue of the CRAC segment of the gp41 protein of HIV. *Biochemistry.* 2008;47(1):124-130. doi:10.1021/bi7018892
221. Zwick MB. The membrane-proximal external region of HIV-1 gp41: a vaccine target worth exploring. *AIDS.* 2005;19(16):1725-1737. doi:10.1097/01.aids.0000189850.83322.41

222. Lorizate M, Huarte N, Sáez-Cirión A, Nieva JL. Interfacial pre-transmembrane domains in viral proteins promoting membrane fusion and fission. *Biochim Biophys Acta.* 2008;1778(7-8):1624-1639. doi:10.1016/j.bbamem.2007.12.018
223. Contarino M, Bastian AR, Kalyana Sundaram RV, et al. Chimeric Cyanovirin-MPER Recombinantly Engineered Proteins Cause Cell-Free Virolysis of HIV-1. *Antimicrob Agents Chemother.* 2013;57(10):4743-4750. doi:10.1128/AAC.00309-13
224. Parajuli B, Acharya K, Yu R, et al. Lytic Inactivation of Human Immunodeficiency Virus by Dual Engagement of gp120 and gp41 Domains in the Virus Env Protein Trimer. *Biochemistry.* 2016;55(44):6100-6114. doi:10.1021/acs.biochem.6b00570
225. Caravilla P, Cruz A, Martin-Ugarte I, et al. Effects of HIV-1 gp41-Derived Virucidal Peptides on Virus-like Lipid Membranes. *Biophys J.* 2017;113(6):1301-1310. doi:10.1016/j.bpj.2017.06.061
226. Cerutti N, Loredo-Varela JL, Caillat C, Weissenhorn W. Antigp41 membrane proximal external region antibodies and the art of using the membrane for neutralization. *Curr Opin HIV AIDS.* 2017;12(3):250-256. doi:10.1097/COH.0000000000000364
227. Montero M, Gulzar N, Klaric KA, et al. Neutralizing epitopes in the membrane-proximal external region of HIV-1 gp41 are influenced by the transmembrane domain and the plasma membrane. *J Virol.* 2012;86(6):2930-2941. doi:10.1128/JVI.06349-11
228. Rujas E, Insausti S, Leaman DP, et al. Affinity for the Interface Underpins Potency of Antibodies Operating In Membrane Environments. *Cell Rep.* 2020;32(7):108037. doi:10.1016/j.celrep.2020.108037
229. Chernomordik LV, Kozlov MM. Protein-lipid interplay in fusion and fission of biological membranes. *Annu Rev Biochem.* 2003;72:175-207. doi:10.1146/annurev.biochem.72.121801.161504
230. Akimov SA, Molotkovsky RJ, Kuzmin PI, Galimzyanov TR, Batishchev OV. Continuum Models of Membrane Fusion: Evolution of the Theory. *Int J Mol Sci.* 2020;21(11):E3875. doi:10.3390/ijms21113875
231. Jaroniec CP, Kaufman JD, Stahl SJ, et al. Structure and Dynamics of Micelle-Associated Human Immunodeficiency Virus gp41 Fusion Domain,. *Biochemistry.* 2005;44(49):16167-16180. doi:10.1021/bi051672a
232. Li Y, Tamm LK. Structure and plasticity of the human immunodeficiency virus gp41 fusion domain in lipid micelles and bilayers. *Biophys J.* 2007;93(3):876-885. doi:10.1529/biophysj.106.102335

233. Lai AL, Moorthy AE, Li Y, Tamm LK. Fusion activity of HIV gp41 fusion domain is related to its secondary structure and depth of membrane insertion in a cholesterol-dependent fashion. *J Mol Biol.* 2012;418(1-2):3-15. doi:10.1016/j.jmb.2012.02.010
234. Qiang W, Sun Y, Weliky DP. A strong correlation between fusogenicity and membrane insertion depth of the HIV fusion peptide. *Proc Natl Acad Sci U S A.* 2009;106(36):15314-15319. doi:10.1073/pnas.0907360106
235. Sáez-Cirión A, Nieva JL. Conformational transitions of membrane-bound HIV-1 fusion peptide. *Biochimica et Biophysica Acta (BBA) - Biomembranes.* 2002;1564(1):57-65. doi:10.1016/S0005-2736(02)00400-5
236. Martin I, Defrise-Quertain F, Decroly E, Vandenbranden M, Brasseur R, Ruysschaert JM. Orientation and structure of the NH₂-terminal HIV-1 gp41 peptide in fused and aggregated liposomes. *Biochim Biophys Acta.* 1993;1145(1):124-133. doi:10.1016/0005-2736(93)90389-h
237. Martin I, Schaal H, Scheid A, Ruysschaert JM. Lipid membrane fusion induced by the human immunodeficiency virus type 1 gp41 N-terminal extremity is determined by its orientation in the lipid bilayer. *J Virol.* 1996;70(1):298-304. doi:10.1128/JVI.70.1.298-304.1996
238. Castano S, Desbat B. Structure and orientation study of fusion peptide FP23 of gp41 from HIV-1 alone or inserted into various lipid membrane models (mono-, bi- and multibi-layers) by FT-IR spectroscopies and Brewster angle microscopy. *Biochim Biophys Acta.* 2005;1715(2):81-95. doi:10.1016/j.bbamem.2005.07.008
239. Gabrys CM, Qiang W, Sun Y, Xie L, Schmick SD, Weliky DP. Solid-state nuclear magnetic resonance measurements of HIV fusion peptide 13CO to lipid 31P proximities support similar partially inserted membrane locations of the α helical and β sheet peptide structures. *J Phys Chem A.* 2013;117(39):9848-9859. doi:10.1021/jp312845w
240. Gordon LM, Mobley PW, Lee W, et al. Conformational mapping of the N-terminal peptide of HIV-1 gp41 in lipid detergent and aqueous environments using ¹³C-enhanced Fourier transform infrared spectroscopy. *Protein Sci.* 2004;13(4):1012-1030. doi:10.1110/ps.03407704
241. Martin I, Dubois MC, Defrise-Quertain F, et al. Correlation between fusogenicity of synthetic modified peptides corresponding to the NH₂-terminal extremity of simian immunodeficiency virus gp32 and their mode of insertion into the lipid bilayer: an infrared

- spectroscopy study. *J Virol.* 1994;68(2):1139-1148. doi:10.1128/JVI.68.2.1139-1148.1994
242. Mobley PW, Waring AJ, Sherman MA, Gordon LM. Membrane interactions of the synthetic N-terminal peptide of HIV-1 gp41 and its structural analogs. *Biochim Biophys Acta.* 1999;1418(1):1-18. doi:10.1016/s0005-2736(99)00014-0
243. Rafalski M, Lear JD, DeGrado WF. Phospholipid interactions of synthetic peptides representing the N-terminus of HIV gp41. *Biochemistry.* 1990;29(34):7917-7922. doi:10.1021/bi00486a020
244. Qiang W, Weliky DP. HIV fusion peptide and its cross-linked oligomers: efficient syntheses, significance of the trimer in fusion activity, correlation of beta strand conformation with membrane cholesterol, and proximity to lipid headgroups. *Biochemistry.* 2009;48(2):289-301. doi:10.1021/bi8015668
245. Nieva JL, Nir S, Muga A, Goñi FM, Wilschut J. Interaction of the HIV-1 fusion peptide with phospholipid vesicles: different structural requirements for fusion and leakage. *Biochemistry.* 1994;33(11):3201-3209. doi:10.1021/bi00177a009
246. Pereira FB, Valpuesta JM, Basañez G, Goñi FM, Nieva JL. Interbilayer lipid mixing induced by the human immunodeficiency virus type-1 fusion peptide on large unilamellar vesicles: the nature of the nonlamellar intermediates. *Chem Phys Lipids.* 1999;103(1-2):11-20. doi:10.1016/s0009-3084(99)00087-0
247. Tristram-Nagle S, Chan R, Kooijman E, et al. HIV fusion peptide penetrates, disorders, and softens T-cell membrane mimics. *J Mol Biol.* 2010;402(1):139-153. doi:10.1016/j.jmb.2010.07.026
248. Ivankin A, Kuzmenko I, Gidalevitz D. Cholesterol mediates membrane curvature during fusion events. *Phys Rev Lett.* 2012;108(23):238103. doi:10.1103/PhysRevLett.108.238103
249. Yao H, Lee M, Liao SY, Hong M. Solid-State Nuclear Magnetic Resonance Investigation of the Structural Topology and Lipid Interactions of a Viral Fusion Protein Chimera Containing the Fusion Peptide and Transmembrane Domain. *Biochemistry.* 2016;55(49):6787-6800. doi:10.1021/acs.biochem.6b00568
250. Yao H, Lee MW, Waring AJ, Wong GCL, Hong M. Viral fusion protein transmembrane domain adopts β -strand structure to facilitate membrane topological changes for virus-cell fusion. *Proc Natl Acad Sci U S A.* 2015;112(35):10926-10931. doi:10.1073/pnas.1501430112

251. Lee M, Yao H, Kwon B, et al. Conformation and Trimer Association of the Transmembrane Domain of the Parainfluenza Virus Fusion Protein in Lipid Bilayers from Solid-State NMR: Insights into the Sequence Determinants of Trimer Structure and Fusion Activity. *J Mol Biol.* 2018;430(5):695-709. doi:10.1016/j.jmb.2018.01.002
252. Liao SY, Lee M, Hong M. Interplay between membrane curvature and protein conformational equilibrium investigated by solid-state NMR. *J Struct Biol.* 2019;206(1):20-28. doi:10.1016/j.jsb.2018.02.007
253. Sreerama N, Venyaminov SY, Woody RW. Estimation of protein secondary structure from circular dichroism spectra: inclusion of denatured proteins with native proteins in the analysis. *Anal Biochem.* 2000;287(2):243-251. doi:10.1006/abio.2000.4879
254. Arrondo JL, Goñi FM. Structure and dynamics of membrane proteins as studied by infrared spectroscopy. *Prog Biophys Mol Biol.* 1999;72(4):367-405. doi:10.1016/s0079-6107(99)00007-3
255. Iloro I, Chehín R, Goñi FM, Pajares MA, Arrondo JLR. Methionine adenosyltransferase alpha-helix structure unfolds at lower temperatures than beta-sheet: a 2D-IR study. *Biophys J.* 2004;86(6):3951-3958. doi:10.1529/biophysj.103.028373
256. Vu DM, Myers JK, Oas TG, Dyer RB. Probing the folding and unfolding dynamics of secondary and tertiary structures in a three-helix bundle protein. *Biochemistry.* 2004;43(12):3582-3589. doi:10.1021/bi036203s
257. Walsh STR, Cheng RP, Wright WW, et al. The hydration of amides in helices; a comprehensive picture from molecular dynamics, IR, and NMR. *Protein Sci.* 2003;12(3):520-531. doi:10.1110/ps.0223003
258. Guyader M, Kiyokawa E, Abrami L, Turelli P, Trono D. Role for human immunodeficiency virus type 1 membrane cholesterol in viral internalization. *J Virol.* 2002;76(20):10356-10364. doi:10.1128/jvi.76.20.10356-10364.2002
259. Liao Z, Graham DR, Hildreth JEK. Lipid rafts and HIV pathogenesis: virion-associated cholesterol is required for fusion and infection of susceptible cells. *AIDS Res Hum Retroviruses.* 2003;19(8):675-687. doi:10.1089/088922203322280900
260. Fabian H, Mantsch HH, Schultz CP. Two-dimensional IR correlation spectroscopy: Sequential events in the unfolding process of the λ Cro-V55C repressor protein. *Proc Natl Acad Sci U S A.* 1999;96(23):13153-13158.

261. Noda I. Two-dimensional correlation analysis useful for spectroscopy, chromatography, and other analytical measurements. *Anal Sci.* 2007;23(2):139-146. doi:10.2116/analsci.23.139
262. Serrano S, Huarte N, Rujas E, Andreu D, Nieva JL, Jiménez MA. Structure-Related Roles for the Conservation of the HIV-1 Fusion Peptide Sequence Revealed by Nuclear Magnetic Resonance. *Biochemistry.* 2017;56(41):5503-5511. doi:10.1021/acs.biochem.7b00745
263. Yang J, Gabrys CM, Weliky DP. Solid-state nuclear magnetic resonance evidence for an extended beta strand conformation of the membrane-bound HIV-1 fusion peptide. *Biochemistry.* 2001;40(27):8126-8137. doi:10.1021/bi0100283
264. Yang J, Prorok M, Castellino FJ, Weliky DP. Oligomeric beta-structure of the membrane-bound HIV-1 fusion peptide formed from soluble monomers. *Biophys J.* 2004;87(3):1951-1963. doi:10.1529/biophysj.103.028530
265. Schibli DJ, Montelaro RC, Vogel HJ. The membrane-proximal tryptophan-rich region of the HIV glycoprotein, gp41, forms a well-defined helix in dodecylphosphocholine micelles. *Biochemistry.* 2001;40(32):9570-9578. doi:10.1021/bi010640u
266. Julien JP, Bryson S, Nieva JL, Pai EF. Structural details of HIV-1 recognition by the broadly neutralizing monoclonal antibody 2F5: epitope conformation, antigen-recognition loop mobility, and anion-binding site. *J Mol Biol.* 2008;384(2):377-392. doi:10.1016/j.jmb.2008.09.024
267. Sanders RW, Moore JP. HIV: A stamp on the envelope. *Nature.* 2014;514(7523):437-438. doi:10.1038/nature13926
268. Wang H, Barnes CO, Yang Z, Nussenzweig MC, Bjorkman PJ. Partially Open HIV-1 Envelope Structures Exhibit Conformational Changes Relevant for Coreceptor Binding and Fusion. *Cell Host Microbe.* 2018;24(4):579-592.e4. doi:10.1016/j.chom.2018.09.003
269. van Gils MJ, Sanders RW. Hitting HIV's Harpoon. *Immunity.* 2018;49(1):14-15. doi:10.1016/j.immuni.2018.07.003
270. Xu K, Acharya P, Kong R, et al. Epitope-based vaccine design yields fusion peptide-directed antibodies that neutralize diverse strains of HIV-1. *Nat Med.* 2018;24(6):857-867. doi:10.1038/s41591-018-0042-6

271. Jacob RA, Moyo T, Schomaker M, Abrahams F, Grau Pujol B, Dorfman JR. Anti-V3/Glycan and Anti-MPER Neutralizing Antibodies, but Not Anti-V2/Glycan Site Antibodies, Are Strongly Associated with Greater Anti-HIV-1 Neutralization Breadth and Potency. *J Virol.* 2015;89(10):5264-5275. doi:10.1128/JVI.00129-15
272. Oakes V, Torralba J, Rujas E, Nieva JL, Domene C, Apellaniz B. Exposure of the HIV-1 broadly neutralizing antibody 10E8 MPER epitope on the membrane surface by gp41 transmembrane domain scaffolds. *Biochimica et Biophysica Acta (BBA) - Biomembranes.* 2018;1860(6):1259-1271. doi:10.1016/j.bbamem.2018.02.019
273. Galiani S, Waithe D, Reglinski K, et al. Super-resolution Microscopy Reveals Compartmentalization of Peroxisomal Membrane Proteins. *J Biol Chem.* 2016;291(33):16948-16962. doi:10.1074/jbc.M116.734038
274. Rujas E, Leaman DP, Insausti S, et al. Functional Optimization of Broadly Neutralizing HIV-1 Antibody 10E8 by Promotion of Membrane Interactions. *J Virol.* 2018;92(8):e02249-17. doi:10.1128/JVI.02249-17
275. Chojnacki J, Staudt T, Glass B, et al. Maturation-dependent HIV-1 surface protein redistribution revealed by fluorescence nanoscopy. *Science.* 2012;338(6106):524-528. doi:10.1126/science.1226359
276. Grouleff J, Irudayam SJ, Skeby KK, Schiøtt B. The influence of cholesterol on membrane protein structure, function, and dynamics studied by molecular dynamics simulations. *Biochim Biophys Acta.* 2015;1848(9):1783-1795. doi:10.1016/j.bbamem.2015.03.029
277. Legler DF, Matti C, Laufer JM, et al. Modulation of Chemokine Receptor Function by Cholesterol: New Prospects for Pharmacological Intervention. *Mol Pharmacol.* 2017;91(4):331-338. doi:10.1124/mol.116.107151
278. McIntosh TJ, Simon SA. Bilayers as Protein Solvents: Role of Bilayer Structure and Elastic Properties. *J Gen Physiol.* 2007;130(2):225-227. doi:10.1085/jgp.200709841
279. Epand RF, Sayer BG, Epand RM. The Tryptophan-Rich Region of HIV gp41 and the Promotion of Cholesterol-Rich Domains. *Biochemistry.* 2005;44(14):5525-5531. doi:10.1021/bi0500224
280. Lorent JH, Diaz-Rohrer B, Lin X, et al. Structural determinants and functional consequences of protein affinity for membrane rafts. *Nat Commun.* 2017;8(1):1219. doi:10.1038/s41467-017-01328-3

281. Lorent JH, Levental KR, Ganesan L, et al. Plasma membranes are asymmetric in lipid unsaturation, packing and protein shape. *Nat Chem Biol.* 2020;16(6):644-652. doi:10.1038/s41589-020-0529-6
282. Yuan Z, Zhang F, Davis MJ, Bodén M, Teasdale RD. Predicting the Solvent Accessibility of Transmembrane Residues from Protein Sequence. *J Proteome Res.* 2006;5(5):1063-1070. doi:10.1021/pr050397b
283. Shen X, Parks RJ, Montefiori DC, et al. In vivo gp41 antibodies targeting the 2F5 monoclonal antibody epitope mediate human immunodeficiency virus type 1 neutralization breadth. *J Virol.* 2009;83(8):3617-3625. doi:10.1128/JVI.02631-08
284. Zhu Z, Qin HR, Chen W, et al. Cross-reactive HIV-1-neutralizing human monoclonal antibodies identified from a patient with 2F5-like antibodies. *J Virol.* 2011;85(21):11401-11408. doi:10.1128/JVI.05312-11
285. Li Y, Svehla K, Louder MK, et al. Analysis of neutralization specificities in polyclonal sera derived from human immunodeficiency virus type 1-infected individuals. *J Virol.* 2009;83(2):1045-1059. doi:10.1128/JVI.01992-08
286. Gray ES, Madiga MC, Moore PL, et al. Broad neutralization of human immunodeficiency virus type 1 mediated by plasma antibodies against the gp41 membrane proximal external region. *J Virol.* 2009;83(21):11265-11274. doi:10.1128/JVI.01359-09
287. Sather DN, Stamatatos L. Epitope specificities of broadly neutralizing plasmas from HIV-1 infected subjects. *Vaccine.* 2010;28 Suppl 2:B8-12. doi:10.1016/j.vaccine.2009.07.085
288. Stamatatos L, Morris L, Burton DR, Mascola JR. Neutralizing antibodies generated during natural HIV-1 infection: good news for an HIV-1 vaccine? *Nat Med.* 2009;15(8):866-870. doi:10.1038/nm.1949
289. Zhou M, Kostoula I, Brill B, Panou E, Sakarellos-Daitsiotis M, Dietrich U. Prime boost vaccination approaches with different conjugates of a new HIV-1 gp41 epitope encompassing the membrane proximal external region induce neutralizing antibodies in mice. *Vaccine.* 2012;30(11):1911-1916. doi:10.1016/j.vaccine.2012.01.026
290. Serrano S, Araujo A, Apellániz B, et al. Structure and Immunogenicity of a Peptide Vaccine, Including the Complete HIV-1 gp41 2F5 Epitope: IMPLICATIONS FOR ANTIBODY RECOGNITION MECHANISM AND IMMUNOGEN DESIGN *. *Journal of Biological Chemistry.* 2014;289(10):6565-6580. doi:10.1074/jbc.M113.527747

291. Salimi H, Johnson J, Flores MG, et al. The lipid membrane of HIV-1 stabilizes the viral envelope glycoproteins and modulates their sensitivity to antibody neutralization. *J Biol Chem.* 2020;295(2):348-362. doi:10.1074/jbc.RA119.009481
292. Carrauilla P, Nieva JL, Goñi FM, Requejo-Isidro J, Huarte N. Two-Photon Laurdan Studies of the Ternary Lipid Mixture DOPC:SM:Cholesterol Reveal a Single Liquid Phase at Sphingomyelin:Cholesterol Ratios Lower Than 1. *Langmuir.* 2015;31(9):2808-2817. doi:10.1021/la504251u
293. Caillat C, Guilligay D, Sulbaran G, Weissenhorn W. Neutralizing Antibodies Targeting HIV-1 gp41. *Viruses.* 2020;12(11):E1210. doi:10.3390/v12111210
294. Song L, Sun ZYJ, Coleman KE, et al. Broadly neutralizing anti-HIV-1 antibodies disrupt a hinge-related function of gp41 at the membrane interface. *Proc Natl Acad Sci U S A.* 2009;106(22):9057-9062. doi:10.1073/pnas.0901474106
295. Kwon B, Mandal T, Elkins MR, Oh Y, Cui Q, Hong M. Cholesterol Interaction with the Trimeric HIV Fusion Protein gp41 in Lipid Bilayers Investigated by Solid-State NMR Spectroscopy and Molecular Dynamics Simulations. *J Mol Biol.* 2020;432(16):4705-4721. doi:10.1016/j.jmb.2020.06.017
296. Sun ZYJ, Cheng Y, Kim M, et al. Disruption of helix-capping residues 671 and 674 reveals a role in HIV-1 entry for a specialized hinge segment of the membrane proximal external region of gp41. *J Mol Biol.* 2014;426(5):1095-1108. doi:10.1016/j.jmb.2013.09.030
297. Torralba J, de la Arada I, Carrauilla P, et al. Cholesterol Constrains the Antigenic Configuration of the Membrane-Proximal Neutralizing HIV-1 Epitope. *ACS Infect Dis.* 2020;6(8):2155-2168. doi:10.1021/acsinfecdis.0c00243
298. Plesnar E, Subczynski WK, Pasenkiewicz-Gierula M. Saturation with cholesterol increases vertical order and smoothes the surface of the phosphatidylcholine bilayer: a molecular simulation study. *Biochim Biophys Acta.* 2012;1818(3):520-529. doi:10.1016/j.bbamem.2011.10.023
299. Shahane G, Ding W, Palaiokostas M, Orsi M. Physical properties of model biological lipid bilayers: insights from all-atom molecular dynamics simulations. *J Mol Model.* 2019;25(3):76. doi:10.1007/s00894-019-3964-0
300. Kucerka N, Perlmutter JD, Pan J, Tristram-Nagle S, Katsaras J, Sachs JN. The effect of cholesterol on short- and long-chain monounsaturated lipid bilayers as

- determined by molecular dynamics simulations and X-ray scattering. *Biophys J.* 2008;95(6):2792-2805. doi:10.1529/biophysj.107.122465
301. Kucerka N, Liu Y, Chu N, Petrache HI, Tristram-Nagle S, Nagle JF. Structure of fully hydrated fluid phase DMPC and DLPC lipid bilayers using X-ray scattering from oriented multilamellar arrays and from unilamellar vesicles. *Biophys J.* 2005;88(4):2626-2637. doi:10.1529/biophysj.104.056606
302. Gallová J, Uhríková D, Kučerka N, Teixeira J, Balgavý P. Hydrophobic thickness, lipid surface area and polar region hydration in monounsaturated diacylphosphatidylcholine bilayers: SANS study of effects of cholesterol and β -sitosterol in unilamellar vesicles. *Biochimica et Biophysica Acta (BBA) - Biomembranes.* 2008;1778(11):2627-2632. doi:10.1016/j.bbamem.2008.08.009
303. Kwong PD, Mascola JR. Human antibodies that neutralize HIV-1: identification, structures, and B cell ontogenies. *Immunity.* 2012;37(3):412-425. doi:10.1016/j.immuni.2012.08.012
304. Caskey M, Klein F, Nussenzweig MC. Broadly neutralizing anti-HIV-1 monoclonal antibodies in the clinic. *Nat Med.* 2019;25(4):547-553. doi:10.1038/s41591-019-0412-8
305. Shnaper S, Sackett K, Gallo SA, Blumenthal R, Shai Y. The C- and the N-terminal regions of glycoprotein 41 ectodomain fuse membranes enriched and not enriched with cholesterol, respectively. *J Biol Chem.* 2004;279(18):18526-18534. doi:10.1074/jbc.M304950200
306. Sutherland M, Kwon B, Hong M. Interactions of HIV gp41's membrane-proximal external region and transmembrane domain with phospholipid membranes from 31P NMR. *Biochim Biophys Acta Biomembr.* 2021;1863(11):183723. doi:10.1016/j.bbamem.2021.183723
307. de la Arada I, Torralba J, Tascón I, et al. Conformational plasticity underlies membrane fusion induced by an HIV sequence juxtaposed to the lipid envelope. *Sci Rep.* 2021;11(1):1278. doi:10.1038/s41598-020-80156-w
308. Garcia-Manyes S, Sanz F. Nanomechanics of lipid bilayers by force spectroscopy with AFM: a perspective. *Biochim Biophys Acta.* 2010;1798(4):741-749. doi:10.1016/j.bbamem.2009.12.019
309. Picas L, Rico F, Scheuring S. Direct measurement of the mechanical properties of lipid phases in supported bilayers. *Biophys J.* 2012;102(1):L01-03. doi:10.1016/j.bpj.2011.11.4001

310. Ebner A, Wildling L, Gruber HJ. Functionalization of AFM Tips and Supports for Molecular Recognition Force Spectroscopy and Recognition Imaging. *Methods Mol Biol.* 2019;1886:117-151. doi:10.1007/978-1-4939-8894-5_7
311. Proksch R, Schäffer T, Cleveland J, Callahan R, Viani M. Finite optical spot size and position corrections in thermal spring constant calibration. *Nanotechnology.* 2004;15:1344. doi:10.1088/0957-4484/15/9/039
312. Lorizate M, Cruz A, Huarte N, Kunert R, Pérez-Gil J, Nieva JL. Recognition and blocking of HIV-1 gp41 pre-transmembrane sequence by monoclonal 4E10 antibody in a Raft-like membrane environment. *J Biol Chem.* 2006;281(51):39598-39606. doi:10.1074/jbc.M605998200
313. Sáez-Cirión A, Arrondo JLR, Gómara MJ, et al. Structural and Functional Roles of HIV-1 gp41 Pretransmembrane Sequence Segmentation. *Biophysical Journal.* 2003;85(6):3769-3780. doi:10.1016/S0006-3495(03)74792-4
314. Reisdorf WC, Krimm S. Infrared amide I' band of the coiled coil. *Biochemistry.* 1996;35(5):1383-1386. doi:10.1021/bi951589v
315. Schwesinger F, Ros R, Strunz T, et al. Unbinding forces of single antibody-antigen complexes correlate with their thermal dissociation rates. *PNAS.* 2000;97(18):9972-9977. doi:10.1073/pnas.97.18.9972
316. Hinterdorfer P, Baumgartner W, Gruber HJ, Schilcher K, Schindler H. Detection and localization of individual antibody-antigen recognition events by atomic force microscopy. *PNAS.* 1996;93(8):3477-3481. doi:10.1073/pnas.93.8.3477
317. Dammer U, Hegner M, Anselmetti D, et al. Specific antigen/antibody interactions measured by force microscopy. *Biophys J.* 1996;70(5):2437-2441. doi:10.1016/S0006-3495(96)79814-4
318. Allen S, Chen X, Davies J, et al. Detection of antigen-antibody binding events with the atomic force microscope. *Biochemistry.* 1997;36(24):7457-7463. doi:10.1021/bi962531z
319. Neuert G, Albrecht C, Pamir E, Gaub HE. Dynamic force spectroscopy of the digoxigenin-antibody complex. *FEBS Lett.* 2006;580(2):505-509. doi:10.1016/j.febslet.2005.12.052
320. Bell GI. Models for the specific adhesion of cells to cells. *Science.* 1978;200(4342):618-627. doi:10.1126/science.347575

321. Evans E, Ritchie K. Strength of a weak bond connecting flexible polymer chains. *Biophys J.* 1999;76(5):2439-2447. doi:10.1016/S0006-3495(99)77399-6
322. Evans E. Energy landscapes of biomolecular adhesion and receptor anchoring at interfaces explored with dynamic force spectroscopy. *Faraday Discuss.* 1998;(111):1-16. doi:10.1039/a809884k
323. Evans E. Probing the relation between force--lifetime--and chemistry in single molecular bonds. *Annu Rev Biophys Biomol Struct.* 2001;30:105-128. doi:10.1146/annurev.biophys.30.1.105
324. Kienberger F, Kada G, Mueller H, Hinterdorfer P. Single Molecule Studies of Antibody–Antigen Interaction Strength Versus Intra-molecular Antigen Stability. *Journal of Molecular Biology.* 2005;347(3):597-606. doi:10.1016/j.jmb.2005.01.042
325. Donius LR, Cheng Y, Choi J, et al. Generation of Long-Lived Bone Marrow Plasma Cells Secreting Antibodies Specific for the HIV-1 gp41 Membrane-Proximal External Region in the Absence of Polyreactivity. *J Virol.* 2016;90(19):8875-8890. doi:10.1128/JVI.01089-16
326. Shao S, Huang WC, Lin C, et al. An Engineered Biomimetic MPER Peptide Vaccine Induces Weakly HIV Neutralizing Antibodies in Mice. *Ann Biomed Eng.* 2020;48(7):1991-2001. doi:10.1007/s10439-019-02398-8